

DEVIATION SADDLE BEHAVIOR AND DESIGN FOR
EXTERNALLY POST-TENSIONED BRIDGES

by

Richard James Beaupre, B.S.C.E.

THESIS

Presented to the Faculty of the Graduate School of
The University of Texas at Austin
in Partial Fulfillment
for the Degree of

MASTER OF SCIENCE IN ENGINEERING

THE UNIVERSITY OF TEXAS AT AUSTIN

August 1988

DEVIATION SADDLE BEHAVIOR AND DESIGN FOR
EXTERNALLY POST-TENSIONED BRIDGES

APPROVED:

To my Mom and Dad, and my special brother Paul

ACKNOWLEDGEMENTS

I wish to express my appreciation to the faculty members who contributed toward this thesis. A special thanks goes to my supervising professors, Dr. John Breen and Dr. Mike Kreger, who patiently and unselfishly directed my research and gave me much needed advice while writing my thesis. It was both an honor and a pleasure to work with them. I am grateful to the staff at the Phil M. Ferguson Structural Engineering Laboratory for their assistance. A special thanks goes to Blake Stasney, Dick Marshall, Pat Ball, Laurie Golding, Sharon Cunningham, Carol Booth, Maxine DeButts, Irene Saathoff, Alec Tahmassebi, Robert Gracia, and Jean Gehrke.

This project was sponsored by the Texas Department of Highways and Public Transportation under project 3-5-85-365.

I appreciate the hard work and endeavor of Lisa Carter who carried out the first phase of this study. Although many graduate students helped during the casting and testing, I would like to extend a special thanks to my friends Willy Ramirez, Bob Anderson, and Dave Barton. Gratitude is also extended to Rodney Heisch and Mike Hebert for their work on the project.

I would also like to thank friends outside of structural engineering for their support and encouragement throughout this endeavor; Esther Zapata, Bruce Vincent, Steve Rohde, Ri-Jen Chou, and Elyse Greene. A special thanks to my roommate Rui DaCosta.

Finally, I would like to thank my family; Dad, Mom, John, Karen, Paul and Jimmy. Without their love and support this goal would have been very difficult to achieve. I appreciate their sacrifice and hope that someday I will be able to return this gift.

TABLE OF CONTENTS

<u>Chapter</u>		<u>Page</u>
1	INTRODUCTION	1
	1.1 General	1
	1.2 State-of-the-Art	4
	1.3 Objective and Scope	16
2	TEST DESCRIPTION AND PROCEDURE	18
	2.1 Test Objectives	18
	2.2 Description and Design of Test Specimens	18
	2.2.1 Specimens 1A and 1B.	19
	2.2.2 Specimens 2A and 2B.	28
	2.2.3 Specimens 3A and 3B	33
	2.2.4 Specimens 4A and 4B	33
	2.2.5 Specimens 5A and 5B.	39
	2.3 Materials	41
	2.3.1 Concrete	41
	2.3.2 Reinforcing Steel	42
	2.3.3 Epoxy Coating	43
	2.3.4 Ducts	43
	2.3.5 Tendons	44
	2.4 Construction and Formwork	44
	2.5 Test Setup	47
	2.6 Instrumentation	52
	2.7 Data Reduction	57
	2.8 Test Procedure	58
3	TEST RESULTS	60
	3.1 Introduction	60
	3.2 Test 1A-Uncoated Link Bar with Stirrups- Straight Span-Three Tendons	66
	3.3 Test 1B-Uncoated Link Bar with Stirrups- Straight Span-Two Tendons	76
	3.4 Test 2A-Uncoated Link Bar Isolated-Test 1B Tendon Configuration	88
	3.5 Test 2B-Uncoated Stirrups Without Link Bar-Test 1B Tendon Configuration	97
	3.6 Test 3A-Epoxy Coated Link Bar with Stirrups- Companion Test of Test 1A	106
	3.7 Test 3B-Epoxy Coated Link Bar with Stirrups- Companion Test of Test 1B	113

TABLE OF CONTENTS (continued)

<u>Chapter</u>	<u>Page</u>
3.8 Test 4A-Uncoated Tendon Loop Bars with Stirrup- Outside of Curved Span-Two Tendons	130
3.9 Test 4B-Uncoated Tendon Loop Bars with Stirrup- Inside of Curved Span-Two Tendons	140
3.10 Test 5A-Epoxy Coated Tendon Loop Bars with Stirrup-Companion Test of Test 4A	150
3.11 Test 5B-Epoxy Coated Tendon Loop Bars with Stirrup-Companion Test of Test 4B	157
3.12 Comparison of Epoxy Coated and Uncoated Reinforcement	165
4 ANALYSIS OF TEST RESULTS	177
4.1 Introduction	177
4.2 Evaluation of Results With Respect To Simplified Analysis Models	177
4.2.1 Direct Tension Model	178
4.2.2 Shear Friction Model	182
4.2.3 Beam Model	195
4.2.4 Analysis Combinations And Comparison of Test Results.	202
4.3 Evaluation of Results With Respect To Strut-Tie Model	219
4.3.1 Analysis Combinations And Comparison To Test Results.	233
4.4 Comparison Of Analysis Methods	238
4.5 Conclusions	244
5 DEVIATOR DESIGN RECOMMENDATIONS	251
5.1 General Approach	251
5.2 Deviation Saddle Geometry And Size	257
5.3 Reinforcement	265
5.4 Design Examples	272
5.5 Conclusions	272
6 CONCLUSIONS AND RECOMMENDATIONS	276
6.1 Brief Summary	276
6.2 Conclusions	282
6.3 Recommendations	286

LIST OF TABLES

<u>Table</u>	<u>Page</u>
4.1 Yield Deviator Loads	203
4.2 Ultimate Deviator Loads	204
4.3 Comparison of Test Results to Simplified Analysis Results - Yield Load Stage - Tests 1A, 1B, 2A, 2B, 3A, 3B	207
4.4 Comparison of Test Results to Simplified Analysis Results - Ultimate Load Stage - Tests 1A, 1B, 2A, 2B, 3A, 3B	208
4.5 Comparison of Test Results to Simplified Analysis Results - Yield Load Stage - Tests 4A, 4B, 5A, 5B	215
4.6 Comparison of Test Results to Simplified Analysis Results - Ultimate Load Stage - Tests 4A, 4B, 5A, 5B	216
4.7 Comparison of Test Results to Strut-Tie Analysis Results- Yield Load Stage - Tests 1A, 1B, 2A, 2B, 3A, 3B	234
4.8 Comparison of Test Results to Strut-Tie Analysis Results - Ultimate Load Stage - Tests 1A, 1B, 2A, 2B, 3A, 3B	235
4.9 Comparison of Test Results to Strut-Tie Analysis Results- Yield Load Stage - Tests 4A, 4B, 5A, 5B	236
4.10 Comparison of Test Results to Strut-Tie Analysis Results - Ultimate Load Stage - Tests 4A, 4B, 5A, 5B	236
5.1 Comparison of Factors of Safety - Tests 4A, 4B, 5A, 5B	259

LIST OF FIGURES

<u>Figure</u>		<u>Page</u>
1.1	External Post-Tensioning in Long Key Bridge	2
1.2	Typical Shapes for Diaphragm Deviators	7
1.3	Typical Shape for Rib Deviators	8
1.4	Typical Shapes for Deviation Saddles	9
1.5	Diaphragm Reinforcement - Example	10
1.6	Pass-Through Tendons	12
1.7a	Deviation Saddle Reinforcement - Example 1	13
1.7b	Deviation Saddle Reinforcement - Example 2	14
1.7c	Deviation Saddle Reinforcement - Example 3	15
2.1a	Box Reinforcement	20
2.1b	Box Reinforcement Schedule	21
2.2	Prototype Deviator Reinforcement	22
2.3	Specimens 1A, 1B, 2A, 2B, 3A, 3B Dimensions	23
2.4a	Specimens 1A, 3A	24
2.4b	Specimens 1B, 3B	25
2.4c	Deviator Reinforcement Bending Diagram Specimens 1A, 1B, 2A, 2B, 3A, 3B	26
2.4d	Specimens 1A and 1B Reinforcement Cage	27
2.5	Prototype Tendon Layout	29
2.6a	Specimen 2A	30
2.6b	Specimen 2B	31
2.6c	Specimens 2A and 2B Reinforcement Cage	32
2.7	Specimens 3A and 3B Reinforcement Cage	34

LIST OF FIGURES (continued)

<u>Figure</u>		<u>Page</u>
2.8	Specimens 4A, 4B, 5A, 5B Dimensions	35
2.9a	Specimens 4A, 4B, 5A, 5B	36
2.9b	Deviator Reinforcement Bending Diagram Specimens 4A, 4B, 5A, 5B	37
2.9c	Specimens 4A and 4B Reinforcement Cage	38
2.10	Specimens 5A and 5B Reinforcement Cage	40
2.11	Box Reinforcement Cage	45
2.12	Formwork	46
2.13	Test Setup	48
2.14a	Testing Concept	49
2.14b	Test Setup, Elevation	50
2.14c	Test Setup, Plan	51
2.15a	Strain Gage Locations on Deviation Saddle Reinforcement Specimens 1A, 1B	53
2.15b	Strain Gage Locations on Deviation Saddle Reinforcement Specimens 2A, 2B	54
2.15c	Strain Gage Locations on Deviation Saddle Reinforcement Specimens 3A, 3B	55
2.15d	Strain Gage Locations on Deviation Saddle Reinforcement Specimens 4A, 4B, 5A, 5B	56
3.1a	Prototype Deviation Angles and Forces	63
3.1b	Prototype Deviation Angles and Forces	64
3.2	Test 1A Loading History	67
3.3	Test 1A Crack Patterns	68
3.4	Test 1A Reinforcement Strain Data - Phase 1	70

LIST OF FIGURES (continued)

<u>Figure</u>		<u>Page</u>
3.5	Test 1A Reinforcement Strain Data - Phase 2	71
3.6	Test 1A Reinforcement Failure Locations	73
3.7	Test 1A - Before and After Failure	74
3.8	Test 1A Strength Comparison	75
3.9	Test 1B Loading History - Phase 1	77
3.10	Test 1B Loading History - Phase 2	78
3.11	Test 1B Crack Patterns	79
3.12	Test 1B Reinforcement Strain Data - Phase 1 (a) ...	81
3.13	Test 1B Reinforcement Strain Data - Phase 1 (b) ...	82
3.14	Test 1B Reinforcement Strain Data - Phase 2	83
3.15	Test 1B Reinforcement Failure Locations	85
3.16	Test 1B - Before and After Failure	86
3.17	Test 1B Strength Comparison	87
3.18	Test 2A Loading History	89
3.19	Test 2A Crack Patterns	90
3.20	Test 2A Reinforcement Strain Data - Phase 1	91
3.21	Test 2A Reinforcement Strain Data - Phase 2	92
3.22	Test 2A Reinforcement Failure Locations	94
3.23	Test 2A - Before and After Failure	95
3.24	Test 2A Strength Comparison	96
3.25	Test 2B Loading History	98
3.26	Test 2B Crack Patterns	99

LIST OF FIGURES (continued)

<u>Figure</u>		<u>Page</u>
3.27	Test 2B Reinforcement Strain Data - Phase 1	100
3.28	Test 2B Reinforcement Strain Data - Phase 2	102
3.29	Test 2B Reinforcement Failure Locations	103
3.30	Test 2B - Before and After Failure	104
3.31	Test 2B Strength Comparison	105
3.32	Test 3A Loading History	107
3.33	Test 3A Crack Patterns	108
3.34	Test 3A Reinforcement Strain Data - Phase 1	110
3.35	Test 3A Reinforcement Strain Data - Phase 2	112
3.36	Test 3A Reinforcement Failure Locations	114
3.37	Test 3A - Before and After Failure	115
3.38	Test 3A Strength Comparison	116
3.39	Test 3B Loading History - Phase 1	118
3.40	Test 3B Loading History - Phase 2	119
3.41	Test 3B Crack Patterns	120
3.42	Test 3B Reinforcement Strain Data - Phase 1 (a) ...	121
3.43	Test 3B Reinforcement Strain Data - Phase 1 (b) ...	122
3.44	Test 3B Reinforcement Strain Data - Phase 1 (c) ...	123
3.45	Test 3B Reinforcement Strain Data - Phase 2	125
3.46	Test 3B Reinforcement Failure Locations	127
3.47	Test 3B - Before and After Failure	128
3.48	Test 3B Strength Comparison	129

LIST OF FIGURES (continued)

<u>Figure</u>		<u>Page</u>
3.49	Test 4A Loading History	131
3.50	Test 4A Crack Patterns	132
3.51	Test 4A Reinforcement Strain Data - Phase 1	134
3.52	Test 4A Reinforcement Strain Data - Phase 2	135
3.53	Test 4A Reinforcement Failure Locations	137
3.54	Test 4A - Before and After Failure	138
3.55	Test 4A Strength Comparison	139
3.56	Test 4B Loading History	141
3.57	Test 4B Crack Patterns	142
3.58	Test 4B Reinforcement Strain Data - Phase 1	143
3.59	Test 4B Reinforcement Strain Data - Phase 2	145
3.60	Test 4B Reinforcement Failure Locations	147
3.61	Test 4B - Before and After Failure	148
3.62	Test 4B Strength Comparison	149
3.63	Test 5A Loading History	151
3.64	Test 5A Crack Patterns	152
3.65	Test 5A Reinforcement Strain Data - Phase 1 (a) ...	153
3.66	Test 5A Reinforcement Strain Data - Phase 1 (b) ...	155
3.67	Test 5A Reinforcement Strain Data - Phase 2	156
3.68	Test 5A Reinforcement Failure Locations	158
3.69	Test 5A - Before and After Failure	159
3.70	Test 5A Strength Comparison	160

LIST OF FIGURES (continued)

<u>Figure</u>		<u>Page</u>
3.71	Test 5B Loading History	161
3.72	Test 5B Crack Patterns	162
3.73	Test 5B Reinforcement Strain Data - Phase 1	164
3.74	Test 5B Reinforcement Strain Data - Phase 2	166
3.75	Test 5B Reinforcement Failure Locations	167
3.76	Test 5B - Before and After Failure	168
3.77	Test 5B Strength Comparison	169
3.78	Comparison of Tests 1A and 3A	170
3.79	Comparison of Tests 1B and 3B	171
3.80	Comparison of Tests 4A and 5A	172
3.81	Comparison of Tests 4B and 5B	173
4.1	Behavioral Models	179
4.2	Direct Tension Model - Tests 1A, 1B, 2A, 3A, 3B ...	181
4.3	Direct Tension Model - Tests 4A, 4B, 5A, 5B	183
4.4	Typical Test Results for Shear Friction Study	185
4.5	Diagonal Tension Cracking Along Previously Uncracked Shear Plane	187
4.6	Shear Friction - Comparison of Mattock Test Results and Design Equations	187
4.7	Shear Friction Model - Tests 1A, 1B, 2B, 3A, 3B ...	189
4.8a	Shear Friction Model - Tests 4A, 4B, 5A, 5B - First Trial	192
4.8b	Shear Friction Model - Tests 4A, 4B, 5A, 5B - Second Trial	193

LIST OF FIGURES (continued)

<u>Figure</u>		<u>Page</u>
4.9	Beam Model - Tests 1A, 3A	197
4.10	Beam Model - Tests 1B, 2B, 3B	198
4.11	Beam Model - Tests 4A, 5A	200
4.12	Beam Model - Tests 4B, 5B	201
4.13	"D" Regions (Shaded Areas) with Nonlinear Strain Distribution	220
4.14	Strut-Tie Models - Primary Reinforcement	224
4.15	Strut-Tie Model - Top Surface Reinforcement - Tests 1A, 3A	226
4.16	Strut-Tie Model - Top Surface Reinforcement - Tests 1B, 3B	227
4.17	Strut-Tie Model - Top Surface Reinforcement - Test 2B	228
4.18	Strut-Tie Model - Top Surface Reinforcement - Tests 4A, 5A	231
4.19	Strut-Tie Model - Top Surface Reinforcement - Tests 4B, 5B	232
4.20	Comparison of Analysis Methods	241
5.1	Horizontal Force Components on Deviators of Curved Span	253
5.2	Modified Deviation Saddle Detail	256
5.3	Early Deviation Saddle Detail	258
5.4	Recommendation for Full Bottom Flange Width Deviation Saddle - Small Radius Curved Spans	261
5.5	Plan and Elevation of Full Bottom Flange Deviation Saddle	263
5.6	Construction Scheme for Box Reinforcement	267

LIST OF FIGURES (continued)

<u>Figure</u>		<u>Page</u>
5.7a	Design Example for Straight Span	272
5.7b	Design Example for Straight Span	273
5.8a	Design Example for Curved Span	274
5.8b	Design Example for Curved Span	275

CHAPTER 1 INTRODUCTION

1.1 General

Since the first use of concrete segmental box girder bridges in the United States in 1973, there have been rapid developments in segmental bridge design and construction. One of the latest and most dramatic developments in segmental technology has been the use of external tendons which are defined as tendons in ducts which are not encased in the concrete of the webs or flanges of the box girder bridge except at the ends of the span (see Fig. 1.1). This innovative type of construction has been shown to provide substantial economic savings, as well as savings in construction time. The economic savings result from use of a more efficient web section because the tendons are moved into the cell-void and out of the web. This greatly reduces the web congestion. Construction time is reduced because of the development of a span-by-span erection scheme. This scheme has proved to be very efficient, enabling some constructors to average over two spans per week. The rapid rate of completion results in both direct savings to the constructor and greatly reduced detour costs, fuel, and time to the motoring public. Because of the economic savings and the anticipated rapidity of construction expected of this novel type of bridge construction, the Texas Department of Highways and Public Transportation selected this bridge type as one of the alternate designs for substantial use in the San Antonio area. Competitive

bidding indicated that constructors favored this alternate and several substantial projects have already been put under construction.

External post-tensioning differs from internal post-tensioning because the tendons are removed from the webs and flanges and placed in the cell-void. Tendon geometry is controlled by passing the tendons through tendon deviators cast monolithically in several of the segments as illustrated in Fig. 1.1. These tendon deviators perform somewhat the same function as hold-down devices in a pretensioning bed. Note in Fig. 1.1 that there are typically some segments of a span which have no physical connection to the tendons. These segments are held in position completely by the compressive forces from their adjacent segments and the combination of friction and multiple shear keys. External tendons usually overlap at the pier to provide continuity to the bridge. After completion of post-tensioning, the tendons are usually grouted in the tendon ducts, which often consist of polyethylene pipes running between anchorage locations and tendon deviators. This provides corrosion protection for the tendons, but the system is generally regarded as unbonded post-tensioned construction for ultimate-strength analysis unless special attempts are made to develop the tendons by bonding to the concrete over longer lengths.

Because this is a relatively new technology and most of these developments have been investigated primarily on an analytical basis, there have been uncertainties about the actual behavior of these

bridges when subjected to loads greater than service loads. Also, there are uncertainties that exist concerning the behavior and proper design criteria for the tendon deviator details. For this reason, a series of studies of this type construction are being conducted at the Ferguson Structural Engineering Laboratory at the University of Texas at Austin. The primary study being conducted is concerned with the overall bridge behavior. The experimental portion of this project includes the construction and testing of a reduced scale three-span continuous externally post-tensioned segmental box girder bridge. A satellite study reported in this thesis documents an experimental investigation of the tendon deviator details and suggests a design methodology for the deviators.

1.2 State-of-the-Art

An excellent, comprehensive review of state-of-the-art developments of external post-tensioning in bridges was completed by Carter (1) who carried out the first phase of the deviator study at the University of Texas at Austin. The following subjects were reported by Carter:

- 1) An extensive history of the worldwide developments leading to the use of external post-tensioning in recent U. S. bridge projects.

- 2) The advantages and disadvantages of the use of external post-tensioning in bridges.

3) Various types of tendon deviators, tendon ducts, and reinforcing schemes.

4) Problem areas concerning deviators. The topics touched on were problems related to each type of deviator, geometry errors of ducts embedded in deviators, force diffusion at deviators, damage to deviators in existing structures, and lack of consistent design philosophy.

5) Related research on the subject of external post-tensioning. This included research on girders with external post-tensioning and research on tendons with respect to characteristics of the deviation, nature of the tendons, tendon protection, and loading.

Carter's thesis also included a description of the testing equipment developed for this study as well as some test results. These will be referred to in subsequent chapters. A brief summary of several pertinent items from Carter's state-of-the-art study in the areas of existing tendon deviators, reinforcement schemes, and the advantages and disadvantages of specific deviator types is presented here since this information is essential to the understanding of the material presented in Chapters 2 through 6.

Deviators maintain the draped profile of the external tendons and provide the only positive attachment of the tendons to the structure other than at the anchorage zones. This makes the deviator a key element of this bridge type.

There have been three basic kinds of tendon deviators utilized in bridges. These include the diaphragm which is shown in Fig. 1.2, the rib or stiffener shown in Fig. 1.3, and the saddle or block shown in Fig. 1.4. These types of deviators are usually monolithically cast in the bridge segments with the correct tendon duct configurations required for the bridge constraints.

Diaphragms (Fig. 1.2) are usually "U" shaped either as shown in the sketch or inverted. The opening in the center of the diaphragm is provided to allow passage through the bridge. The thickness of the diaphragm (along the longitudinal direction of the bridge) usually ranges from 12" to 30", typically depending on the tendon deviation required (there is a minimum radius that the tendon duct can be bent). In some cases, the deviator is wider at the base as shown in Fig. 1.2(b). The reinforcing scheme for the diaphragm is typically a mesh of horizontal and vertical reinforcement bars which extend into the flanges and the webs. Also, local confinement reinforcement is usually provided around the tendon ducts. An example of diaphragm reinforcement is shown in Fig. 1.5. The advantage of using this type of deviator is that the compressive strength of the concrete may be utilized to resist the deviation forces in this detail. A compression strut can develop from immediately above the tendon duct to the top flange which provides this detail with exceedingly high strength. However, many disadvantages exist with this detail. It creates added dead load for the bridge, sometimes offsetting the savings from the

efficient web thickness. Other disadvantages are construction related. The formwork for the diaphragm and the geometry for the tendon pass throughs become very complicated especially for a curved span. This is illustrated in Fig. 1.6.

The stiffener or rib shaped deviators (Fig. 1.3) generally extend along the full web height and extend out approximately a foot from the web. The transverse width is usually increased at the toe and the head of the rib as shown in the sketch. This type of deviator is commonly used for retrofit measures where external tendons are added to strengthen an existing bridge, although it has been utilized in new bridge design. This type of deviator represents a compromise between the saddle and the diaphragm. As in the diaphragm, the geometry can become very complicated for the pass through tendons, especially for curved spans.

The block or saddle (Fig. 1.2) is just as its name implies, a relatively small block of concrete located at the intersection of the web and bottom flange. The reinforcing for this detail is usually in the form of links and bent bars anchored into the web and flanges. Some examples of some reinforcing schemes used in early practice in the United States are shown in Figs. 1.7a-c. Advantages of utilizing this detail in a bridge are the insignificant additional weight for the structure, the formwork is less complicated than that required for diaphragms, and geometry complications are minimized because tendon pass throughs are not required. However, the disadvantage is

that the deviator capacity may be greatly reduced compared to the diaphragm because there is no compression strut formed after cracking as in the diaphragm or rib. Therefore, the deviator force must be tied back into the box by reinforcement so that it requires greater attention to detailing than that required for a diaphragm or rib.

1.3 Objective and Scope

From the extensive survey of existing tendon deviators performed by Carter (1), it was determined that the deviation saddle was the most prevalent type of tendon deviator. It is obvious that the deviation saddle is also the weakest of the three basic types of tendon deviators. However, if the safety of deviation saddles is confirmed by tests, then this type offers the most advantages for reducing the structure weight, facilitating the fabrication of segments, and minimizing geometry complications. Therefore, the laboratory investigation was directed towards the study of deviation saddles.

The objectives of the study were to:

- 1) Investigate deviator behavior with respect to strength and ductility.
- 2) Evaluate several typical deviator designs with respect to efficiency and adequacy of details and to overall performance.
- 3) Define behavioral models for deviators.
- 4) Determine the effects of using epoxy coated reinforcement in deviators.

5) Establish design criteria for deviators.

The scope of the experimental program included the fabricating and testing to ultimate of ten reduced scale models of deviation saddles. A specially designed testing apparatus applied load to the deviator just as it would be loaded in a bridge. This generalized test setup could accommodate a variety of specimen sizes, tendon layouts and loading schemes.

The prototype for the first six deviator specimens was chosen from representative details in existing structures in the United States. With the goal of simplification and standardization of the deviator design, the geometry and reinforcing scheme were modified for later models. Tendon configurations varied for the models. Since epoxy coated reinforcement is used in many coastal bridges, some of the test specimens incorporated this type of reinforcement to study its effect on behavior. Description of the specimens and testing procedure are presented in Chapter 2. The data from this test series are presented in Chapter 3. Based on the results of this investigation, analysis techniques are formulated in Chapter 4, and deviator design recommendations are suggested in Chapter 5. Final conclusions and recommendations are given in Chapter 6.

CHAPTER 2
TEST DESCRIPTION AND PROCEDURE

2.1 Test Objectives

The deviation saddle investigation began by looking at typical details of deviation saddles used in early practice in the United States. These details were then modelled and tested (1). In later tests, deviation saddle details were modified with the goal of simplification and standardization. The tests had the following objectives:

- 1) Investigate deviation saddle behavior with respect to ductility and strength.
- 2) Evaluate the design of the prototype deviation saddle with respect to details and overall performance.
- 3) Evaluate the design of the modified deviation saddle with respect to details and overall performance.
- 4) Establish design models for deviation saddle behavior.
- 5) Evaluate the effects of using epoxy coated reinforcement in deviation saddles.
- 6) Establish design criteria for deviation saddles.

2.2 Description and Design of Test Specimens

A total of ten specimens were fabricated and tested including the two that were completed by Carter (1). Two test specimens were fabricated in each reduced scale single cell box section. They were

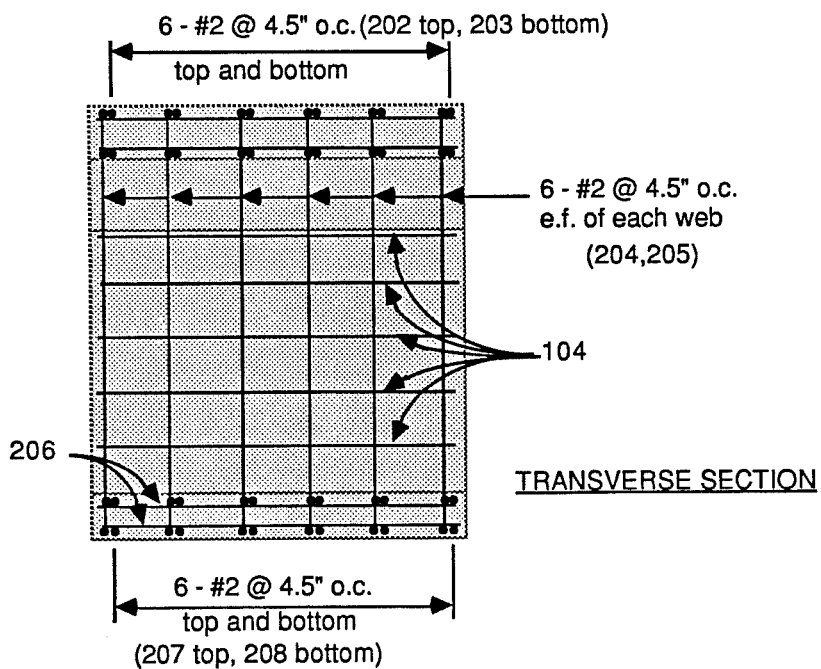
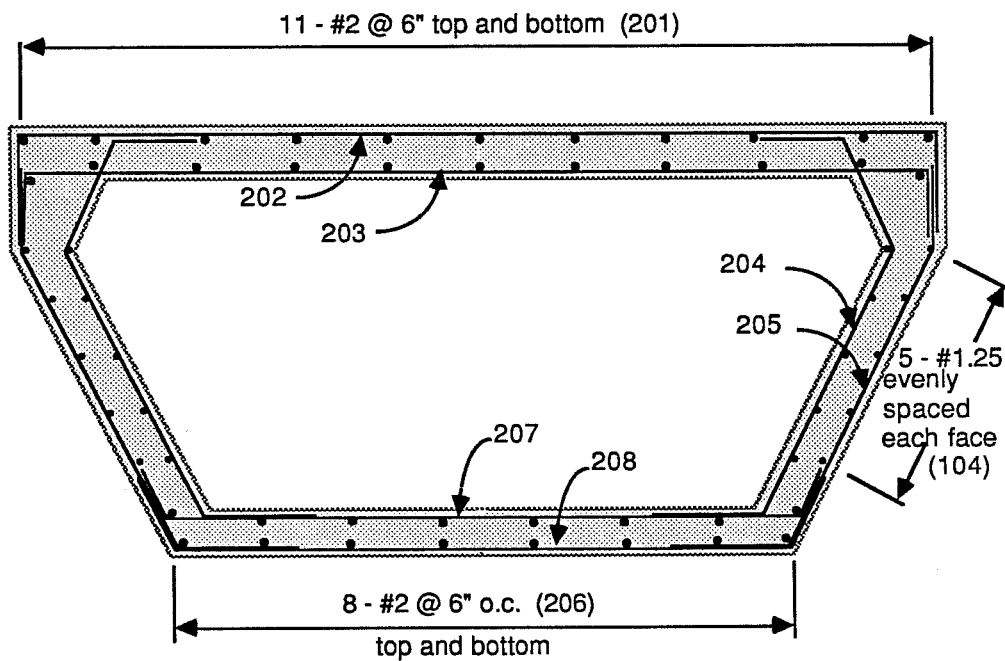


Figure 2.1a Box Reinforcement (From Ref. 1)

Schedule No.	Bend Type	Bar Size	Length	Pieces required
201	straight	#2	23"	22
206	straight	#2	23"	16
104	straight	#1.25	23"	20
202	A	#2	72"	6
203	B	#2	66"	6
204	C	#2	39.25"	12
205	D	#2	36.25"	12
207	E	#2	59"	6
208	F	#2	57"	6

BEND TYPES (All dimensions out-to-out)

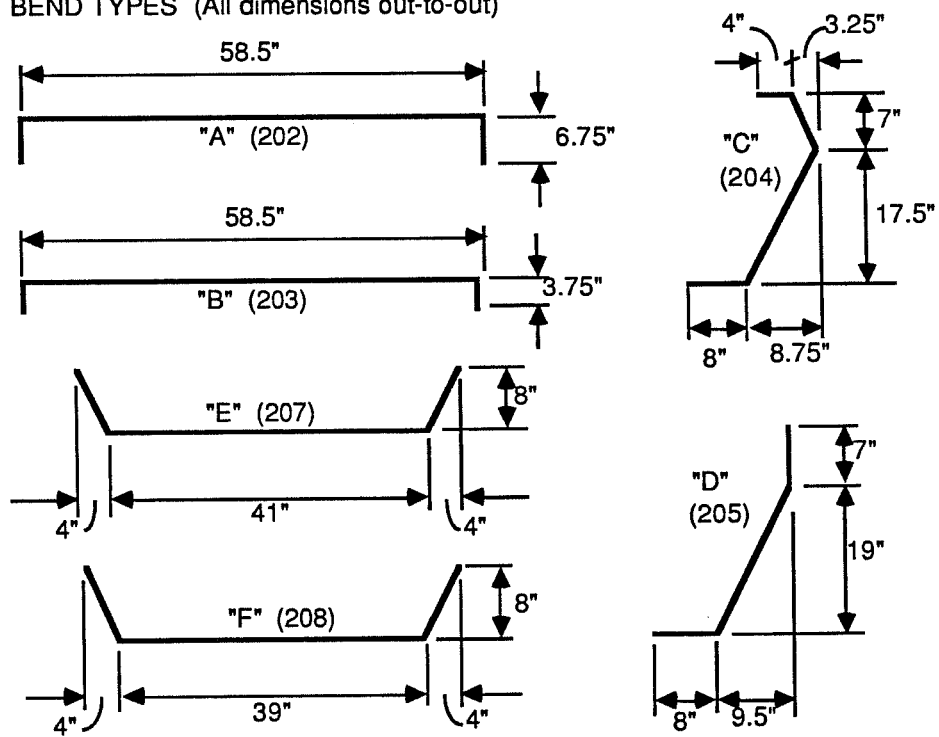
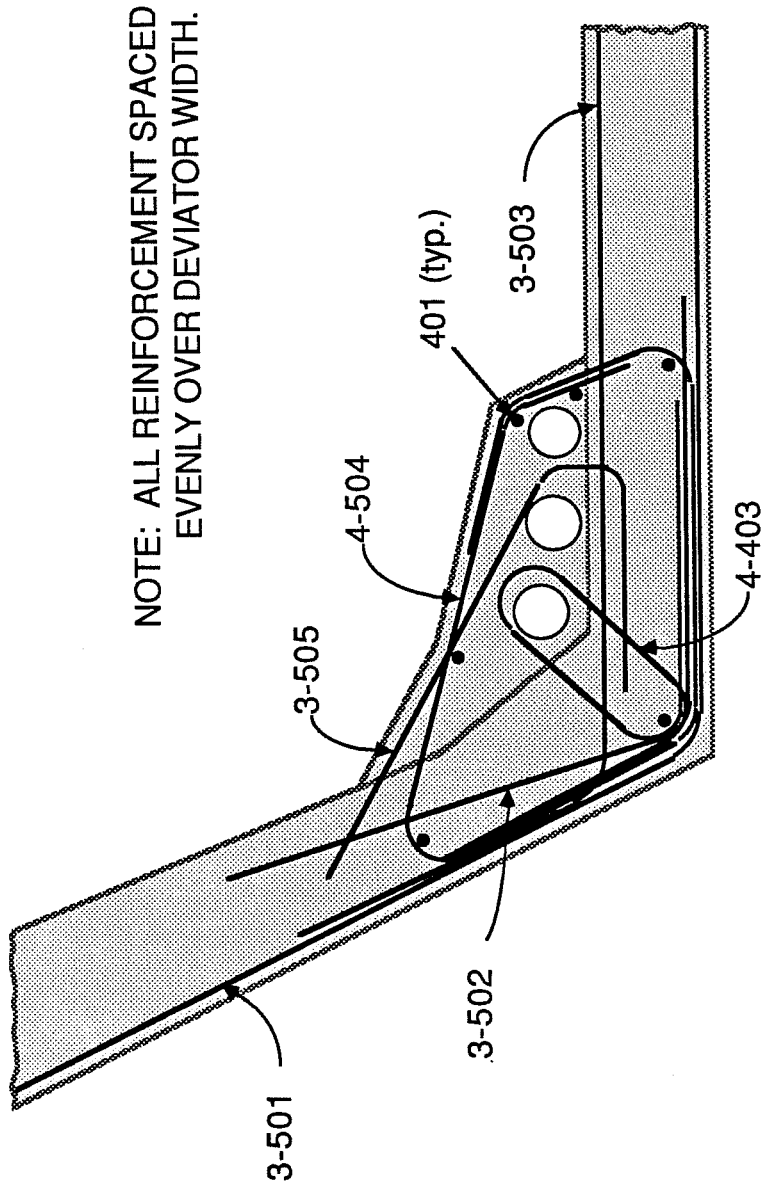


Figure 2.1b Box Reinforcement Schedule (From Ref. 1)



NOTE: ALL REINFORCEMENT SPACED
EVENLY OVER DEVIATOR WIDTH.

Figure 2.2 Prototype Deviator Reinforcement (From Ref. 1)

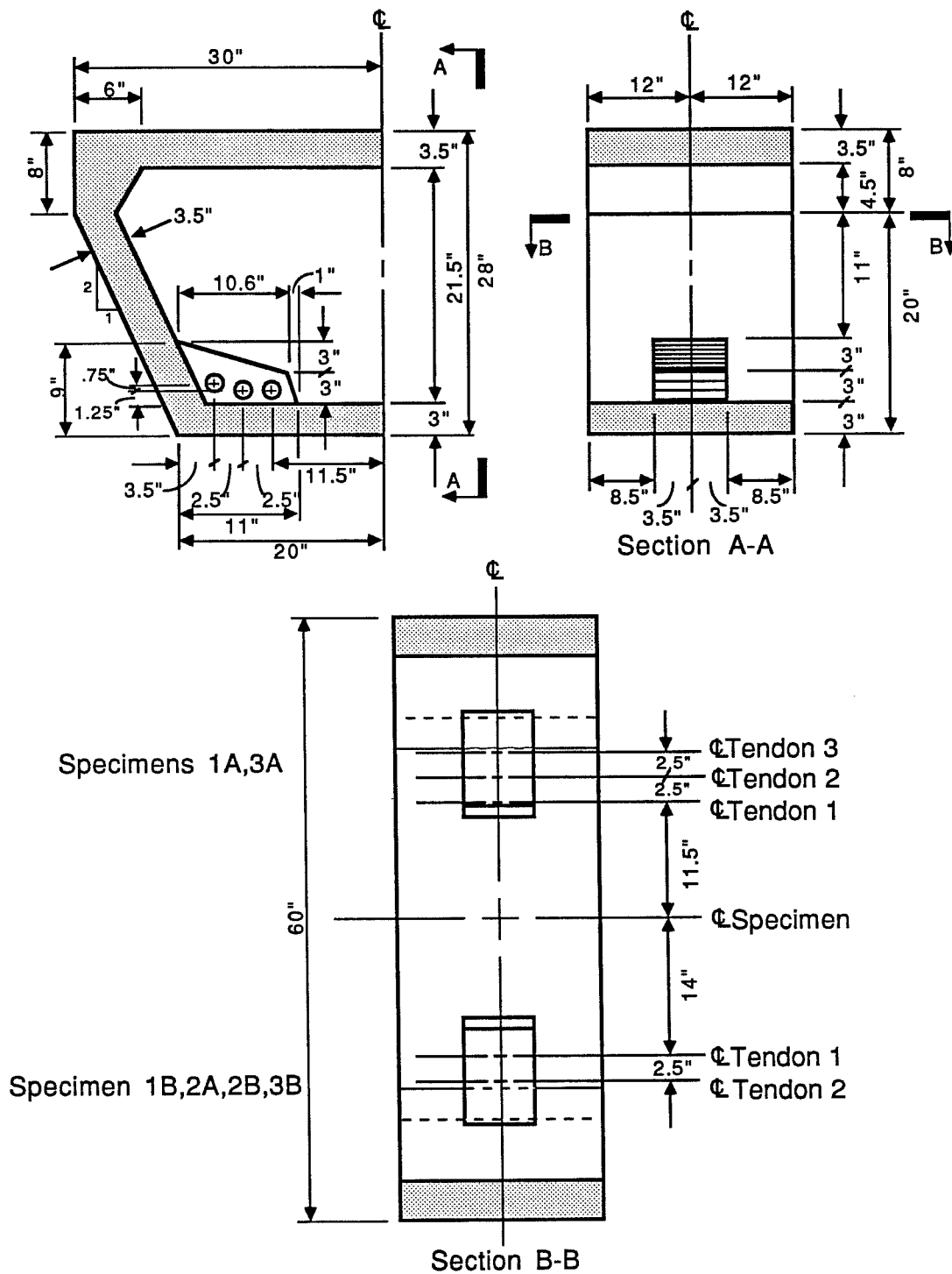


Figure 2.3 Specimens 1A, 1B, 2A, 2B, 3A, 3B Dimensions (From Ref. 1)

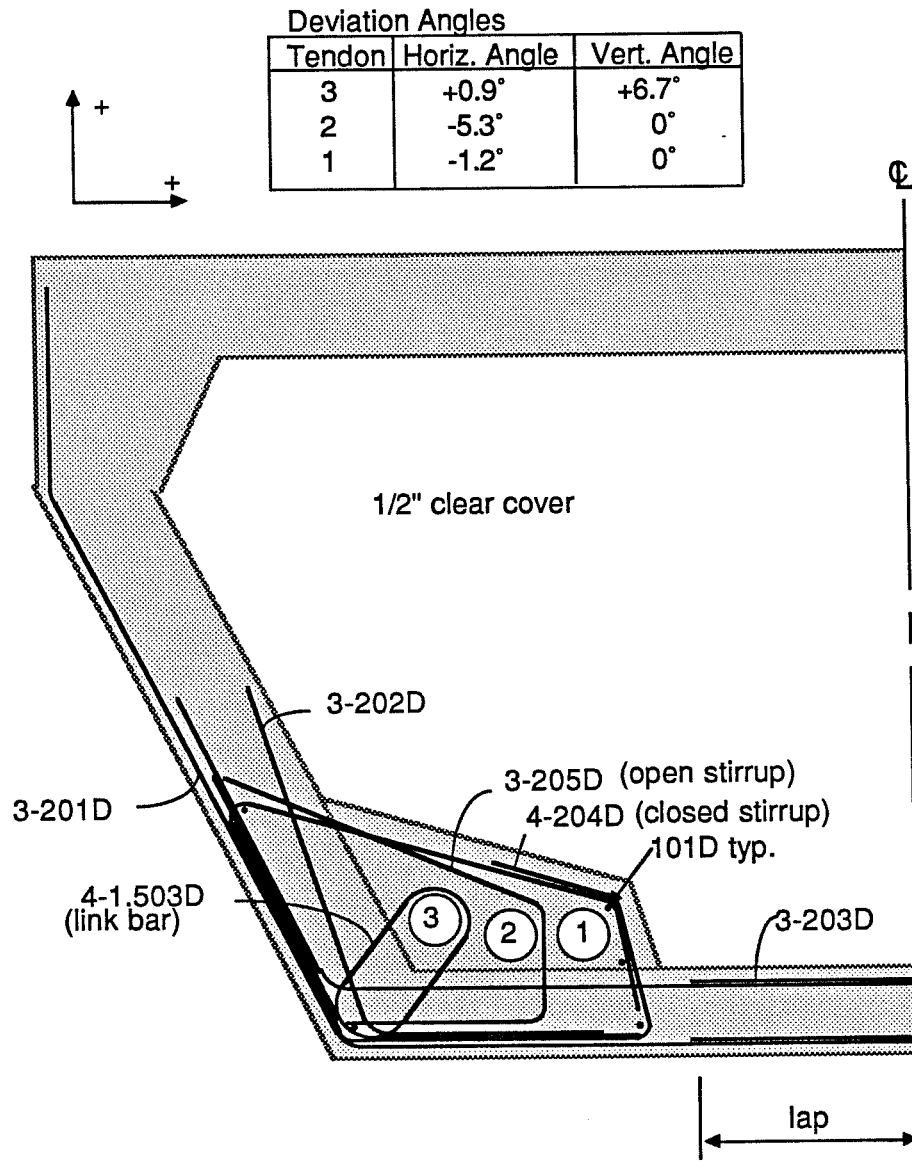


Figure 2.4a Specimens 1A, 3A

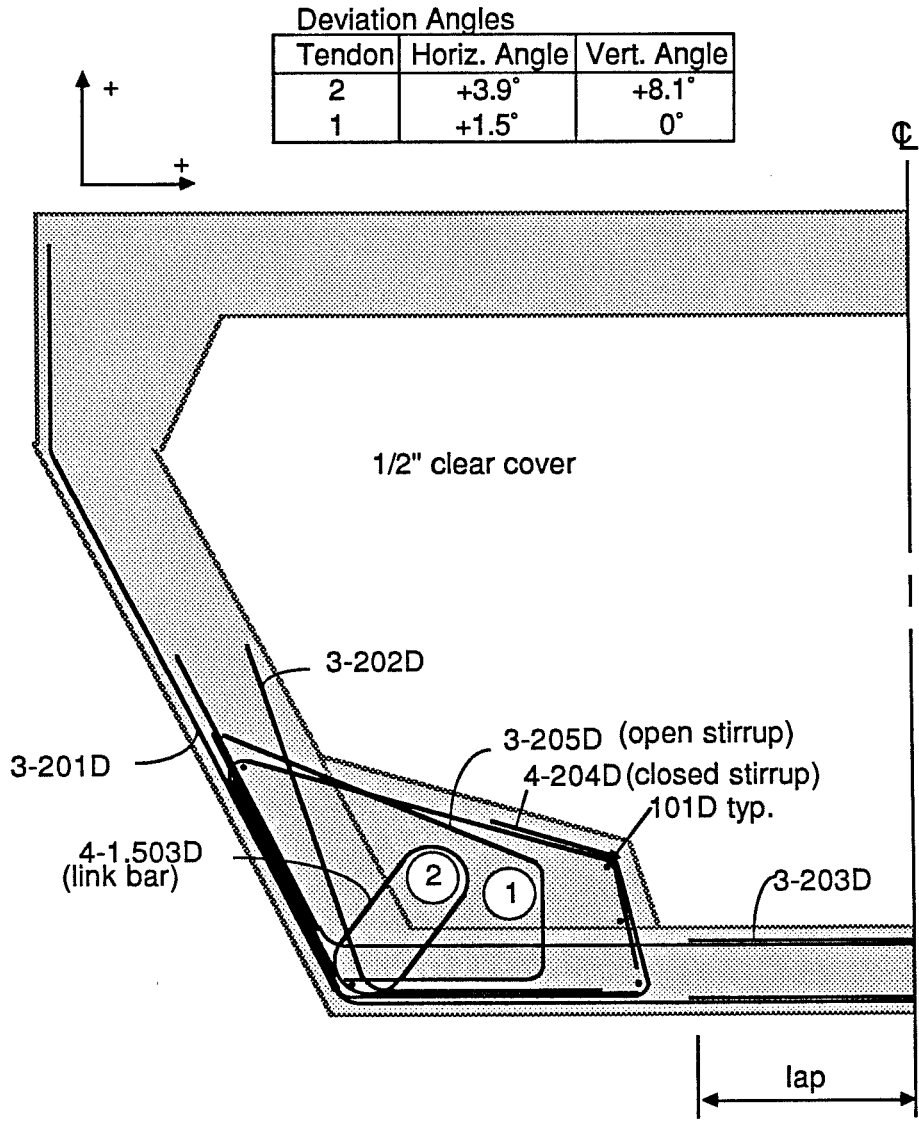
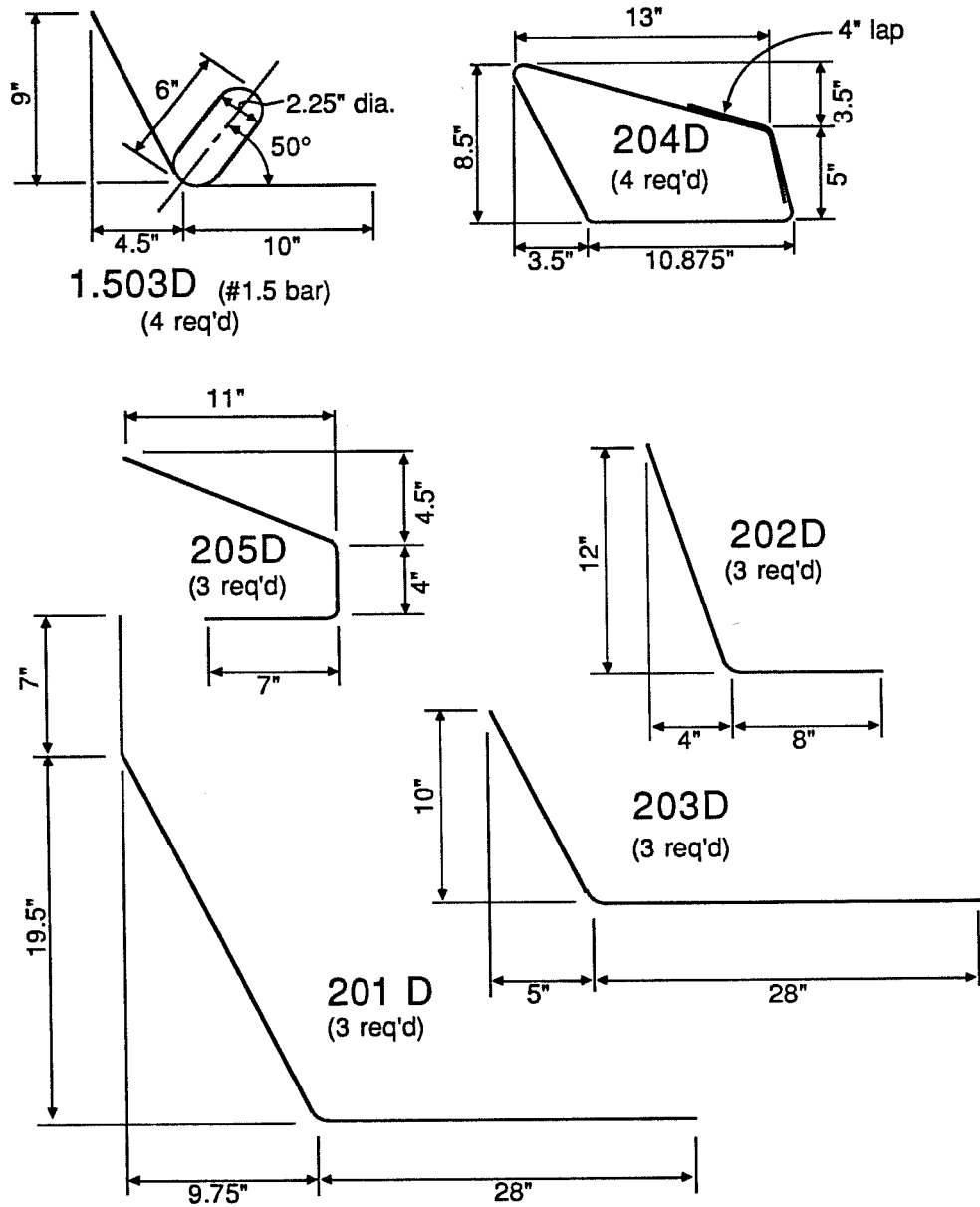


Figure 2.4b Specimens 1B, 3B

DEVIATOR REINFORCEMENT BENDING DIAGRAM



NOTE: Diameter of bends = 1" unless otherwise noted.

Figure 2.4c Deviator Reinforcement Bending Diagram
Specimens 1A, 1B, 2A, 2B, 3A, 3B (From Ref. 1)

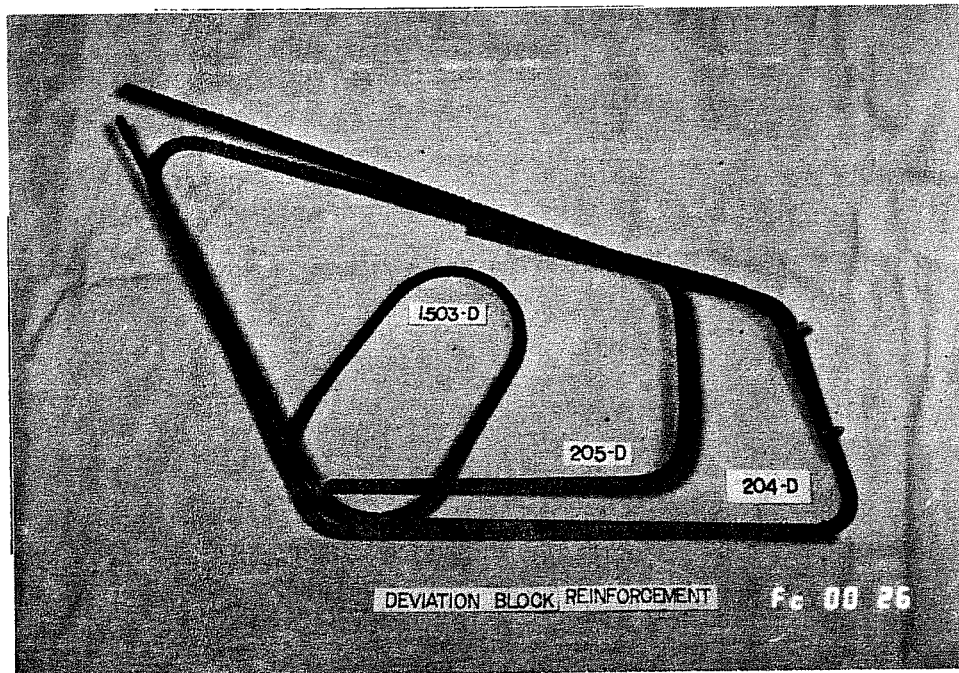
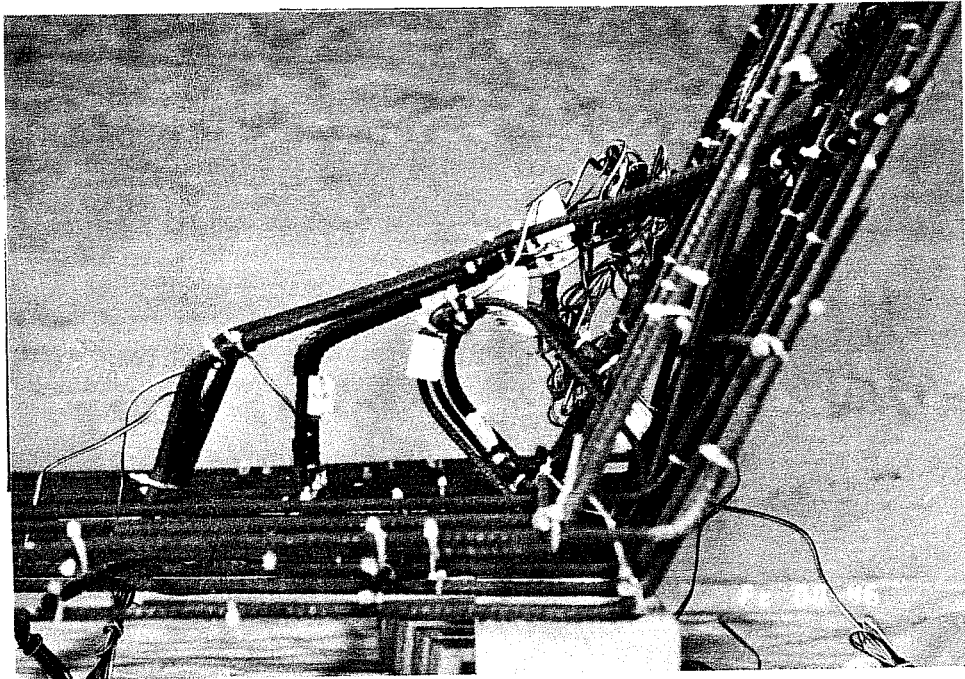
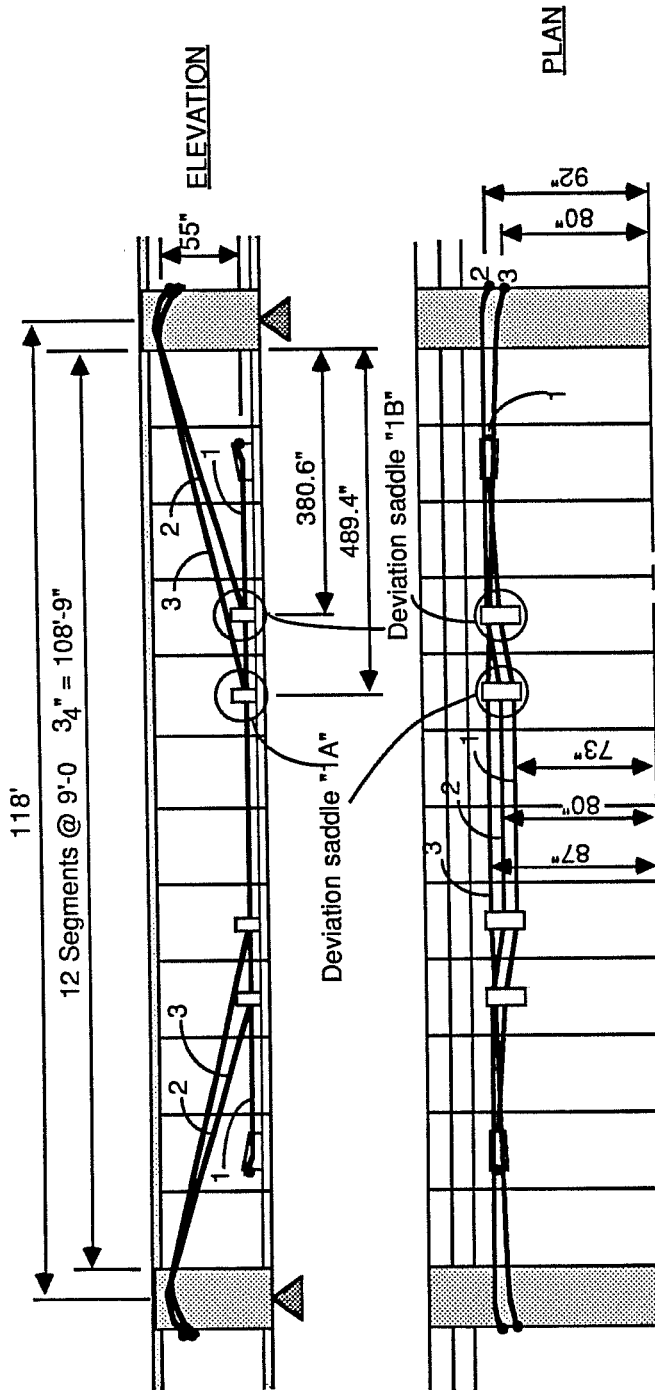


Figure 2.4d Specimens 1A and 1B Reinforcement Cage

the bottom flange and the web to provide extra reinforcement for the box section (201D, 202D, 203D).

Deviation saddle 1A was representative of a prototype deviation saddle that is located farthest from the pier. It was assumed that such a saddle would deviate half the tendons of a span, and that the tendon which deviates vertically has a smaller vertical deviation than a tendon that is deviated closer to the pier (Fig. 2.5). Deviation saddle 1B was representative of a prototype deviation saddle which would be located closer to the pier and adjacent to the deviation saddle described above. It was assumed that such a saddle would deviate one less tendon and that the tendon which deviates vertically has a greater vertical deviation than a tendon which is deviated farther from the pier (Fig. 2.5). Tendon deviation angles for the prototype structure are shown in Fig. 2.5, and tendon deviation angles for specimens 1A and 1B are shown in Fig. 2.4a-b.

2.2.2 Specimens 2A and 2B. The objective for specimens 2A and 2B was to isolate the behavior of the individual reinforcement patterns of specimens 1A and 1B. Reinforcement details for specimen 2A were based on providing the link bar (1.503D) alone. Specimen 2B reinforcement details were based on providing the two types of stirrups (204D,205D) without the link bars (Fig. 2.6a-c). The tendon patterns were identical to specimen 1B. Also, additional reinforcement was placed in the bottom flange and web similar to specimens 1A and 1B (201D,202D,203D).



Tendon 1 : 12-0.5" dia. strands
 2 : 19-0.5" dia. strands
 3 : 19-0.5" dia. strands

DEVIATION ANGLES:

Test	Tendon	Horiz. Angle	Vert. Angle
Deviation Saddle "1A"	3	+0.82°	+6.41°
	2	-3.68°	0
	1	-3.68°	0
Deviation Saddle "1B"	2	+2.93°	+8.22°
	1	+1.84°	0

Figure 2.5 Prototype Tendon Layout (From Ref. 1)

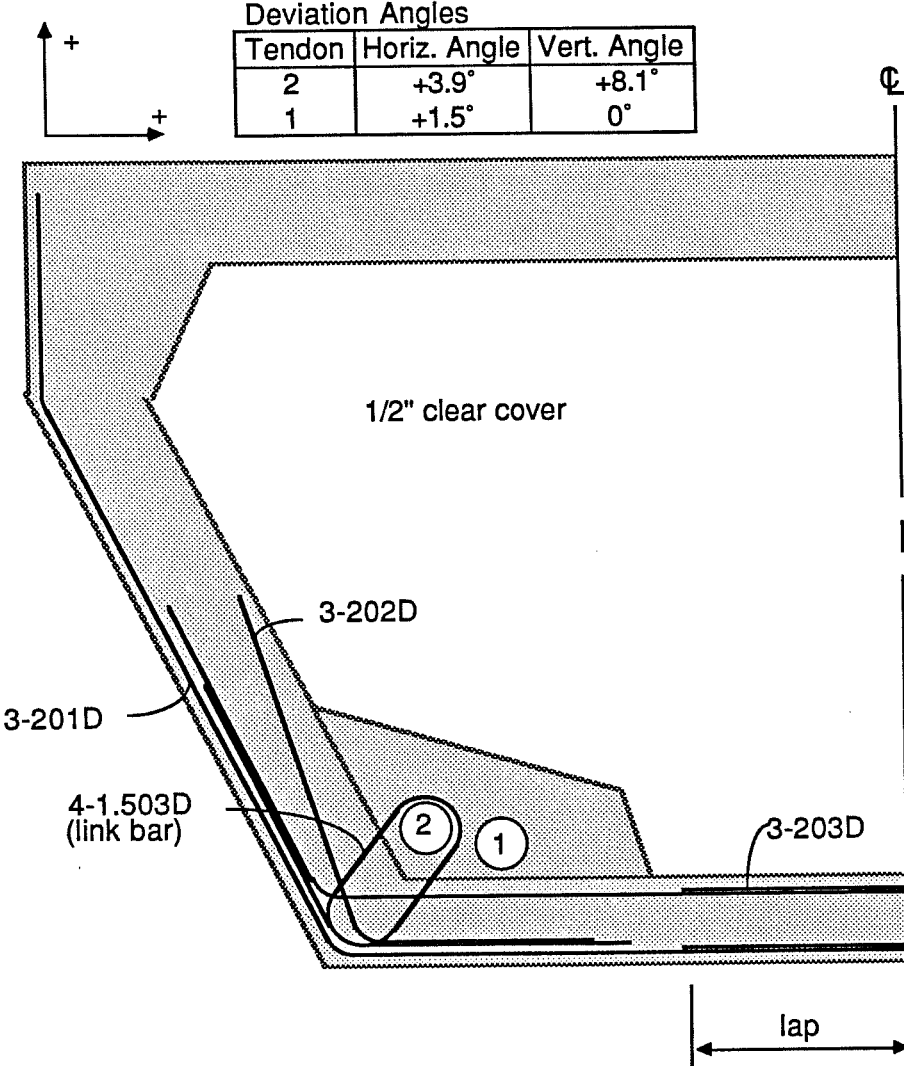


Figure 2.6a Specimen 2A

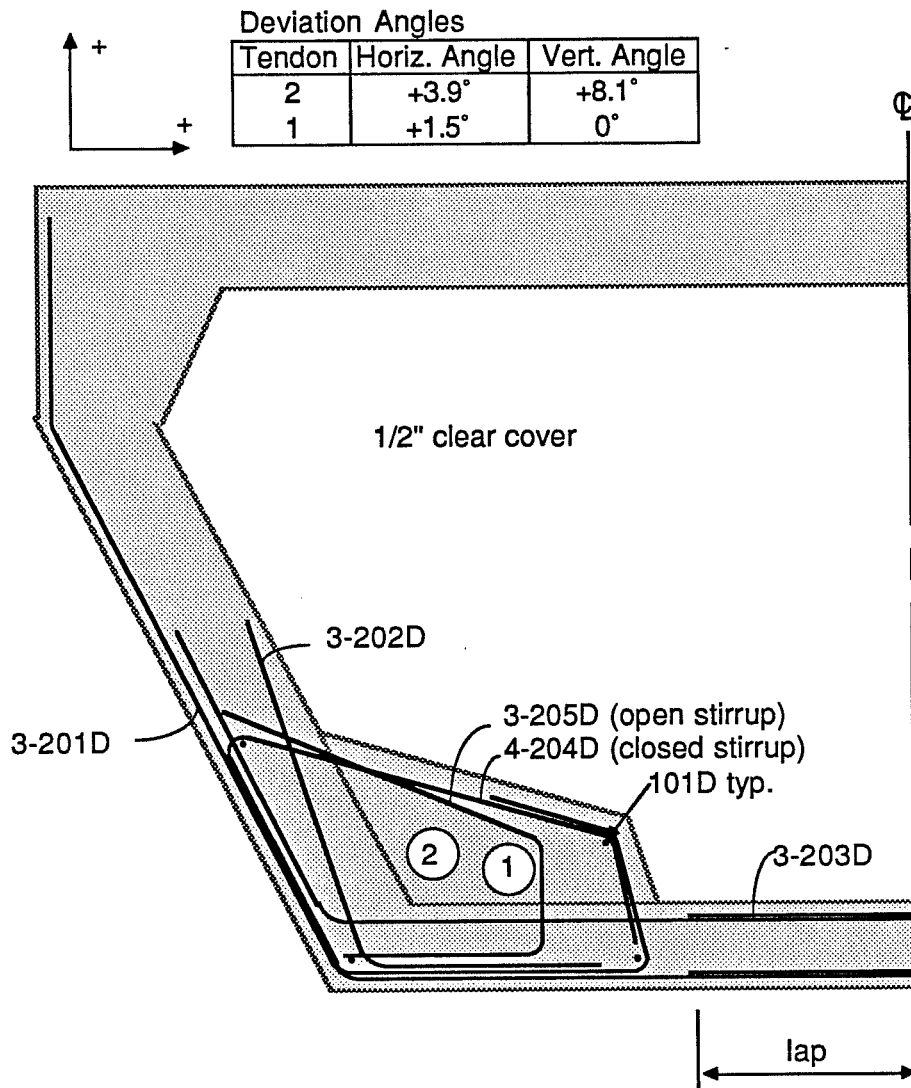


Figure 2.6b Specimen 2B

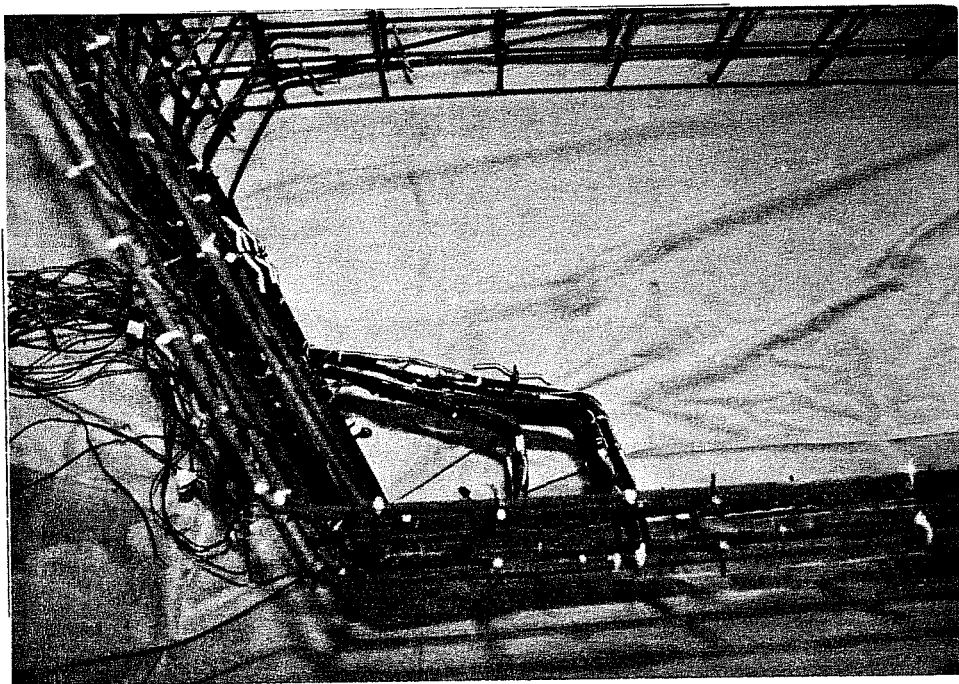
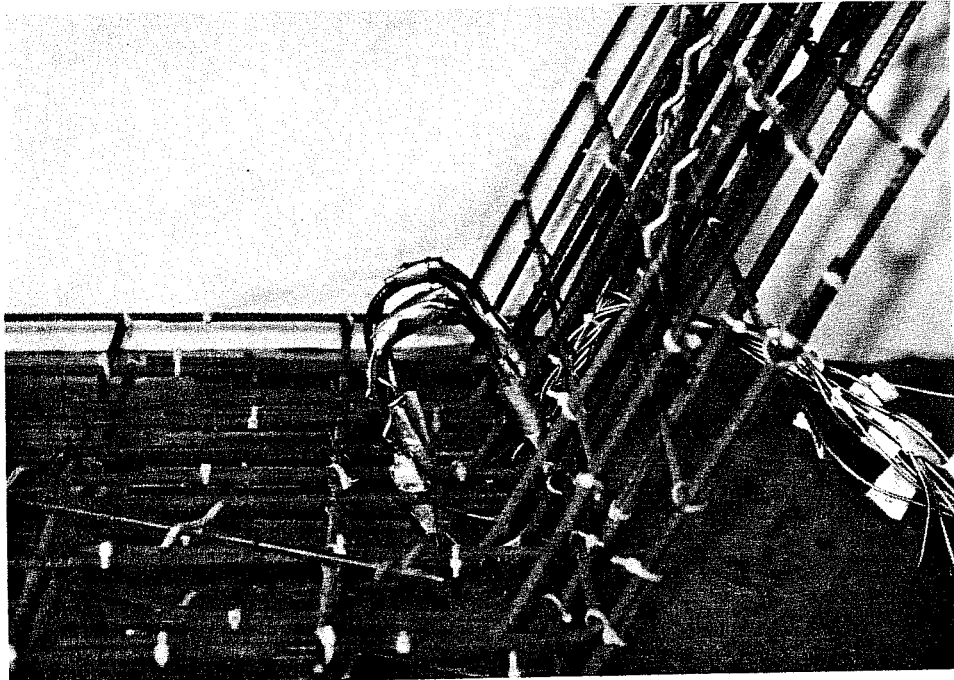


Figure 2.6c Specimens 2A and 2B Reinforcement Cage

2.2.3 Specimens 3A and 3B. The objective for specimens 3A and 3B was to determine if epoxy coated reinforcement has any effect on the behavior and the strength of a deviation saddle. Reproductions of specimens 1A and 1B were fabricated, except that the reinforcement was epoxy coated, and comparison tests of 1A and 1B were performed (Fig. 2.7).

2.2.4 Specimens 4A and 4B. The objective for specimens 4A and 4B was to evaluate some modified reinforcement details utilized in deviation diaphragms of curved bridges that are being built in San Antonio, Texas, but to utilize these reinforcement details in a deviation saddle. This was an attempt to simplify and standardize reinforcement patterns for typical deviation saddle details. The scale factor used for the models was 1/5. Refer to Fig. 2.8 for model dimensions. The reason for the smaller scale factor was to reduce post-tensioning forces required to fail the deviation saddle which were approaching test setup capacity on previous tests. Reinforcement was the same for both specimens 4A and 4B. Both specimens had two tendons, but had different tendon patterns. The geometry of the deviation saddle was also different than the previous specimens in an attempt to make fabrication easier. The deviation saddle had a horizontal top surface and vertical sides (see Fig. 2.8).

The deviation saddle reinforcement shown in Fig. 2.9a-c had two types of bar bend details. A separate inner loop (1.2501D) encloses each tendon similar to the link bar in the previous

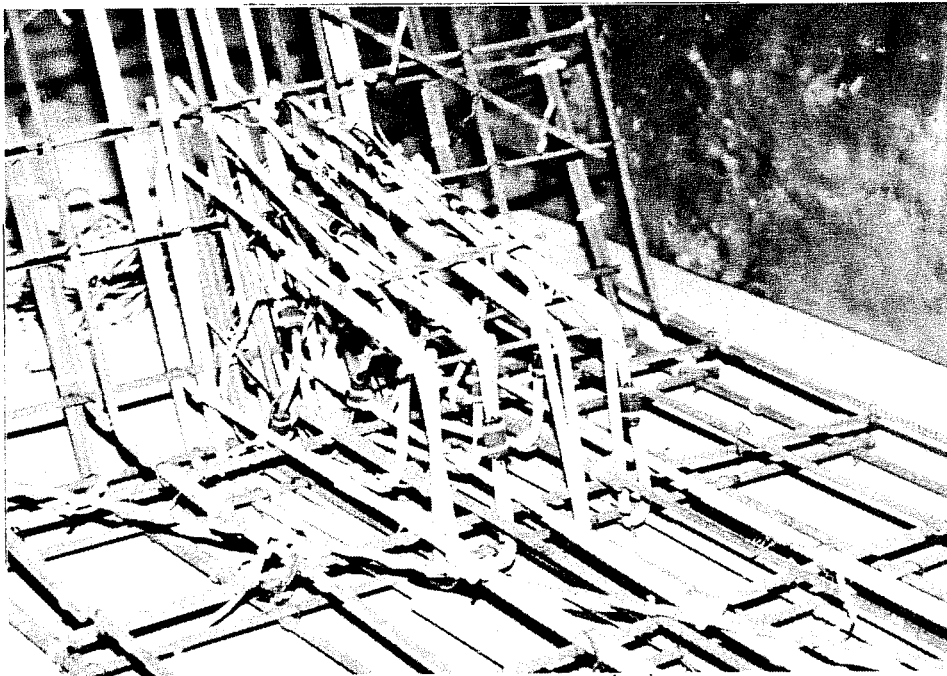
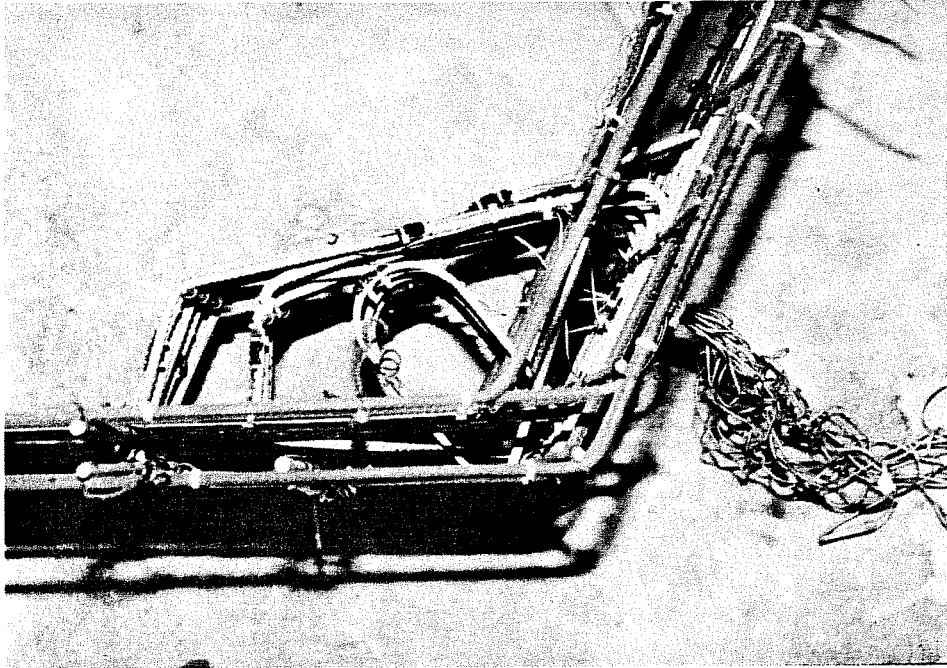


Figure 2.7 Specimens 3A and 3B Reinforcement Cage

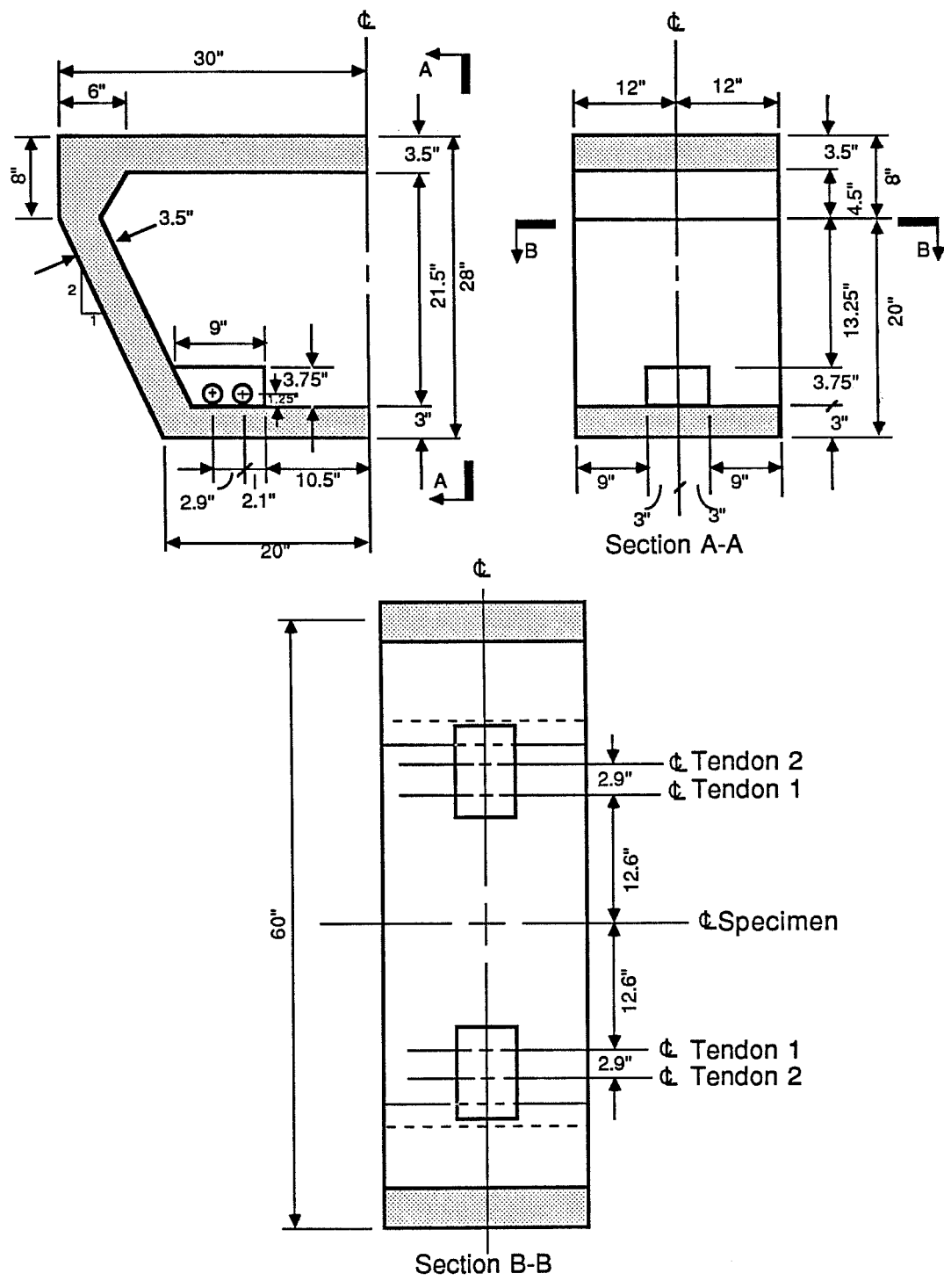


Figure 2.8 Specimens 4A, 4B, 5A, 5B Dimensions

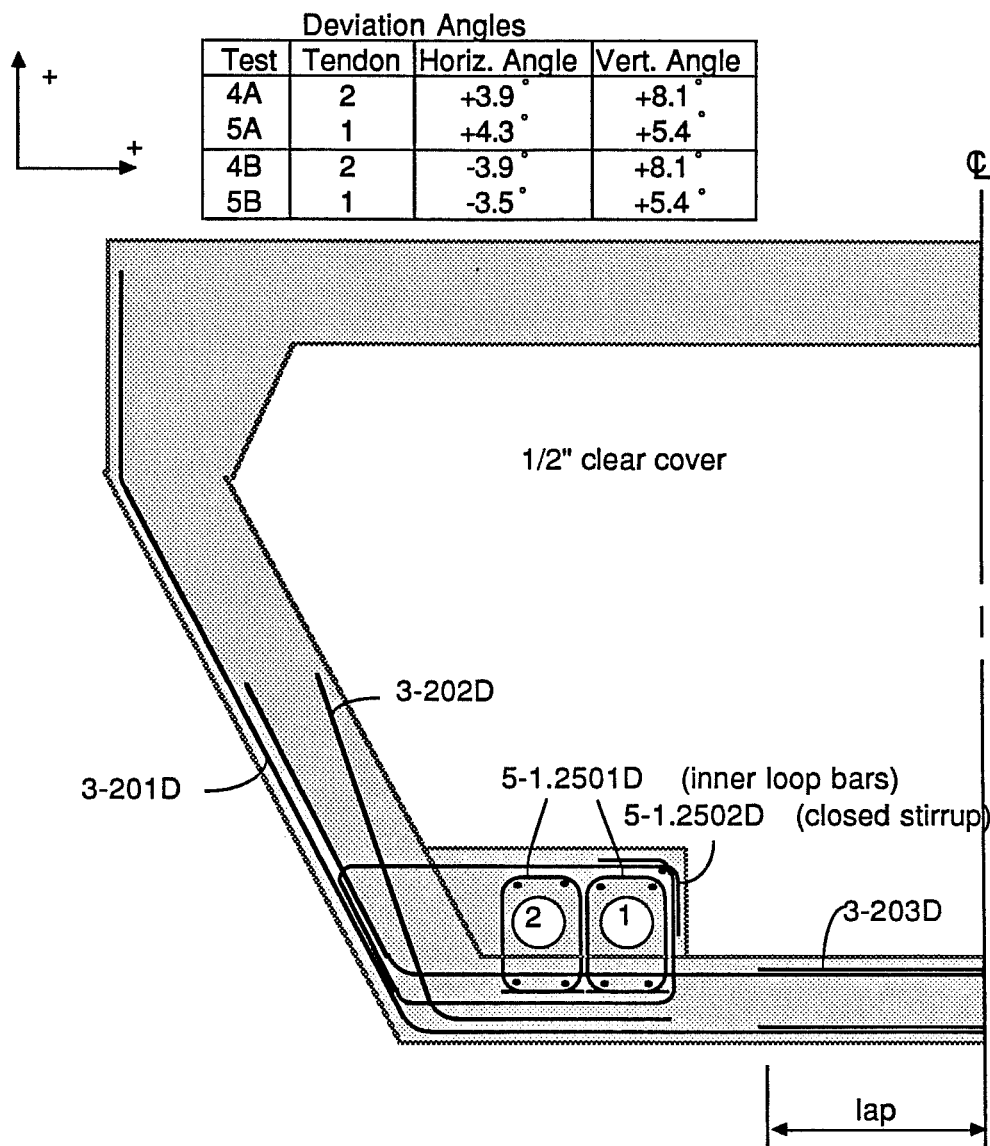


Figure 2.9a Specimens 4A, 4B, 5A, 5B

DEVIATOR REINFORCEMENT BENDING DIAGRAM

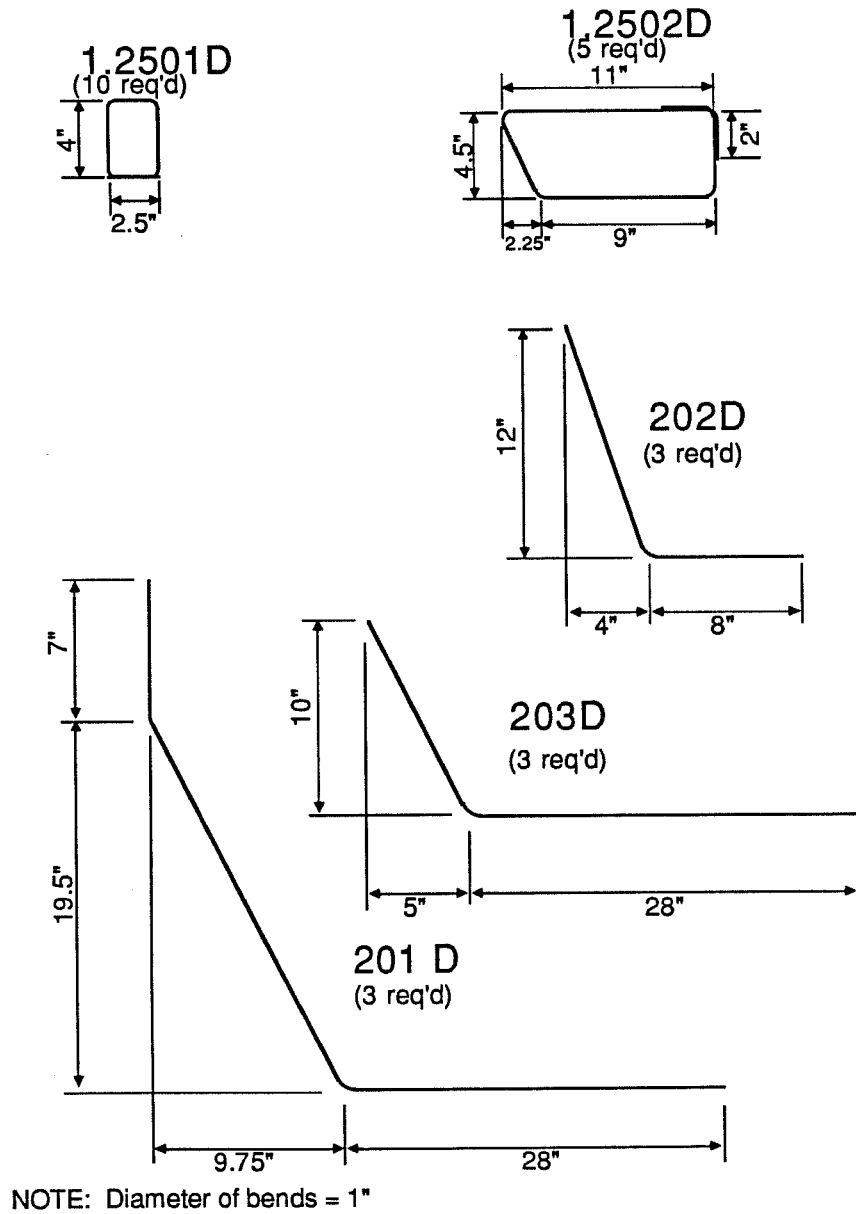


Figure 2.9b Deviator Reinforcement Bending Diagram
Specimens 4A, 4B, 5A, 5B

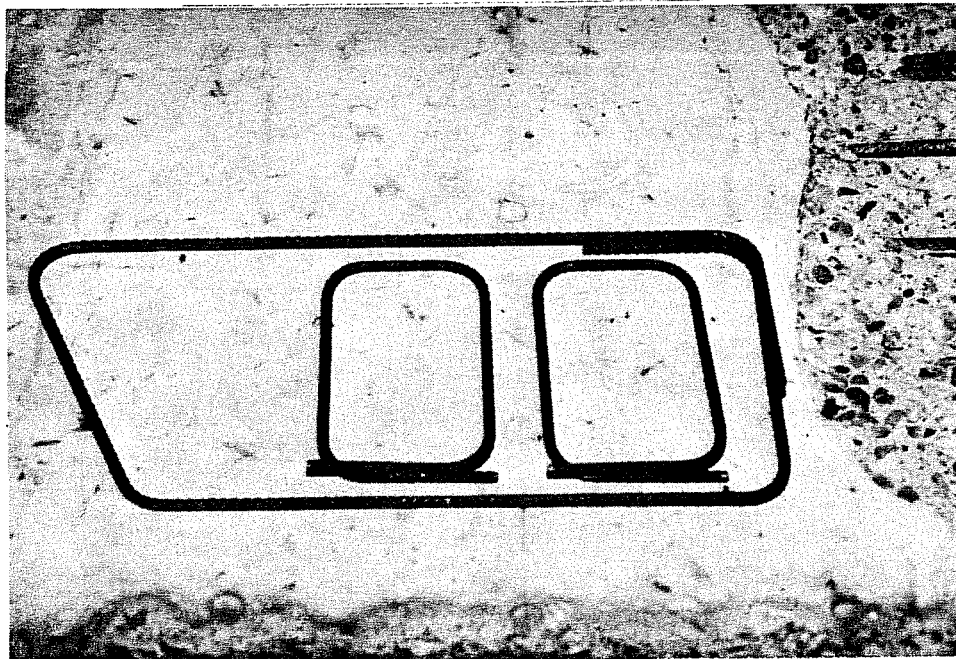
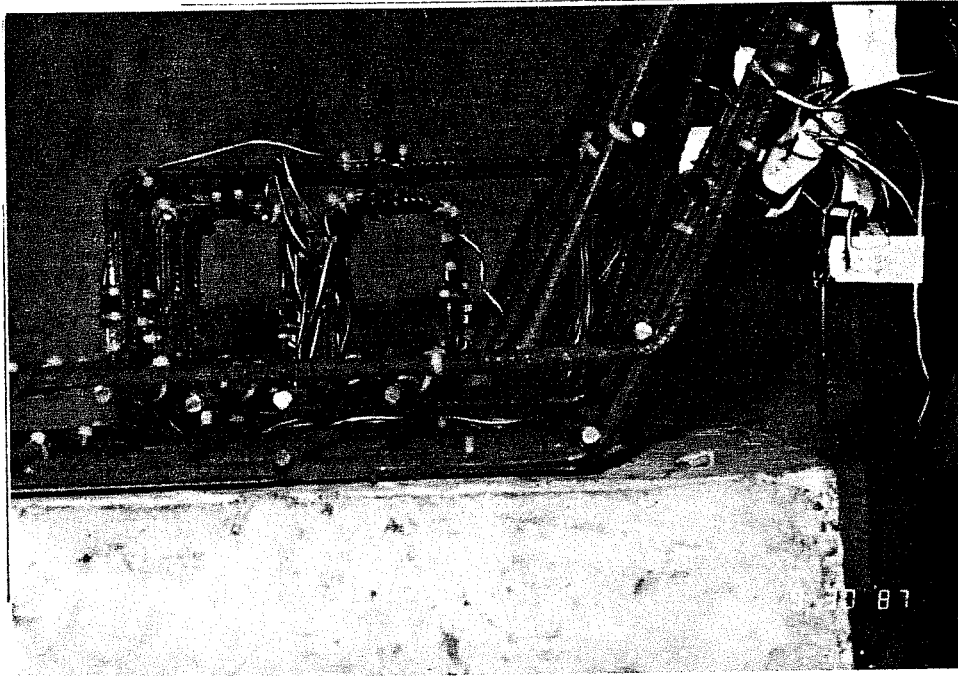


Figure 2.9c Specimens 4A and 4B Reinforcement Cage

specimens. These bars were anchored under the top mat of reinforcement of the bottom flange. The other type of reinforcement was a closed stirrup (1.2502D) which enclosed the entire deviation saddle. This bar was anchored under the top mat of reinforcement of the bottom flange and in the web wall (Fig.2.9a-c). Also, additional reinforcement was placed in the bottom flange and web similar to specimens 1A and 1B to provide local junction reinforcement (201D,202D,203D).

The tendon patterns for both specimens were based on a worst case scenario for a curved span in a highway bridge with a 250 foot radius of curvature and 110 foot span. Specimen 4A was representative of a deviation saddle located on the outside of the curve; whereas, specimen 4B was representative of a deviation saddle located on the inside of the curve. Also, it was assumed both tendons are vertically deviated. The vertical deviation for both tendons was the same for both specimens. See Fig. 2.9a for tendon deviation angles.

2.2.5 Specimens 5A and 5B. The objective for specimens 5A and 5B was to further evaluate the effect of epoxy coated reinforcement on the behavior and the strength of the deviation saddle. Reproductions of specimens 4A and 4B were fabricated except that the reinforcement was epoxy coated. Comparison tests of 4A and 4B were performed (Fig. 2.10).

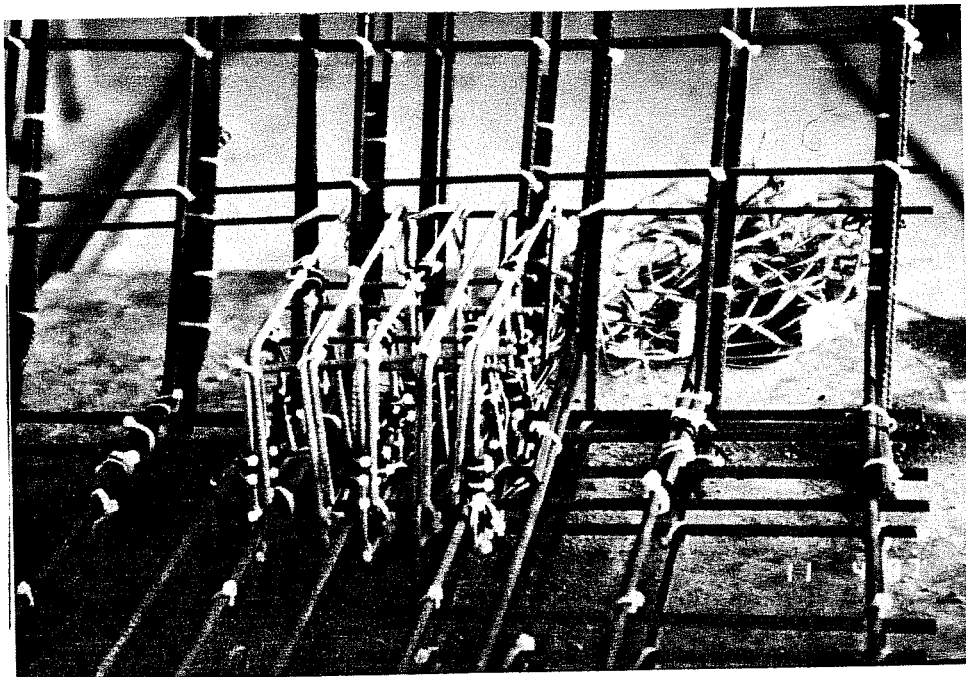
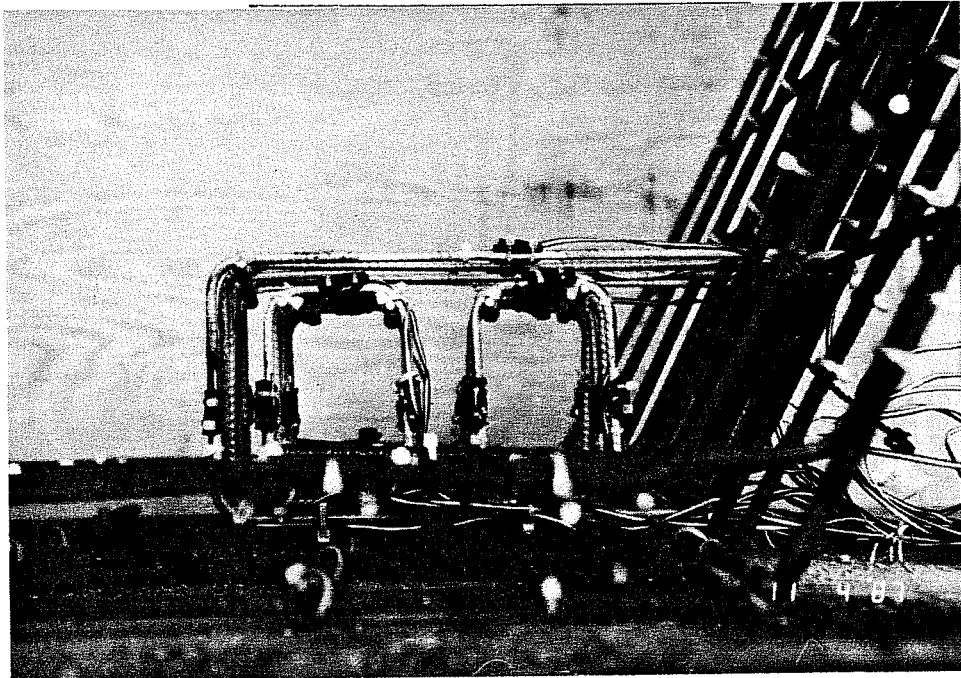


Figure 2.10 Specimens 5A and 5B Reinforcement Cage

2.3 Materials

A special attempt was made to ensure that all materials used for the test specimens modelled the basic properties used for the prototype structures.

2.3.1 Concrete. Concrete was delivered to the laboratory from a local ready-mix company. A 6000 psi mix was used which is typical of the strengths used on segmental bridge construction. The mix design was as follows:

	SSD lb/yd ³
Cement	611
Sand	1355
Aggregate	1680
Water	290

The mix was slightly different for specimen 1 because a different ready-mix company was used. A retarder was added to the mix since the ready-mix company was located at a great distance from the laboratory. The largest aggregate size used was 3/8 inch since minimum cover and bar spacing was 1/2 inch. The mix did not contain any fly ash, air-entrainments, or super-plasticizers. Some water was added to the mixes at time of the delivery for specimens 1 and 2 to increase the slump which ranged from 6 to 8 inches for specimens 2 to 5, and approximately 3 inches for specimen 1.

The concrete strength was measured by the standard strength test using 6 x 12 inch cylinders loaded at a rate of 35 psi per second

at the time of testing of the deviation saddles. The concrete strengths at testing were as follows:

	<u>Strength (psi)</u>
Test 1A	5650
Test 1B	5650
Test 2A	5700
Test 2B	5750
Test 3A	6000
Test 3B	5800
Test 4A	5700
Test 4B	5700
Test 5A	5400
Test 5B	5400

All cylinders were cured in the same manner as the test specimen.

2.3.2 Reinforcing Steel. The reinforcement used in typical prototype deviation saddles are generally deformed #4 or #5 bars. For the modelling of the deviation saddles it was preferred to use the same number of reinforcing bars as the prototype, and since the scaling factors for the deviation saddles were $1/3$ and $1/5$, it was necessary to use deformed microreinforcing bars. The microreinforcing bars range in sizes #1.25, #1.5, and #2. The sizes are referred to by their nominal diameter expressed in eighths of an inch to correspond to the ASTM standard reinforcing bar designation.

When originally tested the sample bars did not display a well-defined yield plateau, so they were heat treated to more correctly represent reinforcing bar ductility. The heat treatment included the following steps:

- 1) Cut bars into 94 in. lengths
- 2) Subcritical anneal at 1150°F for one hour
- 3) Remove bars, turn end for end, and repeat step 2
- 4) Air cool

From averages of reinforcement strength tests for sizes #1.5 and #2, the yield stress was 45 ksi and the ultimate stress was 63 ksi. This resulted in a yield strain of 1550 micro inches/inch. The size #1.25 had an average yield stress of 36 ksi and an average ultimate stress of 51 ksi. This resulted in a yield strain of 1240 micro inches/inch.

2.3.3 Epoxy Coating. For the specimens with the epoxy coated reinforcement, the bars were bent and then sent to an epoxy coating company. The coating was done by a method of dipping the bars in a tank of epoxy. The target coating thickness was 3 mils, and the measured coating thickness was 7 mils. This discrepancy was due to the method of coating since it is difficult to control the thickness. A method of coating which utilizes an electro-static sprayer is more accurate, but could not be done because the bars were already bent. Only the bars that were placed in the deviation saddle were coated since only the immediate deviation saddle zone was of interest.

2.3.4 Ducts. The typical duct used in prototype deviation saddles is a rigid duct that is bent for the required deviation angles. To model this, 1-1/2 inch nominal diameter electrical conduit was bent with an hydraulic pipe bender for the required deviation angles of the test specimen.

2.3.5 Tendons. The typical strand size used in post-tensioned segmental bridges is 0.6 inch diameter. In the deviation saddle tests, 3/8 inch diameter was mostly used, but in some tests when more area of tendons was required, 1/2 inch diameter was used to replace some of the 3/8 inch strand. For the sake of modelling, it does not matter because the only concern is to provide sufficient total tendon area to ensure suitable forces on the deviators.

2.4 Construction and Formwork

The reinforcement cage was assembled from microreinforcing bars bent to their correct configuration (Fig. 2.11).

The formwork for the box section was reusable, and the formwork for the deviation saddle was constructed for each specimen. The formwork for the box section consisted of eight pieces which were covered with sheet metal to facilitate reuse. The formwork was assembled around the reinforcement cage. The specimen was cast on its side to simplify forming. The box section formwork was fastened to the formwork base with lag bolts, and the deviation saddle formwork was fastened to the box formwork with brackets and screws. The deviation saddle formwork facilitated an opening which was utilized for placement of the concrete, and then was subsequently closed after the deviation saddle was full. All formwork joints were sealed with silicone to prevent leakage of mortar (Fig. 2.12).

The concrete was placed in the formwork by shovel. The concrete was thoroughly consolidated, worked around reinforcement and

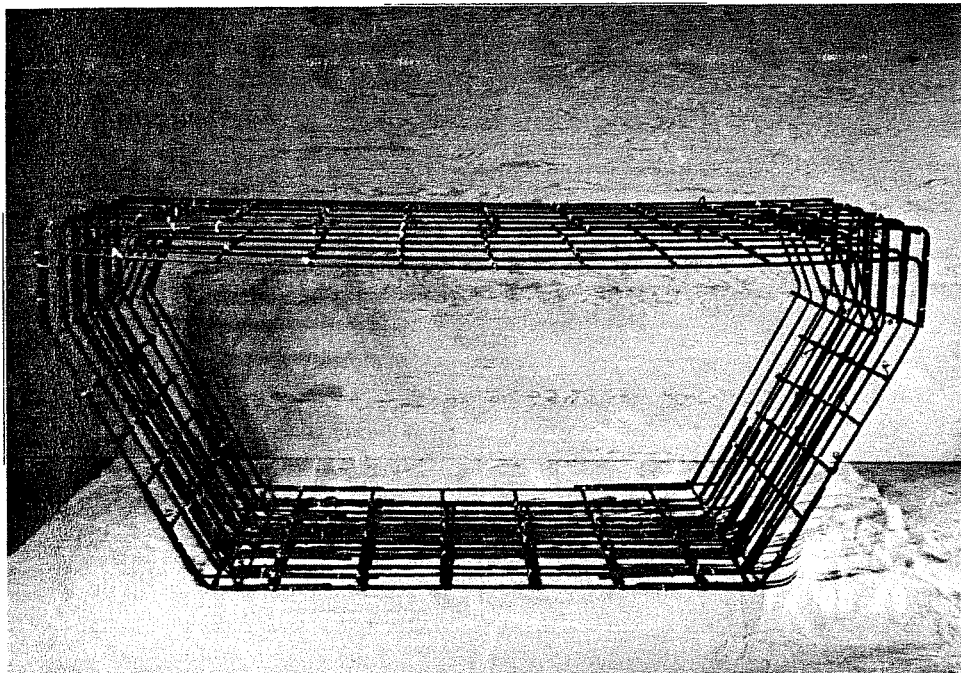
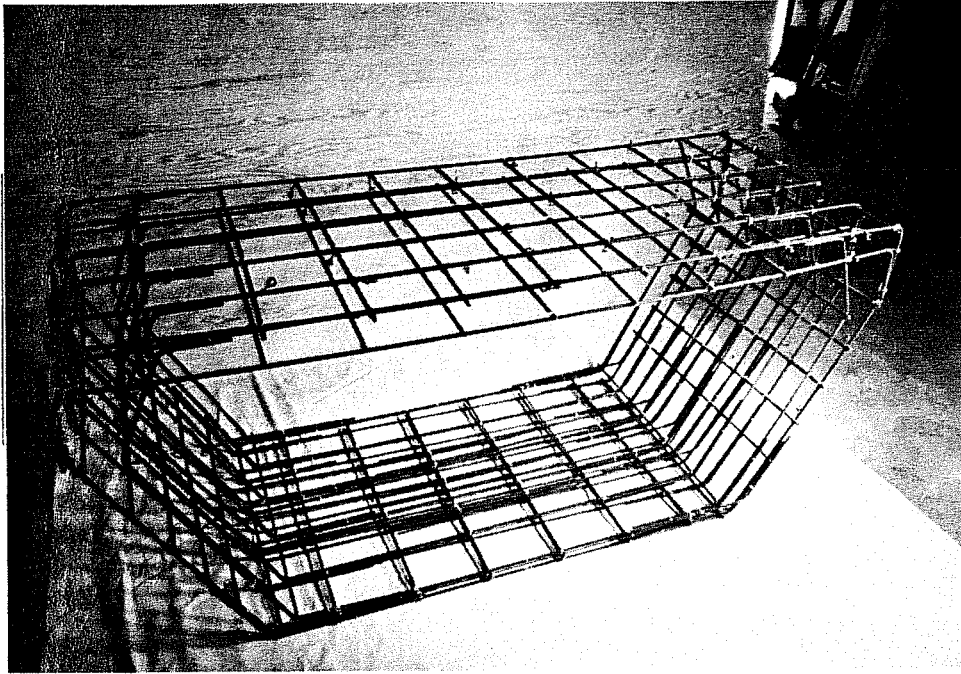


Figure 2.11 Box Reinforcement Cage

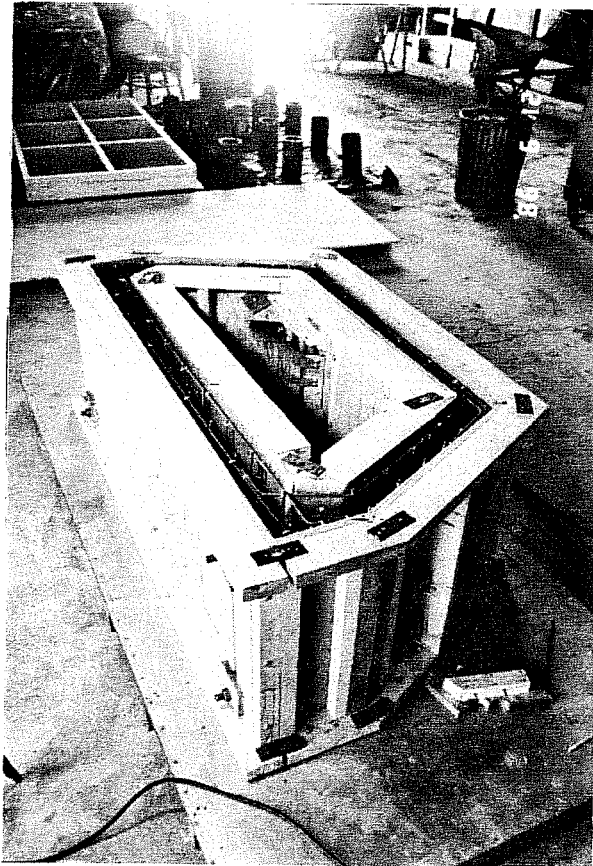


Figure 2.12 Formwork

into corners of formwork. The forms were normally stripped the next day, and moist cured with burlap and plastic for several days.

2.5 Test Setup

In comparison with the size of the test specimens, the size of the test setup was substantial because of the large post-tensioning forces which were necessary to fail the test specimens (Fig. 2.13). The tendons were anchored at lever frames located at opposite ends of the test setup. The lever frames were pinned at their base and bore on hydraulic rams at their top. The lever frames were adaptable to many tendon patterns which facilitated study of different types of deviation saddles. The basic concept for the design of the setup was to load the deviator just as it would be loaded in a bridge. This was accomplished by loading the tendons to some low initial stress with a stressing ram, and then by moving out the lever frames, continue loading the tendons to failure of the deviation saddle (Fig. 2.14a-c). For an in-depth description of the components of the test setup, refer to Carter (1).

The test setup facilitated the determination of the individual tendon forces by several methods. In any case, it was possible to determine the total force of all the tendons because the tendons were anchored vertically in the center of the lever frame at the north end of the test setup, so that the total tendon force was twice the force in the hydraulic rams at the top of the frame. In the case of a test with two tendons, it was possible by knowing the

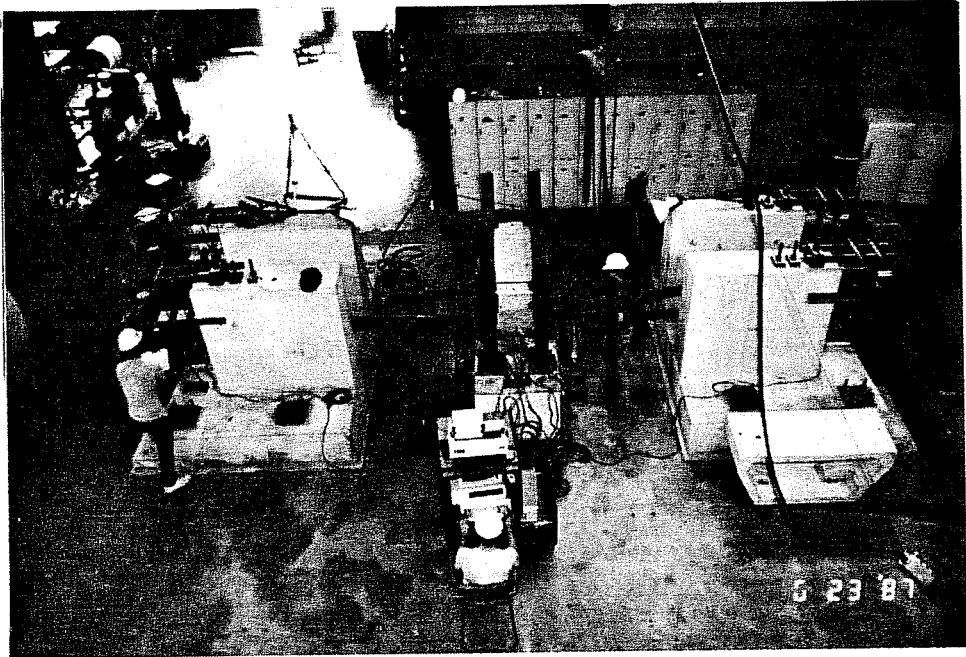
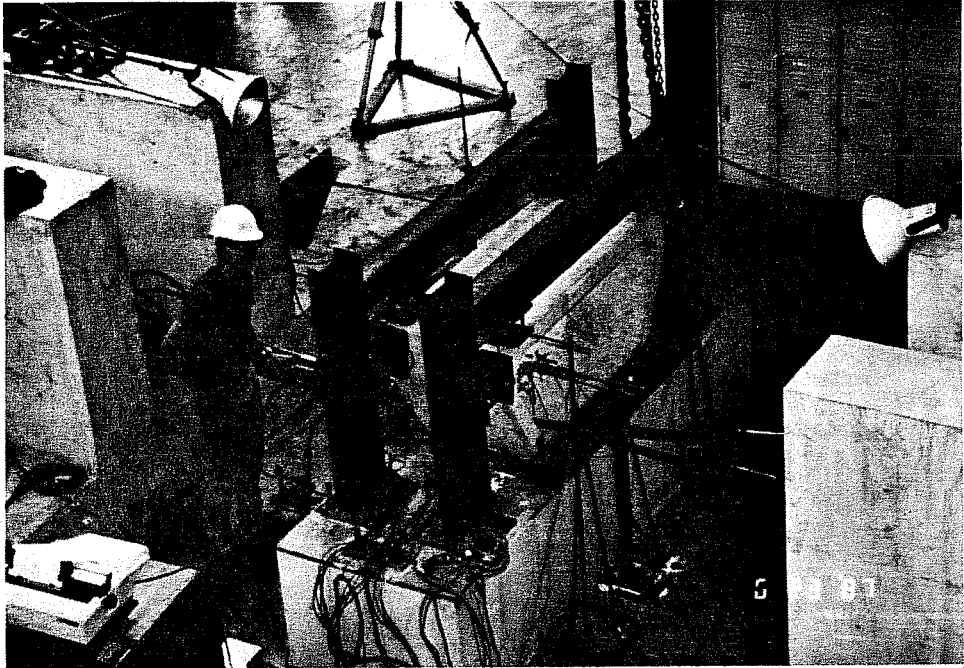


Figure 2.13 Test Setup

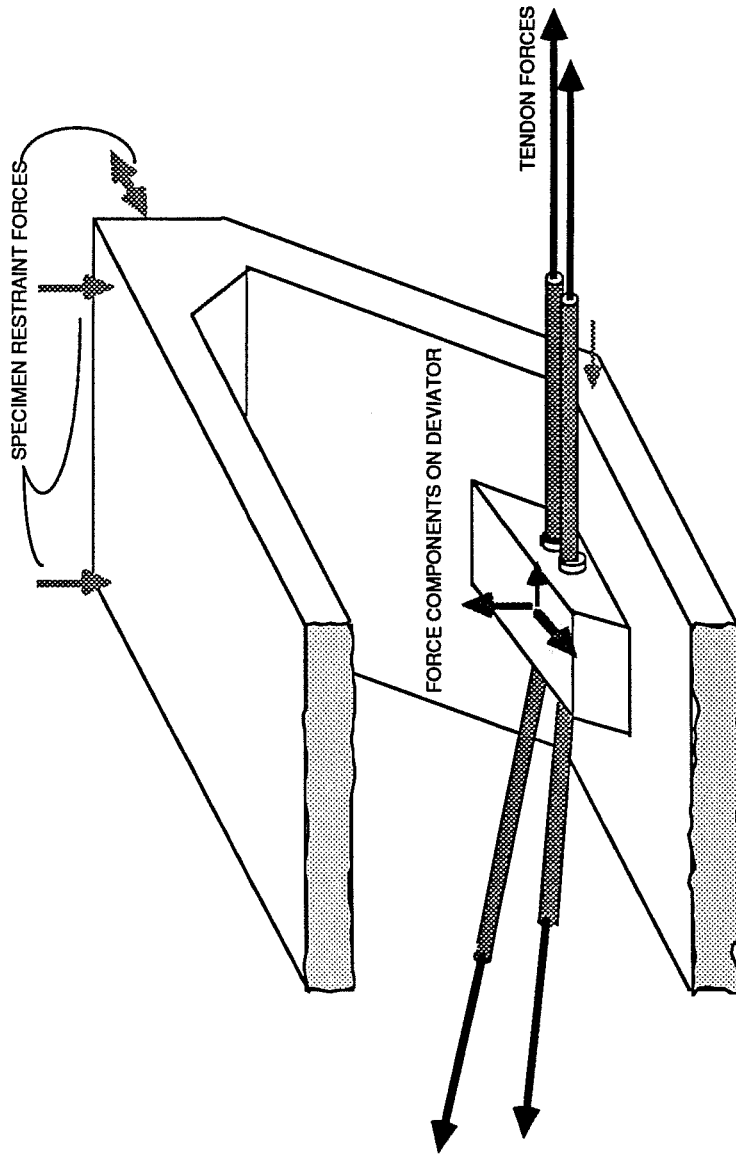


Figure 2.14a Testing Concept (From Ref. 1)

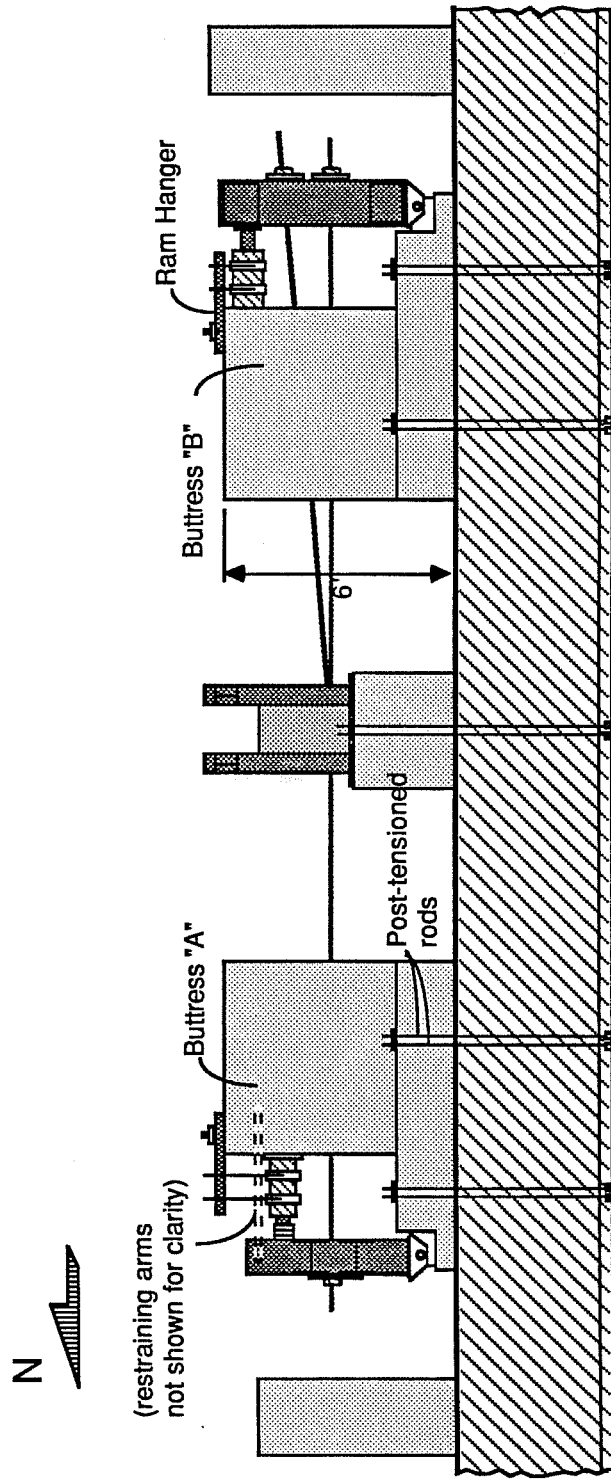


Figure 2.14b Test Setup, Elevation (From Ref. 1)

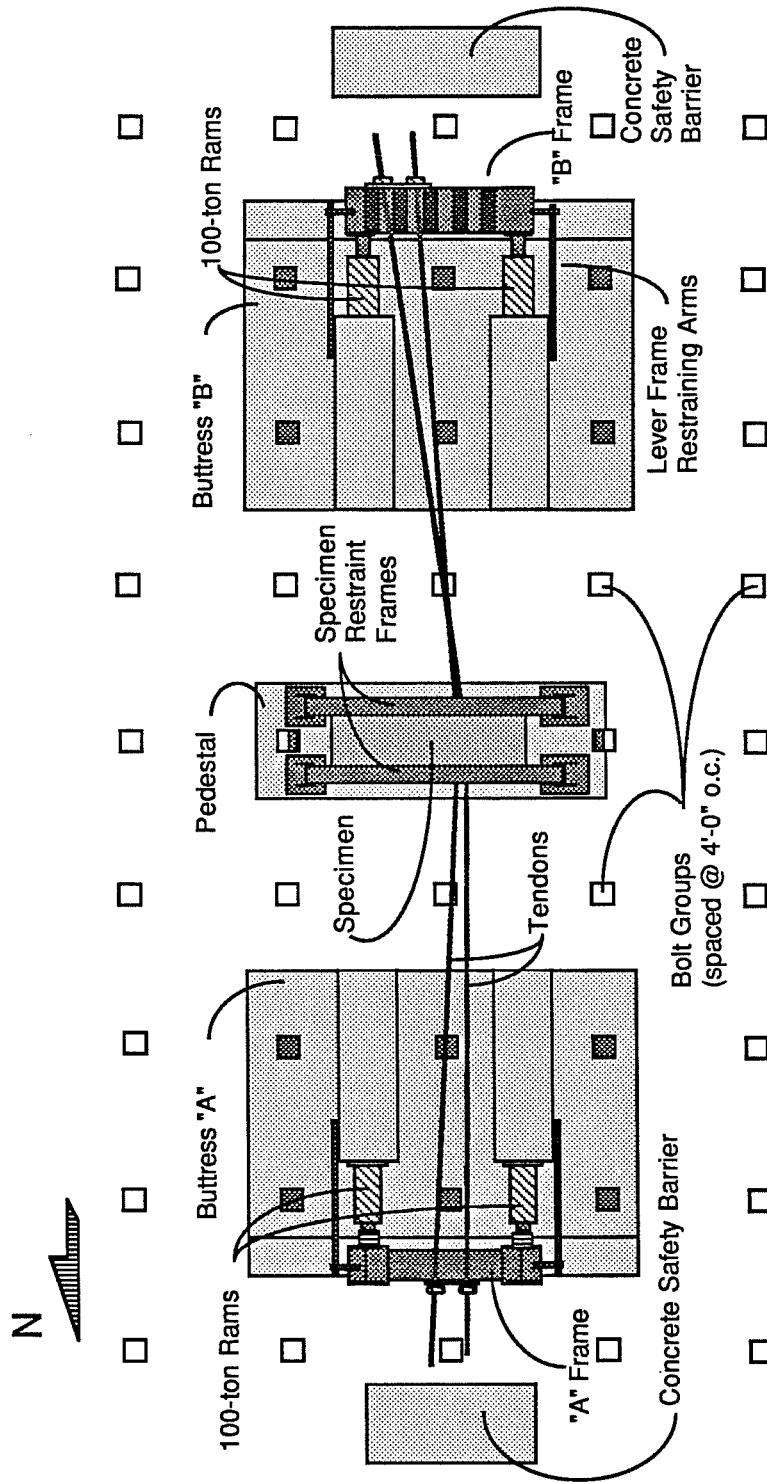


Figure 2.14c Test Setup, Plan (From Ref. 1)

force in the rams at the top of the lever frame and the location of the tendon anchorages on the frame to determine by static equilibrium the force in each tendon. In the case of a test with three tendons, the total force was known by the method stated above, and individual forces could be determined by the ratio of the strain gages placed on the individual tendons. Other possibilities for tendon force calculations were to determine forces from elongation measurements taken during the movement of the frame and add this stress to the initial stress of the tendons, or to assume that the initial stress in each tendon was approximately equal, and divide the load according to the tendon area.

2.6 Instrumentation

Strain gages were utilized for two different purposes in the testing of the deviation saddles. Strain gages were placed internally on the reinforcement of the deviation saddle to attempt to determine contributions of individual reinforcement bars. Refer to Fig. 2.15a-d for gage locations and designations. Strain gages were also placed externally on the tendons to monitor the stress in the individual tendons. The type of strain gages used were from Micro-Measurements, gage type EA-06-062AP-120.

Potentiometers and dial gages were utilized in the test to monitor the movement of the test specimen and also to attempt to determine the relative movement of the deviation saddle with respect to the box section. Refer to Carter (1) for general setup of

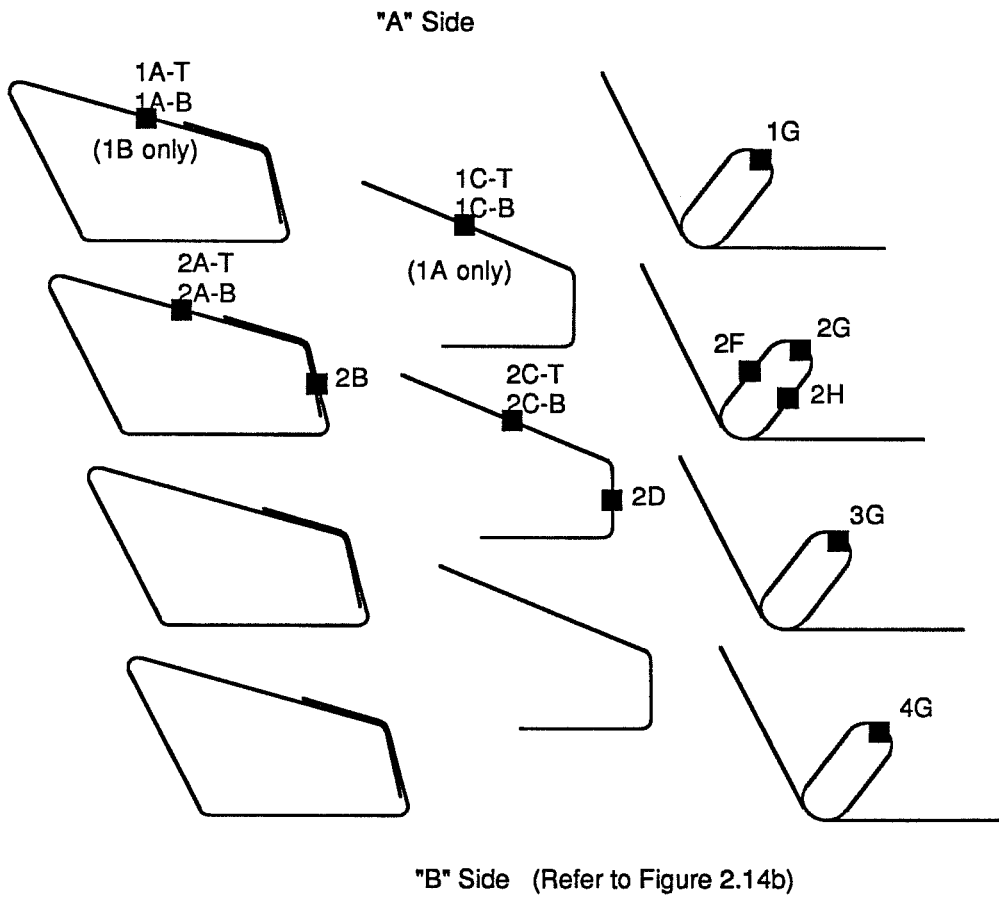


Figure 2.15a Strain Gage Locations on Deviation Saddle Reinforcement Specimens 1A, 1B

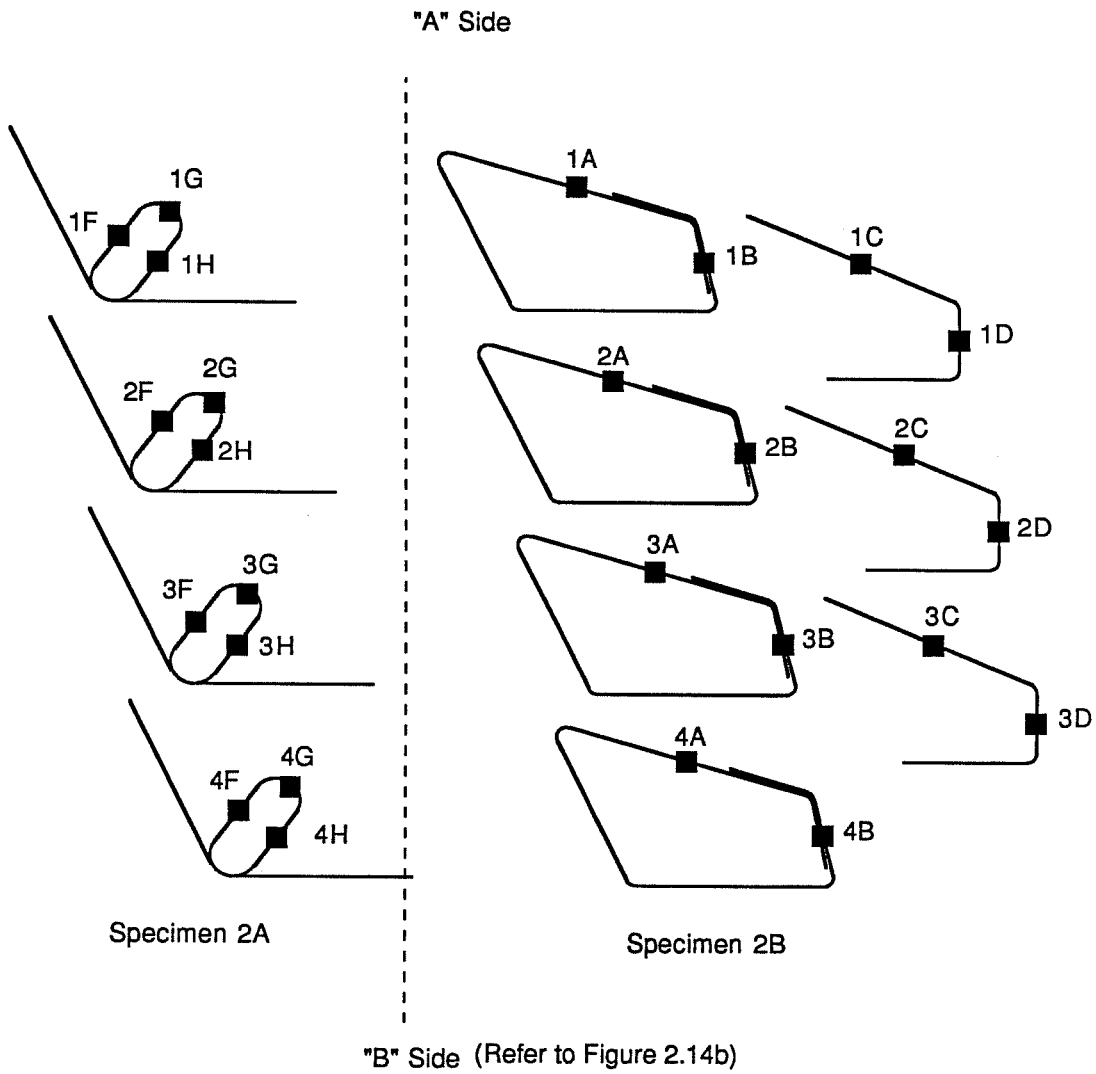


Figure 2.15b Strain Gage Locations on Deviation Saddle Reinforcement Specimens 2A, 2B

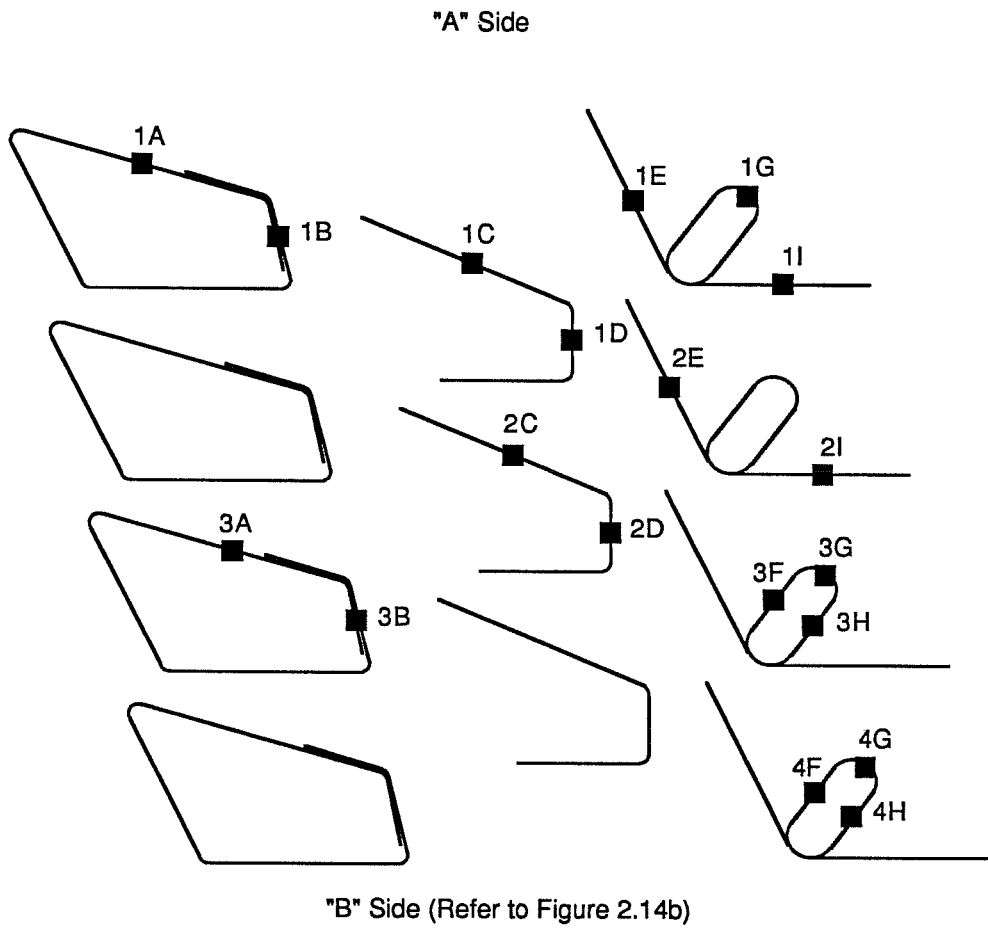


Figure 2.15c Strain Gage Locations on Deviation Saddle Reinforcement Specimens 3A, 3B

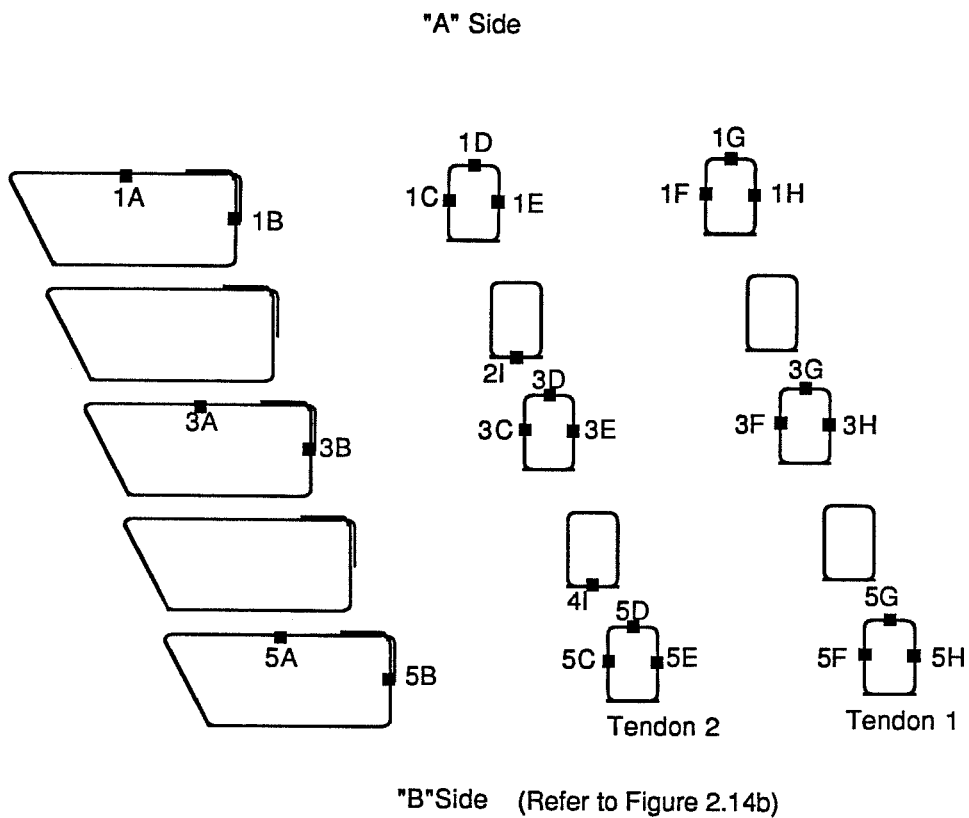


Figure 2.15d Strain Gage Locations on Deviation Saddle Reinforcement Specimens 4A, 4B, 5A, 5B

potentiometers and dial gages. For the latter purpose, the instrumentation was not very effective because it had to be removed before failure of the deviation saddle to prevent it from being damaged. For the most part, large deformations did not occur until the last few load stages if at all. Potentiometers were also located at the lever frames to measure elongations during the load stages.

Pressure transducers were utilized to determine the force in the hydraulic rams at the lever frame which in turn gives the force in the tendons.

A personal computer (IBM XT or Hewlett Packard Vectra), an electronic scanner (Hewlett Packard), and a 2-volt and 10-volt power supply were utilized to compile the electronic data of the strain gages, potentiometers, and pressure transducers. An in-house computer program converted this raw voltage data to corresponding engineering units which was then compiled into spreadsheet form for data reduction and analysis.

2.7 Data Reduction

There were no special considerations here, although, it was important to get accurate calibrations for the ram pressure transducers and hydraulic rams since slight inaccuracy in the ratio of the ram areas would cause an artificial imbalance in the tendon stresses.

2.8 Test Procedure

The testing procedure involved the following steps:

1) Individual stressing of each tendon to some low initial stress so as to not induce internal cracking of the deviation saddle.

2) Increasing the load on the deviation saddle by moving out the lever frame at the north end of the test setup in a controlled deformation mode. Increments were usually an amount of 0.1 inch at the location of the hydraulic rams. The loading to failure of the deviation saddle was generally completed in two stages. The first stage was ended when it was apparent from the strain gages that some of reinforcement had reached yield, and there was some visible surface cracking.

3) Unloading the deviation saddle to its initial starting tendon stress by moving in the lever frame. This is done by utilizing hydraulic needle valves to bleed off the load in the hydraulic rams at the top of the lever frame. If it was apparent that the deviation saddle would require higher forces to fail than was initially anticipated and if the movement of the lever frame that was just unloaded would not have enough extension, the lever frame at the opposite end would be extended out before starting phase two. This would enable the tendons to be at a higher stress at the start of the next phase.

4) Increasing the load in all tendons as in step 2, but proceeding to failure of the deviation saddle. In some of the tests,

it was not possible to fail the deviation saddle because of an inadequate amount of tendon area, so it was necessary to abort the test and start over with a greater amount of tendon area. Test 1B procedure was slightly different, but the above intended outcome was attained (1).

CHAPTER 3 TEST RESULTS

3.1 Introduction

In the following presentation of test results, a detailed summary of the observed physical behavior of each specimen will be presented and specific conclusions will be made about the behavior of the deviation saddles subjected to a full range of loadings. In the next chapter, these results will be integrated with analysis methods to determine deviation saddle strength. Comments will be made about observed strength and ductility for the different deviation saddle details and tendon configurations discussed in Chapter 2. Comparisons will also be made between the epoxy coated and uncoated reinforcement.

For each test, the following test results are presented in figures:

- 1) Total tendon vector force and direction acting on the deviation saddle from phase 1 to the highest load stage before failure are presented in a time history graph. In a few tests, which had an insufficient amount of tendon area at the beginning of the test to fail the specimen and hence had to be stopped and the tendon area increased, these data are presented in two separate figures, one for phase 1 and the other for phase 2. The prototype nominal design jacking load reference force, D_0 , and direction, θ_0 , which will be discussed later for the strength comparisons are plotted on these graphs. In tests 1B, 2A, 2B, and 3B, the prototype direction differs

from that of the applied loading direction by a small amount because of limitations of the available angles of the testing apparatus. Also, a difference in stress amongst the tendons will also cause the applied loading direction to be slightly different from the prototype direction. However, for the evaluation of the prototype deviation saddle detail, these small differences in direction have an insignificant effect.

2) Crack patterns for each individual test are given. The cracks were marked on the specimen in the early stages of testing when it was felt that it was safe to be near the specimen. The cracks were then mapped on scaled drawings. The deviation saddle was monitored at a distance during later stages of testing for safety reasons.

3) Strain gage data for each phase of the test are presented in graph form with total vector force plotted on the vertical axis and strain plotted on the horizontal axis. To reduce the large quantity of strain data, averages of the strain gages across the deviation saddle at the same location on the same pattern were used. Figures 2.15a-d shows the location of individual strain gages. In some cases, only one gage was available for a particular location. The maximum number of different strain gage locations within the deviation saddle was nine. The averages appeared to be a reliable indicator of the individual behavior of the different reinforcement patterns. There was some variation in corresponding strain gages across the deviation saddle.

In some tests, the strain was higher on the "A" side than the "B" side. In others, the reverse occurred which was probably due to placement or curvature of the ducts such that the tendon would bear more on one side of the deviation saddle than on the other. However, no tendon kinked at the face of the deviation saddle and no cover was spalled at the duct openings.

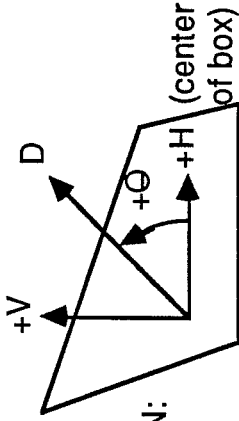
Inset diagrams show the locations of the strain gages on the reinforcement. Another inset diagram shows the forces with relative magnitudes which acted on the deviation saddle. All graphs show the nominal design jacking load reference force, D_0 , which will be discussed later for the strength comparisons. All graphs except phase 1 and phase 1(a) show the ultimate force, D_{ult} , since some strain gages failed before the ultimate state was reached. This was typical in very ductile specimens. The graphs also show the yield strain of the reinforcement.

4) Reinforcement failure locations are noted in a figure. Failures of the reinforcement are classified as fracture of the bar, failure of the lap splice, or pullout of the bar.

5) Photographs before and after failure are shown.

6) Strength comparisons for the critical stages of the test are presented in a bar graph. The symbol D is the total vector force acting on the deviation saddle, and the symbol θ is the total vector force direction. The sign convention is as shown in Figs. 3.1a-b. The positive horizontal axis is directed towards the center of the box.

PROTOTYPE DEVIATION ANGLES/FORCES



SIGN CONVENTION:

Specimens 1A,3A

TENDON	Aps	.8fpuAps/9	HORIZONTAL		VERTICAL	
			dev. angle	force	dev. angle	force
1	1.836 sq.in.	44.06 kips	-3.68°	-2.83 kips	0	0
2	2.907 sq.in.	69.77 kips	-3.68°	-4.48 kips	0	0
3	2.907 sq.in.	69.77 kips	+0.82°	+1.00 kips	+6.41°	7.79 kips

$V_o = 7.79$ kips
 $H_o = -6.31$ kips
 $D_o = 10.02$ kips
 $\Theta_o = 129.01^\circ$

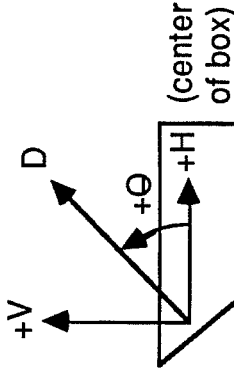
Specimens 1B,2A,2B,3B

TENDON	Aps	.8fpuAps/9	HORIZONTAL		VERTICAL	
			dev. angle	force	dev. angle	force
1	1.836 sq.in.	44.06 kips	+1.84°	+1.41 kips	0	0
2	2.907 sq.in.	69.77 kips	+2.93°	+3.57 kips	+8.22°	9.98 kips

$V_o = 9.98$ kips
 $H_o = 4.98$ kips
 $D_o = 11.15$ kips
 $\Theta_o = 63.48^\circ$

Figure 3.1a Prototype Deviation Angles and Forces (From Ref. 1)

PROTOTYPE DEVIATION ANGLES/FORCES



SIGN CONVENTION:

Specimens 4A,5A

TENDON	Aps	.8fpuAps/25	HORIZONTAL		VERTICAL	
			dev. angle	force	dev. angle	force
1	4.09 sq.in.	35.34 kips	+4.3°	+2.65 kips	+5.4°	3.33 kips
2	4.09 sq.in.	35.34 kips	+3.9°	+2.40 kips	+8.1°	4.98 kips

$V_o = +8.31$ kips
 $H_o = +5.05$ kips
 $D_o = +9.72$ kips
 $\theta_o = 58.71^\circ$

Specimens 4B,5B

TENDON	Aps	.8fpuAps/25	HORIZONTAL		VERTICAL	
			dev. angle	force	dev. angle	force
1	4.09 sq.in.	35.34 kips	-3.5°	-2.16 kips	+5.4°	3.33 kips
2	4.09 sq.in.	35.34 kips	-3.9°	-2.40 kips	+8.1°	4.98 kips

$V_o = +8.31$ kips
 $H_o = -4.56$ kips
 $D_o = +9.48$ kips
 $\theta_o = 118.76^\circ$

Figure 3.1b Prototype Deviation Angles and Forces

The symbol D_0 is the nominal design reference force for the specimen and is the reduced scale total maximum allowable vector force of the prototype tendons. Overload of the structure was not considered in the determination of the maximum allowable tendon force. The maximum allowable tendon force is the allowable initial jacking force which is 80% of the ultimate strength of the tendon ($0.8(f_{pu})(A_{ps})$). The symbol θ_0 is the prototype nominal jacking load vector force direction. Figures 3.1a-b give D_0 and θ_0 for all tests as well as the horizontal and vertical components of D_0 (H_0 and V_0).

The bar graphs in each section show the ratio D/D_0 plotted on the vertical axis and the critical stages plotted on the horizontal axis. If the ratio D/D_0 is greater than 1, it means that the critical stage would not occur under service dead load plus jacking load conditions. The ratio D/D_0 is equal to the deviation saddle factor of safety. The critical stages occur at microcracking, visible cracking, yield, and ultimate. Microcracking occurs at the first apparent jump in strain indicated by the strain gages. Visible cracking was noted when the first crack appeared. In some tests, these two stages occurred simultaneously. Yield of the reinforcement was noted when the strain from any of the strain gages reached the yield strain. Ultimate capacity was apparent due to the explosive nature of the failure. In some tests, the last load stage did not correspond to the maximum load since there were progressive stages of failure before the concrete broke up and the reinforcement was exposed.

The results for test 1A and test 1B were presented by Carter (1) but will be presented here again to facilitate correlations with the other tests.

3.2 Test 1A-Uncoated Link Bar with Stirrups-Straight Span-Three Tendons

Specimen 1A was a typical prototype deviation saddle detail from a straight span bridge. The reinforcement scheme was a link bar with two stirrups. This detail is discussed in Sec. 2.2.1 and is illustrated in Fig. 2.4a. Three tendons were deviated which represented a tendon configuration of a deviation saddle located closest to the center of a span (see Fig. 2.5). The corner tendon had both a vertical deviation and a slight horizontal deviation directed away from the web, and the other two tendons had just horizontal deviation directed towards the web.

The total vector force and direction which acted on the specimen are shown in Fig 3.2. The crack patterns are shown in Fig. 3.3. The first crack to form was on the side face of the deviation saddle. It appears that initial cracking was influenced by the large horizontal force of tendons 1 and 2 and was possibly a splitting crack due to the high compressive force. A failure mechanism formed whereby the top of the deviation saddle (from the tendon ducts up) moved towards the web. Estimated maximum crack width before failure was 1/8 in. at the intersection of the web wall and the top surface of the deviation saddle.

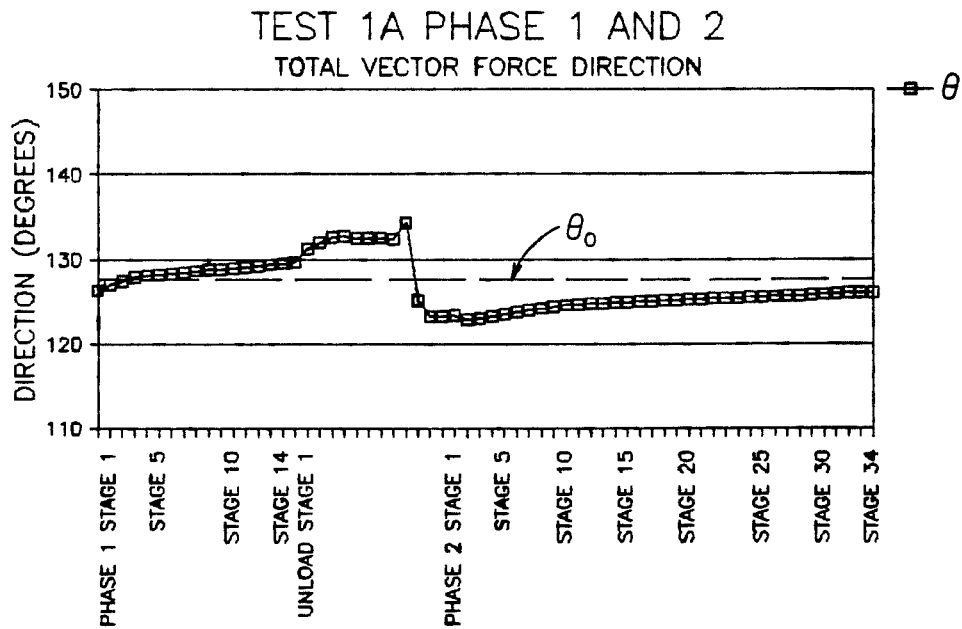
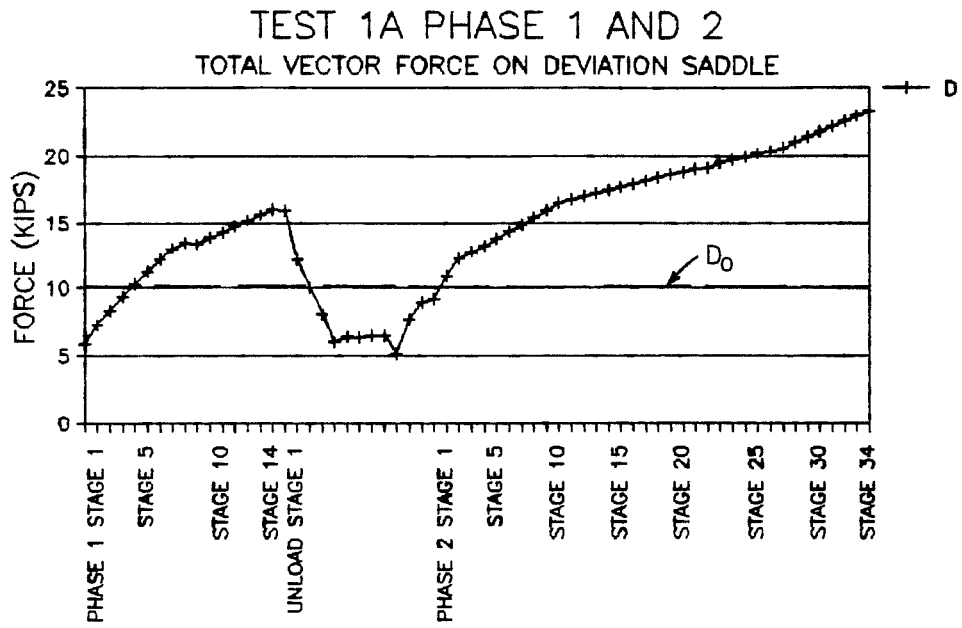


Figure 3.2 Test 1A Loading History

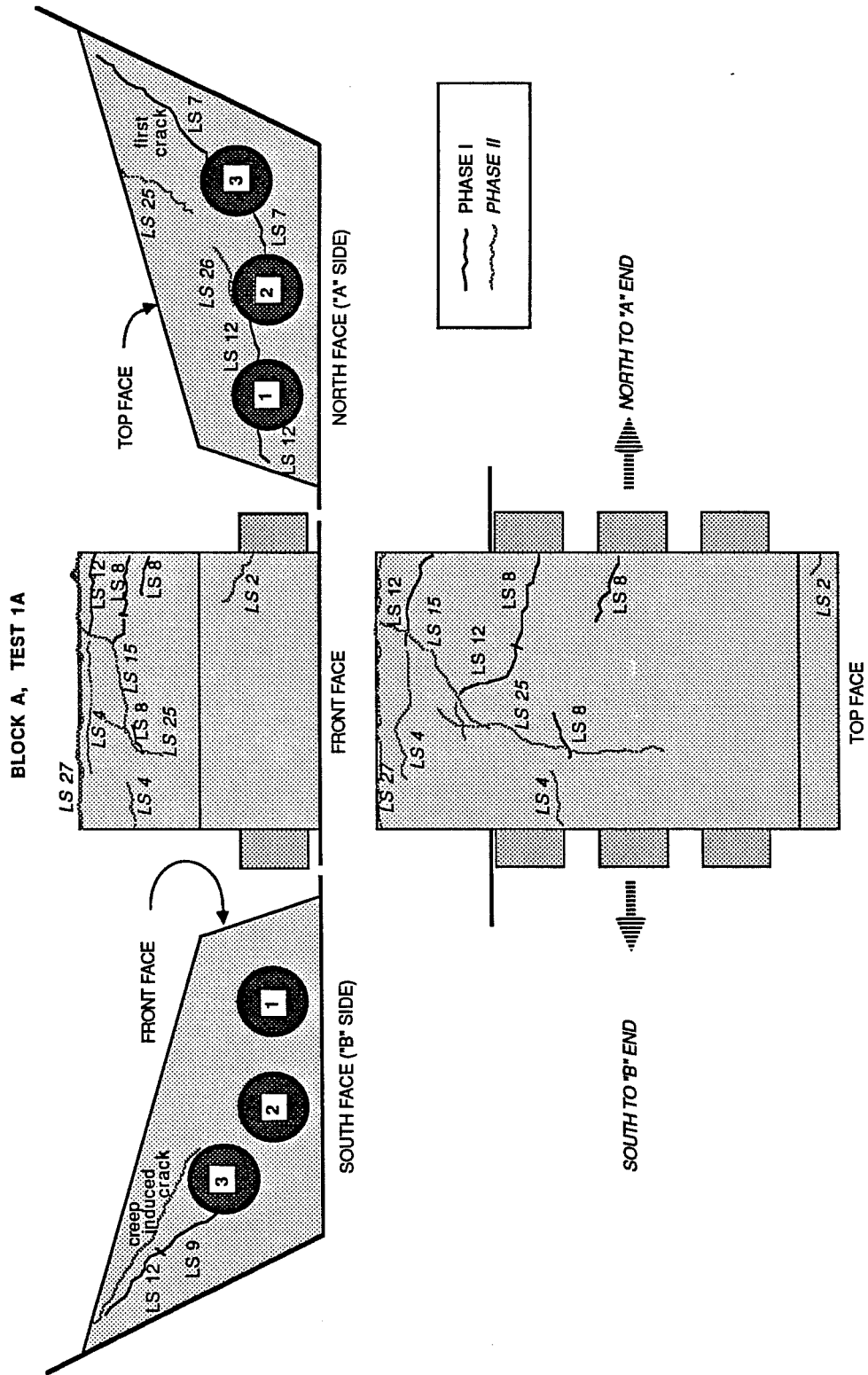


Figure 3.3 Test 1A Crack Patterns (From Ref. 1)

The observations from the strain data shown in Fig. 3.4 for phase 1 in which loading was discontinued before final failure are as follows:

1) The link bars had the highest strain at the "G" and "H" gage, while, the "F" gage had almost zero strain in comparison. The "G" gage location yielded after the last load stage.

2) The strain increased until the end of phase 1 in the "A" and "C" gages which were located on the top surface reinforcement. The strain in the "A" gage was slightly greater than that in the "C" gage.

3) The strain in the front face reinforcement ("B" gage) increased until load stage 7, then it started to decrease. Load stage 7 corresponded to the first visible crack.

4) The strain in the vertical leg of the open stirrup ("D" gage) was increasing to the end of phase 1.

The observations from the strain data shown in Fig. 3.5 for the ultimate loading of phase 2 are as follows:

1) The strains in the "G" and "H" gages on the link bar were the highest of all the reinforcement. These gages showed reinforcement yield before failure of the specimen.

2) At about load stage 10 ($D=16.5$ k), the strain began to increase in the "F" gage of the link bar and the "D" gage of the open stirrup. These gages reached yield several load stages before failure.

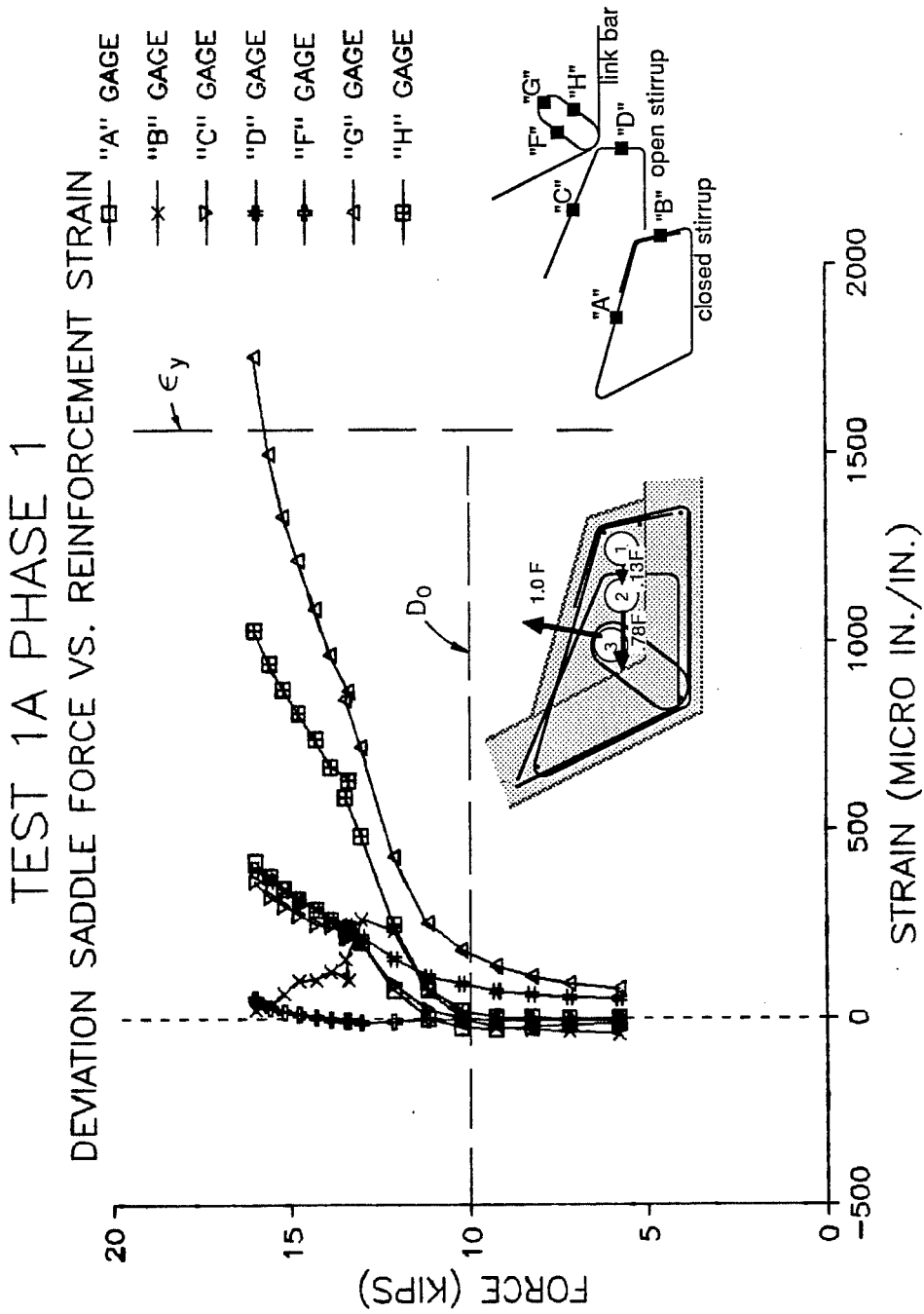


Figure 3.4 Test 1A Reinforcement Strain Data - Phase 1

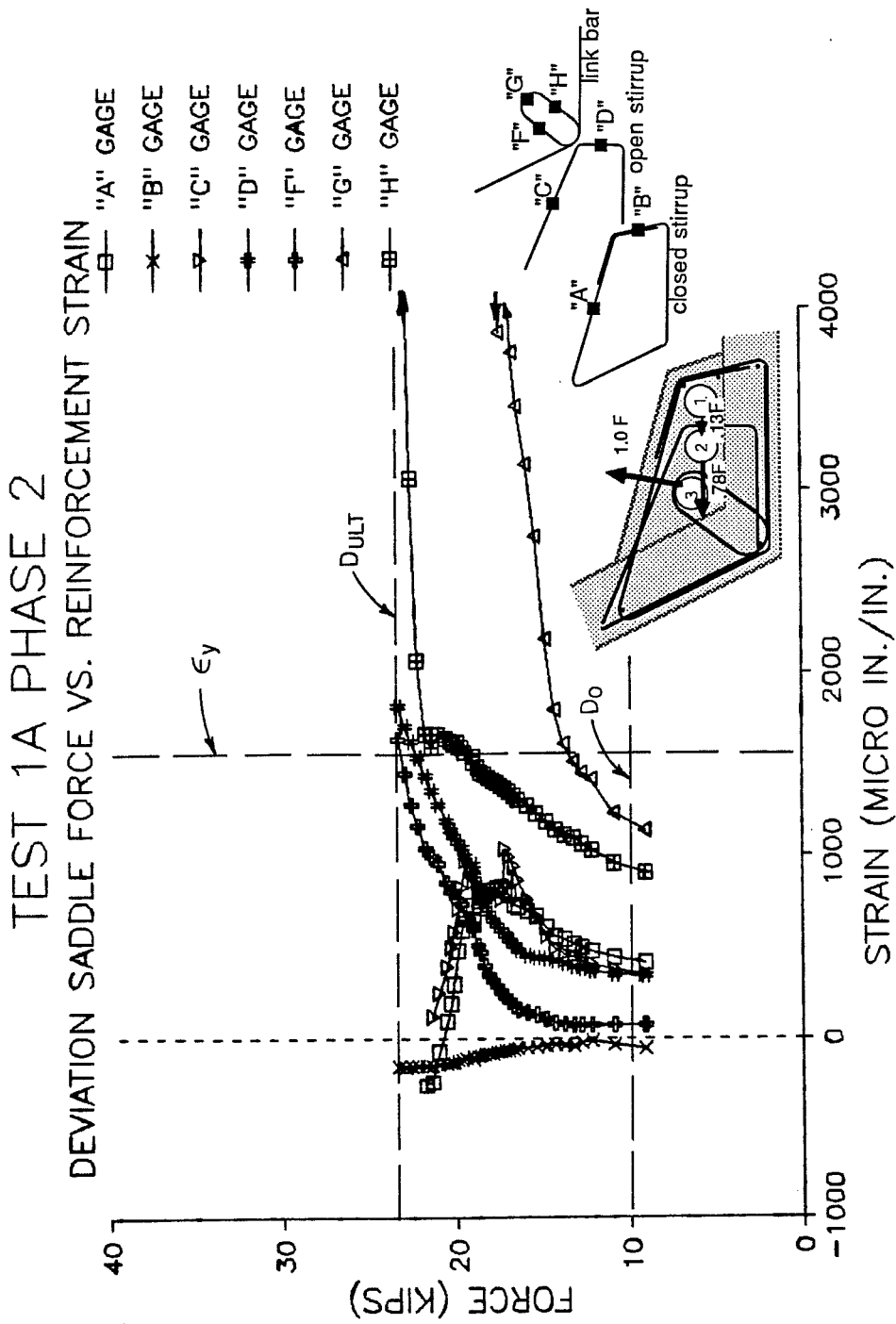


Figure 3.5 Test 1A Reinforcement Strain Data - Phase 2

3) At about load stage 20 ($D=18.8$ k), the strain began to decrease in the "A" and "C" gages at the top surface.

4) The strain in the "B" gage remained compressive.

A rational explanation for the strain data is that at early load stages the link bar ("F", "G", "H" gages) and the vertical leg of the open stirrup ("D" gage) strained due to direct tension. At later load stages they strained due to direct tension and shear friction. At early load stages, the reinforcement in the top surface ("A", "C" gages) strained due to the formation of a bending element above the ducts. The straining was reduced in the top surface reinforcement due to the failure mechanism. The reinforcement in the front face ("B" gage) had little or no contribution to the strength other than in developing the top surface reinforcement since it remained in compression.

The failure locations of the reinforcement and the before and after failure photographs are shown in Figs. 3.6 and 3.7. The bar graph of the strength comparisons (Fig. 3.8) can be used to make conclusions about the deviation saddle detail for this tendon configuration. There was no distinct jump in the strain gages, so microcracking was not noted. This detail has sufficient strength against visible cracking, but the ratio D/D_0 at first yielding seems marginal. The factor of safety against failure is sufficient. A comparison between the D/D_0 ratios for yield and ultimate reveals that the failure was ductile. Also, the horizontal deformation of the

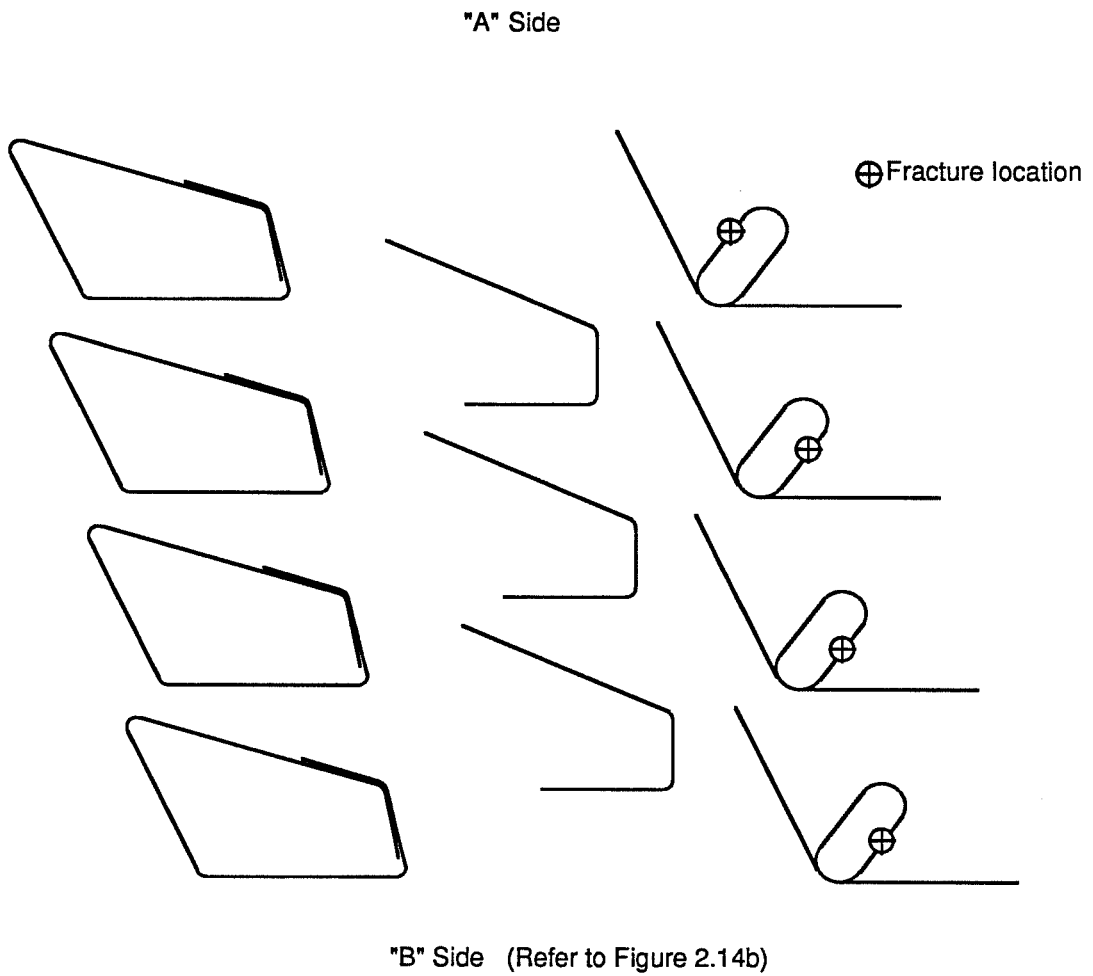


Figure 3.6 Test 1A Reinforcement Failure Locations

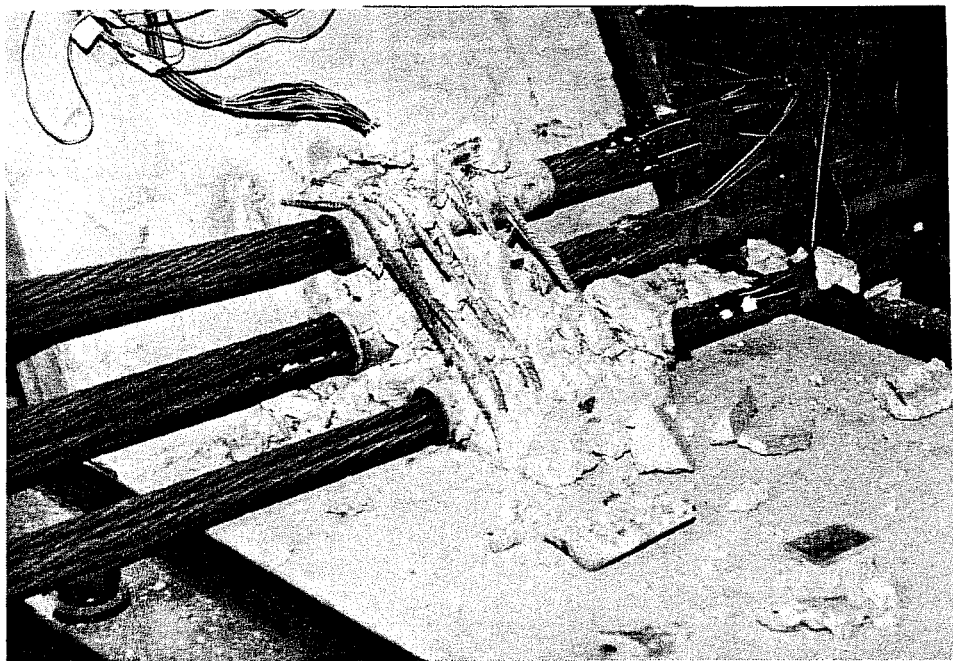
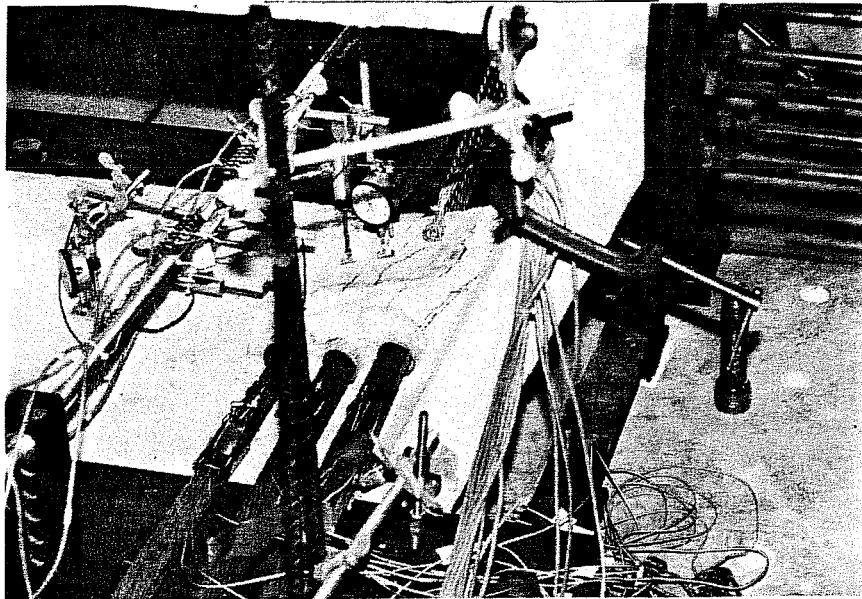


Figure 3.7 Test 1A - Before and After Failure

TEST 1A
RATIO D/D₀ AT CRITICAL STAGES

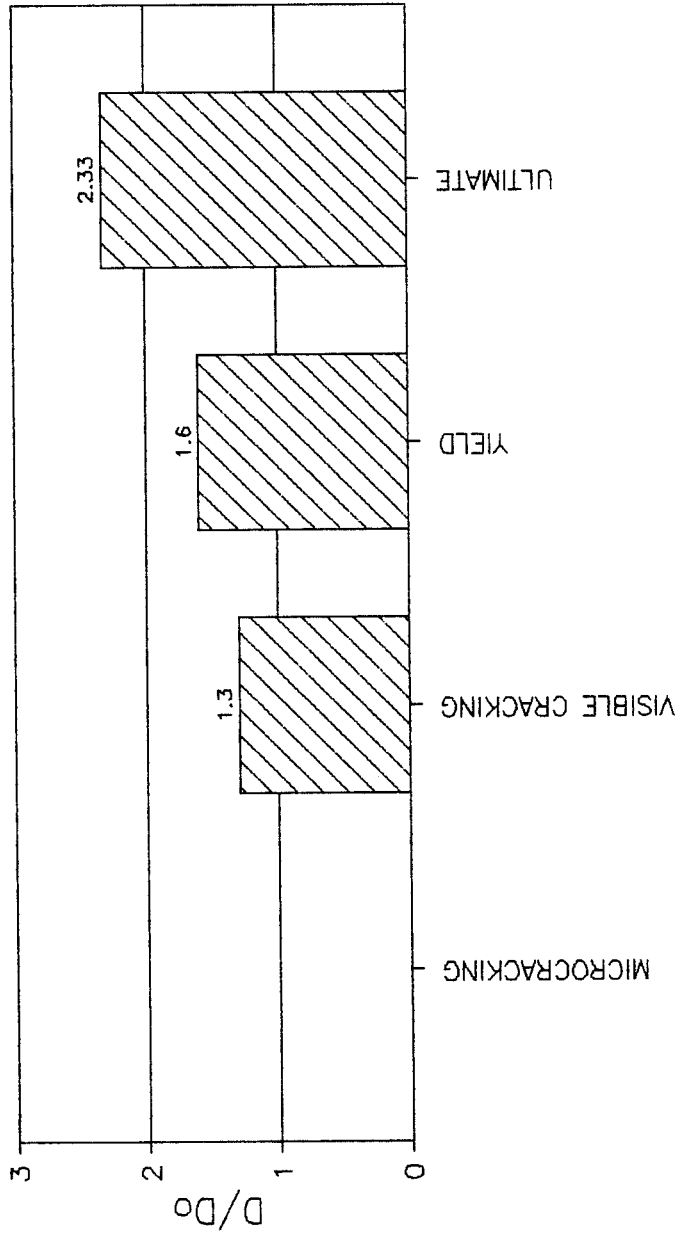


Figure 3.8 Test 1A Strength Comparison

failure mechanism gave advanced warning of the impending explosive failure.

3.3 Test 1B-Uncoated Link Bar with Stirrups-Straight Span-Two Tendons

Specimen 1B reinforcement scheme was identical to that of specimen 1A. However, the tendon configuration was different. This deviation saddle only deviated two tendons which represented a deviation saddle located closer to the piers than that of specimen 1A (see Fig. 2.5). The corner tendon had both a vertical deviation and a horizontal deviation directed away from the web, and the other tendon only had a slight horizontal deviation away from the web. This detail is discussed in Sec. 2.2.1 and is illustrated in Fig. 2.4b.

The total vector force and direction which acted on the deviation saddle for phase 1 and 2 are shown in Figs. 3.9 and 3.10. The crack patterns are shown in Fig. 3.11. The first crack to form was across the top surface and down one side of the deviation saddle. This might be expected since the tendon 2 deviation force was approximately perpendicular to the top surface. As indicated by the larger number of cracks on the top surface, the tensile stresses were higher on the top surface of this specimen than that of specimen 1A. Cracks were very small and failure was sudden. Estimated maximum crack width was 0.02 in. on the top surface above tendon 2.

This test had two stages for phase 1 (1(a),1(b)) since an inadequate amount of tendon area was initially provided to fail the

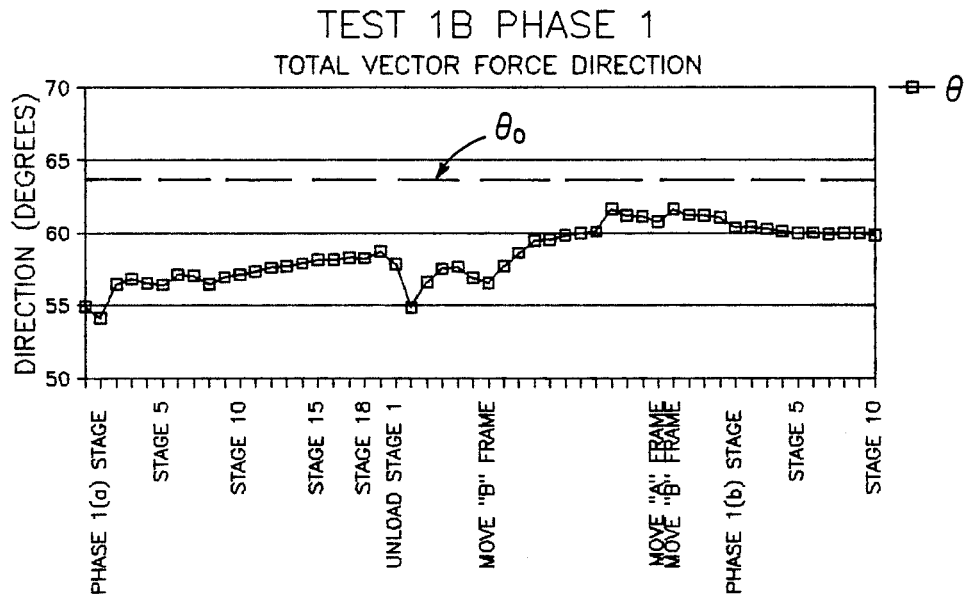
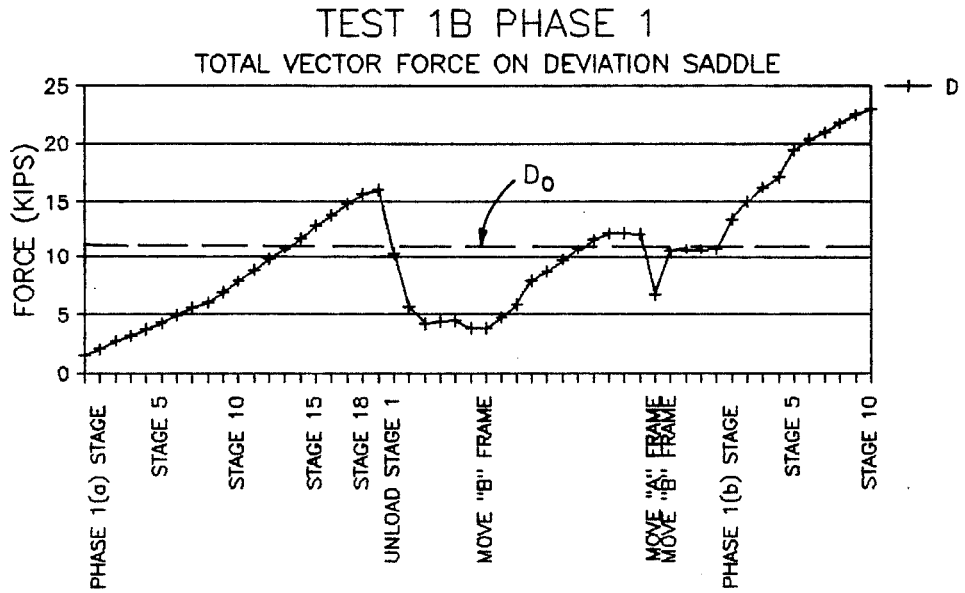


Figure 3.9 Test 1B Loading History - Phase 1

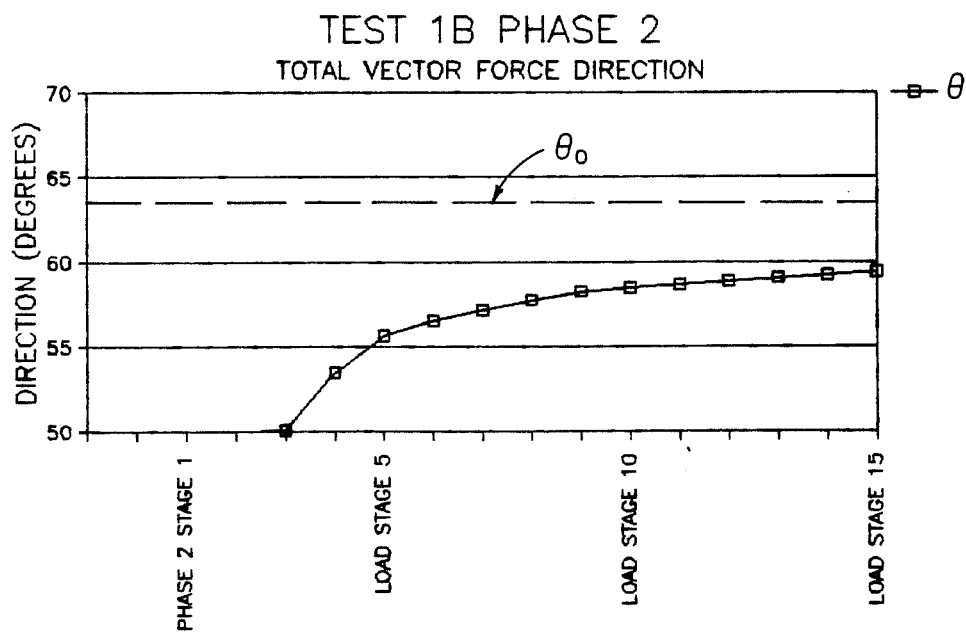
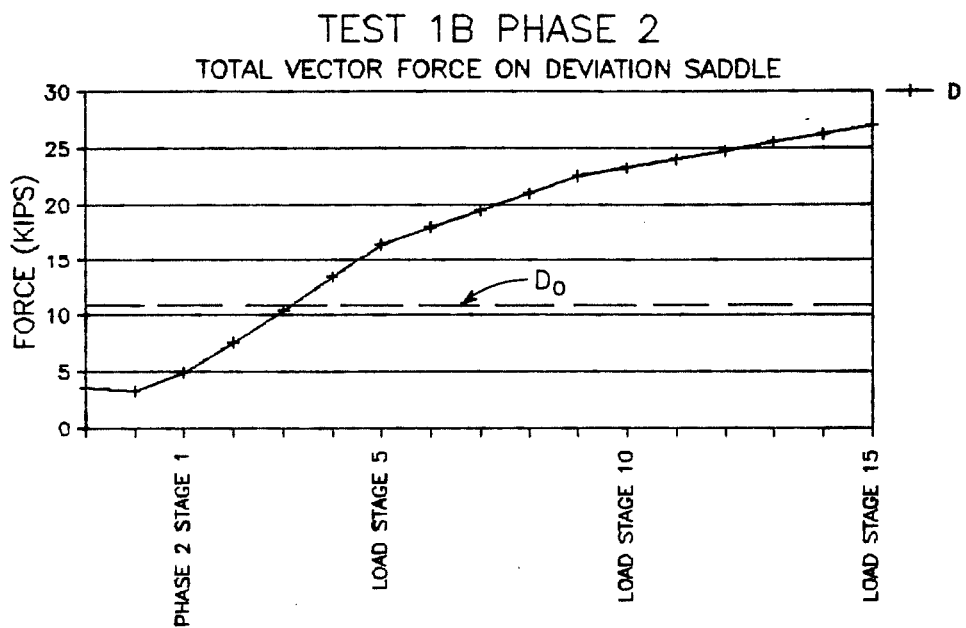


Figure 3.10 Test 1B Loading History - Phase 2

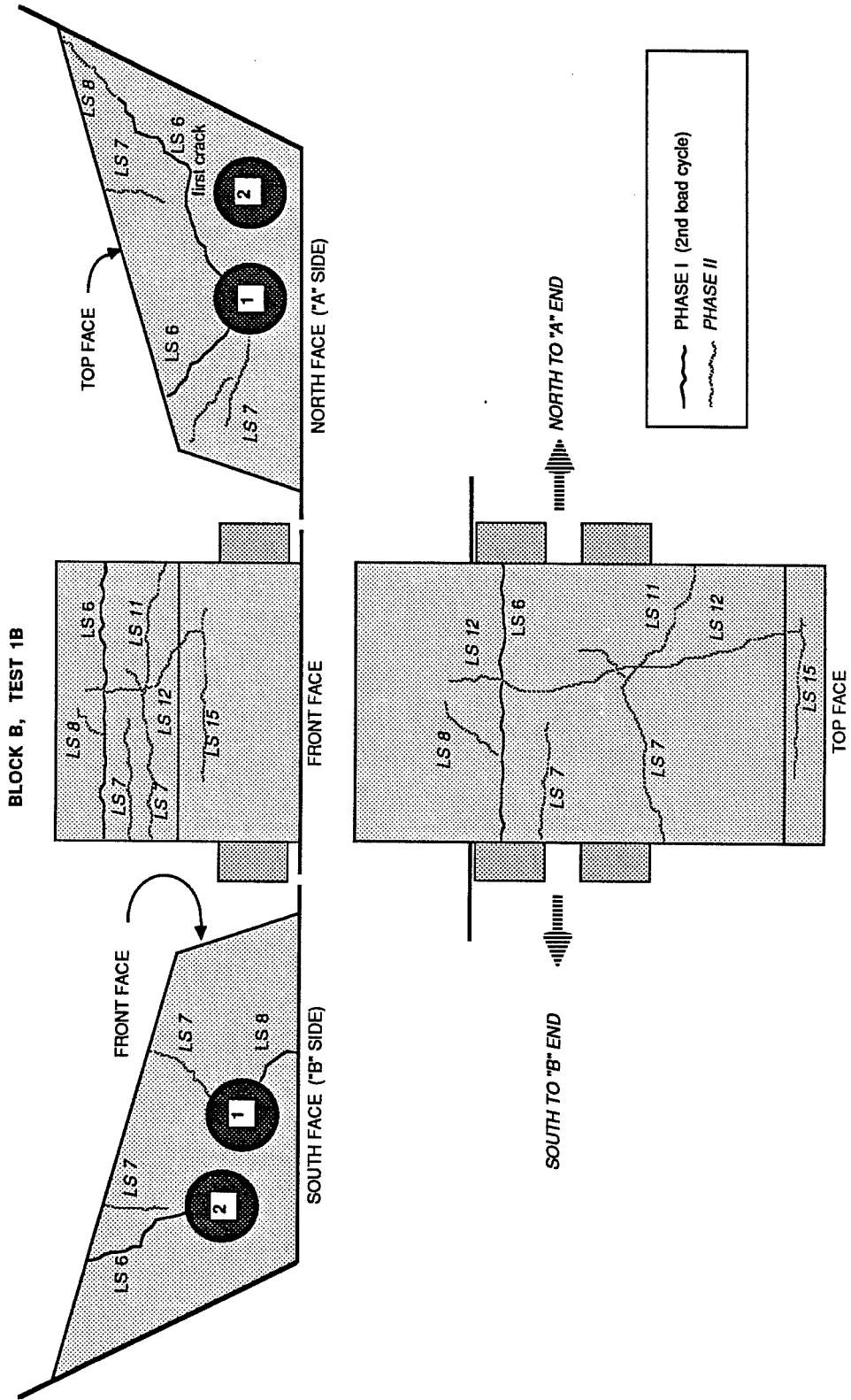


Figure 3.11 Test 1B Crack Patterns (From Ref. 1)

specimen. The following observations can be made with regard to phase 1(a) strain data shown in Fig. 3.12:

- 1) The gages at the top surface of the deviation saddle ("A", "C" gages) had the greatest strain during phase 1(a) with the "A" gage having the larger value.

- 2) The "G" and "H" gages on the link bar reinforcement had the second highest strain. Unfortunately, the "F" gage was not functioning for this test.

- 3) The strain in the "B" gage at the front face of the deviation saddle began to decrease after microcracking occurred.

- 4) The "D" gage on the open stirrup remained at almost zero strain.

Phase 1(b) strain data shown in Fig. 3.13 are similar to phase 1(a) except that the slope decreased for the "H" gage data of the link bar indicating a stiffness decrease and the vertical leg of the open stirrup ("D" gage) began straining. The strain in the link bar and the outer stirrup reached yield at the end of this phase.

The strain gage plot for the phase 2 ultimate load cycle is shown in Fig. 3.14. The following observations can be made:

- 1) The link bar had the greatest strain of all reinforcement patterns. The strain in the "F", "G", and "H" gages was above yield at the end of this phase.

- 2) The strain in the reinforcement of the top surface of the deviation saddle ("A", "C" gages) had also yielded.

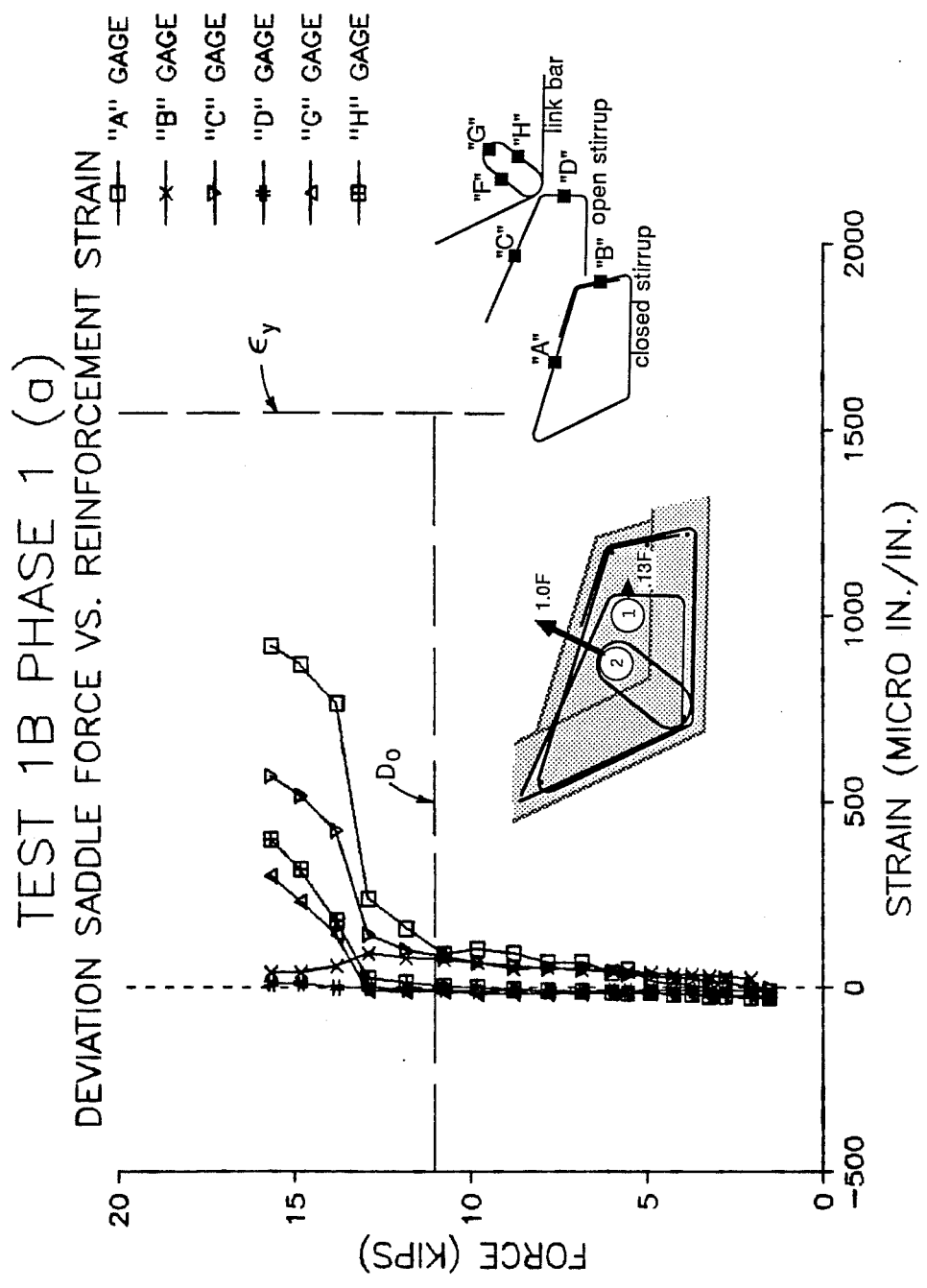


Figure 3.12 Test 1B Reinforcement Strain Data - Phase 1 (a)

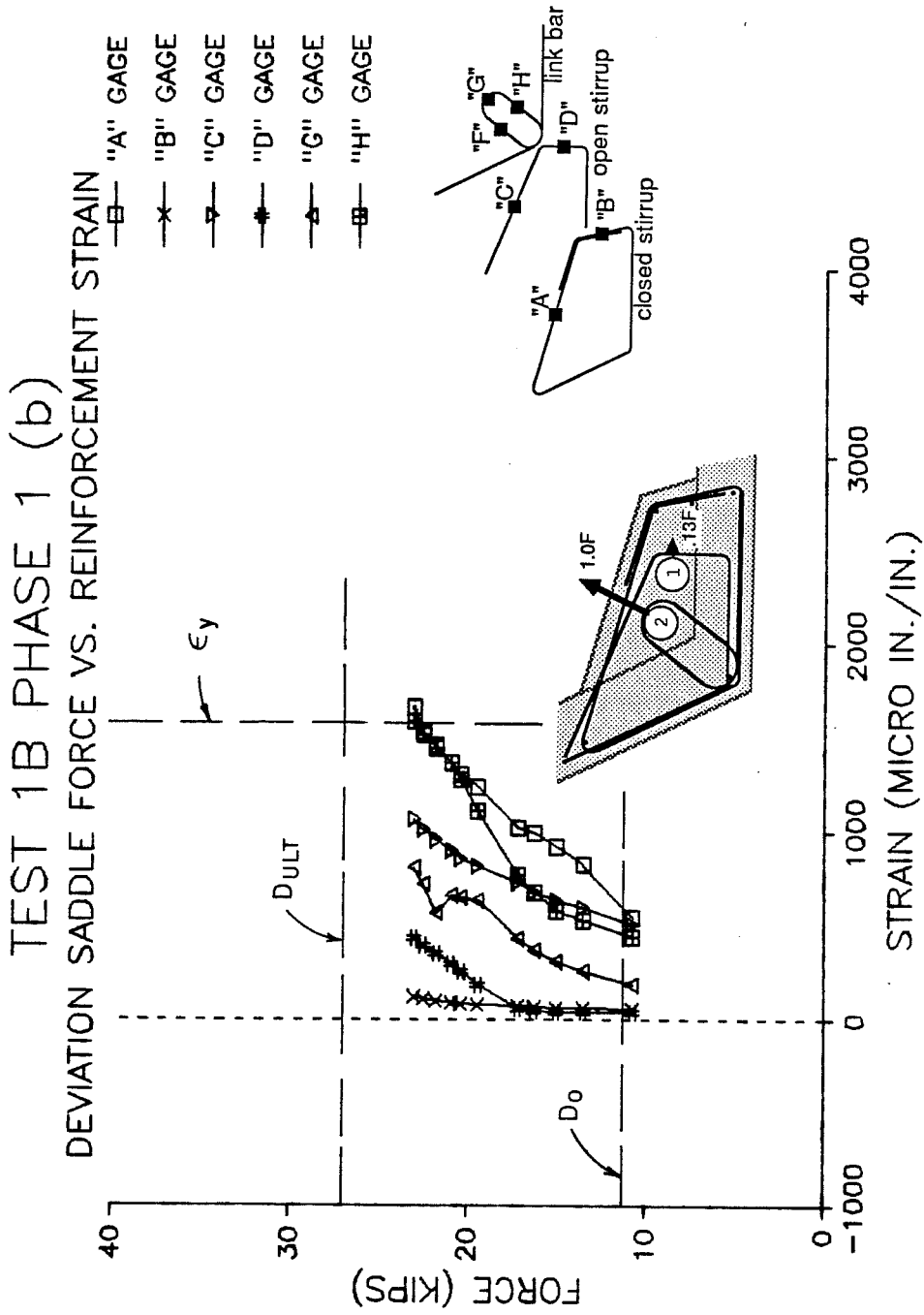


Figure 3.13 Test 1B Reinforcement Strain Data - Phase 1 (b)

TEST 1B PHASE 2

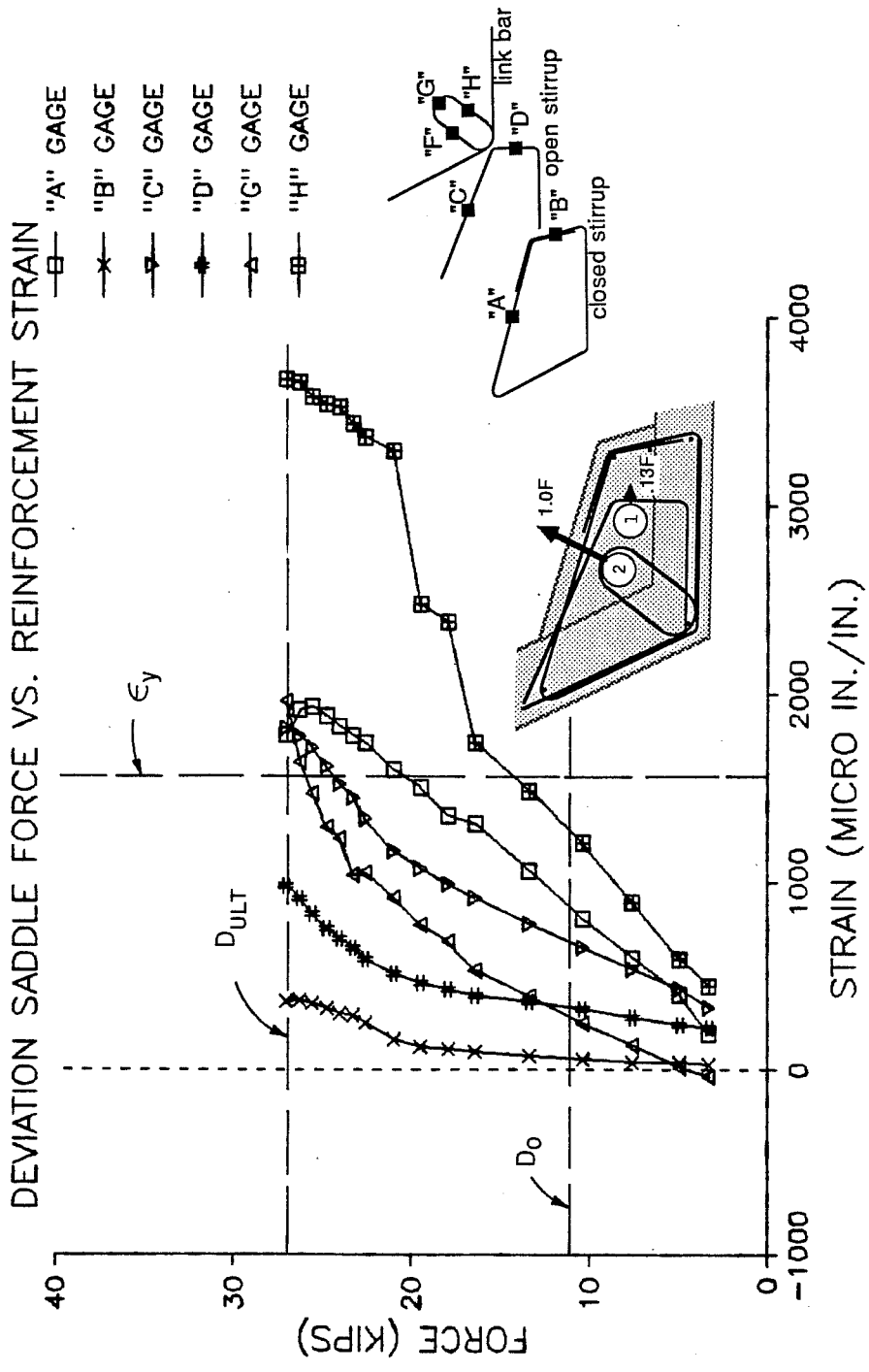


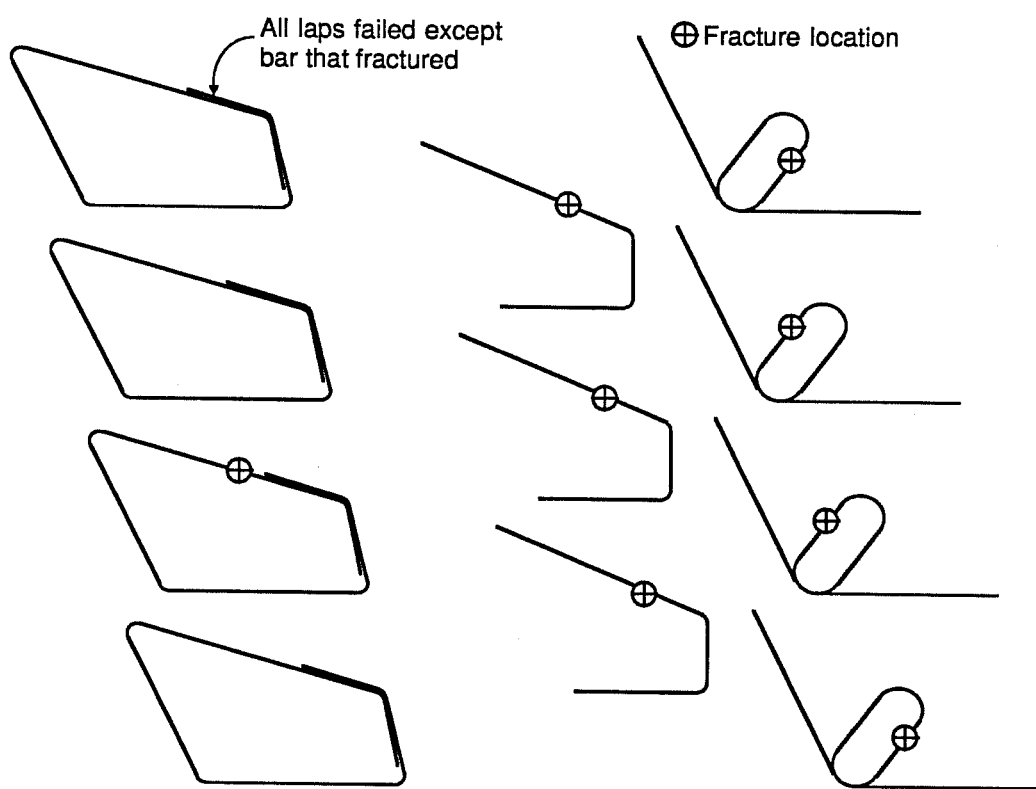
Figure 3.14 Test 1B Reinforcement Strain Data - Phase 2

3) The vertical leg of the open stirrup ("D" gage) and the reinforcement in the front face of the deviation saddle ("B" gage) had some tensile strain, but they did not yield.

A reasonable explanation for the strain data is that the link bar ("F", "G", "H" gages) strained due to direct tension, the reinforcement in the top surface ("A", "C" gages) strained due to the formation of a bending element above the ducts, and the vertical leg of the open stirrup and front leg of the closed stirrup ("D", "B" gages) strained due to direct tension and shear friction. It is obvious from the strain data that shear friction did not influence the failure of this specimen as much as it did in specimen 1A since the vertical leg of the open stirrup and the front face reinforcement did not yield.

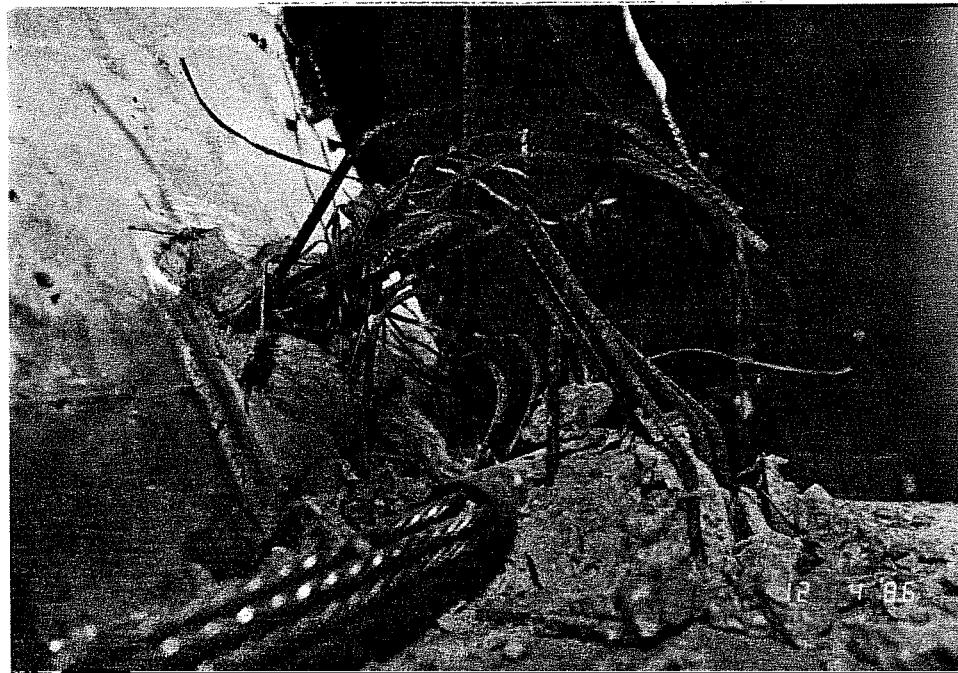
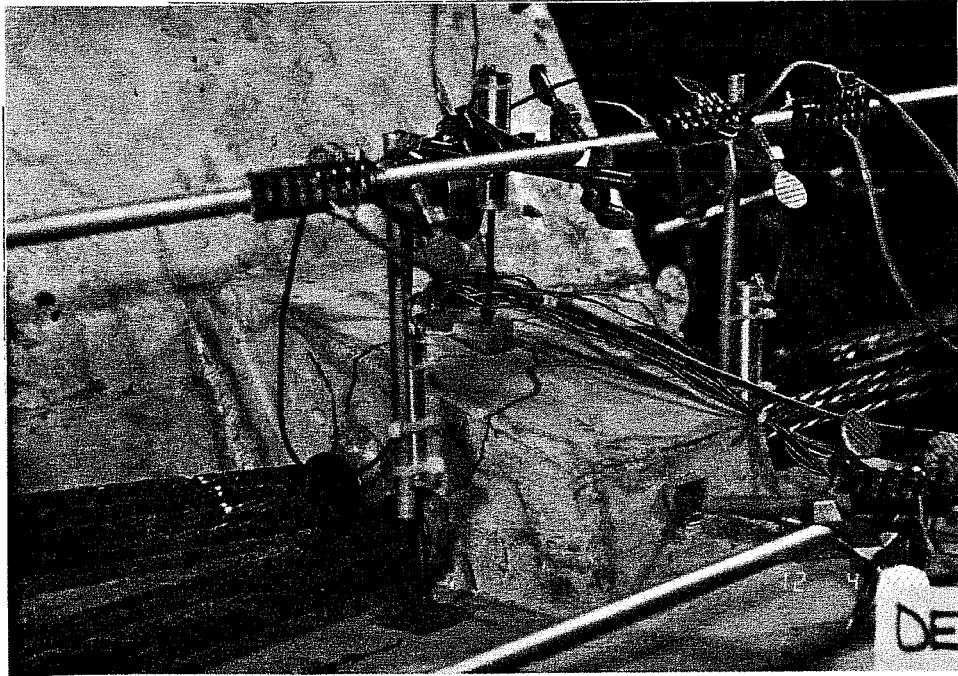
The reinforcement failure locations are shown in Fig. 3.15 and the before and after failure photographs are shown in Fig. 3.16. From the strength comparisons (Fig. 3.17), it appears that this deviation saddle detail is adequately safeguarded against cracking and yielding, and it has a sufficient factor of safety against failure. However, the ductility is low which is indicated by the relatively small difference between the D/D_0 ratio for yield and ultimate, and the fine cracks that had formed.

"A" Side



"B" Side (Refer to Figure 2.14b)

Figure 3.15 Test 1B Reinforcement Failure Locations



TEST 1B
RATIO D/D₀ AT CRITICAL STAGES

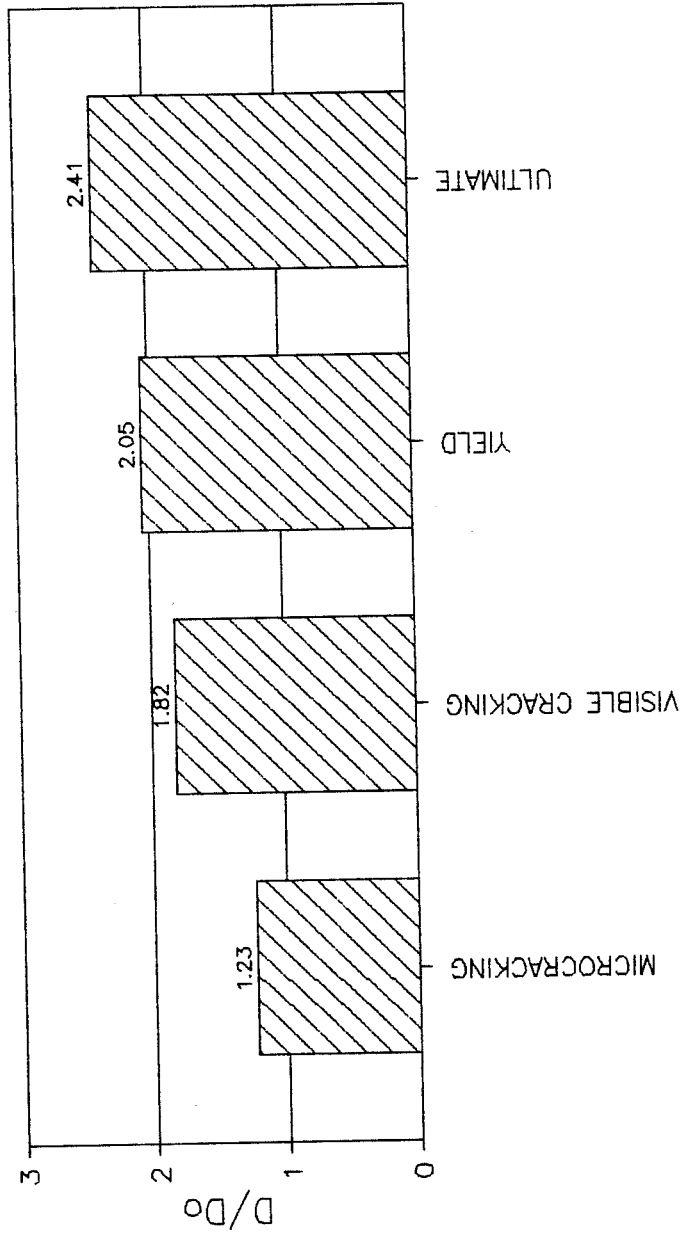


Figure 3.17 Test 1B Strength Comparison

3.4 Test 2A-Uncoated Link Bar Isolated-Test 1B Tendon Configuration

The objective of test 2A was to isolate the behavior of the link bar of specimens 1A and 1B. This specimen was not intended to be a properly detailed deviation saddle, and it was expected to have an abnormally low factor of safety (D/D_0 ratio) for ultimate. The tendon configuration utilized for this test was identical to test 1B. This detail is discussed in Sec. 2.2.2 and is illustrated in Fig. 2.6a.

The total vector force and direction which acted on the specimen are shown in Fig. 3.18. The crack patterns are as might be expected for a specimen without face reinforcement (Fig. 3.19). There was no crack distribution on the top surface of the deviation saddle. Estimated maximum crack width was $1/4$ in. at the side face of the deviation saddle.

The observations that can be made from the phase 1 nominal loading strain data (Fig. 3.20) are as follows:

- 1) The strain jumped dramatically at load stage 5 in the bottom leg ("H" gage) and the top ("G" gage) of the link bar. The first crack appeared at load stage 5.

- 2) The top leg ("F") of the link bar had almost zero strain.

The observations that can be made from the ultimate loading phase 2 strain data (Fig. 3.21) are as follows:

- 1) The "G" and "H" gages are again strained the greatest amount in this reinforcement pattern. Unfortunately, the gages failed at an early load stage, probably when reinforcement yielded.

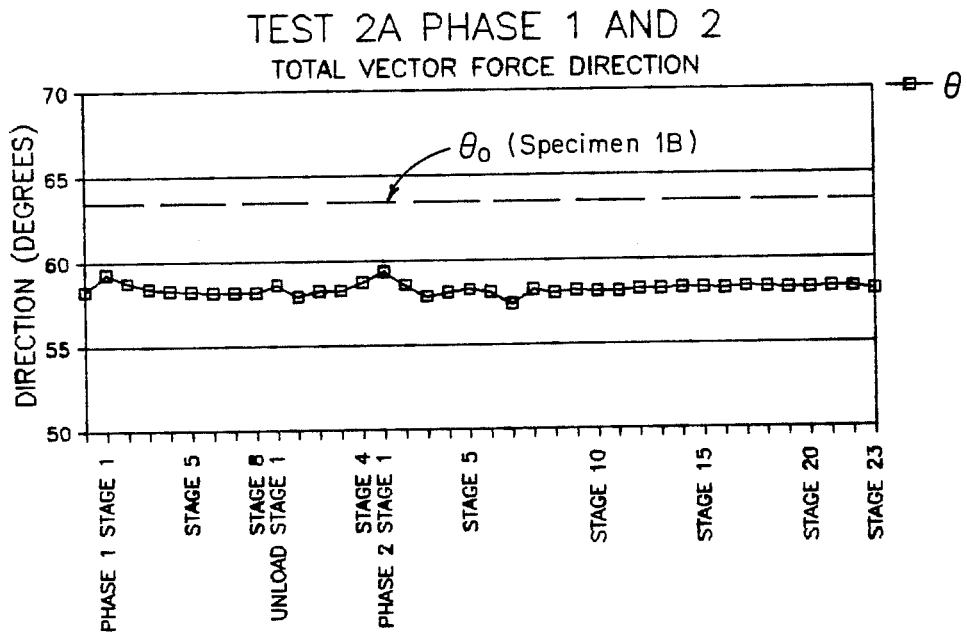
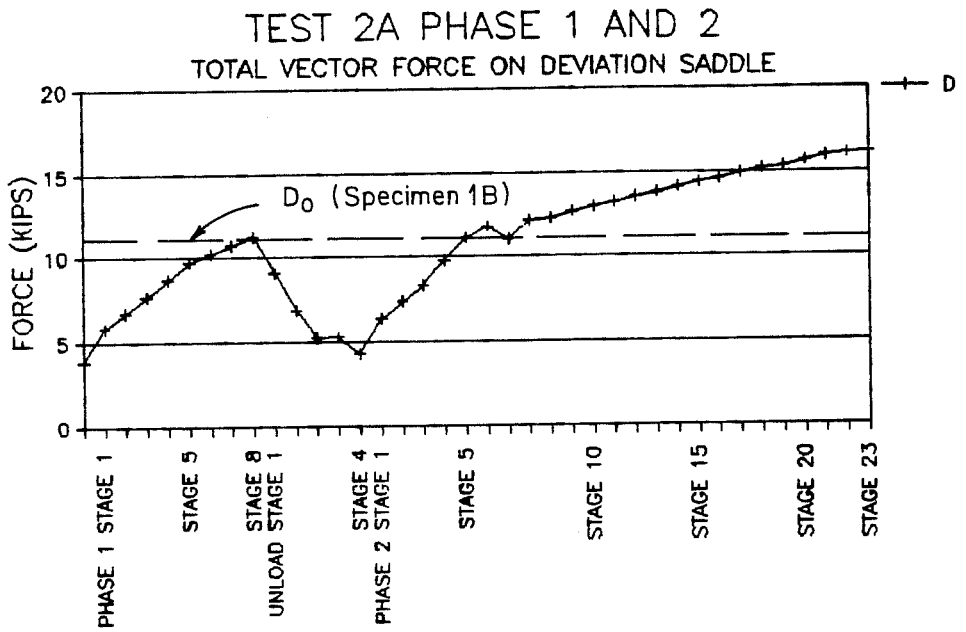


Figure 3.18 Test 2A Loading History

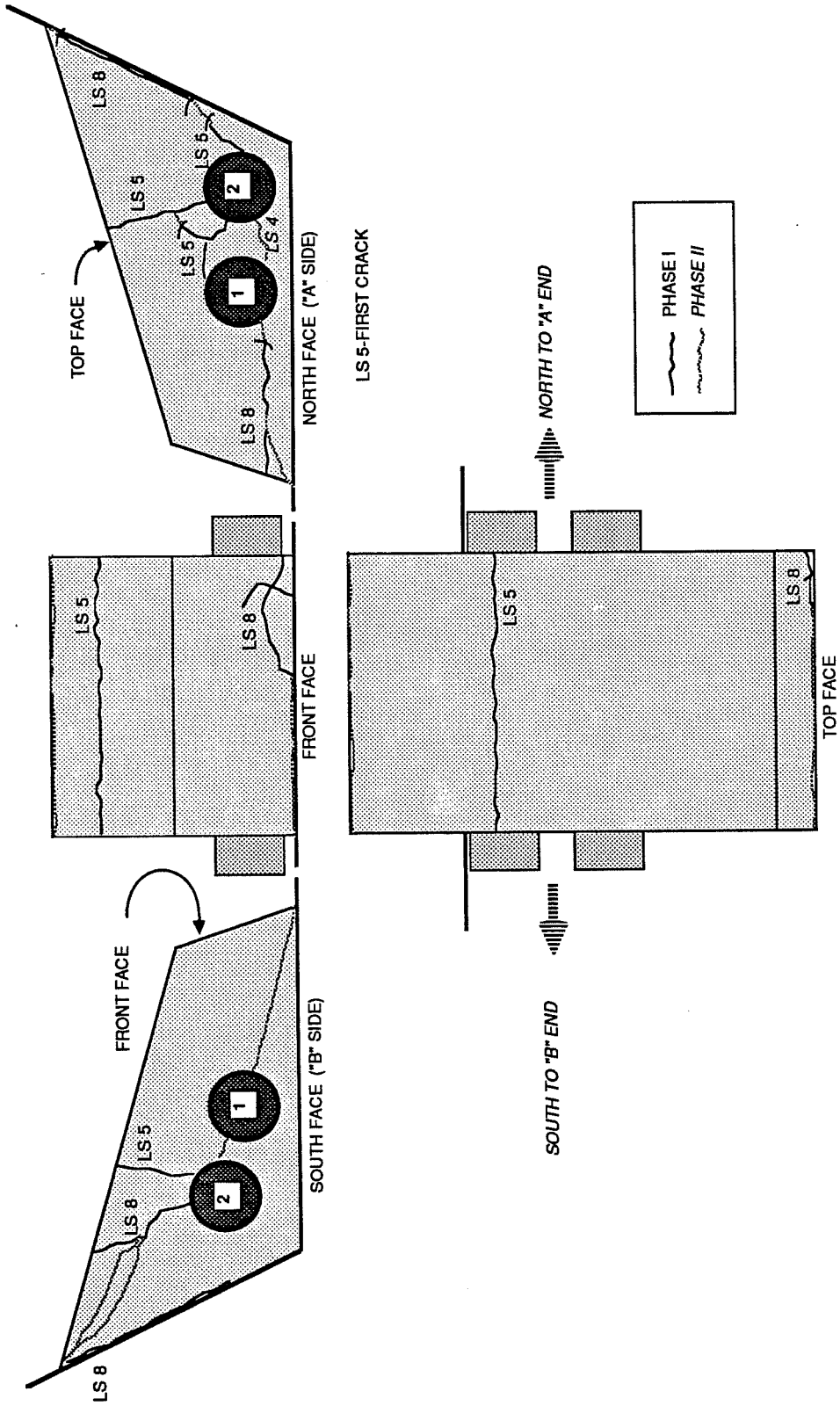


Figure 3.19 Test 2A Crack Patterns

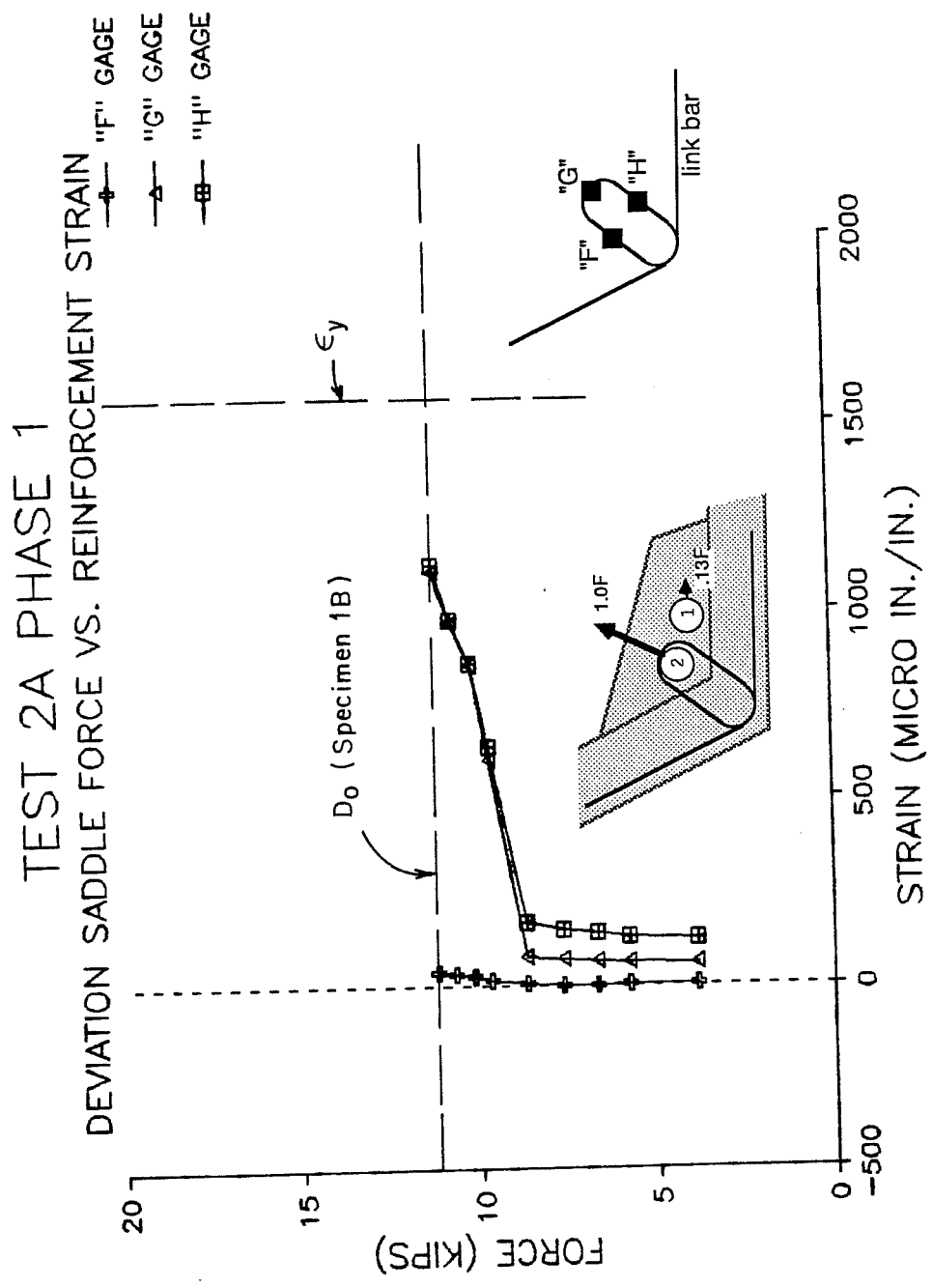


Figure 3.20 Test 2A Reinforcement Strain Data - Phase 1

TEST 2A PHASE 2

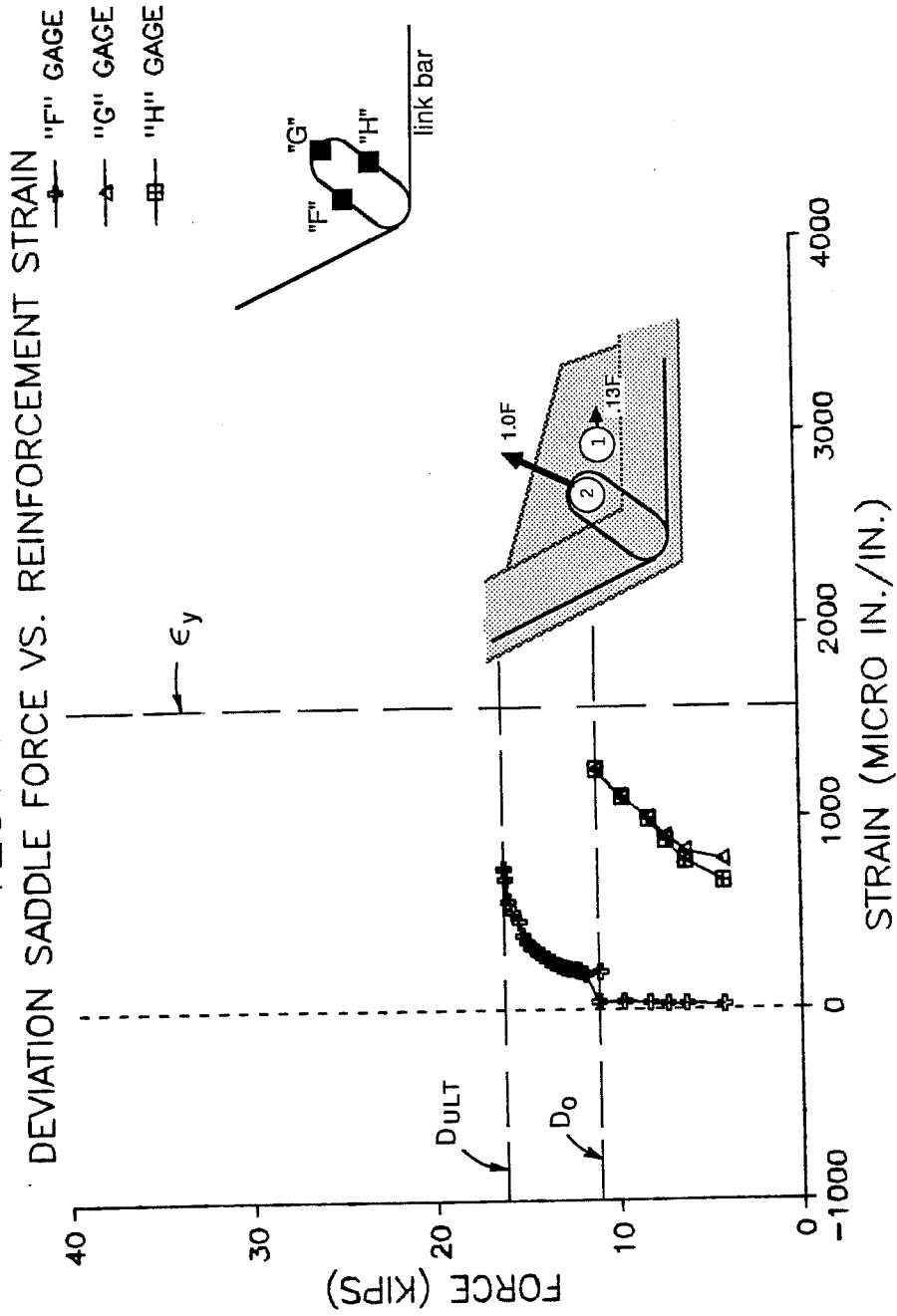


Figure 3.21 Test 2A Reinforcement Strain Data - Phase 2

2) The "F" gage began to strain, but it had a lower strain than the other locations on the link bar. This marked difference with the "H" gage could be due to the location of the gage which was almost in the web, or this could be an indication that a different strain exists in each leg of the link bar.

The main conclusion that can be made is simply that the link bar resisted the direct tension of the deviation force of tendon 2. The relatively small tendon 1 deviation force was most likely resisted by shear friction.

The reinforcement failure locations are shown in Fig. 3.22. The premise that the strains were higher in the bottom leg of the link bar is probably unlikely since fractures occurred on both sides. The before and after photographs (Fig.3.23) show the wide cracks. The strength was compared with the nominal D_0 computed for the original prototype detail having all reinforcement even though only the link bar was provided. Hence, this test should have significantly lower D/D_0 values than a normal deviation saddle design. Figure 3.24 shows that even for this radically reduced design the ultimate strength is sufficient to resist the nominal jacking loads, but the factor of safety at yield and ultimate is too low. Also, cracking of the specimen would occur under nominal load. The specimen was very ductile which was apparent from the large cracks that had formed and the ratio of ultimate to yield load.

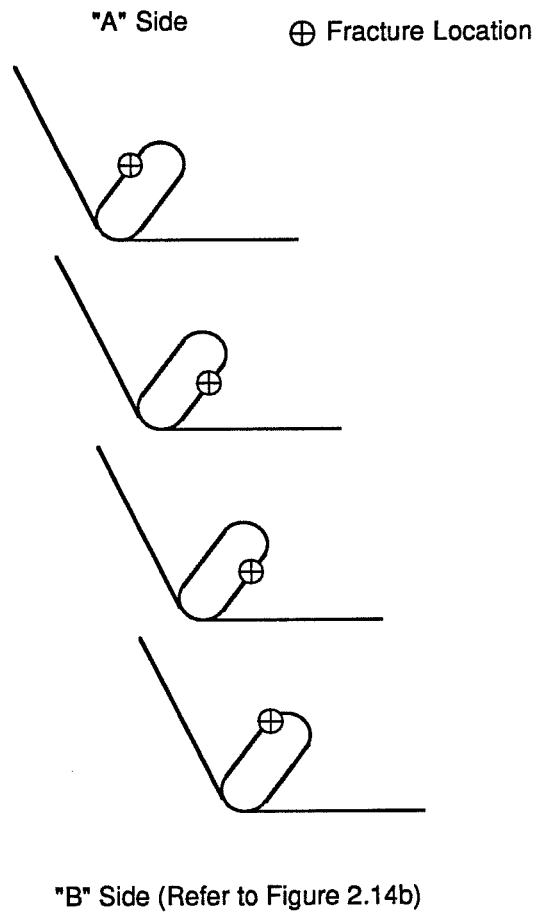


Figure 3.22 Test 2A Reinforcement Failure Locations

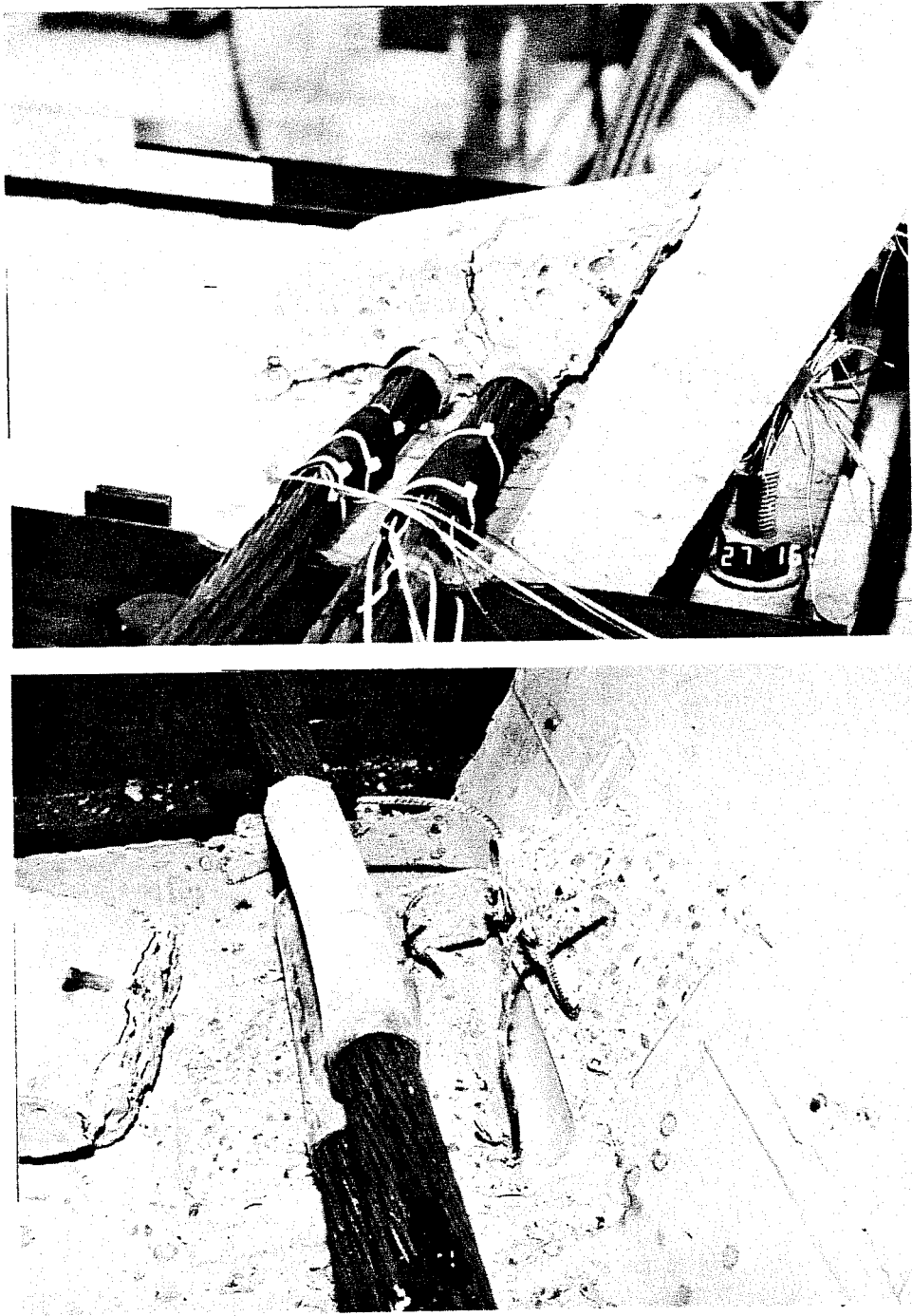


Figure 3.23 Test 2A - Before and After Failure

TEST 2A
RATIO D/D₀ AT CRITICAL STAGES

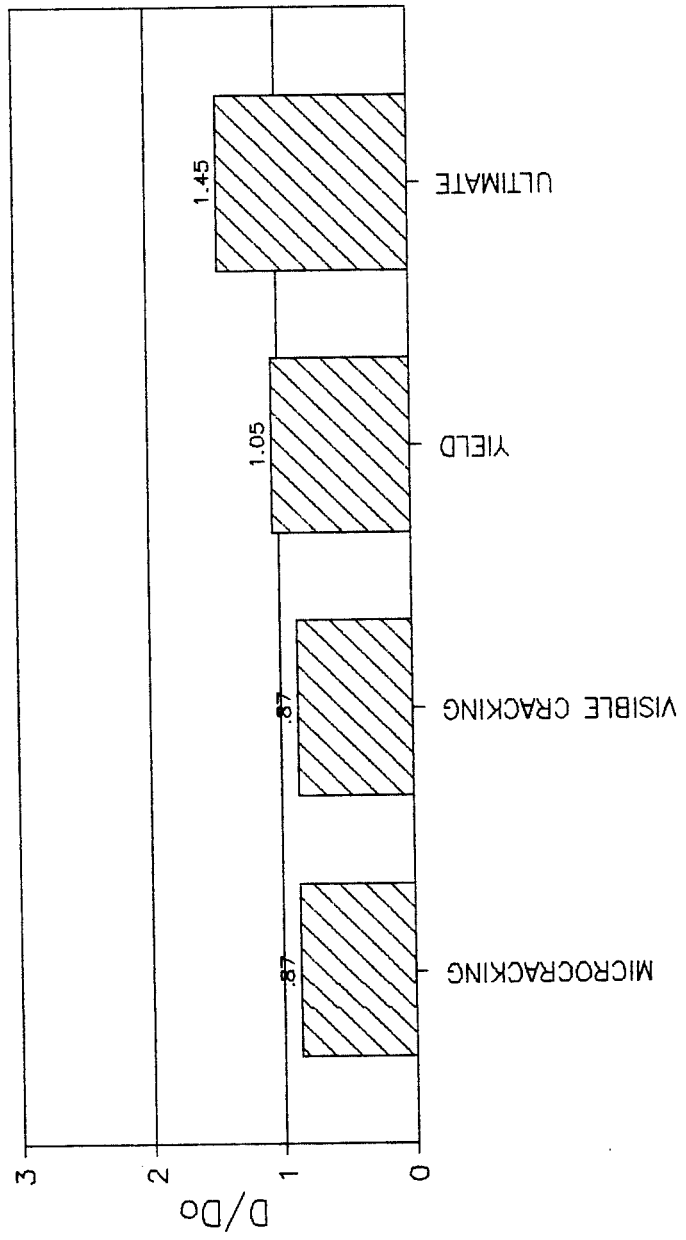


Figure 3.24 Test 2A Strength Comparison

3.5 Test 2B-Uncoated Stirrups Without Link Bar-Test 1B Tendon Configuration

The objective of specimen 2B was similar to that of specimen 2A. The reinforcement scheme was the two types of stirrups of specimens 1A and 1B without the link bar. This was not intended to be a properly detailed deviation saddle, and it was expected that the factor of safety (D/D_0 ratio) for ultimate would be abnormally low. The tendon configuration utilized for this specimen was identical to test 1B. This detail is discussed in Sec. 2.2.2 and is illustrated in Fig. 2.6b.

The total vector force and direction which acted on the specimen are shown in Fig. 3.25. In the load history plot, it is apparent that the load dropped off in phase 2 at load stage 18. This was due to the progressive collapse of the deviation saddle. The crack pattern for the top surface shown in Fig. 3.26 is different from that of Test 2A. The top surface cracks were distributed because of the surface reinforcement. Estimated maximum crack width was 1/8 in. and 1/2 in. respectively before and after the collapse of the top surface at the side faces of deviation saddle.

The observations that can be made from the nominal jacking loading phase 1 strain data (Fig. 3.27) are as follows:

- 1) The deviation saddle top surface reinforcement ("A", "C" gages) had the greatest strain. The large jump in strain concurred with the top surface crack at load stage 12.

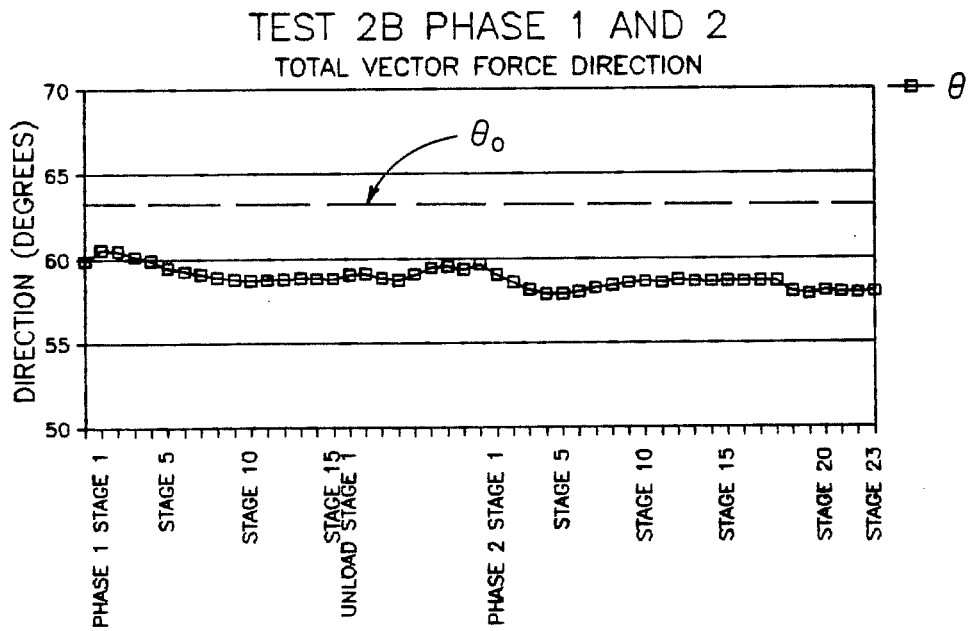
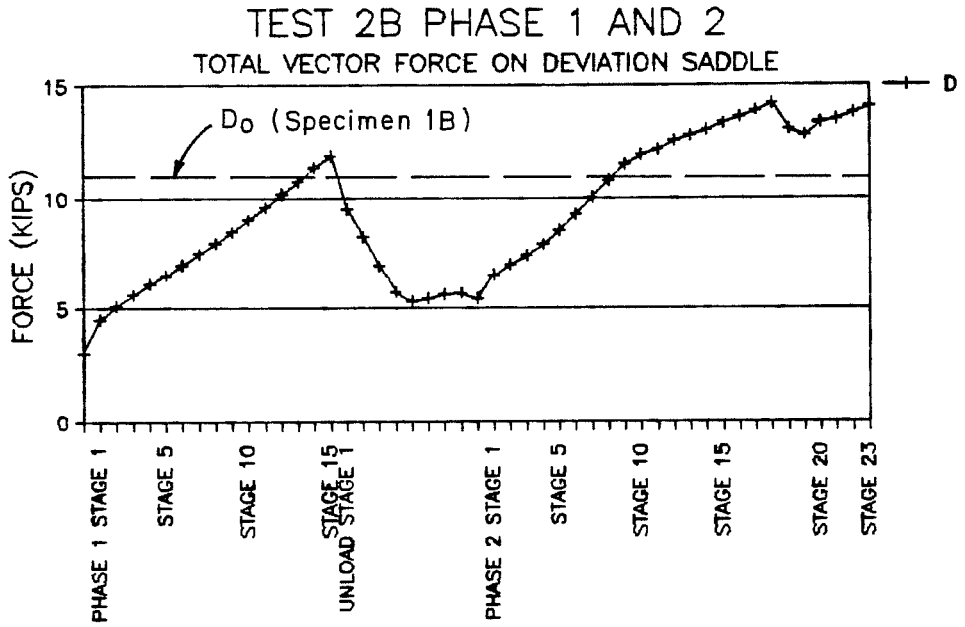


Figure 3.25 Test 2B Loading History

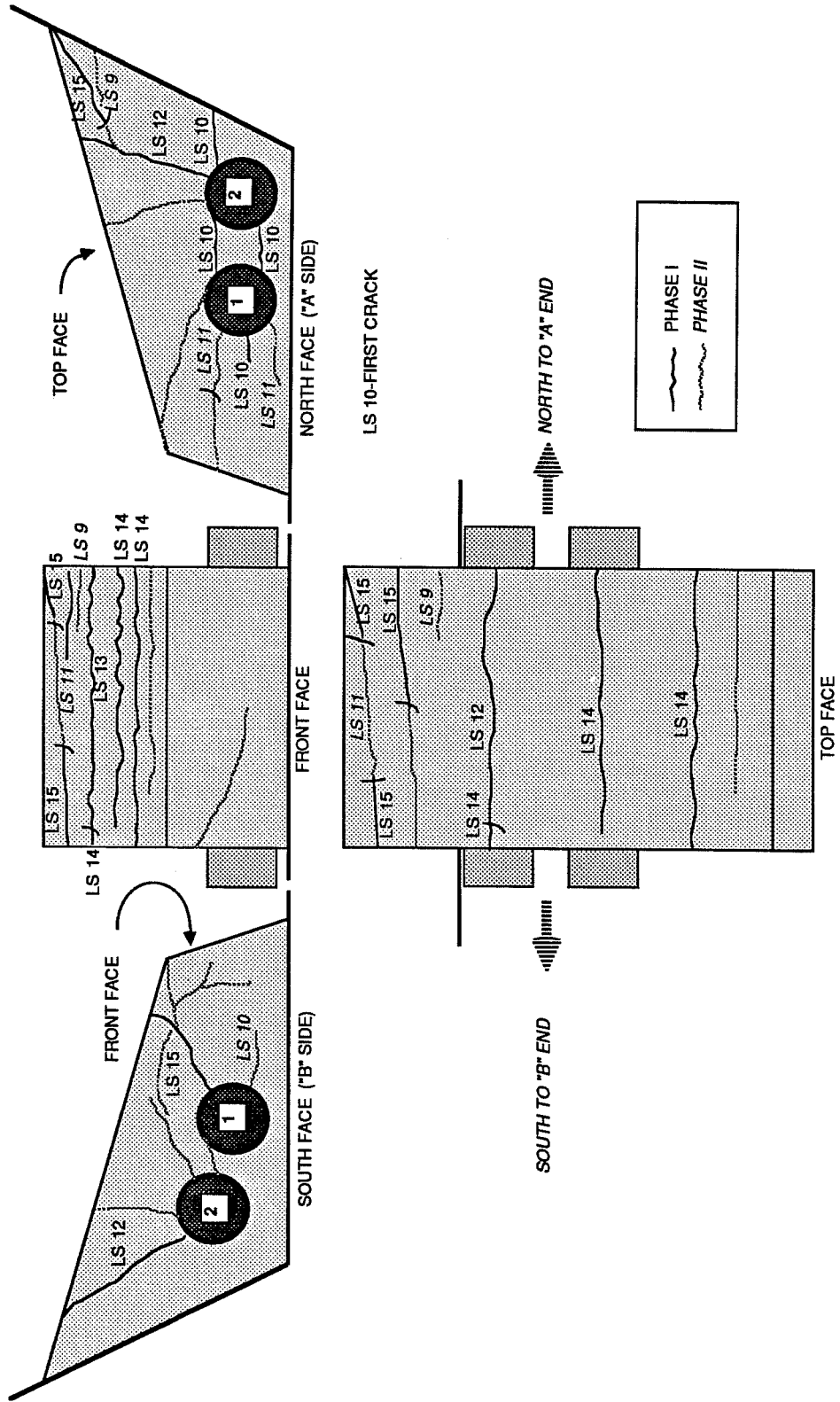


Figure 3.26 Test 2B Crack Patterns

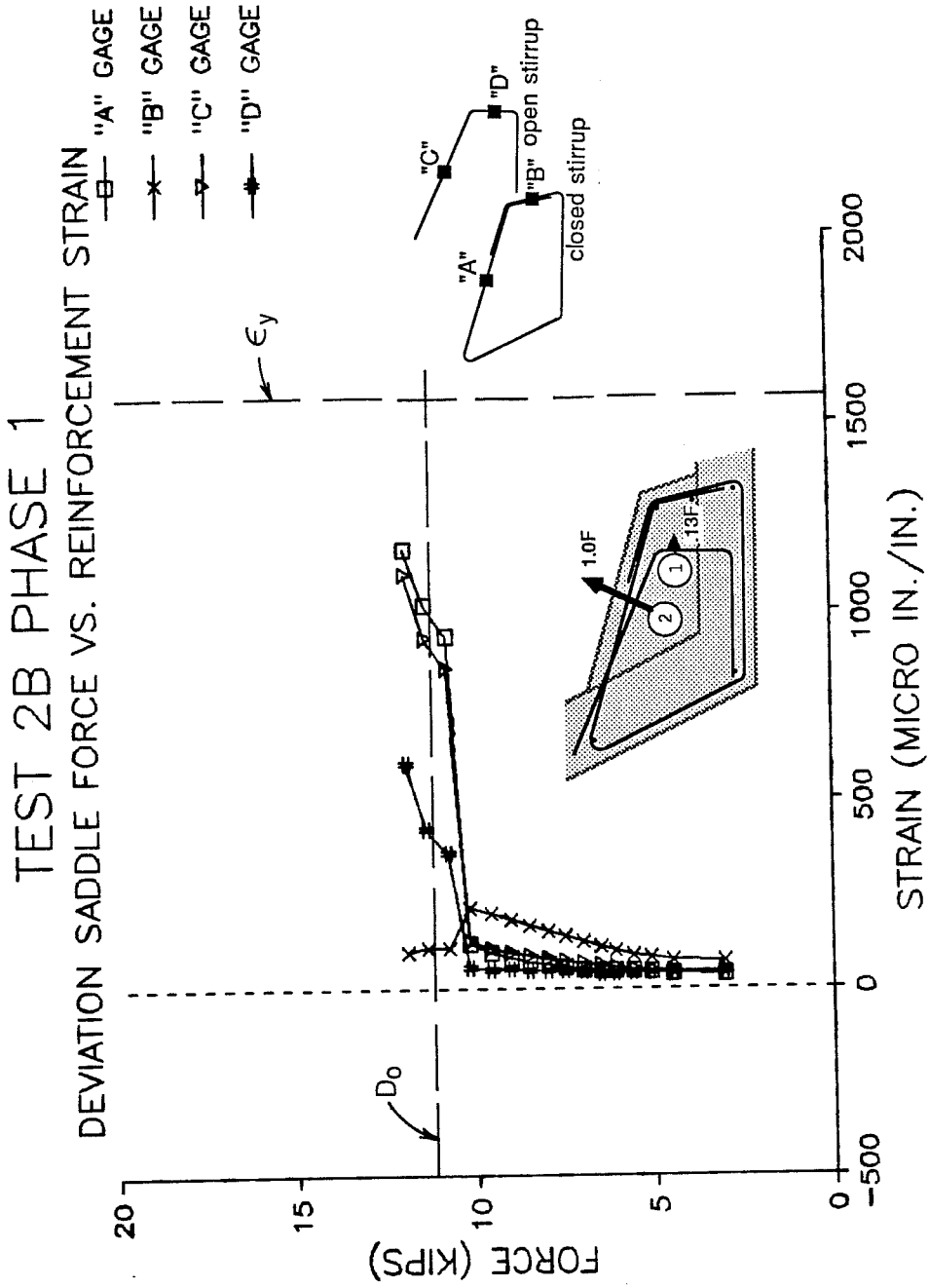


Figure 3.27 Test 2B Reinforcement Strain Data - Phase 1

2) The strain began to decrease in the reinforcement in the front face ("B" gage) after the top surface cracked at load stage 12.

3) There was also a jump in strain in the vertical leg of the open stirrup ("D") at load stage 13.

The ultimate loading phase 2 strain data (Fig. 3.28) observations are as follows:

1) The top surface reinforcement ("A", "C" gages) had the highest strain and reached yield during this phase.

2) The "D" gage on the vertical leg of the open stirrup failed during this phase, so it is not possible to know if this location yielded.

3) The reinforcement in the front face ("B" gage) did not yield.

A reasonable explanation of the strain data is that a bending element formed above the ducts which strained the top surface reinforcement. The strain in the vertical leg of the open stirrup and the reinforcement in the front face was due to direct tension and shear friction.

The reinforcement failure locations are shown in Fig. 3.29. The lap splice on the outer stirrup was the weakest junction in this specimen. The before and after photographs show the tension net that formed after the top surface collapse (Fig. 3.30). Again as in test 2A, the strength is compared to the D_0 of the complete prototype detail (Fig. 3.31) even though the two types of stirrups were placed

TEST 2B PHASE 2

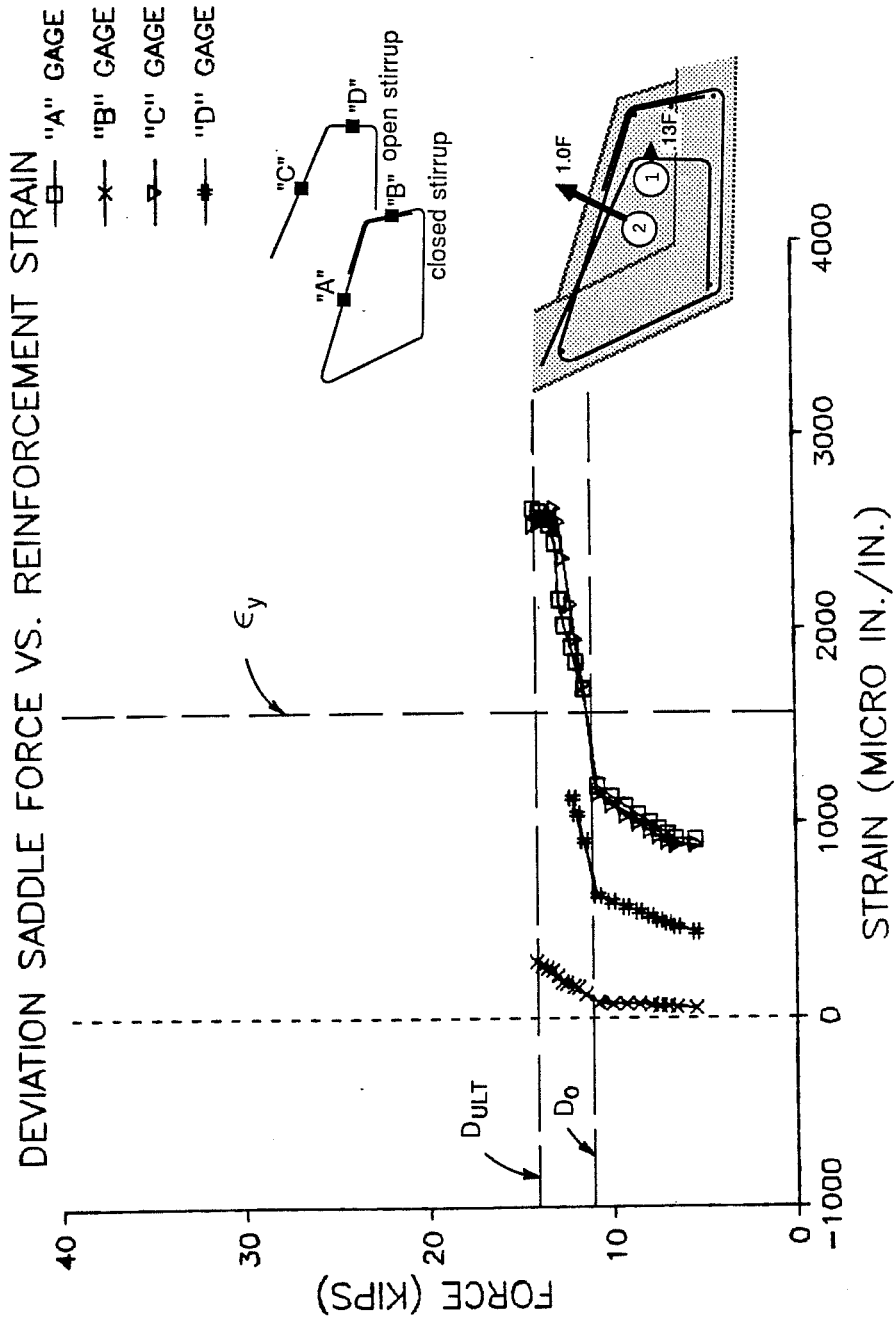
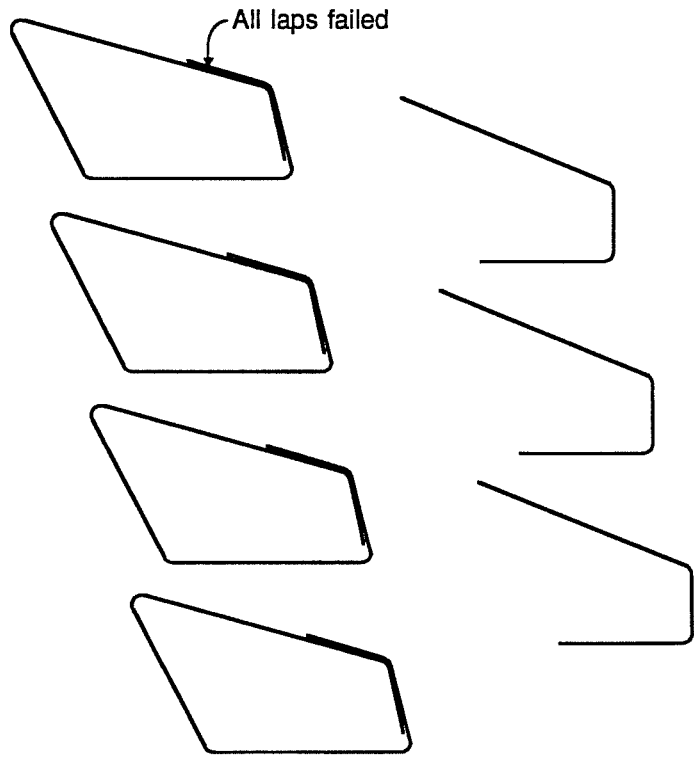


Figure 3.28 Test 2B Reinforcement Strain Data - Phase 2

"A" Side



"B" Side (Refer to Figure 2.14b)

Figure 3.29 Test 2B Reinforcement Failure Locations

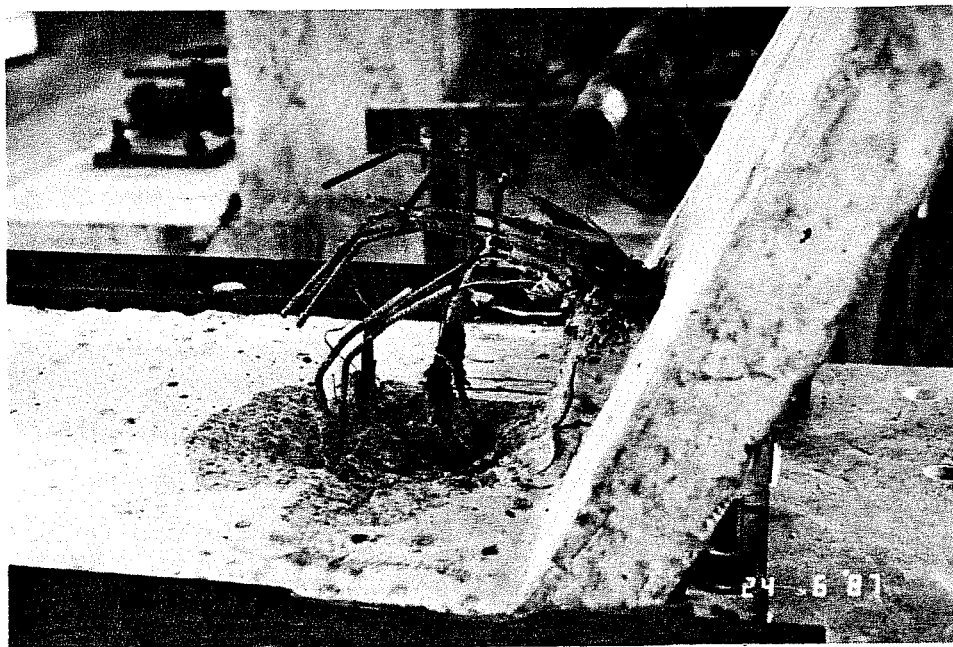
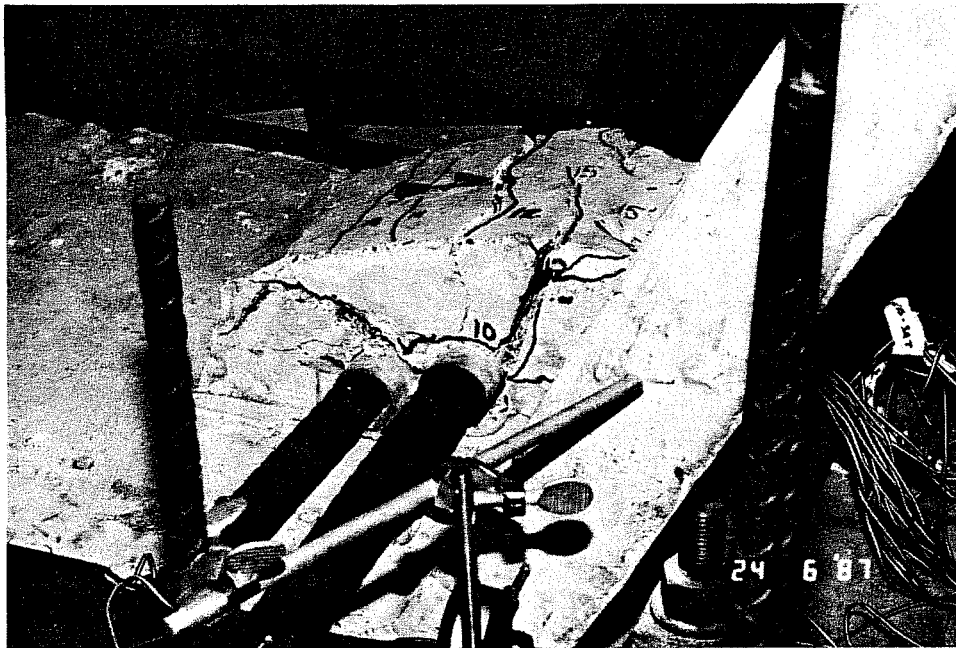


Figure 3.30 Test 2B - Before and After Failure

TEST 2B
RATIO D/D_o AT CRITICAL STAGES

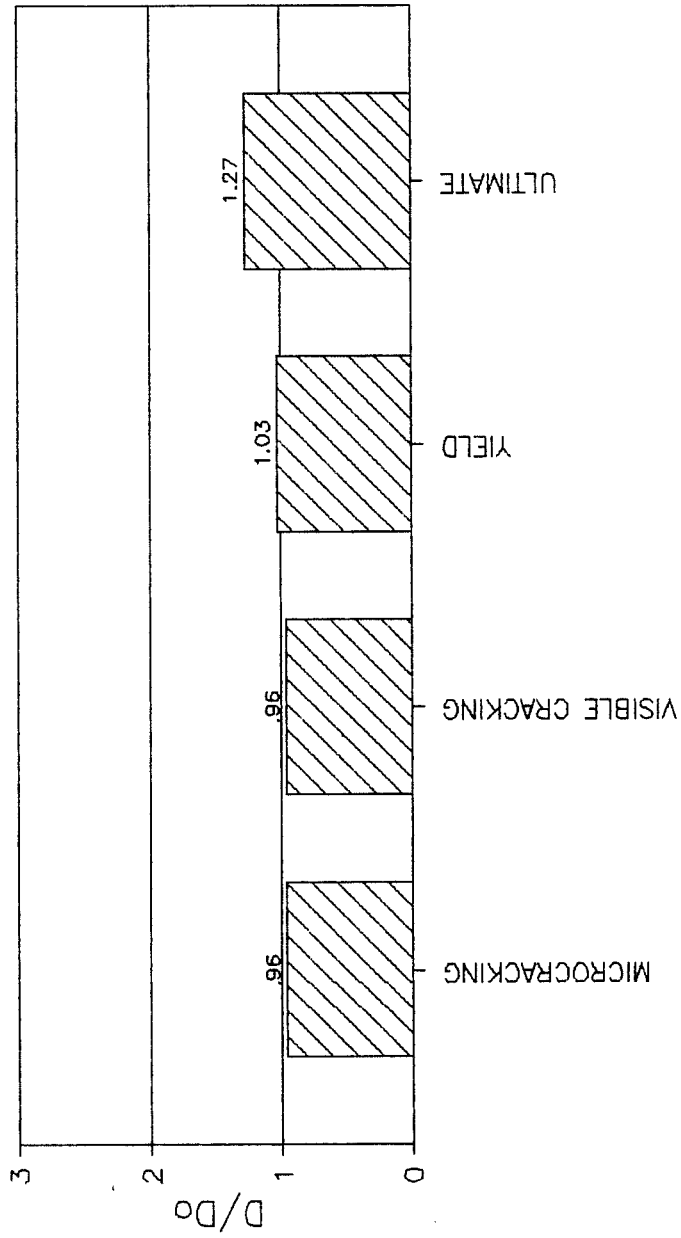


Figure 3.31 Test 2B Strength Comparison

without the link bar. The bar graph shows that the ultimate strength is sufficient, but the factor of safety is too low. Cracking would occur under nominal design load conditions.

3.6 Test 3A-Epoxy Coated Link Bar with Stirrups-Companion Test of Test 1A

The objective of specimen 3A was to determine if epoxy coated reinforcement has any effect on the behavior and strength of a deviation saddle. This test is a direct comparison test with test 1A. Refer to Sec. 3.12 for a comparison between epoxy coated and uncoated reinforcement. The only difference in the specimens should have been that this reinforcement was epoxy coated, but other differences developed that were not apparent until after fabrication. These included the placement of a reinforcement chair at the top surface of the deviation saddle that was not placed in specimen 1A, and also the leading of the strain gage wires out of the specimens at different locations. The strain gage wires came out the top of the deviation saddle in specimen 1A, and they came out the outside of the box section in specimen 3A. Another difference that developed was that the specimen was inadvertently cracked (see Fig. 3.33) when the tendons were placed in the deviation saddle. This may have affected the strain data for phase 1.

The total vector force and direction which acted on the specimen are shown in Fig. 3.32. The crack patterns are shown in Fig.

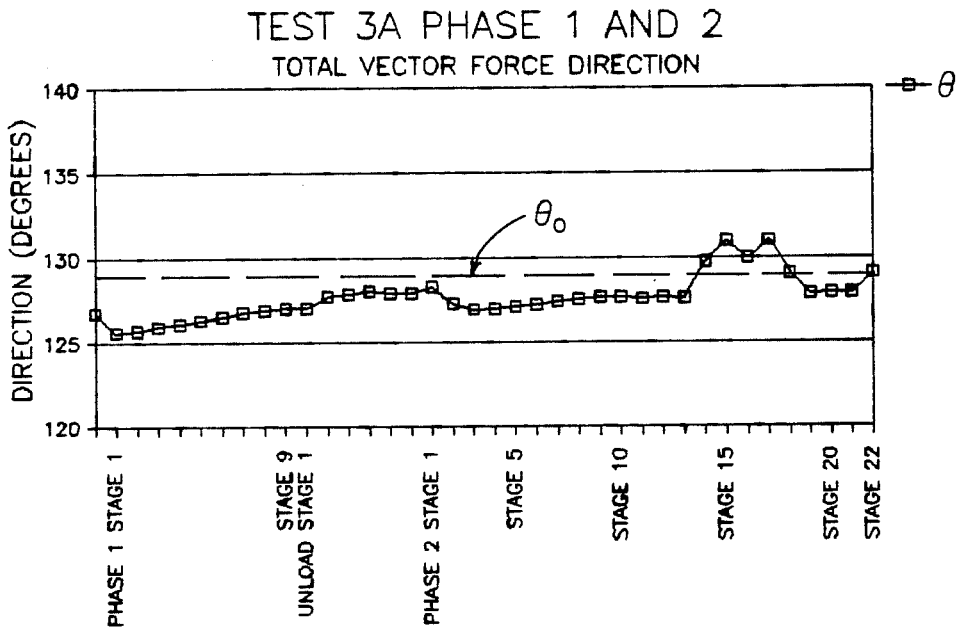
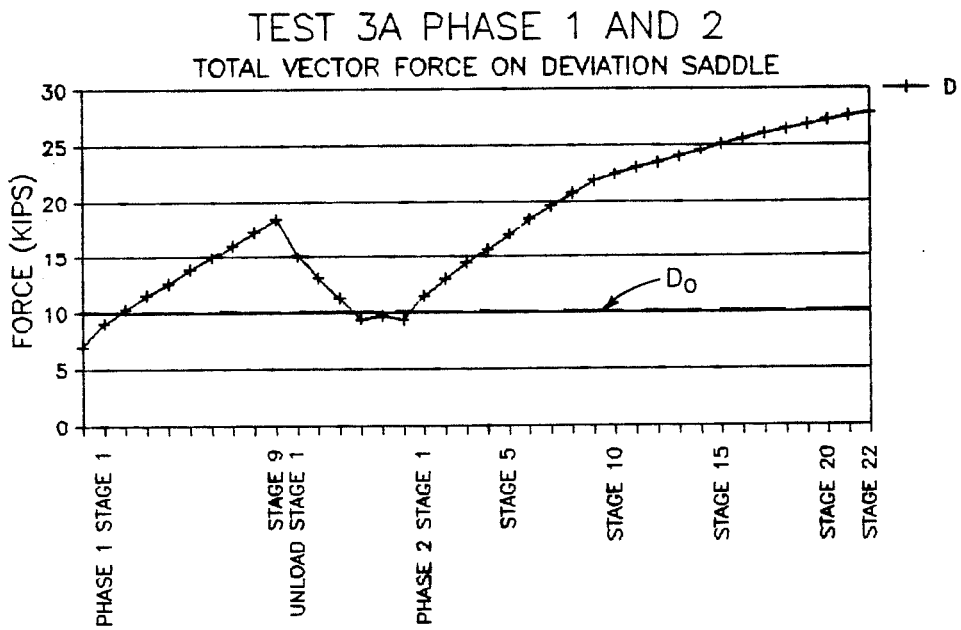


Figure 3.32 Test 3A Loading History

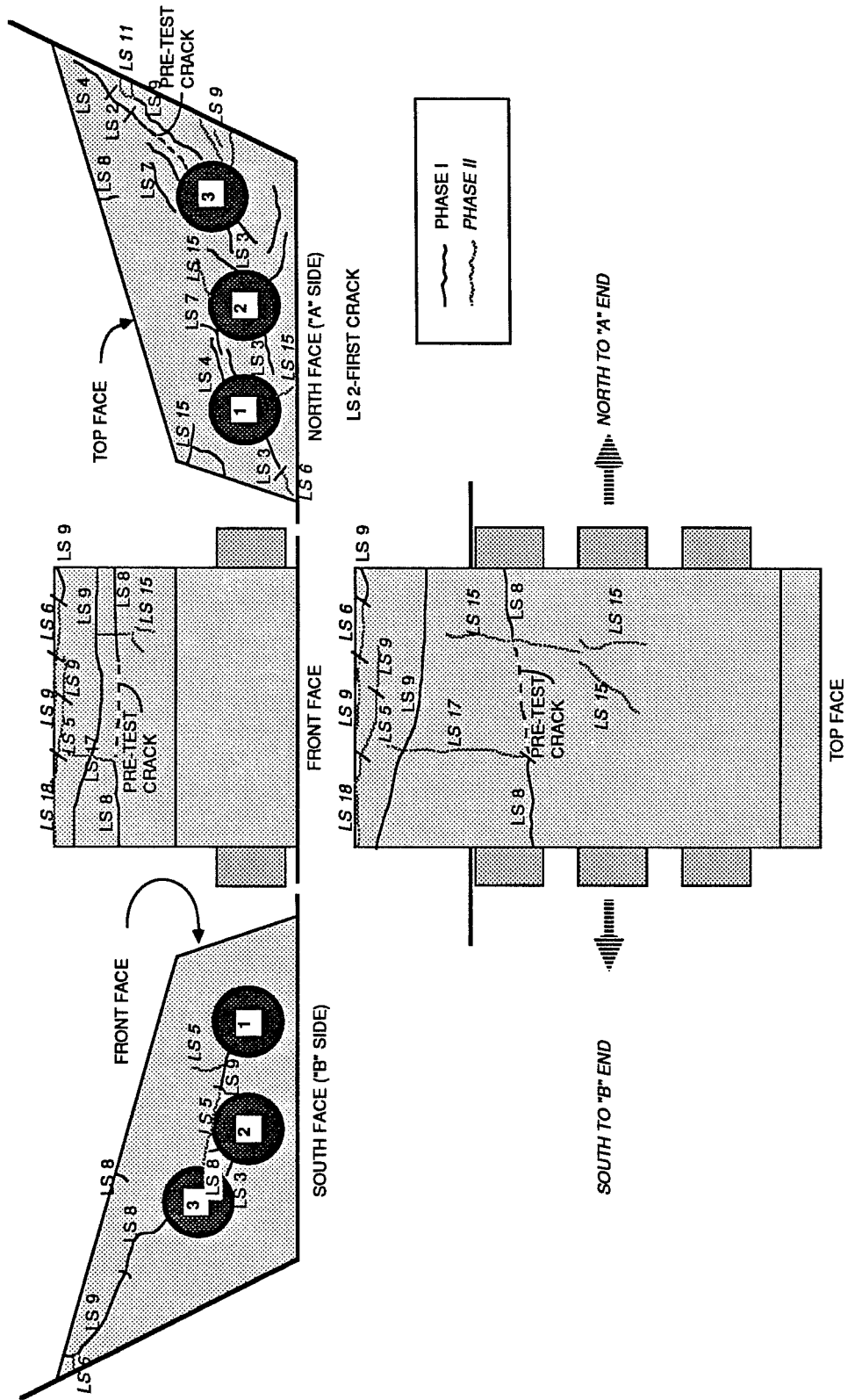


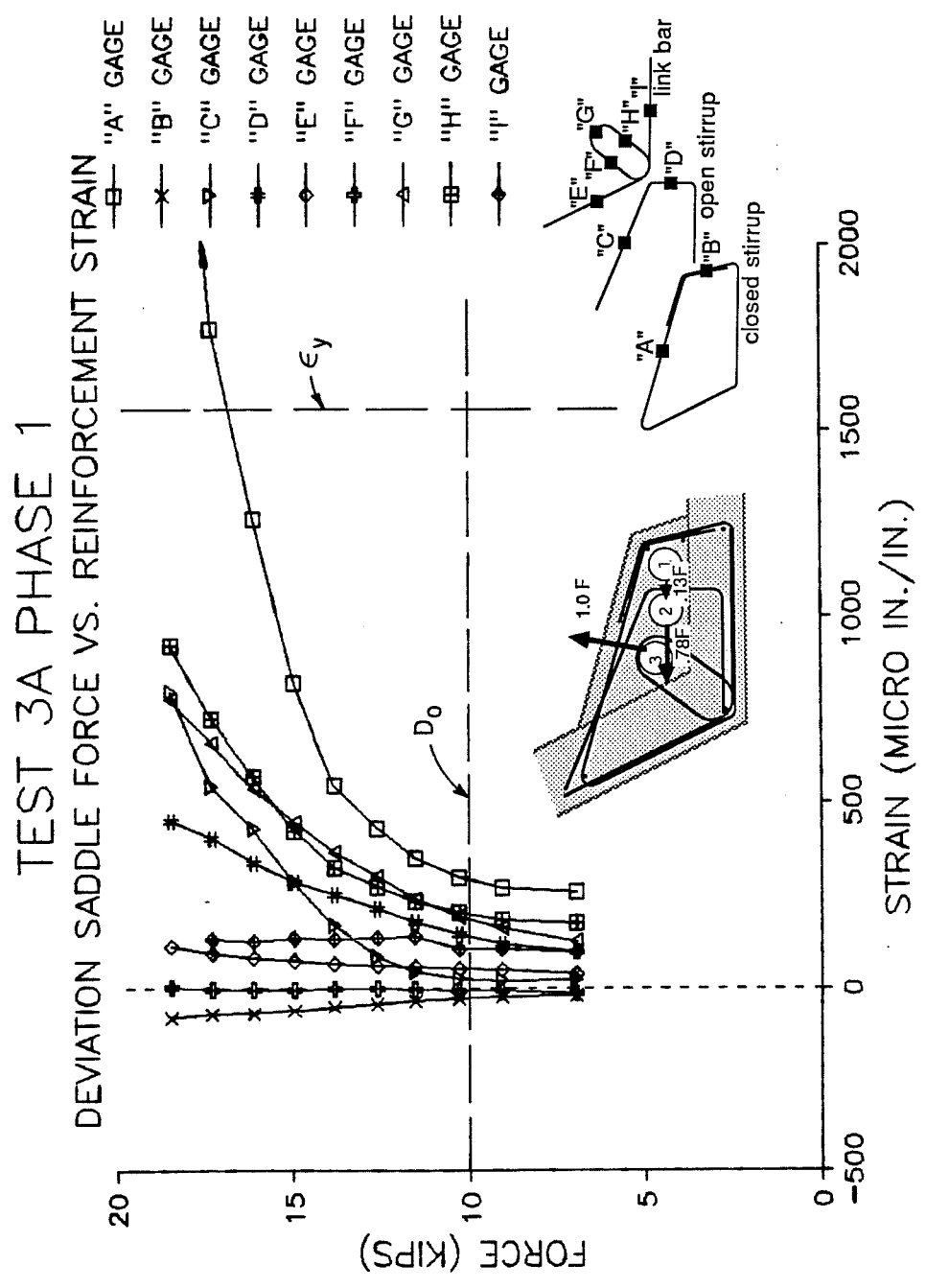
Figure 3.33 Test 3A Crack Patterns

3.33 and are very similar to those of test 1A, but there are more cracks on the side faces than in test 1A. The first crack to form was on the side face of the deviation saddle. As was stated for test 1A, it appears that initial cracking was influenced by the large horizontal force of tendons 1 and 2 and was possibly a splitting crack due to the high compressive force. The same failure mechanism formed as in test 1A, whereby, the top of the deviation saddle (from the tendon ducts up) moved towards the web. Estimated maximum crack width was 1/8 in. at the intersection of the web wall and the top surface of the deviation saddle. Level of ductility appeared to be the same as that of test 1A.

The following observations can be made about the phase 1 strain data shown in Fig. 3.34:

1) The "A" gage located on the reinforcement at the top surface of the deviation saddle was the first to yield, whereas, in test 1A the link bar reinforcement was the first to yield. The "C" gage which was located on the other top surface reinforcement strained much less than the "A" gage. These strains were much higher than the strains at the top surface reinforcement in test 1A.

2) The bottom leg and the top of the link bar ("G", "H" gages) strained while the top leg of the link bar ("F" gage) did not. This was also the case in test 1A and could be due to the location of the "F" gage.



3) The "D" gage located on the vertical leg of the open stirrup strained steadily as in test 1A.

4) The "B" gage located on the front face reinforcement remained in compression during phase 1 which was different from test 1A. This might be attributed to the cracking of the specimen before testing.

5) The "E" and "I" gages which were located on the ends of the link bar strained a small amount. These gage locations were not in specimen 1A.

The observations which can be made for the ultimate loading phase 2 strain data shown in Fig. 3.35 are as follows:

1) The "A" gage on the top surface reinforcement had the highest strain in the deviation saddle. As was observed in test 1A, the strain began to drop off before failure. This was also true for the "C" gage, but the strain was lower. The strain in both gages reached yield during this phase. This did not occur in test 1A.

2) The link bar ("F", "G", "H" gages) did not strain as much as it did in test 1A. The same trend was seen in test 1A with the "F" gage having a low strain until the shear deformation of the failure mechanism started and the strain began increasing. The link bar at the "F" gage and the "H" gage did not yield as they did in test 1A. Only at the "G" gage location did yielding occur.

3) The "D" gage of the vertical leg of the open stirrup had a greater amount of strain than that in test 1A.

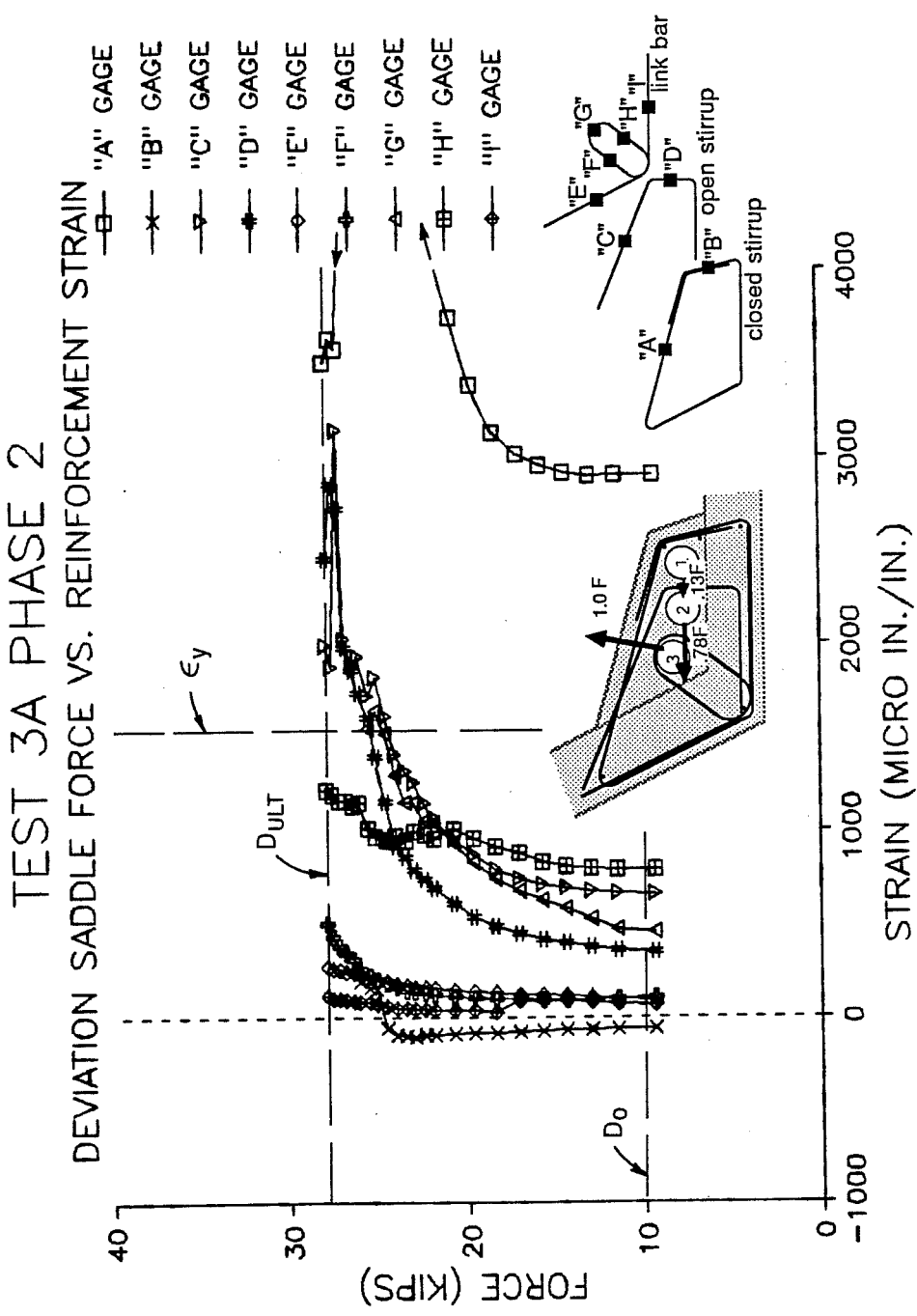


Figure 3.35 Test 3A Reinforcement Strain Data - Phase 2

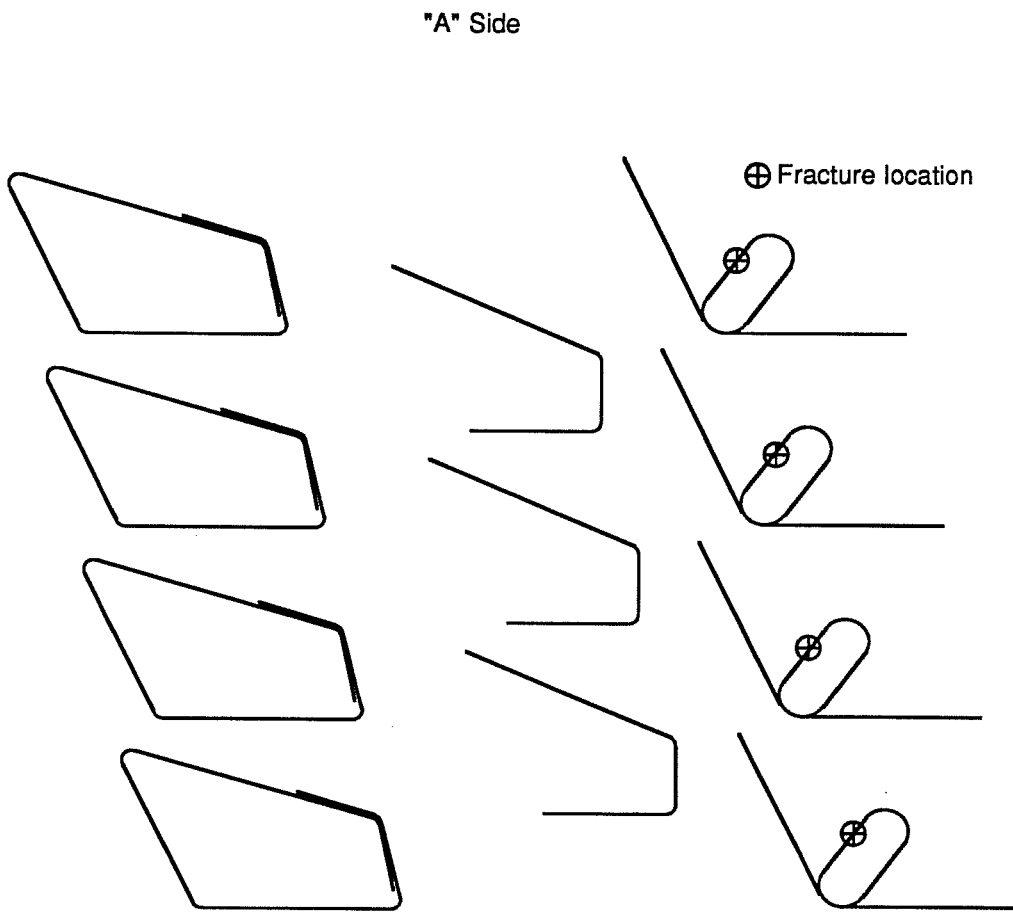
4) The "E" and "I" gage locations on the link bar had strained a small amount as in phase 1.

The conclusions about the reinforcement behavior that can be made with respect to the strain data are basically the same as those of test 1A. The differences were that there was more bending resistance from the top surface reinforcement, and also a redistribution of the strains in the reinforcement that resisted shear friction (some higher and some lower).

The reinforcement failure locations (Fig. 3.36) are strong evidence for the premise that the link bars in addition to resisting direct tension force from tendon 3 also resisted shear friction because they were fractured at the surface of the shear plane. The before and after failure photographs are shown in Fig. 3.37. The comparisons of strength are made in the bar graph shown in Fig 3.38. There was no apparent jump in strain gage values, so microcracking was not noted. The D/D_0 ratio for visible cracking reveals a low factor of safety. However, this detail has an adequate factor of safety against yielding and failure. There is significant ductility which is indicated by the large difference in the D/D_0 ratios for yield and ultimate and the size of the crack widths.

3.7 Test 3B-Epoxy Coated Link Bar with Stirrups-Companion Test of Test 1B

The objective of specimen 3B was to determine if epoxy coated reinforcement has any effect on the behavior and strength of a



"B" Side (Refer to Figure 2.14b)

Figure 3.36 Test 3A Reinforcement Failure Locations

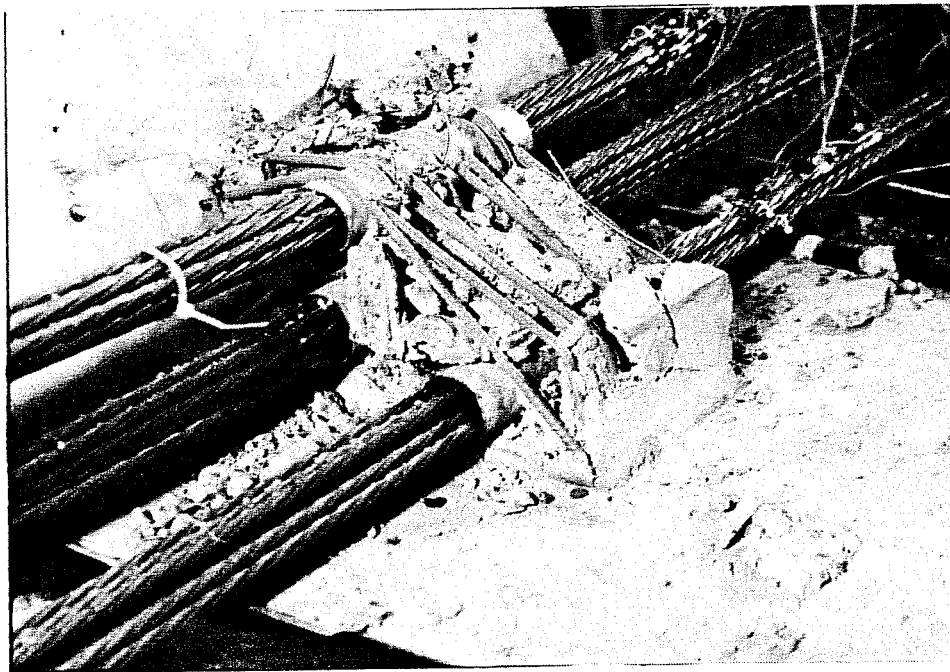
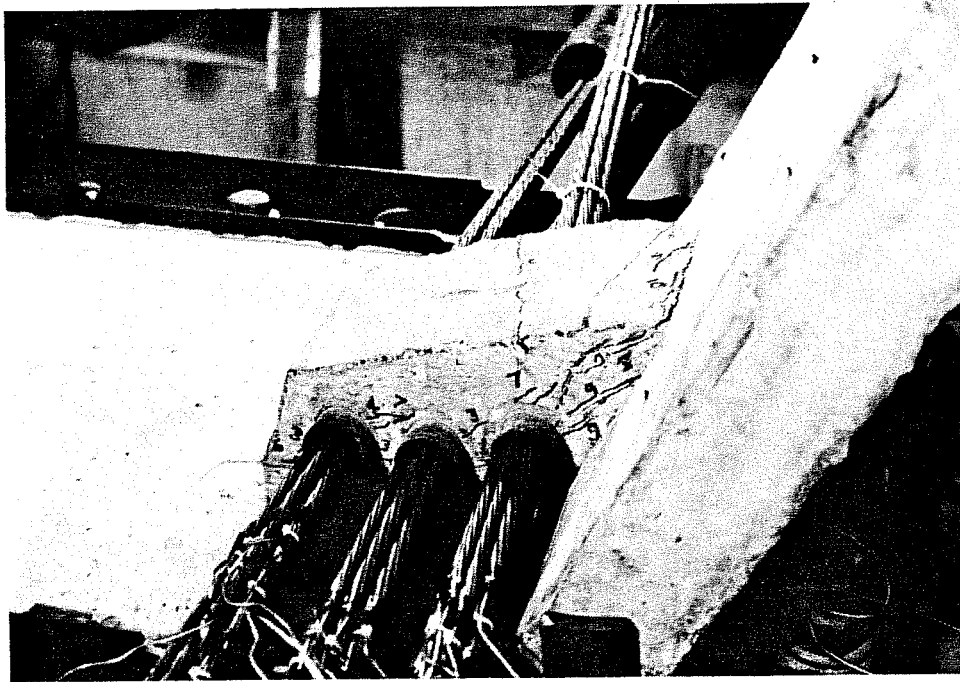


Figure 3.37 Test 3A - Before and After Failure

TEST 3A
RATIO D/D₀ AT CRITICAL STAGES

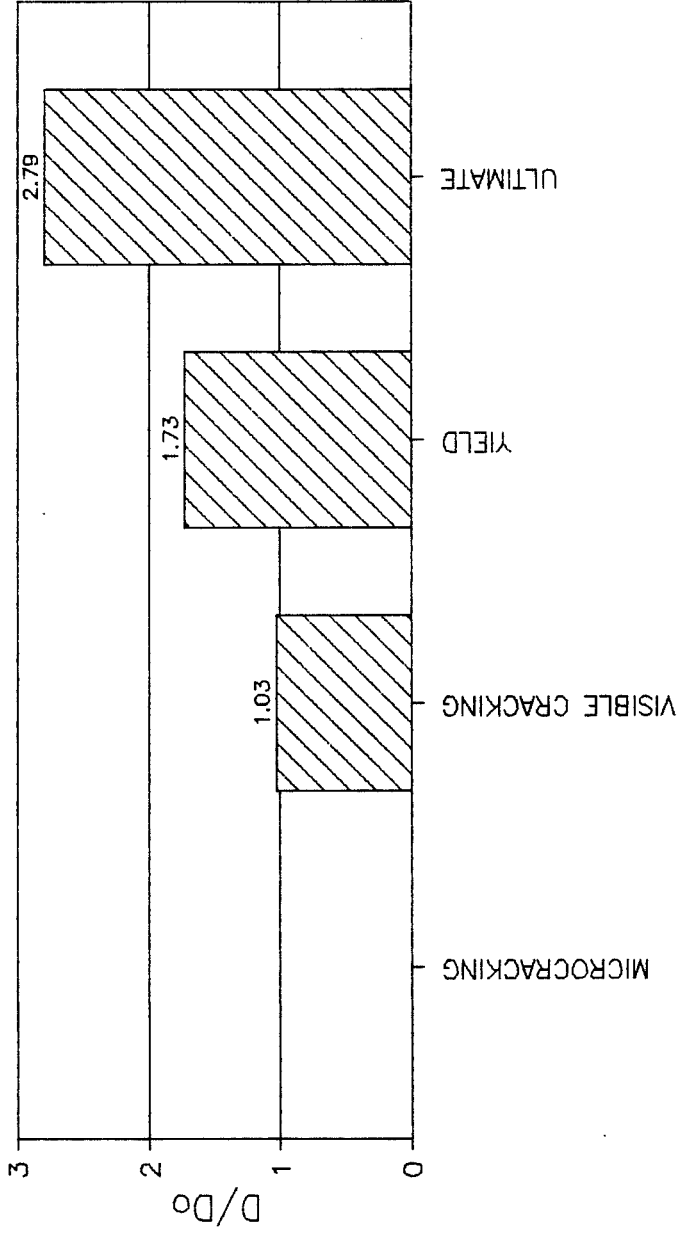


Figure 3.38 Test 3A Strength Comparison

deviation saddle. As in test 3A, this test is a direct comparison test of test 1B except with epoxy coated reinforcement. Refer to Sec. 3.12 for the comparison of epoxy coated and uncoated reinforcement. The same minor inconsistencies of an extra bar chair and changed lead wire locations were present between this specimen and specimen 1B as were mentioned for specimen 1A and 3A.

The total vector force and direction which acted on the specimen are shown in Figs. 3.39 and 3.40. There were three loading stages for phase 1 (1(a),1(b),1(c)) because of two unsuccessful attempts to fail the specimen due to insufficient tendon capacity. The crack patterns for this test shown in Fig. 3.41 are similar to those of test 1B. The first crack formed on the top surface and down the sides of the deviation saddle above tendon 2. Estimated maximum crack width was 0.02 in. Level of ductility appeared to be the same as that of test 1B.

The observations for the strain data of all of phase 1 (Figs. 3.42 through 3.44) are as follows:

- 1) The "A" gage of the top surface reinforcement had the highest strain of all gages. It was the first gage to yield as was the case in test 1B. The "C" gage of the other top surface reinforcement had a lower strain. In phase 1(c), the "A" gage strain was four times as high as that of test 1B.

- 2) The strain jumped in all three gages of the link bar ("F", "G", "H" gages) at load stage 5 of phase 1(a). This is unlike test 2A

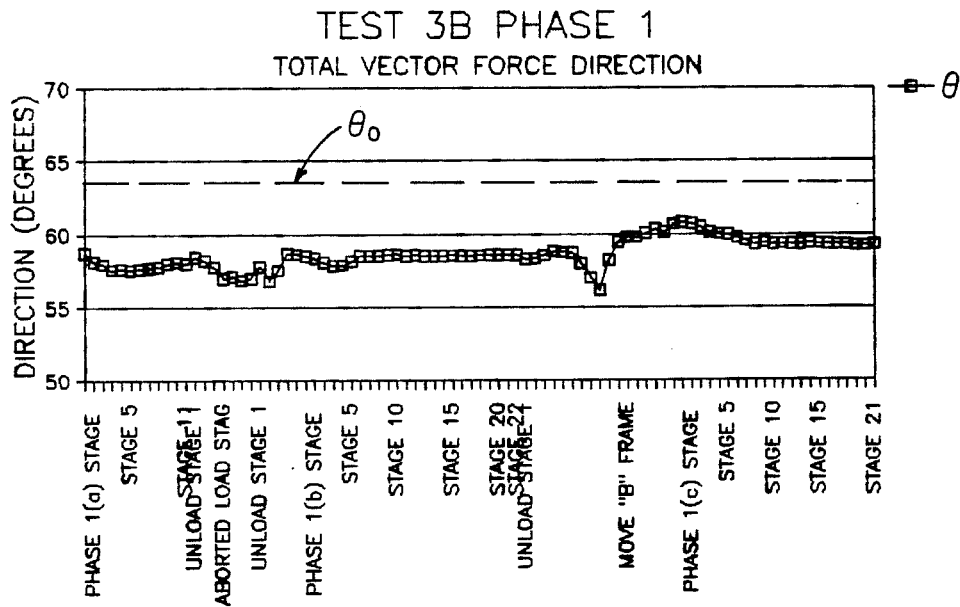
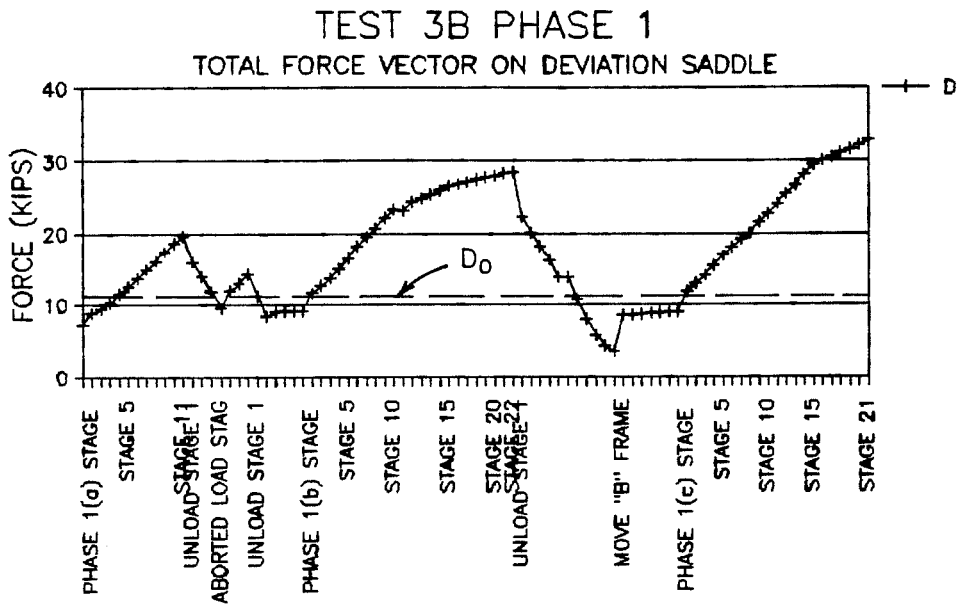


Figure 3.39 Test 3B Loading History - Phase 1

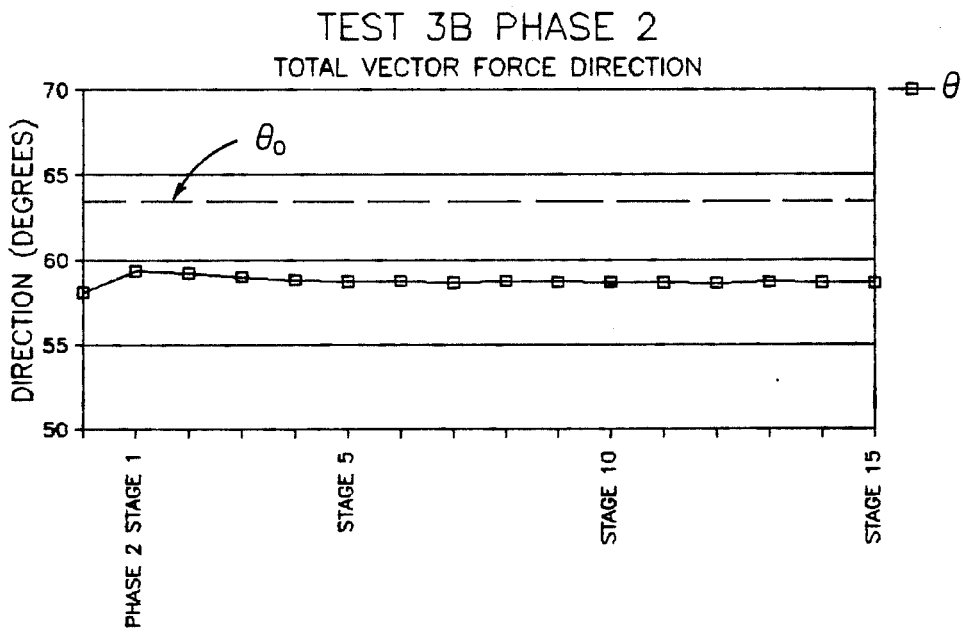
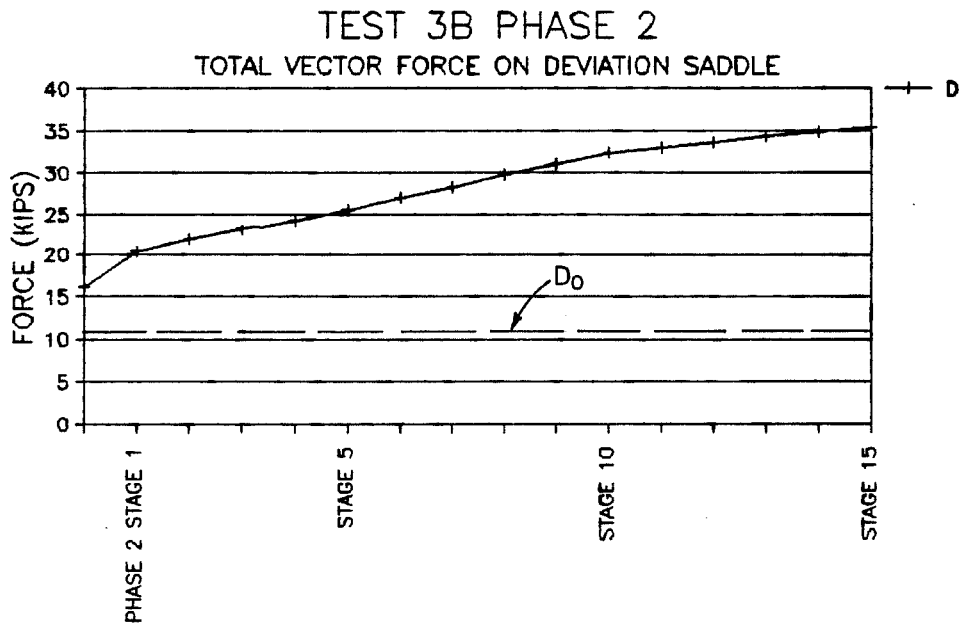


Figure 3.40 Test 3B Loading History - Phase 2

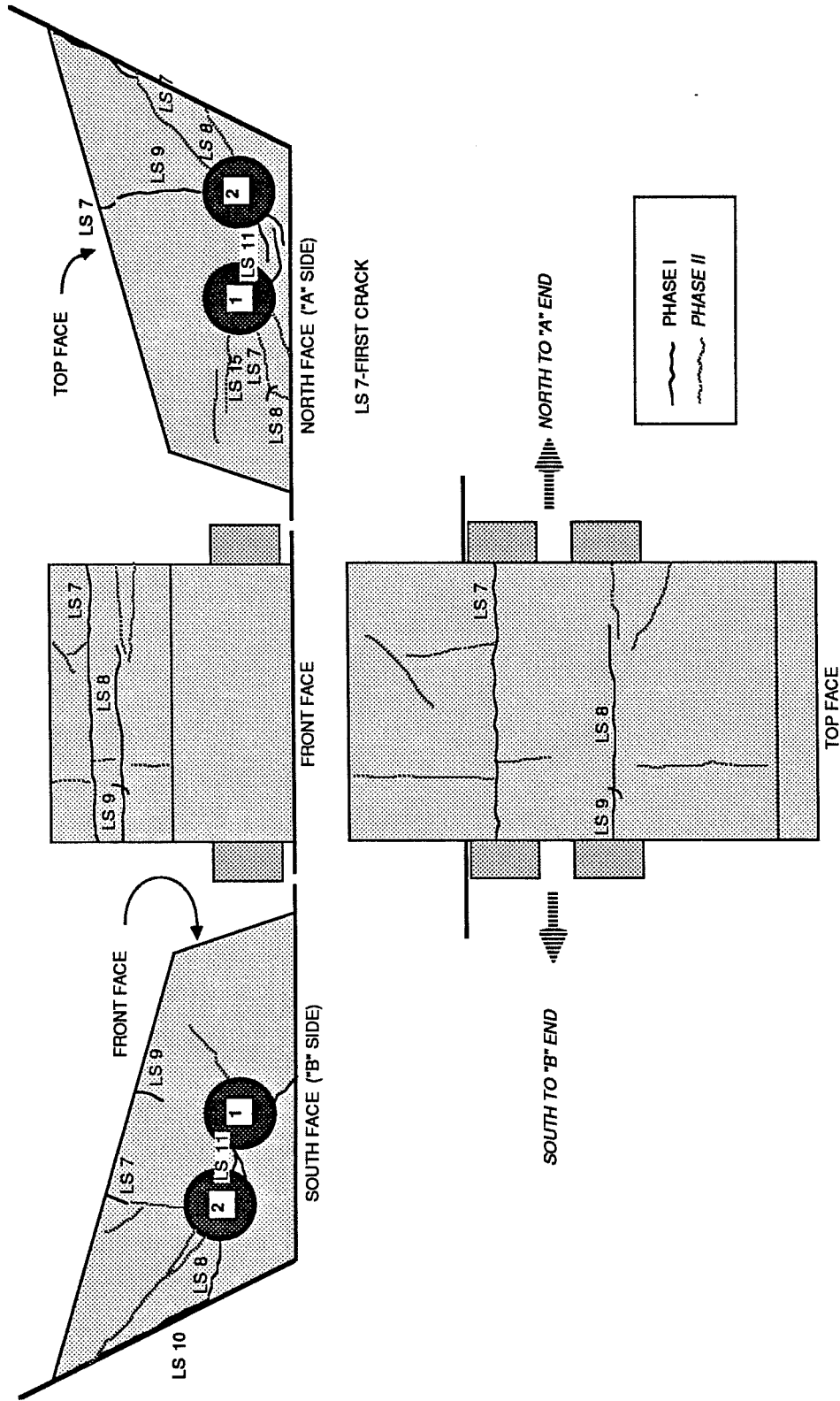


Figure 3.41 Test 3B Crack Patterns

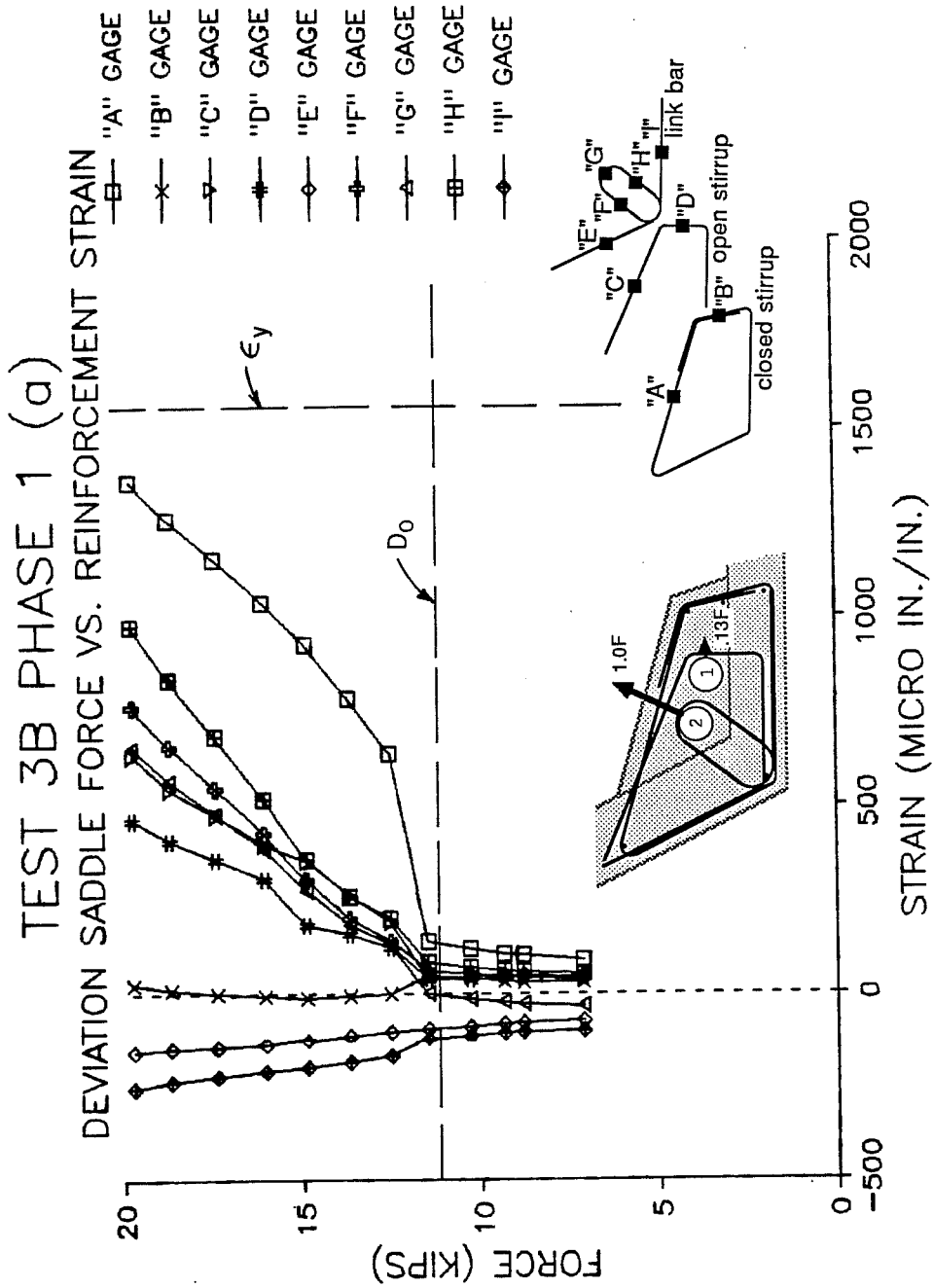


Figure 3.42 Test 3B Reinforcement Strain Data - Phase 1 (a)

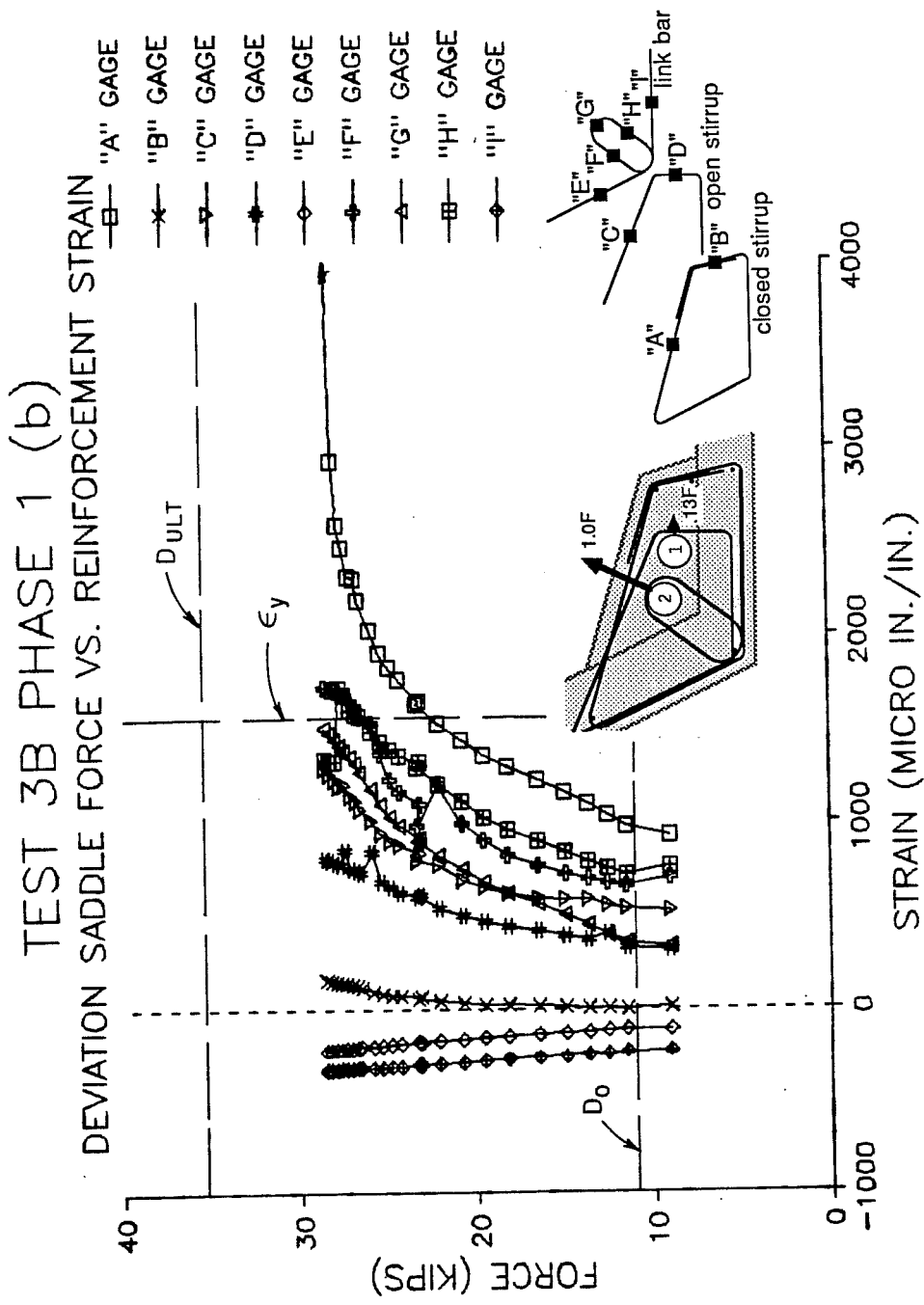
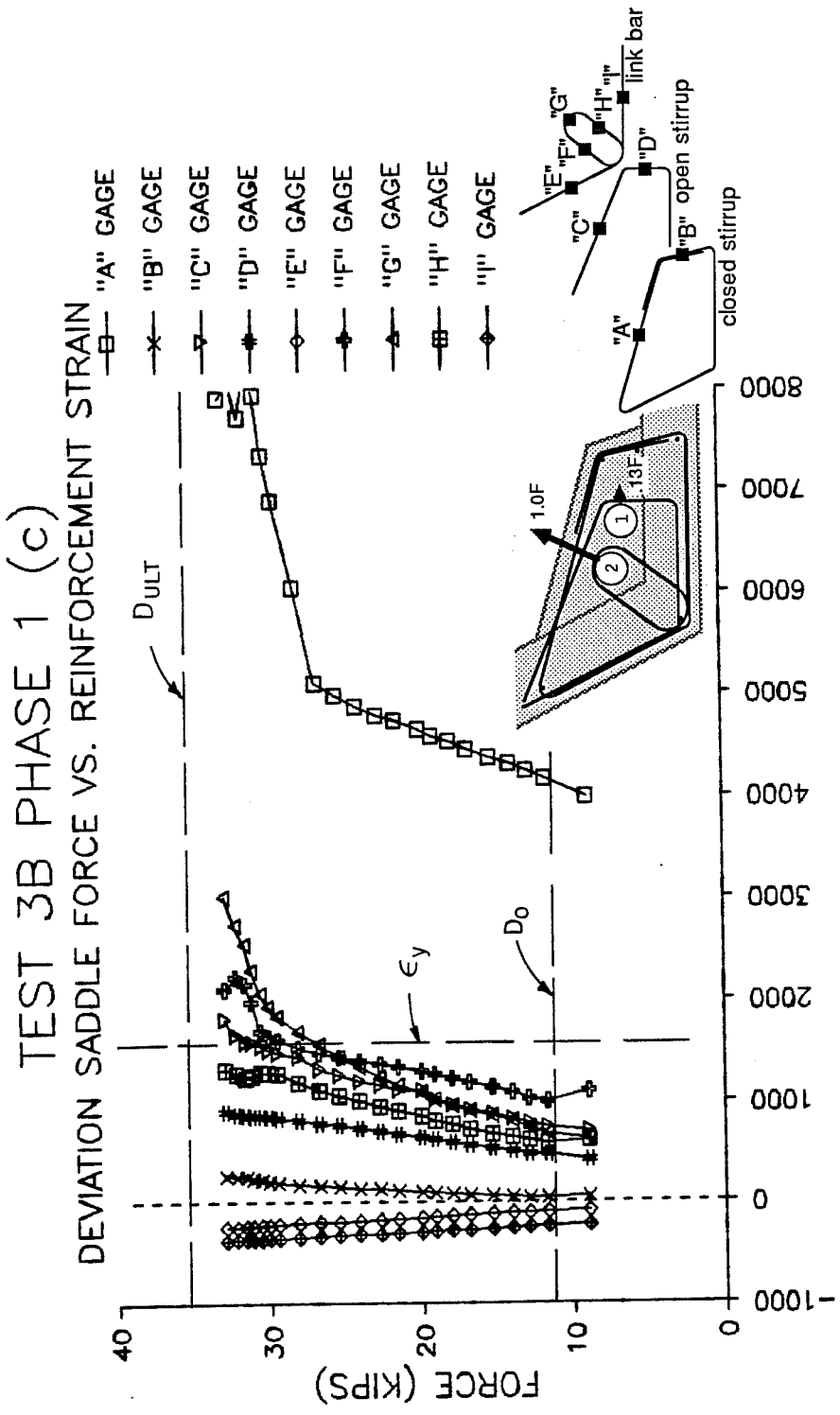


Figure 3.43 Test 3B Reinforcement Strain Data - Phase 1 (b)



STRAIN (MICRO IN./IN.)

Figure 3.44 Test 3B Reinforcement Strain Data - Phase 1 (c)

where the "F" gage did not appreciably strain until phase 2. A comparison cannot be made with test 1B because its "F" gage had failed. The link bar yielded in phase 1(b).

3) The "D" gage of the vertical leg of the open stirrup strained steadily in all three phases, but it did not yield. In test 1B, the "D" gage did not strain until the second load stage. The "B" gage at the front face of deviation saddle strained very little. The strain of gage "B" reduced after microcracking as was apparent in test 1B.

4) The "E" and "I" gages at the ends of the link bar remained in compression. These gage locations did not exist in test 1B.

The observations that can be made about the strain data for the ultimate loading phase 2 (Fig. 3.45) are as follows:

1) As in phase 1, the strain was greatest in the "A" gage of the top surface reinforcement. This strain was three times greater than that of test 1B. The "C" gage which was on the other top surface reinforcement increased greatly several load stages before failure. The "A" gage appeared to have failed several load stages before failure.

2) All locations on the link bar ("F", "G", "H" gages) yielded as was the case in phase 1.

3) The "D" gage of the vertical leg of the open stirrup strained steadily until failure of the specimen, as it did in test 1B, but it did not yield.

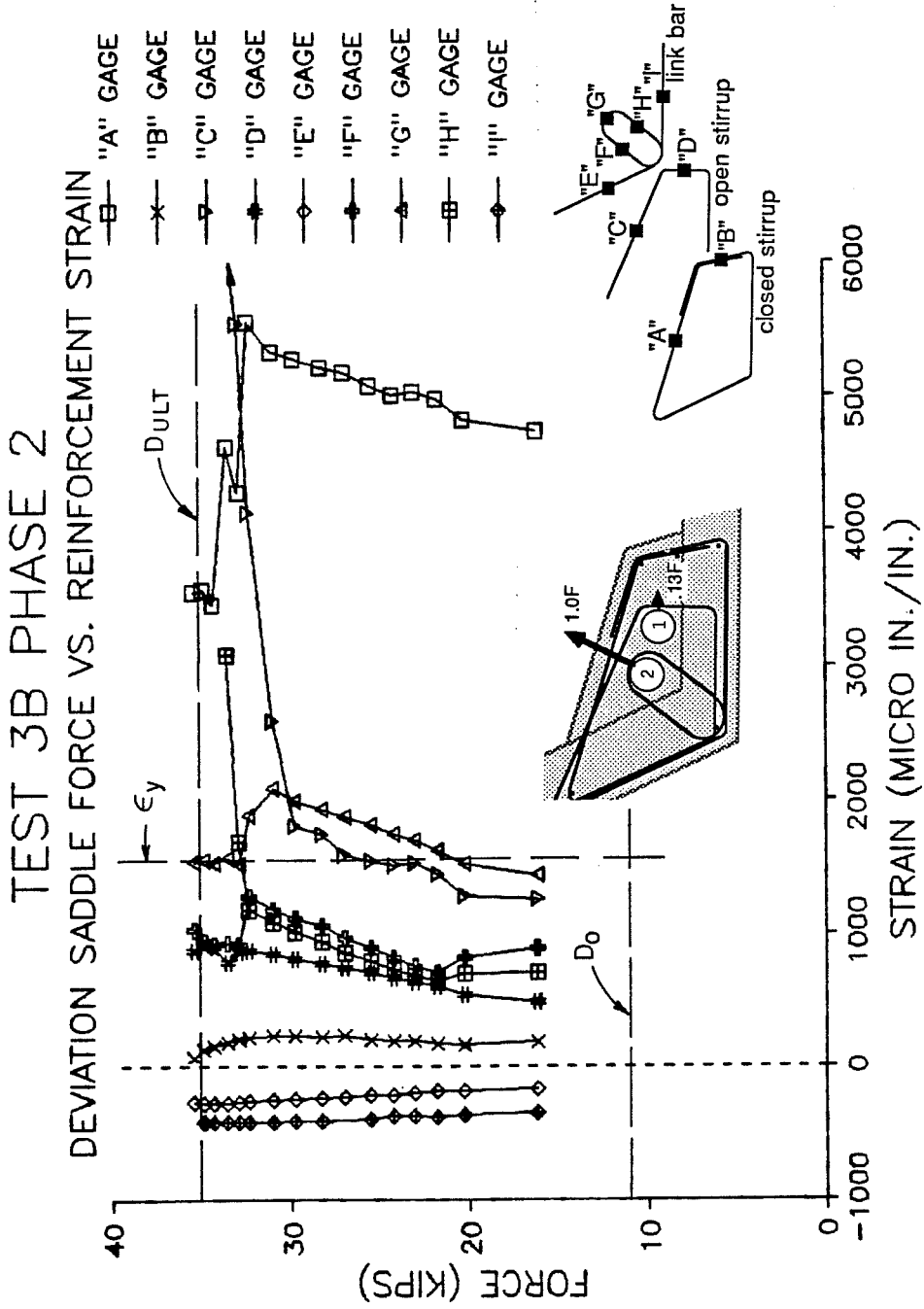


Figure 3.45 Test 3B Reinforcement Strain Data - Phase 2

4) The strain in the "B" gage on the reinforcement in the front face remained at a low strain during this phase and was almost at zero strain at failure. This was not the case in test 1B where the strain was somewhat higher.

5) The "E" and "I" gages of the link bar remained in compression.

The conclusions about the reinforcement behavior with respect to the strain data are basically the same as those of test 1B, although there were some differences. The strains were significantly greater in the top surface reinforcement. The great increase in strain in the open stirrup ("C" gage) near failure must be related to the pullout of this bar from the web wall. The early increase in strain in some gages that did not strain until higher loads in test 1B must be associated with the lower bond between the concrete and the reinforcement. The ends of the link bar ("E", "I" gages) remained in compression because the bottom flange and the web were being compressed, and possibly the link bar stress had developed closer to the hook location.

The reinforcement failure locations are shown in Fig. 3.46. The failure was typical of the other failures which had the same tendon configuration except that the open stirrup had pulled out from the web wall indicating some development insufficiency. The before and after photographs are shown in Fig. 3.47. The strength comparisons are shown in Fig. 3.48. The detail is adequately safeguarded against

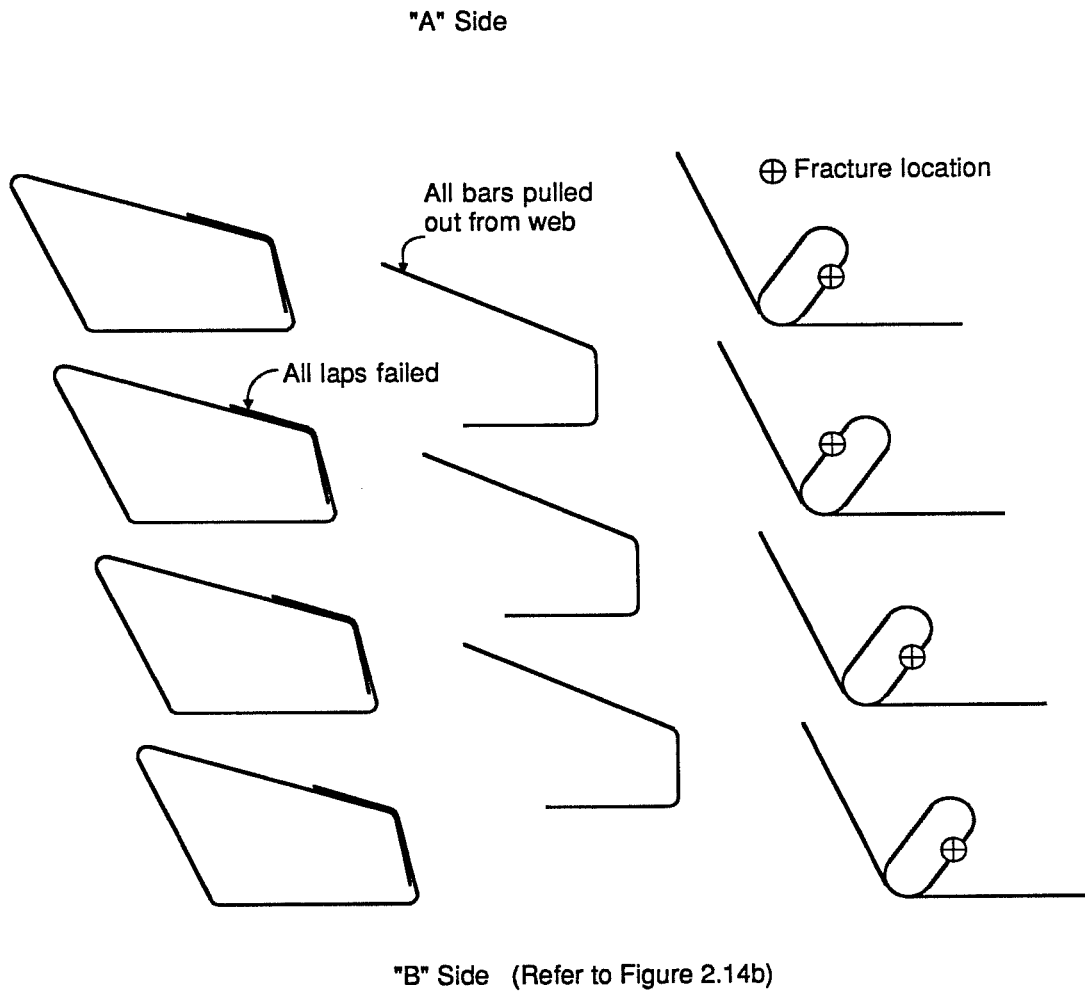


Figure 3.46 Test 3B Reinforcement Failure Locations

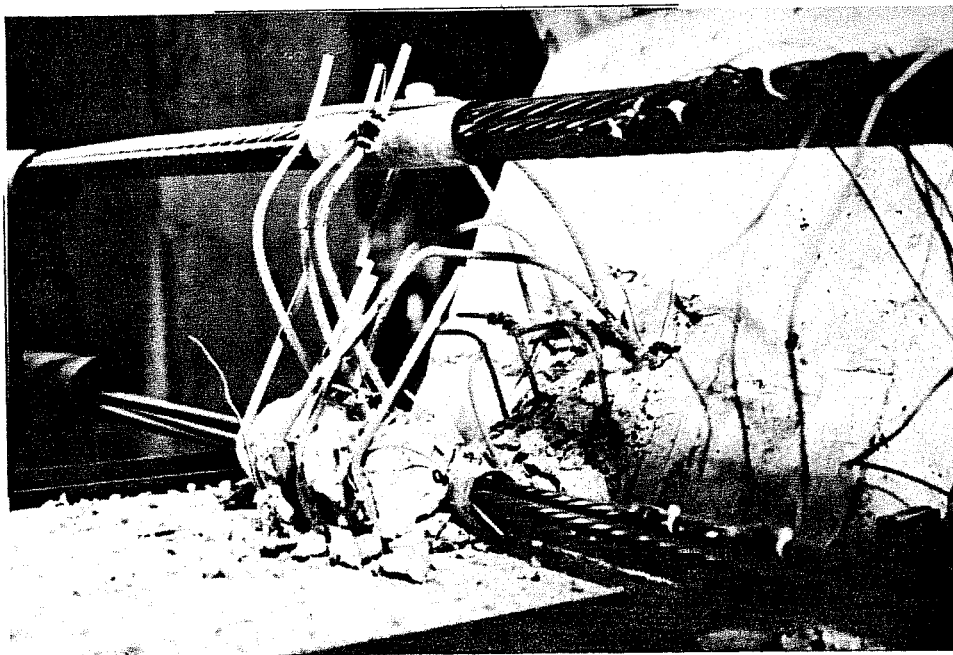
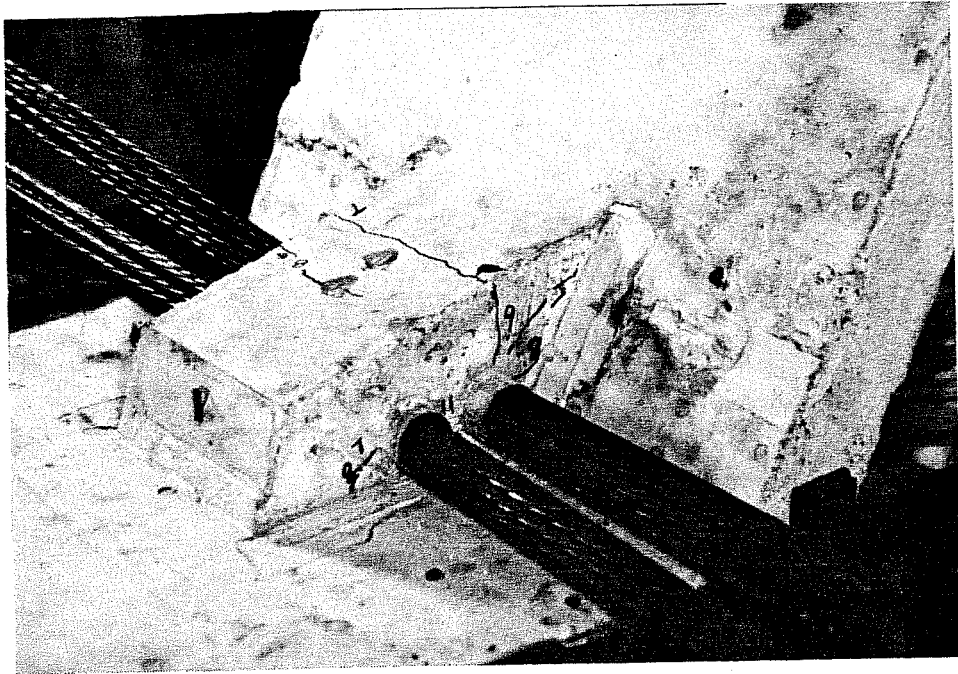


Figure 3.47 Test 3B - Before and After Failure

TEST 3B
RATIO D/D₀ AT CRITICAL STAGES

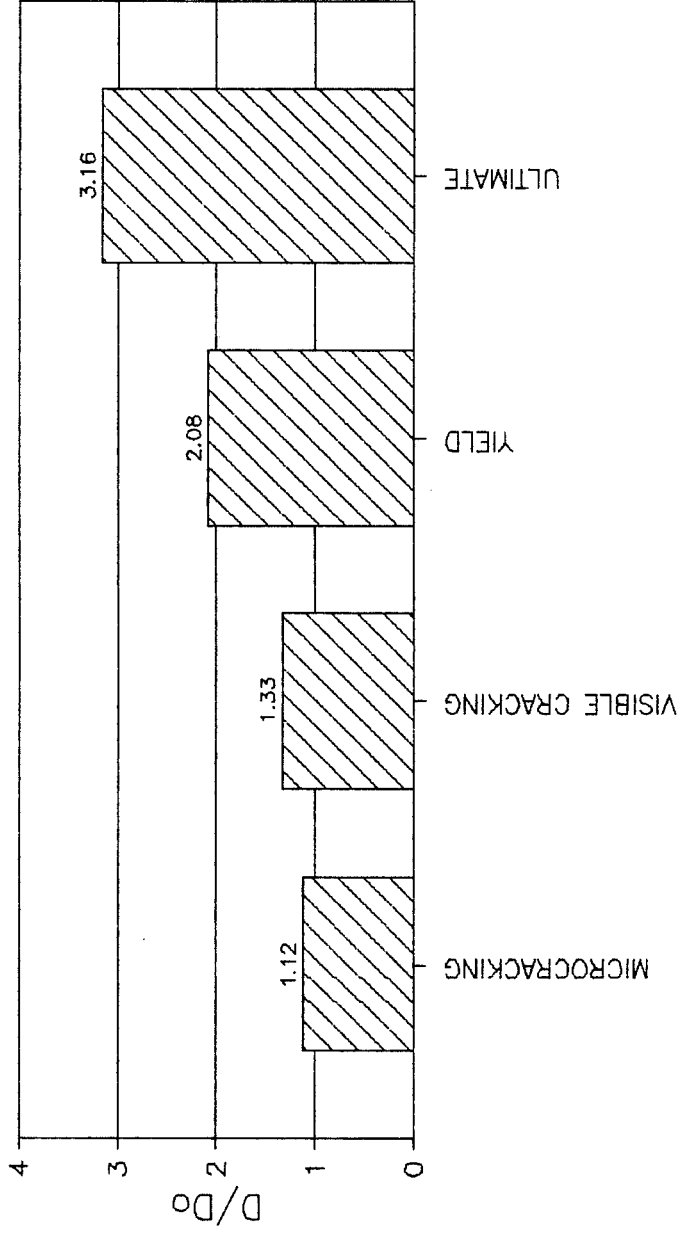


Figure 3.48 Test 3B Strength Comparison

cracking, and it has a ample factor of safety against yielding and failure. The specimen was not ductile, even though there is a large difference between the D/D_0 ratio for yield and ultimate. The cracks were very small and there was little sign of impending failure in the specimen.

3.8 Test 4A-Uncoated Tendon Loop Bars with Stirrup-Outside of Curved Span-Two Tendons

The objective of specimen 4A was to evaluate a modified reinforcement scheme and deviation saddle geometry. This was an attempt to standardize reinforcement patterns for typical deviation saddle details. The reinforcement patterns utilized were a small rectangular closed loop which enclosed each tendon and an outer closed stirrup which encloses the entire deviation saddle. These bars were anchored under the top mat of reinforcement of the bottom flange. The tendon configuration was representative of a deviation saddle on the outside of a small radius curve. Both tendons had vertical and horizontal deviations. This detail is discussed in Sec. 2.2.4 and is illustrated in Fig. 2.9a.

The total vector force and direction which acted on the specimen are shown in Fig. 3.49. The crack patterns are shown in Fig. 3.50. The first crack appeared on the top surface of the specimen right above tendon 2. Only one more crack formed in phase 1. In phase 2, a failure mechanism formed in which the front of the deviation saddle from the middle of tendon 2 to the front face remained as one

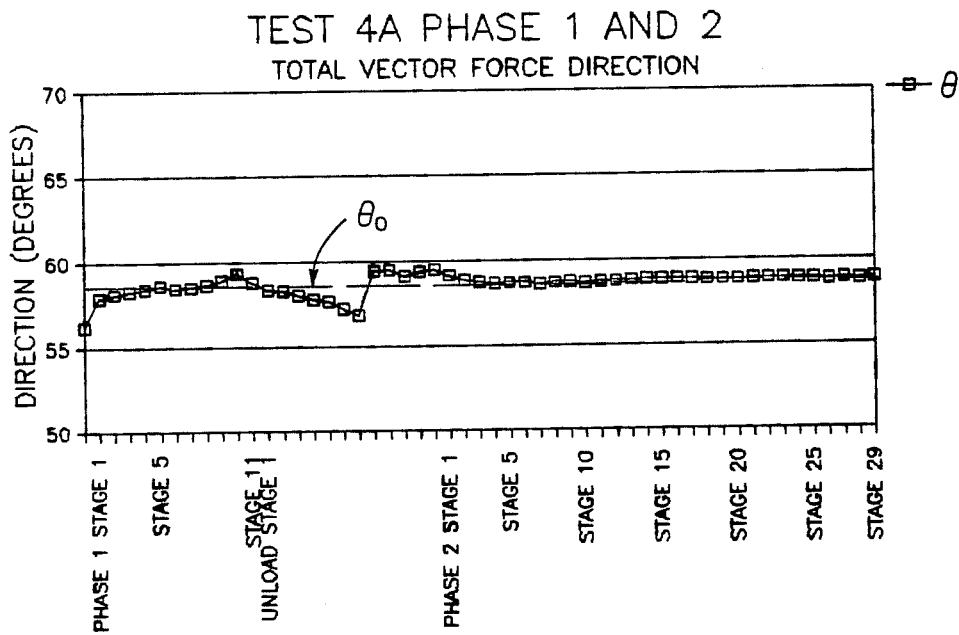
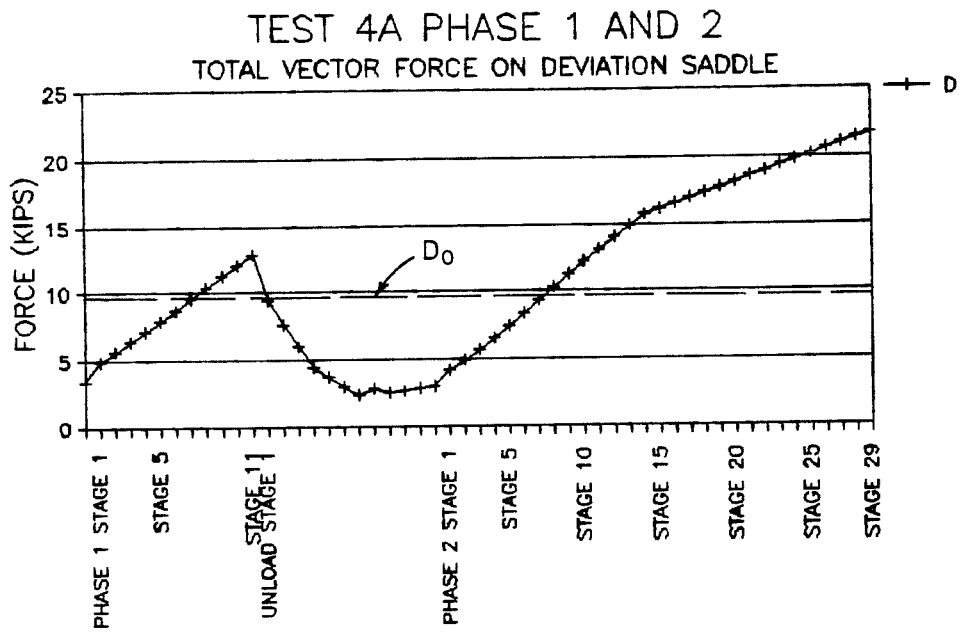


Figure 3.49 Test 4A Loading History

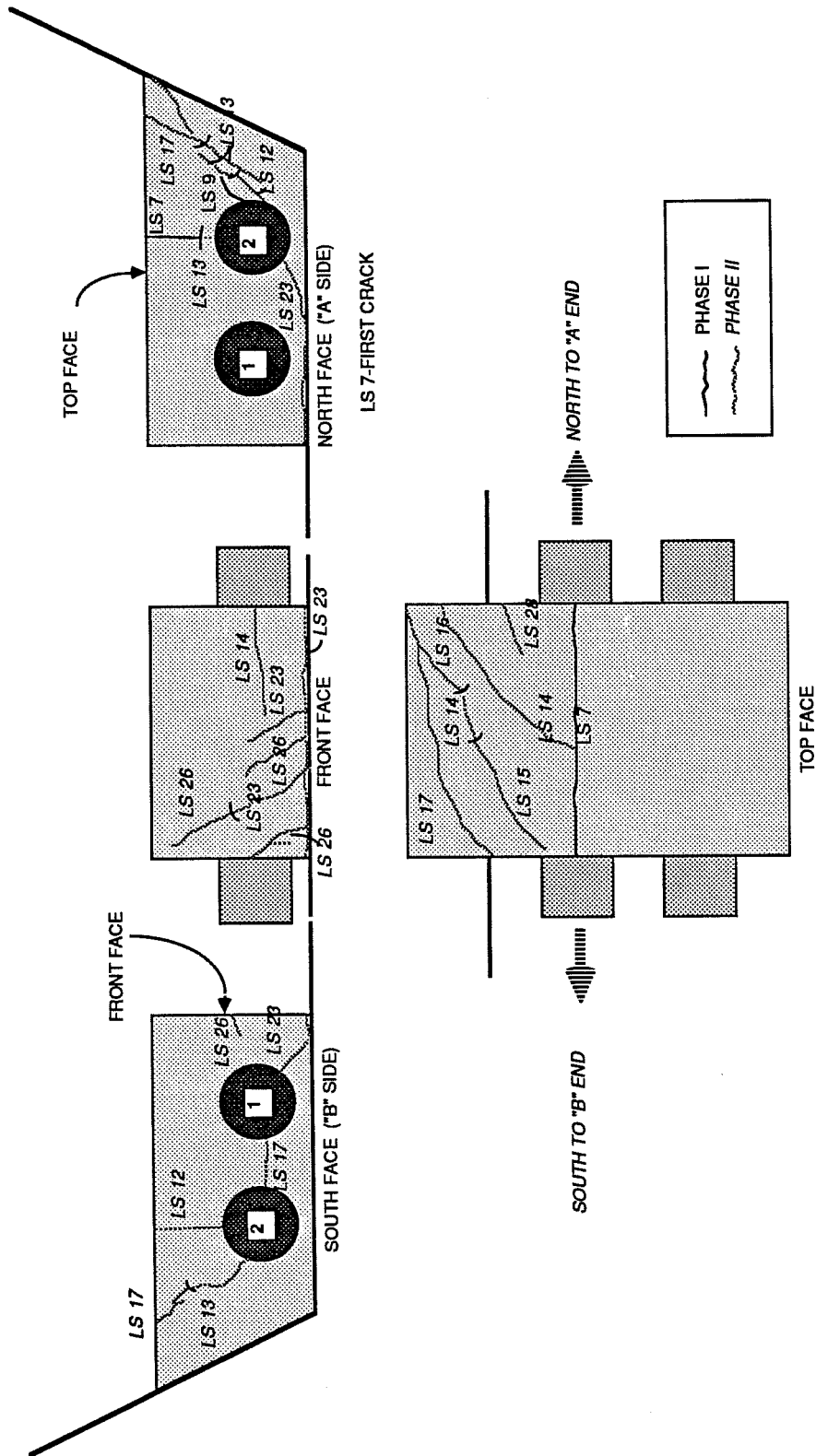


Figure 3.50 Test 4A Crack Patterns

wedge which stayed attached to the front face reinforcement upon failure. Estimated maximum crack width was 1/4 in. at the north side face of the deviation saddle.

It is important to note that after yield of the reinforcement, the strain gages frequently failed. This was due to the smaller bar size used in these specimens. The observations from the phase 1 strain data (Fig. 3.51) are as follows:

- 1) The strain was highest in the reinforcement at the locations of the gages right above tendon 2 ("A", "D" gages). These were the only gage locations that yielded.

- 2) The gages on the vertical bars between the ducts ("E", "F" gages) had the second highest strain and were almost the same value with the "E" gage value slightly greater than the "F" gage value.

- 3) The other gages had a lower strain. It is interesting to note that the strains in the gages in the different bars located parallel in the front face of the deviation saddle ("B", "H" gages) had identical strains.

The observations that can be obtained from the ultimate load phase 2 strain data of Fig. 3.52 are as follows:

- 1) The most striking observation is that the strain in the reinforcement at all gage locations had yielded. This indicates highly efficient use of the reinforcement.

TEST 4A PHASE 1

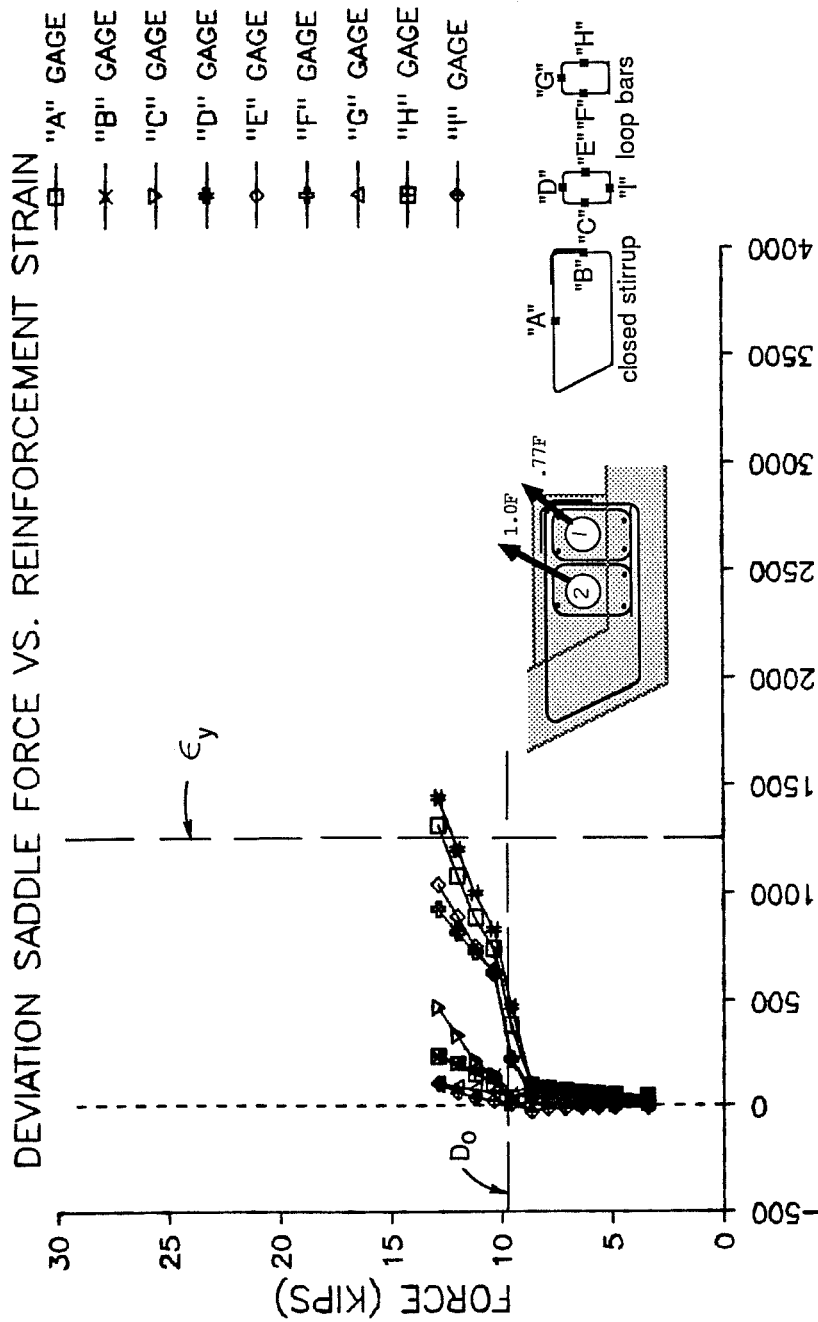


Figure 3.51 Test 4A Reinforcement Strain Data - Phase 1

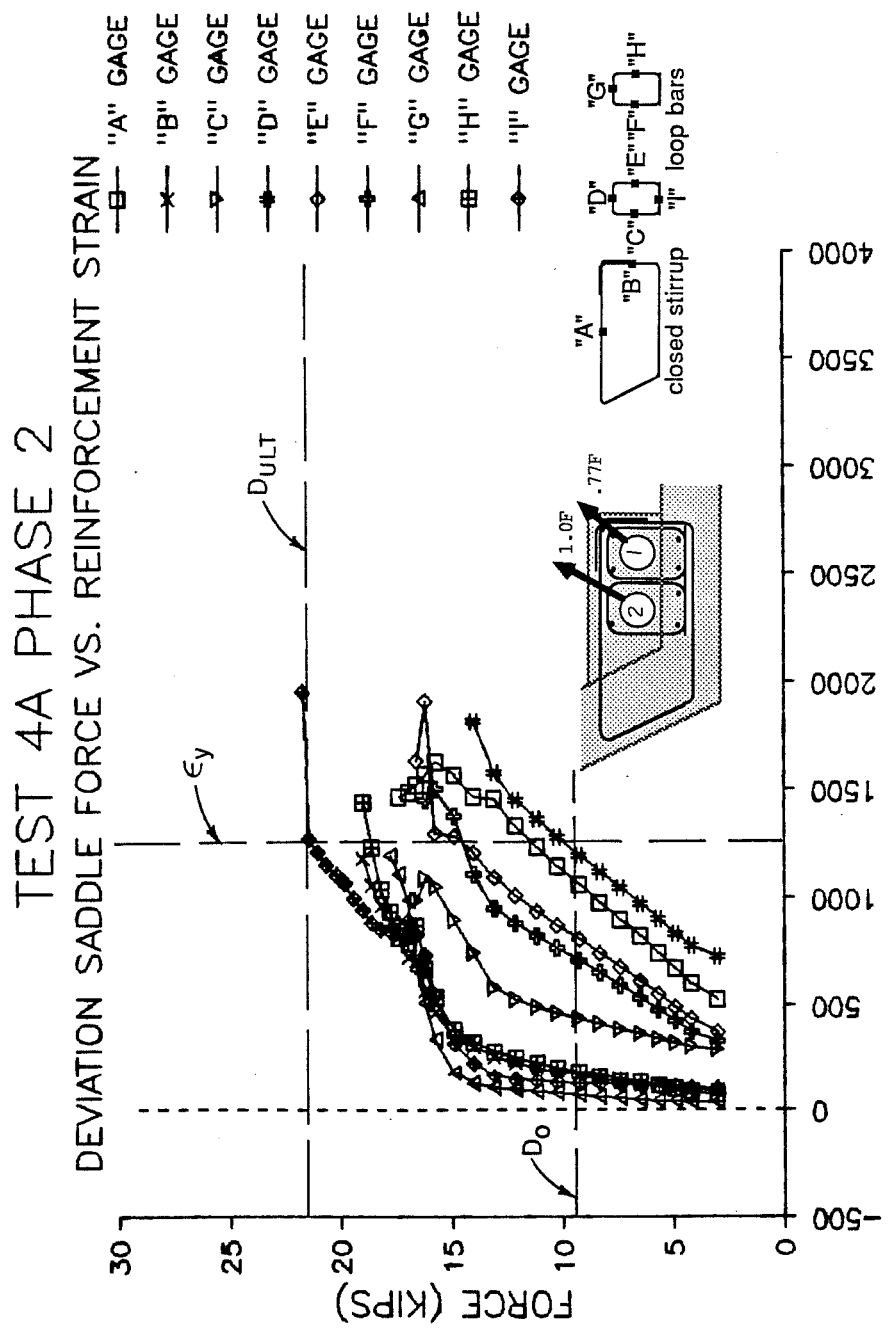


Figure 3.52 Test 4A Reinforcement Strain Data - Phase 2

2) All gages except the "I" gage which was located on the tendon 2 inner loop bar under the top mat of reinforcement electrically failed prior to complete destruction of the deviation saddle.

The conclusions that can be drawn from this strain data are that the inner loops and the vertical leg of the closed stirrup were straining due to direct tension and shear friction. As in the other deviation saddle details, a bending element was formed at the top surface of the deviation saddle. The top of the closed stirrup was straining due to the tensile forces from this bending element.

The failure was very interesting since both sides of the inner loop of tendon 2 fractured while all the laps failed on the tendon 1 inner loops (Fig. 3.53). The outer stirrups were also fractured right above tendon 2. This failure was the only one where damage occurred to the box section. The top mat reinforcement was pulled up about 1/4 in. when the failure occurred. The before and after failure photographs are shown in Fig. 3.54. The strength comparisons in Fig. 3.55 reveal that the factor of safety against cracking and yielding is too low, although the ultimate strength is adequate for this deviation saddle detail. The failure was very ductile which is seen by the large difference between the ratio D/D_0 for yield and ultimate and the wide cracks that had formed.

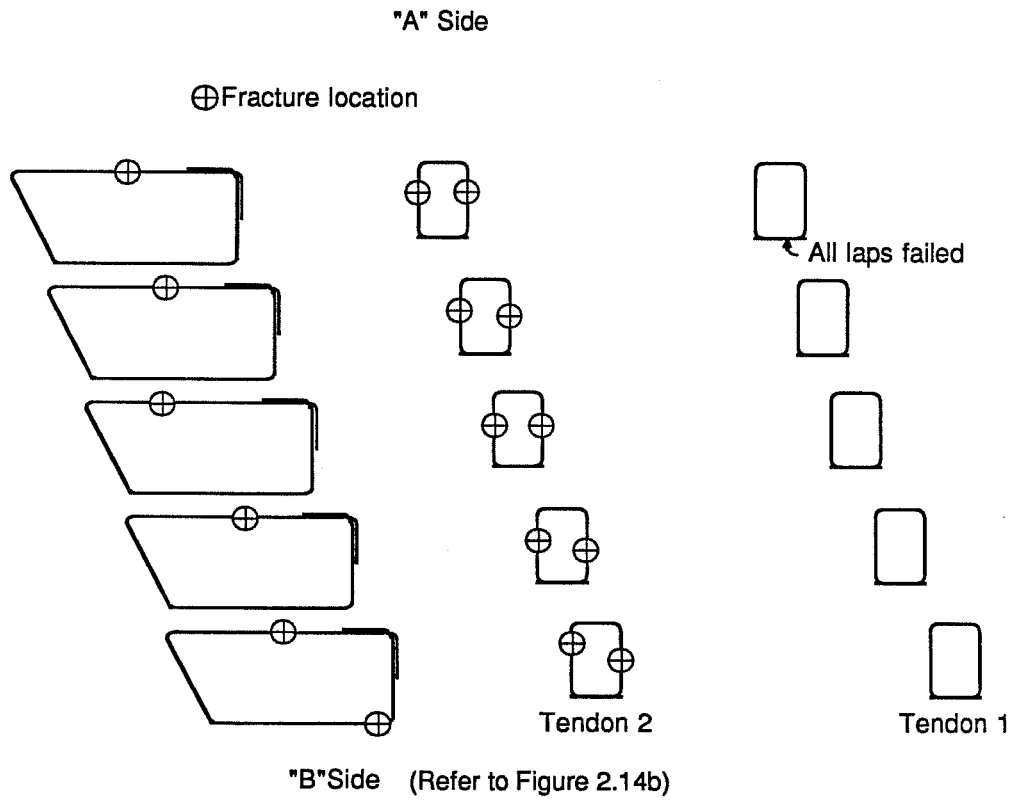


Figure 3.53 Test 4A Reinforcement Failure Locations

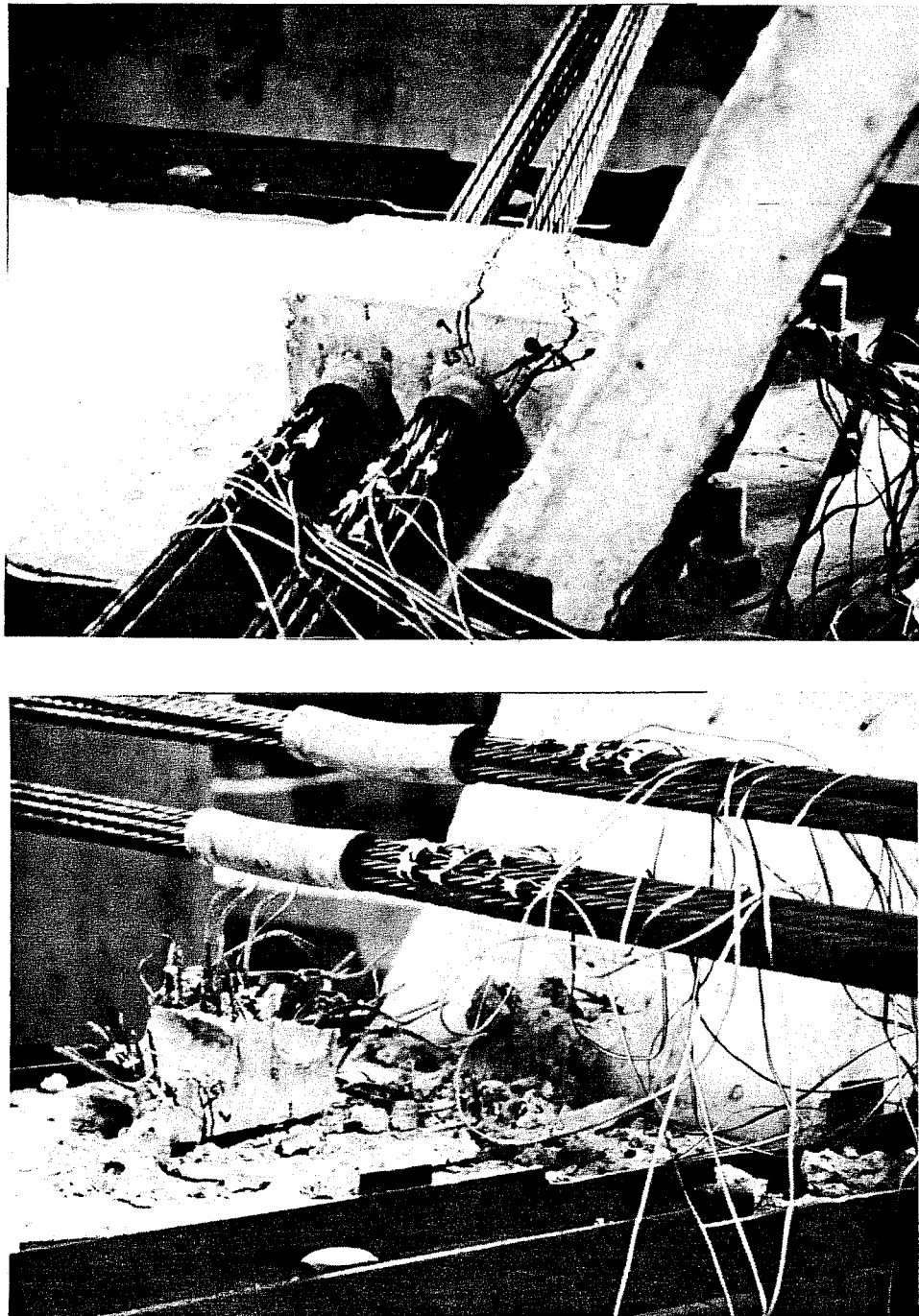


Figure 3.54 Test 4A - Before and After Failure

TEST 4A
RATIO D/D₀ AT CRITICAL STAGES

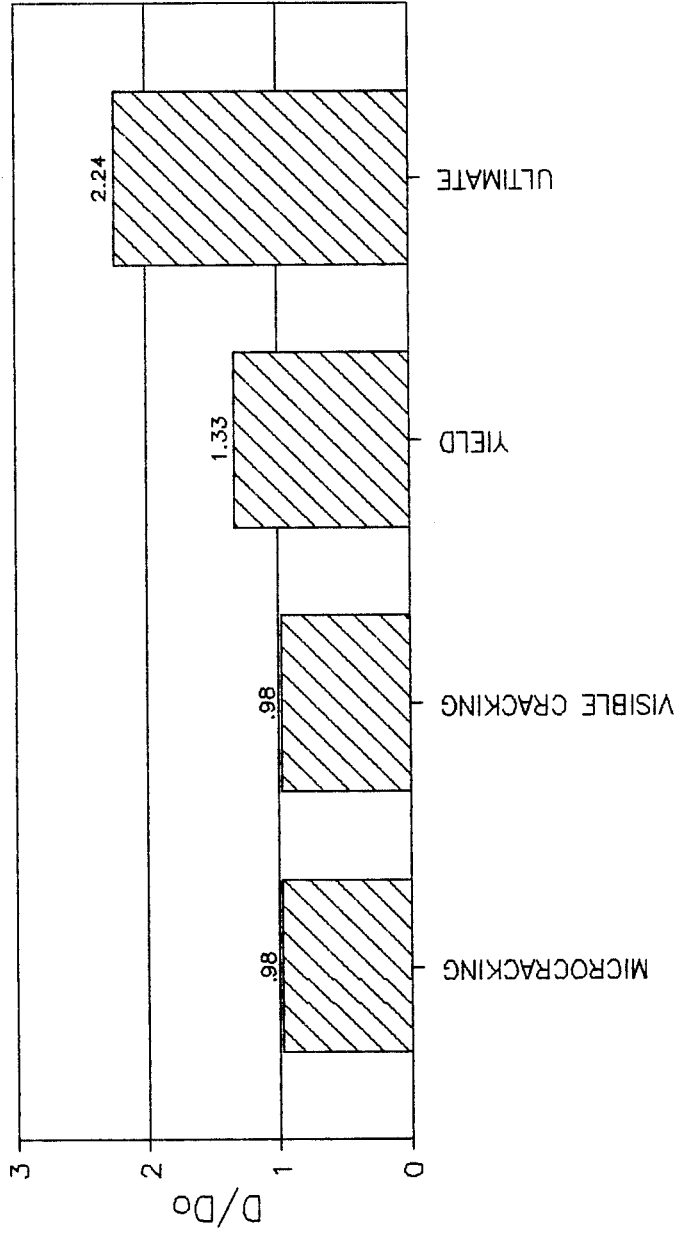


Figure 3.55 Test 4A Strength Comparison

3.9 Test 4B-Uncoated Tendon Loop Bars with Stirrup-Inside of Curved Span-Two Tendons

Specimen 4B detail was identical to specimen 4A detail. However, the tendon configuration was different. The tendon configuration was representative of a deviation saddle on the inside of a small radius curved span. Both tendons had vertical and horizontal deviations. This detail is discussed in Sec. 2.2.4 and is illustrated in Fig. 2.9a.

The total vector force and direction which acted on the specimen are shown in Fig. 3.56. The crack patterns are shown in Fig. 3.57. The first crack to appear was on the side face of the deviation saddle at load stage 18 of phase 1. This appears to be a splitting crack due to the concentrated deviation force of the tendons. In phase 2, at a very low load a crack formed across the top of the deviation saddle. The explanation for this must be that the load path was different after the initial cracking of the side face. The crack widths were significantly smaller for this test than test 4A. Estimated maximum crack width was 1/16 in. which occurred at the intersection of the web wall and the top surface.

The observations that can be made for the phase 1 strain plot of Fig. 3.58 are as follows:

- 1) The strain gages did not have an abrupt jump as those of test 4A.

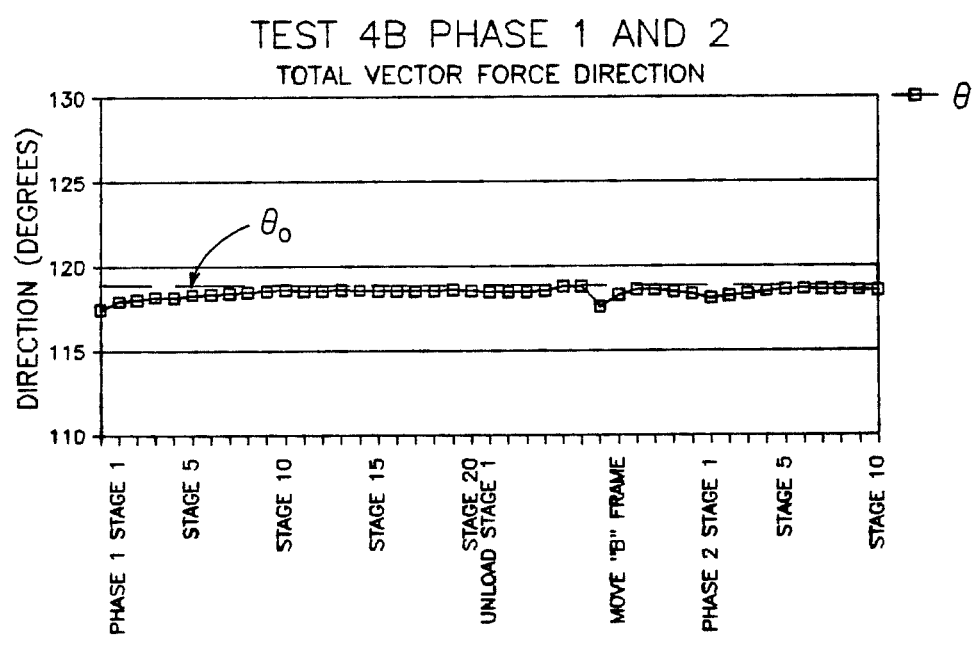
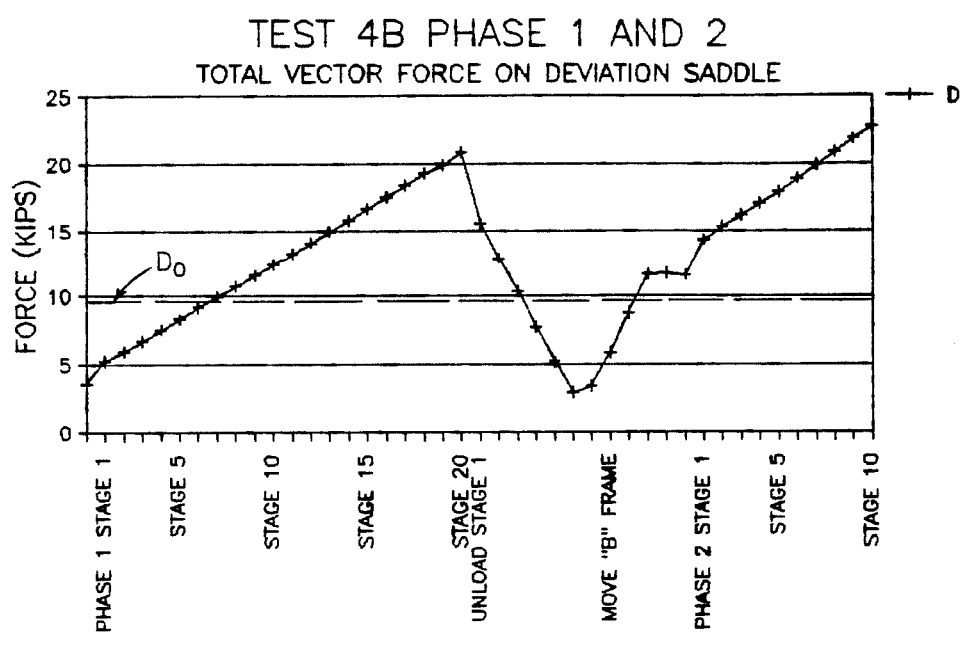


Figure 3.56 Test 4B Loading History

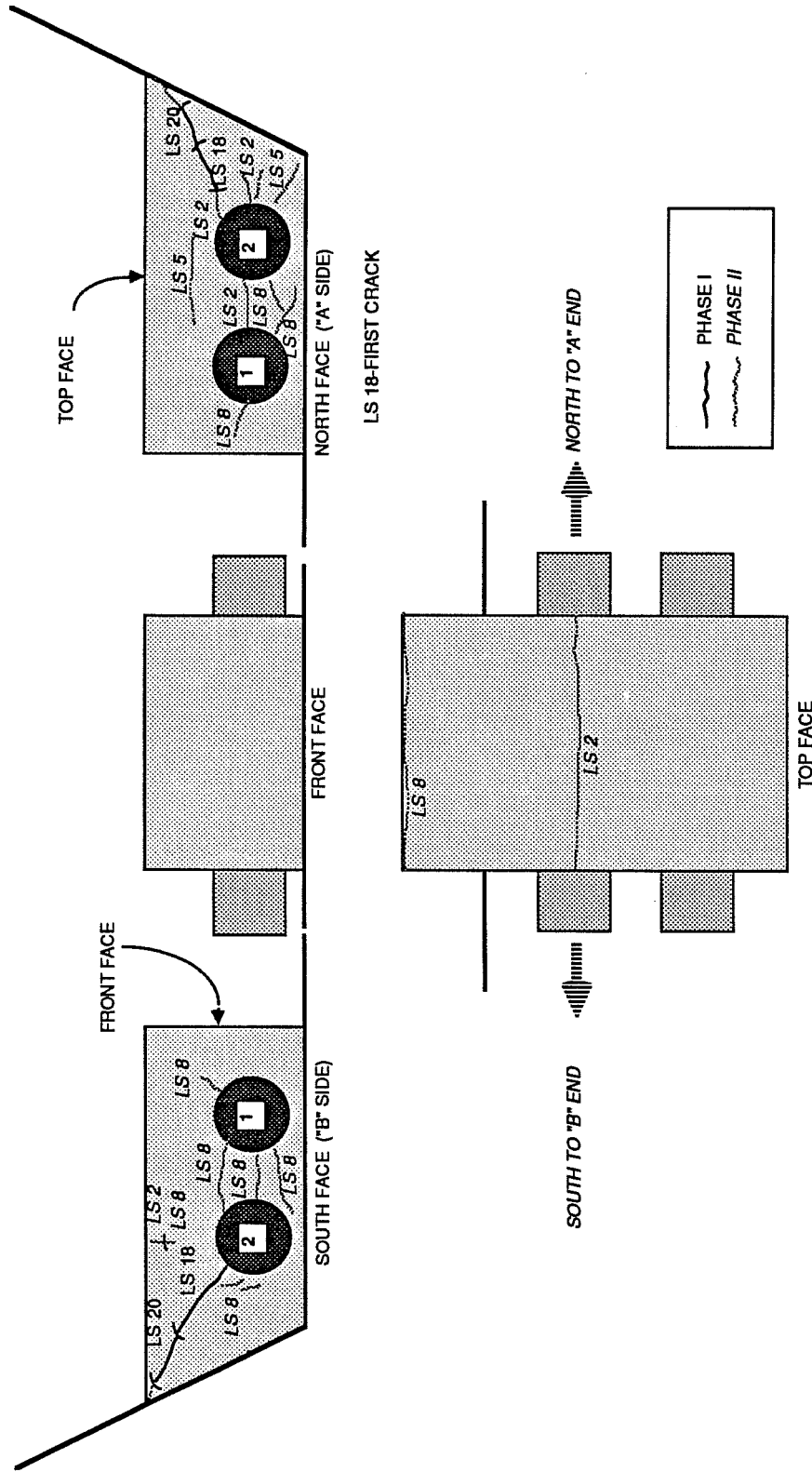


Figure 3.57 Test 4B Crack Patterns

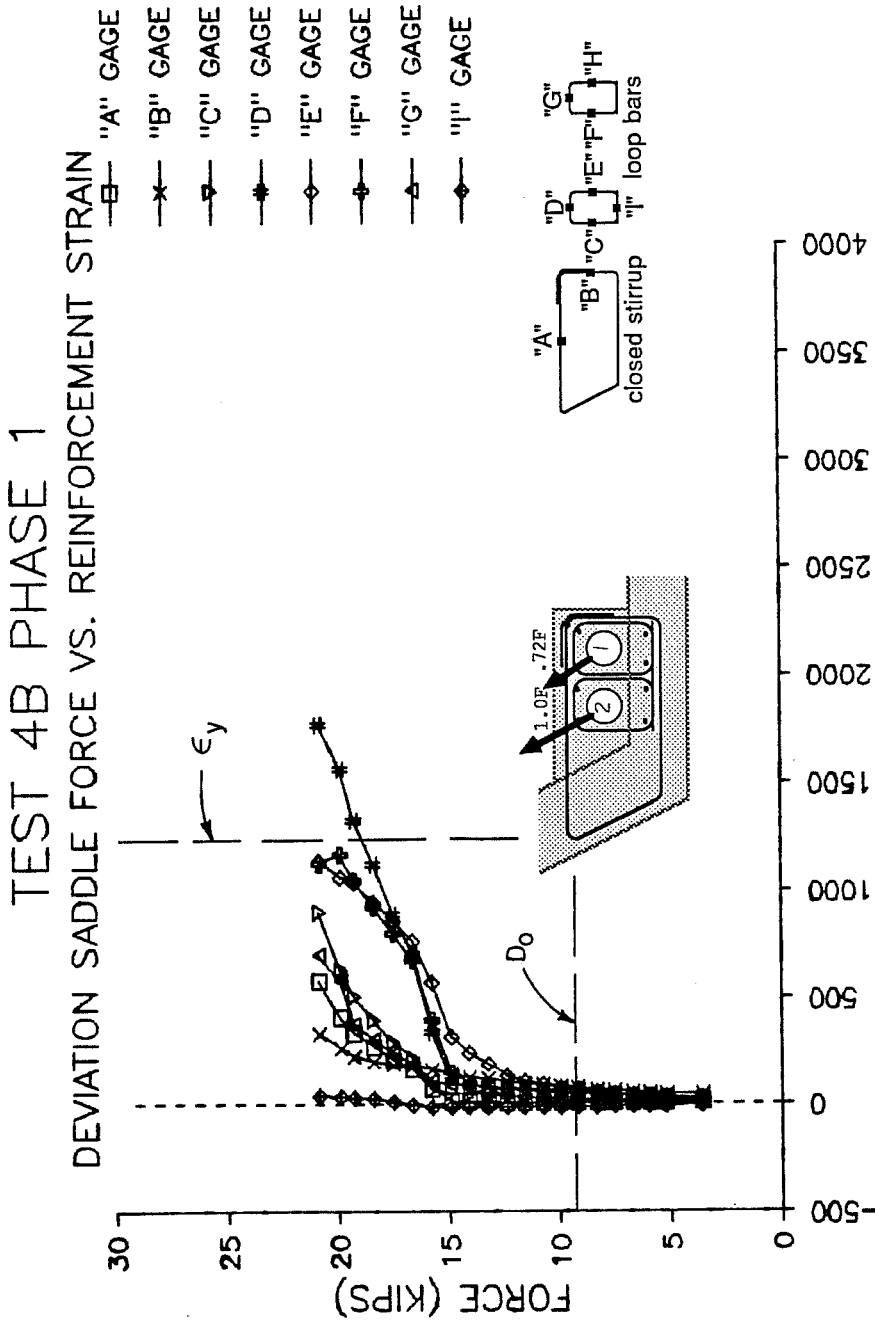


Figure 3.58 Test 4B Reinforcement Strain Data - Phase 1

2) The gage "D" above tendon 2 on the inner loop had the highest strain just as it did in test 4A, and it was the first gage to yield.

3) The "E" and the "F" gages located on the vertical bars between the ducts on the inner loops had the second highest strain and had almost identical values as was the case in test 4A. Unfortunately, the "H" gage had failed, so it is not possible to make a comparison with the "B" gage located near it.

4) The "A" gage located on the top of the closed stirrup had a smaller strain than that of test 4A.

5) The "I" gage of the tendon 2 inner loop strained very little which was not the case in test 4A.

The observations from the strain data for the ultimate loading phase 2 (Fig. 3.59) are as follows:

1) The strain in the "D" gage which was located on the top of the inner loop for tendon 2 was the greatest of all the gages until the last load stage.

2) A trend that was seen in test 1A and 3A was present in this test. The strain was decreasing at the later load stages in the "A" and "D" gages which were located near the top surface of the deviation saddle.

3) The strain in the "B" gage which was located at the front face began to increase in the last three load stages.

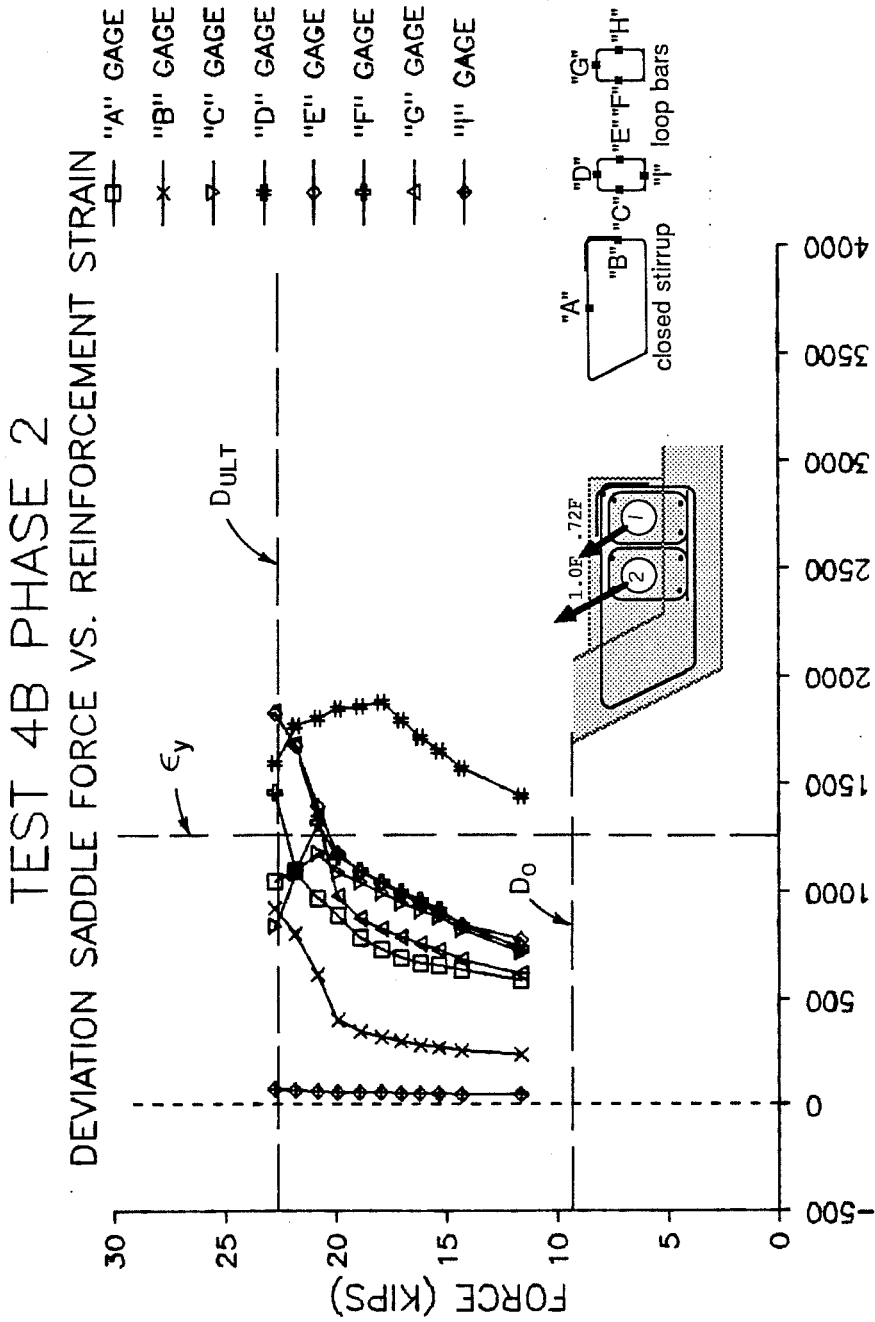


Figure 3.59 Test 4B Reinforcement Strain Data - Phase 2

4) The strain remained constant in the "I" gage which was located on the bottom of the inner loop for tendon 2.

5) All gage locations except the "B" and "I" gages appeared to reach the yield strain but at higher loads than that of test 4A.

6) The straining of the closed stirrup at the "A" gage was much less than that of test 4A.

As in test 4A, a reasonable explanation for the strain data for phase 1 and 2 is that the inner loops and the vertical leg of the closed stirrup strained due to direct tension and shear friction, and the top of the closed stirrup strained due to the tensile forces of a bending element which had formed above the ducts. This bending element appeared to have less influence on the strength of the deviation saddle than that of test 4A which was indicated by the lower strains.

The reinforcement failure locations are shown in Fig. 3.60. It is interesting to note that tendon 2 burst out of the deviation saddle first and then approximately two seconds later, tendon 1 burst out. This test was the only one where this occurred. It is also important to note that all inner loop fractures were on the side where the tendon vector force was directed. The before and after photographs are shown in Fig 3.61. The strength comparisons are shown in Fig. 3.62. This detail would have no serviceability or strength problems since the factors of safety are sufficient. There was less ductility for this test than that of test 4A. This is confirmed by the smaller

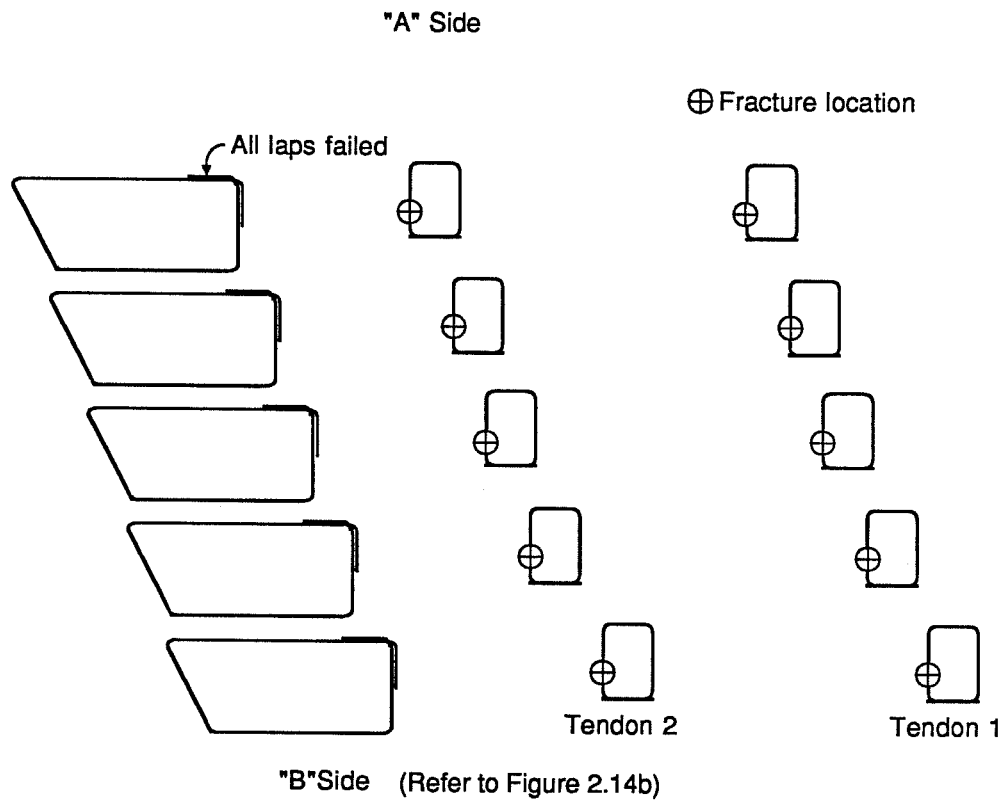


Figure 3.60 Test 4B Reinforcement Failure Locations

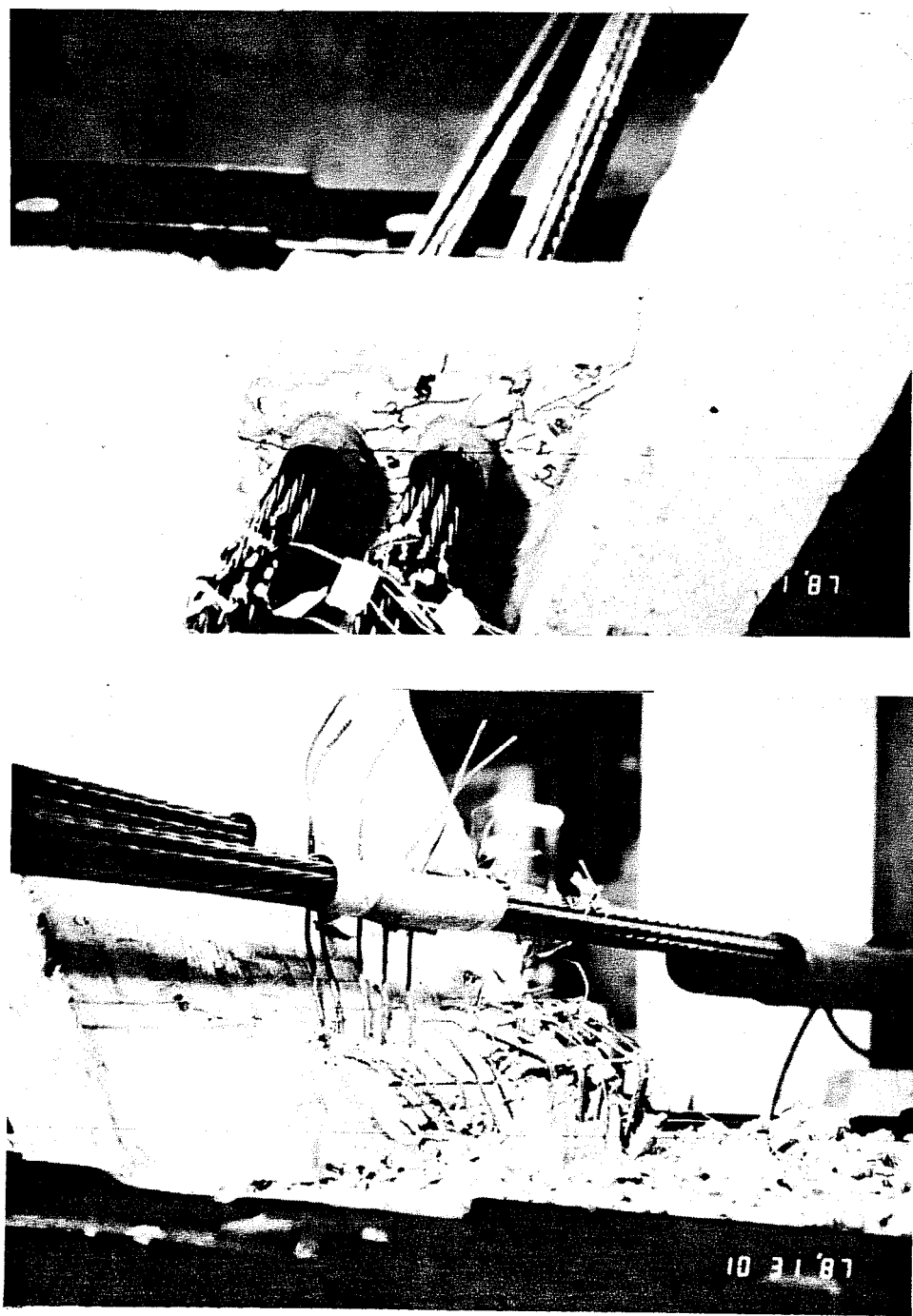


Figure 3.61 Test 4B - Before and After Failure

TEST 4B
RATIO D/D₀ AT CRITICAL STAGES

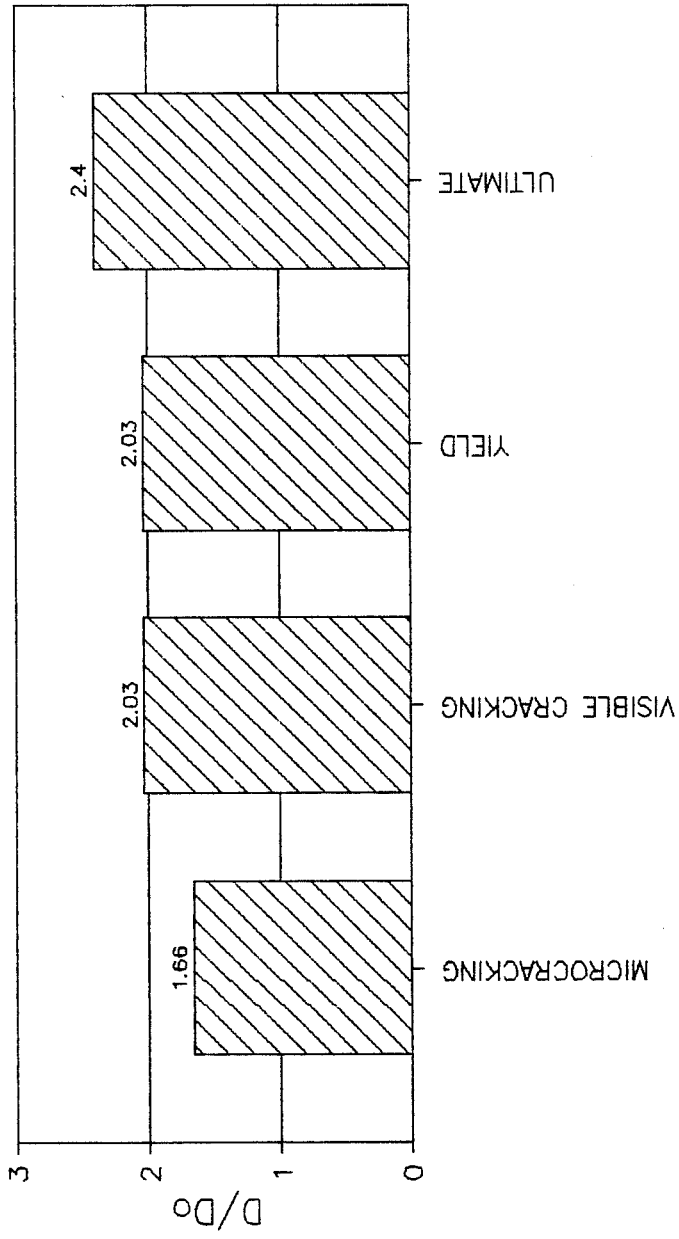


Figure 3.62 Test 4B Strength Comparison

difference in the D/D_0 ratio for yield and ultimate and the smaller cracks that formed.

3.10 Test 5A-Epoxy Coated Tendon Loop Bars with Stirrup-Companion Test of Test 4A

The objective of specimen 5A was to further evaluate the effect of epoxy coated reinforcement on the behavior and strength of the deviation saddle. This is a direct comparison test to test 4A. The only difference between the two specimens was that the reinforcement was epoxy coated for this test. This detail is discussed in Sec. 2.2.4 and is illustrated in Fig. 2.9a. Refer to Sec. 3.12 for a comparison between epoxy coated and uncoated reinforcement. The total force vector and direction which acted on this specimen are shown in Fig. 3.63. The crack patterns are shown in Fig. 3.64. They are very similar to those of test 4A, although, the same failure mechanism that formed in test 4A did not occur in this test. This difference may have been due to the lack of bond between the concrete and the reinforcement. Estimated maximum crack width was 1/8 in. located at the side faces of the deviation saddle.

The observations for the phase 1(a) strain data shown in Fig. 3.65 are as follows:

- 1) The "D" location on the tendon 2 inner loop had the greatest strain in phase 1 just as it did in test 4A. The reason being that this gage was directly above the tendon 2 force.

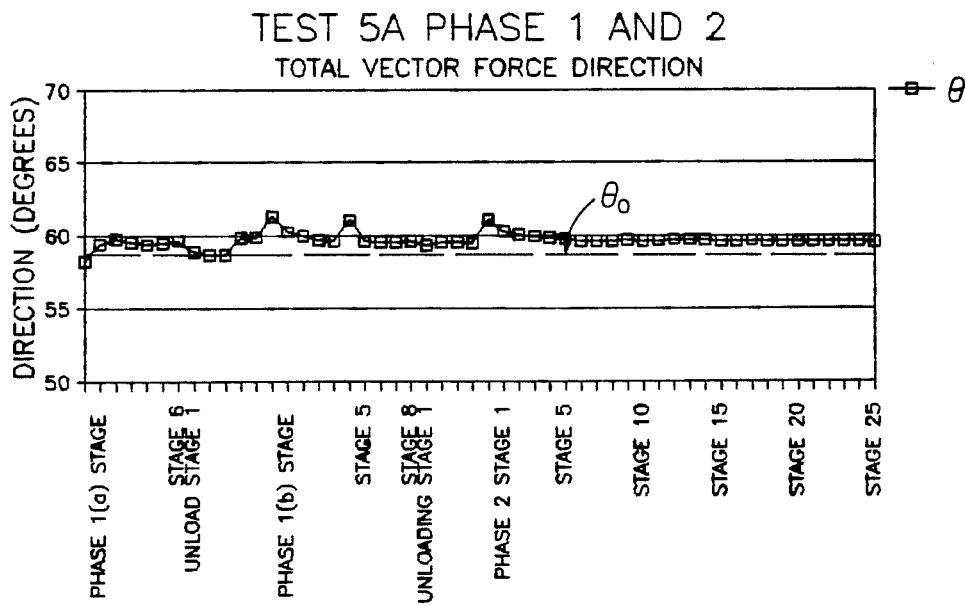
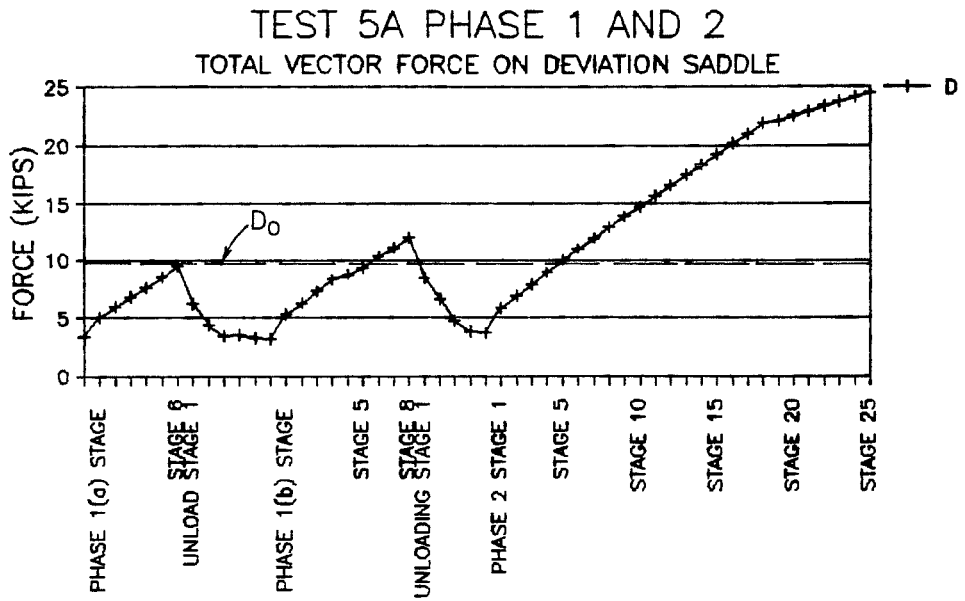


Figure 3.63 Test 5A Loading History

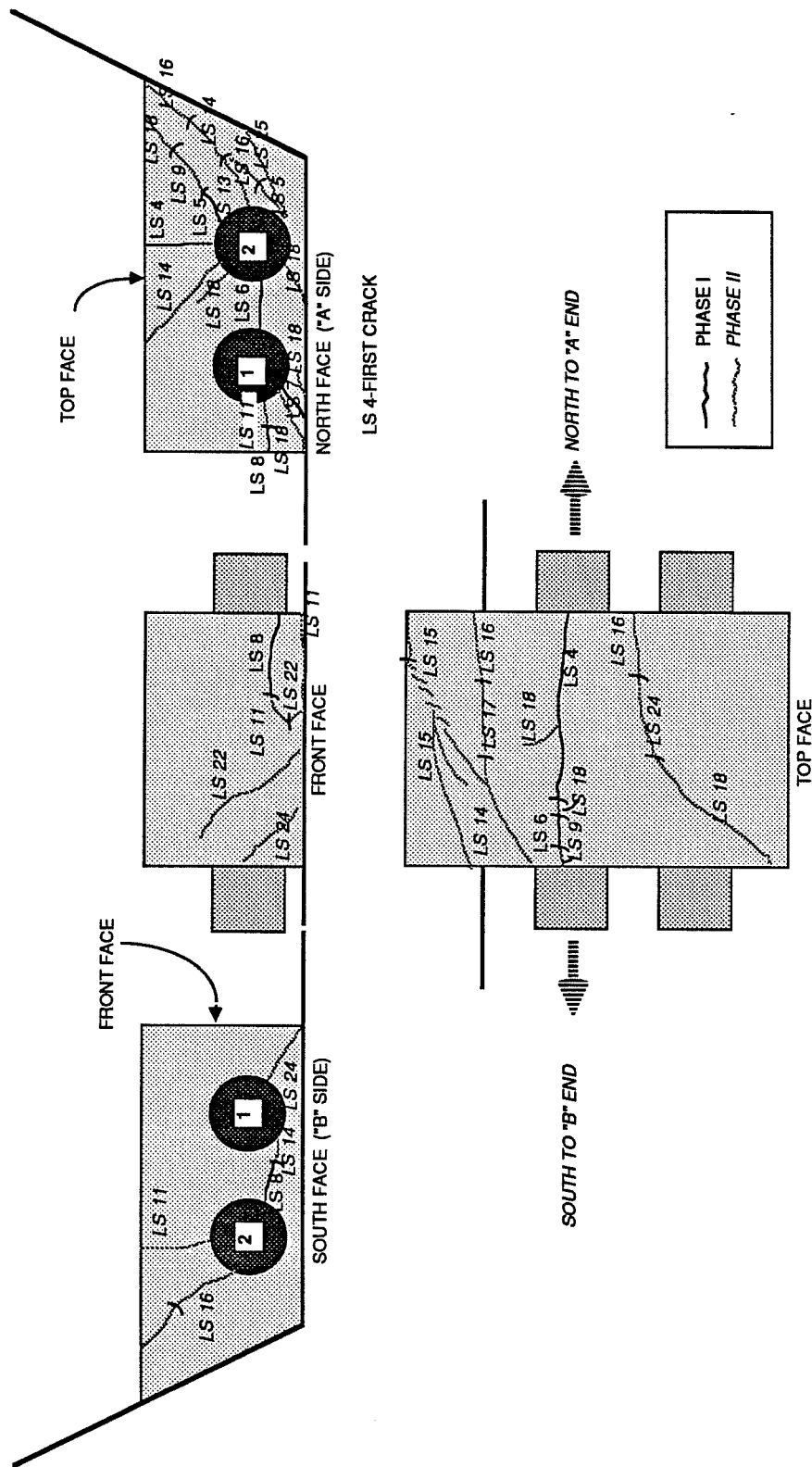
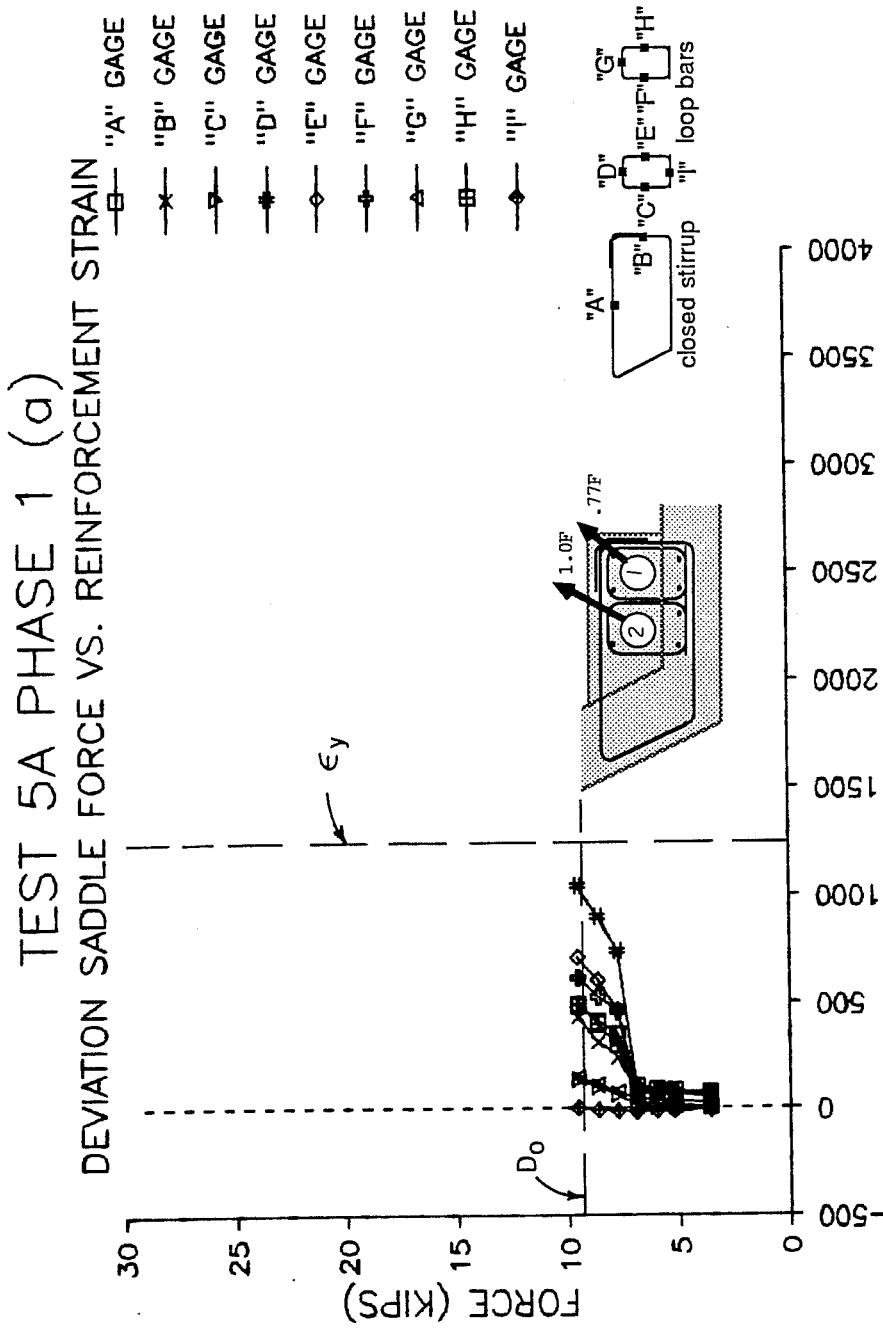


Figure 3.64 Test 5A Crack Patterns



STRAIN (MICRO IN./IN.)
Figure 3.65 Test 5A Reinforcement Strain Data - Phase 1 (a)

2) The "E" and "F" gages located on the inner loop between the ducts had the second highest strain with the "E" gage strain being slightly greater than the "F" gage strain.

3) The "B" and the "H" gage which were respectively located on the inner loop and on the closed stirrup had the third highest strain with the "H" gage strain being slightly greater than "B" gage strain. Coincidentally, the strain in the "A" and the "H" gages were almost identical.

4) The strains in the other gages were lower with the strain in the "I" gage remaining at zero.

The observations for the phase 1(b) and the ultimate loading phase 2 (Figs. 3.66 and 3.67) are as follows:

1) The strain in the "D" gage located on the top of the tendon 2 inner loop was the first to reach yield in phase 1(b).

2) All gage locations indicated yield in phase 2 except the "I" gage that was located on the bottom of the tendon 2 inner loop. This was similar to test 4A except all the gages had indicated yielding. All gages electrically failed before the last load except the "I" gage.

3) Comparing the strain plots for test 4A and test 5A, it appears that the strains are higher in the gages of test 5A.

A reasonable explanation for the phase 1 and phase 2 strain data is the same as that stated for test 4A. The inner loops and the vertical leg of the closed stirrup were straining due to direct

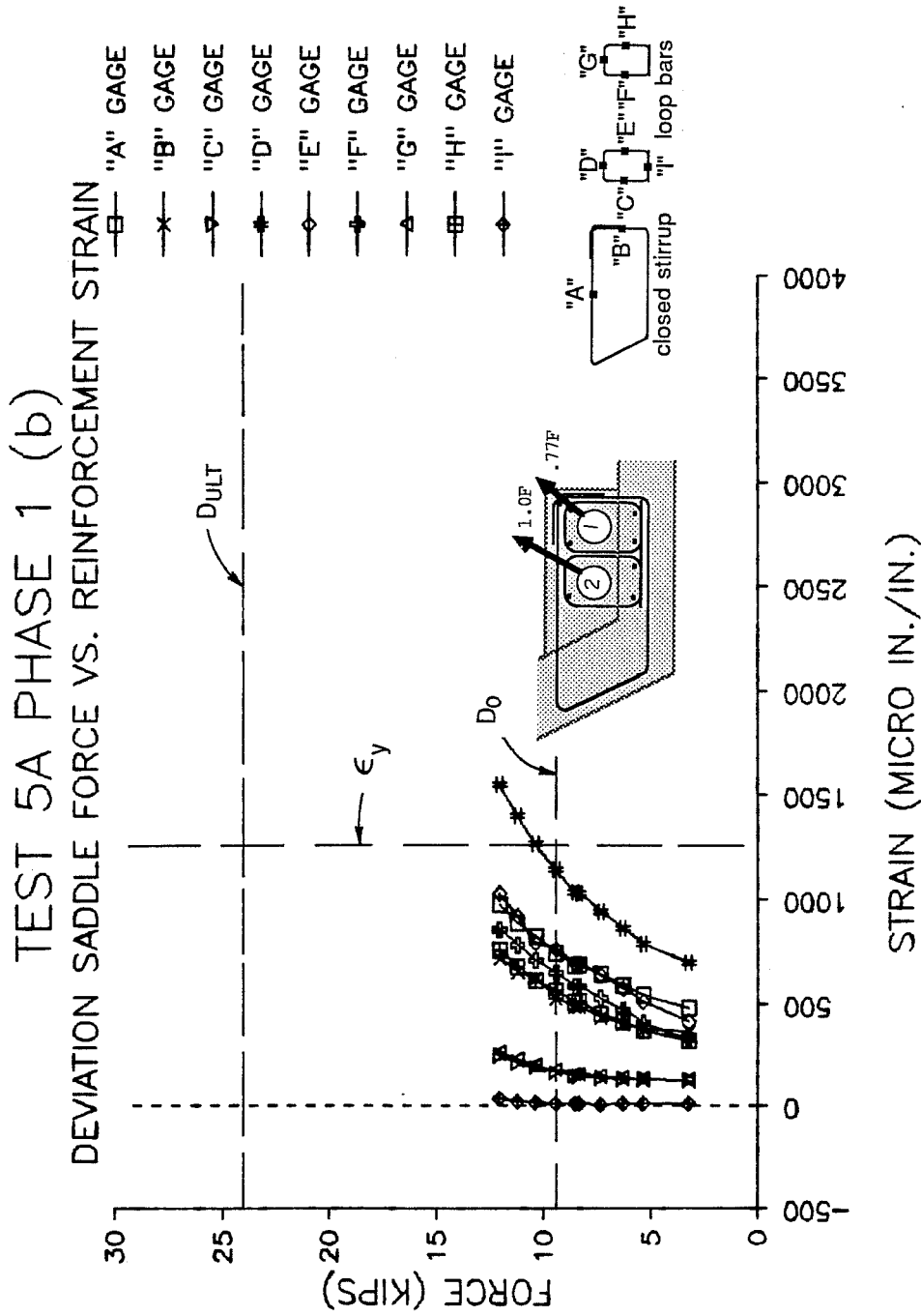
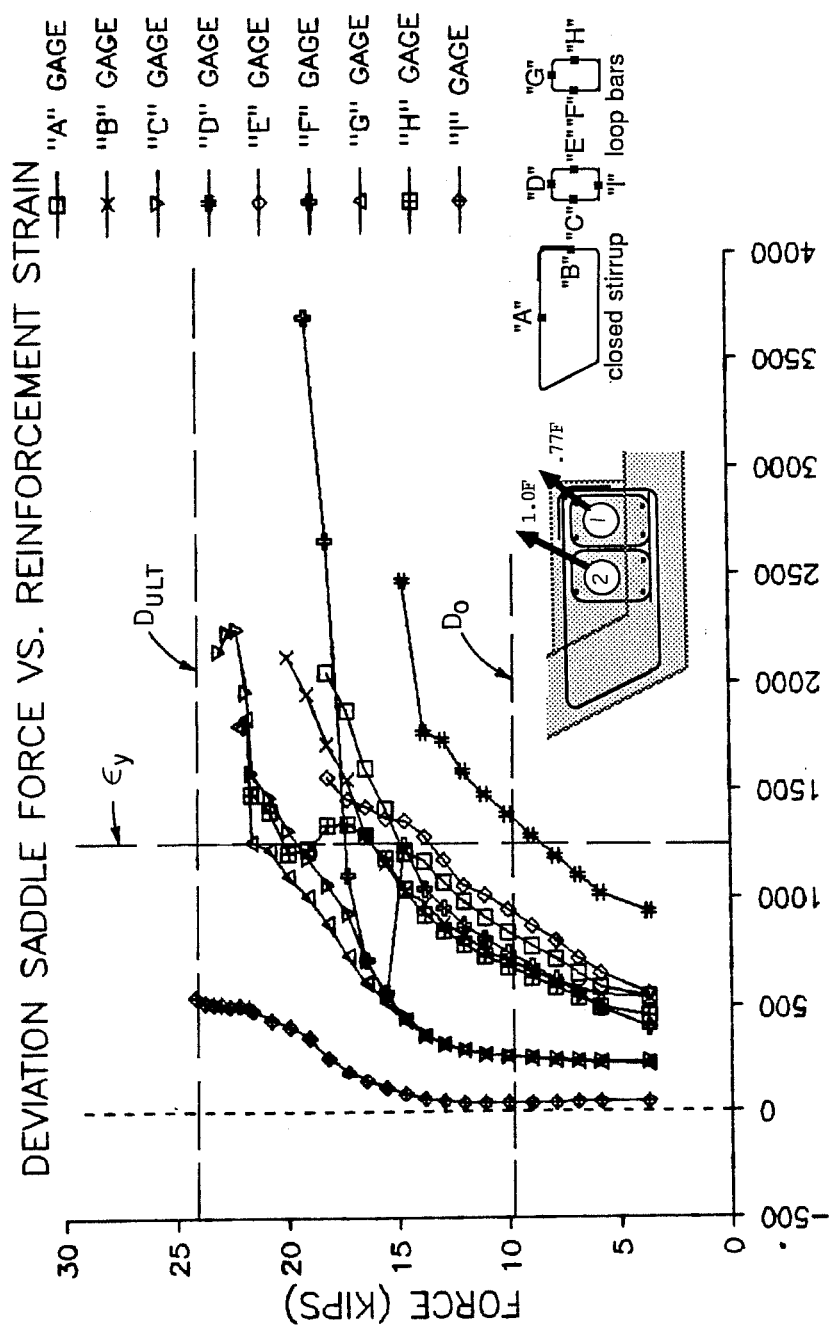


Figure 3.66 Test 5A Reinforcement Strain Data - Phase 1 (b)

TEST 5A PHASE 2



STRAIN (MICRO IN./IN.)
Figure 3.67 Test 5A Reinforcement Strain Data - Phase 2

tension and shear friction, and the top of the closed stirrup was straining due to the formation of the bending element at the top surface above the ducts.

The reinforcement failure locations are shown in Fig. 3.68. The locations of the fractures on the inner loops were on the side towards which the tendon force was directed. The before and after photographs are shown in Fig. 3.69. The comparisons of the strength are shown in Fig. 3.70. It is apparent that the detail is inadequate as far as preventing cracking under service load conditions and for yielding, but the detail has a sufficient factor of safety for the ultimate strength. The specimen had good ductility which was apparent from the crack widths and the large difference between the D/D_0 ratio for yield and ultimate.

3.11 Test 5B-Epoxy Coated Tendon Loop Bars with Stirrup-Companion Test of Test 4B

The objective of specimen 5B was to further evaluate if epoxy coated reinforcement has any effect on the behavior and strength of a deviation saddle. This is a direct comparison test to test 4B. The only difference was that the reinforcement was epoxy coated. This detail is discussed in Sec. 2.2.4 and is illustrated in Fig. 2.9a. Refer to Sec. 3.12 for a comparison between the epoxy coated and the uncoated reinforcement. The total force vector and direction which acted on the specimen are shown in Fig. 3.71. The crack patterns are shown in Fig. 3.72. The crack patterns for test 5B and 4B are very

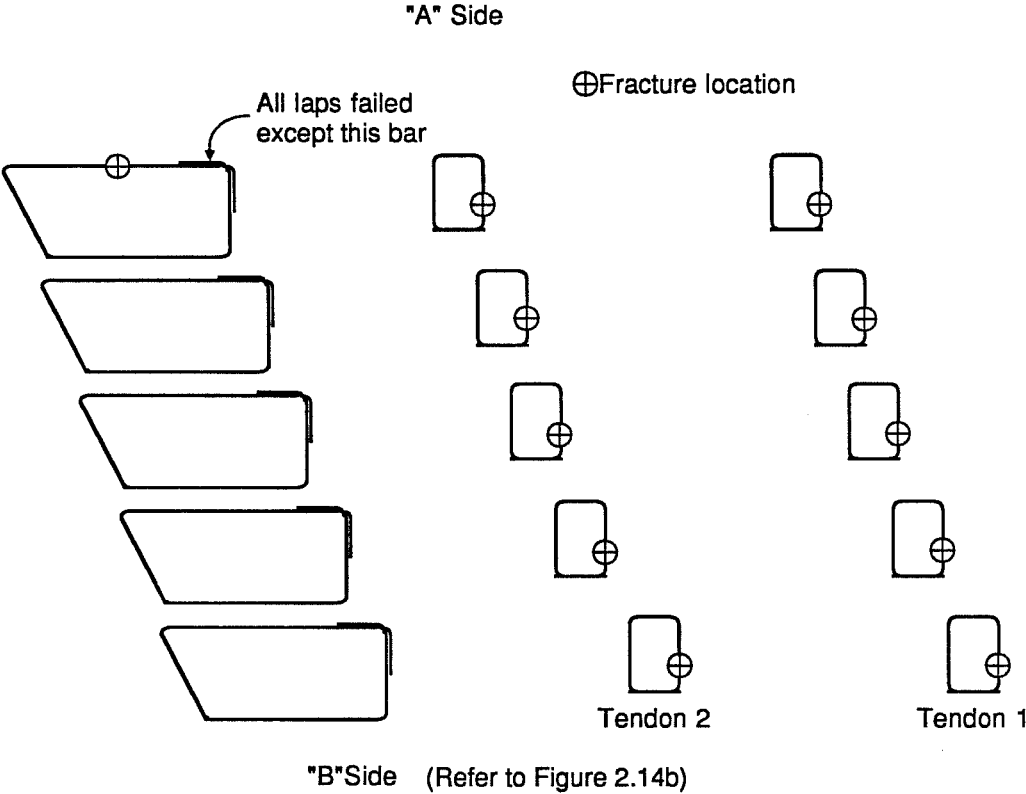


Figure 3.68 Test 5A Reinforcement Failure Locations

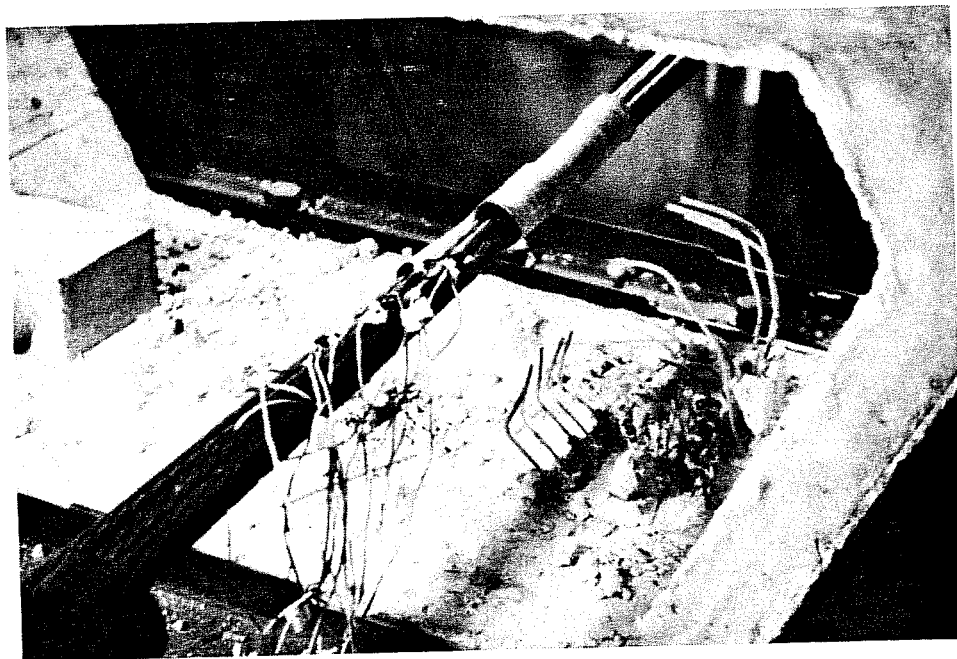
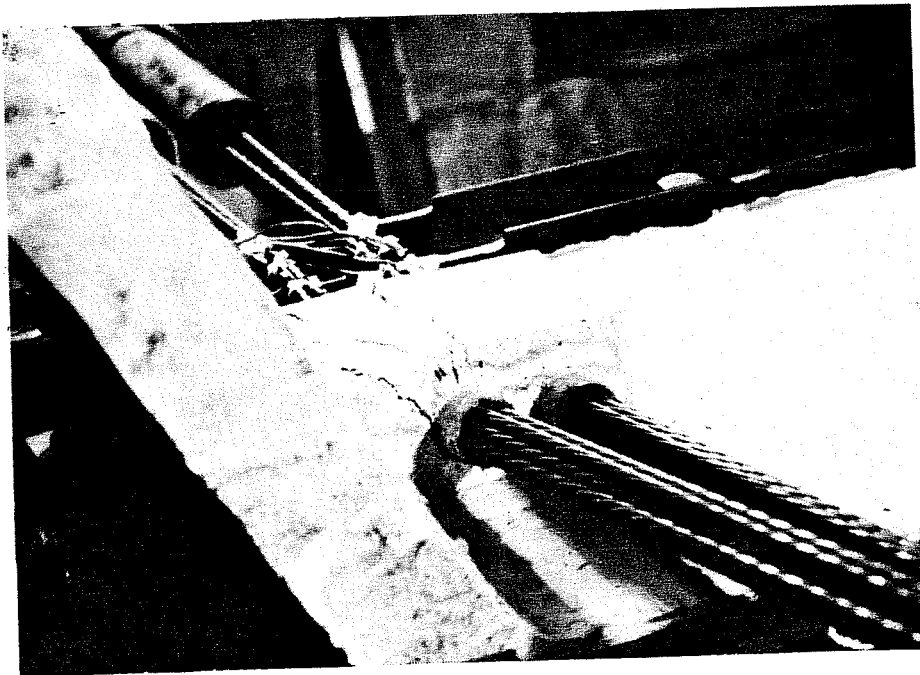


Figure 3.69 Test 5A - Before and After Failure

TEST 5A
RATIO D/D₀ AT CRITICAL STAGES

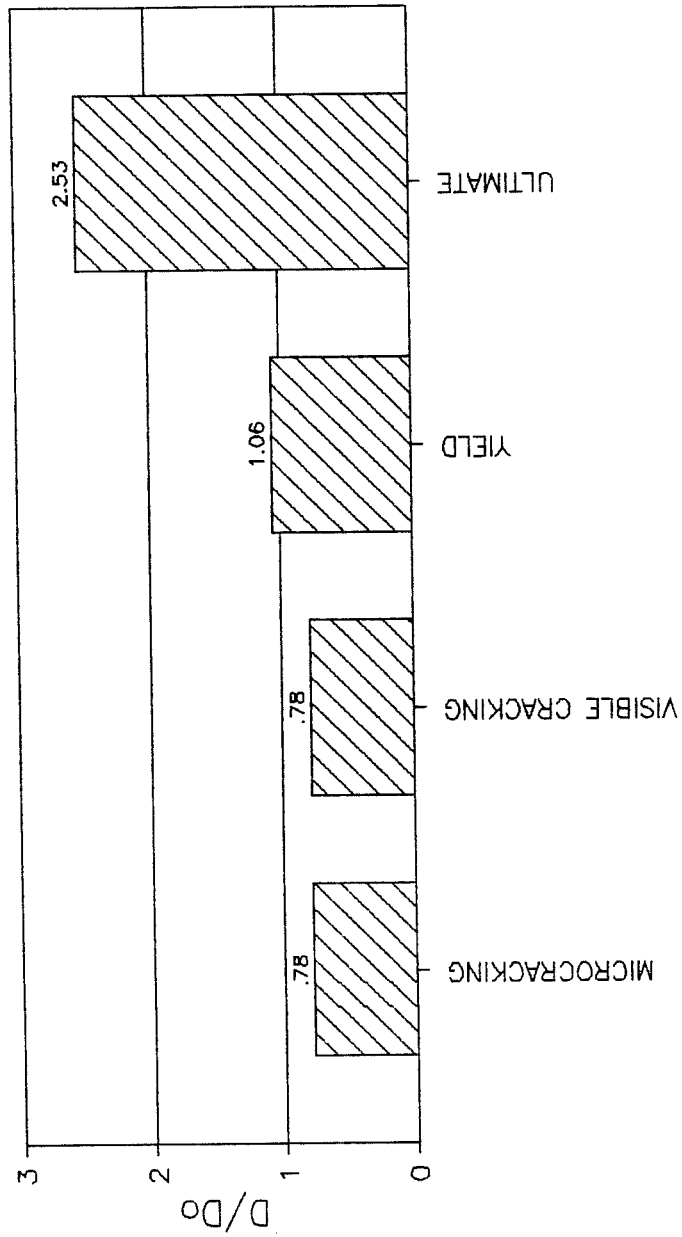


Figure 3.70 Test 5A Strength Comparison

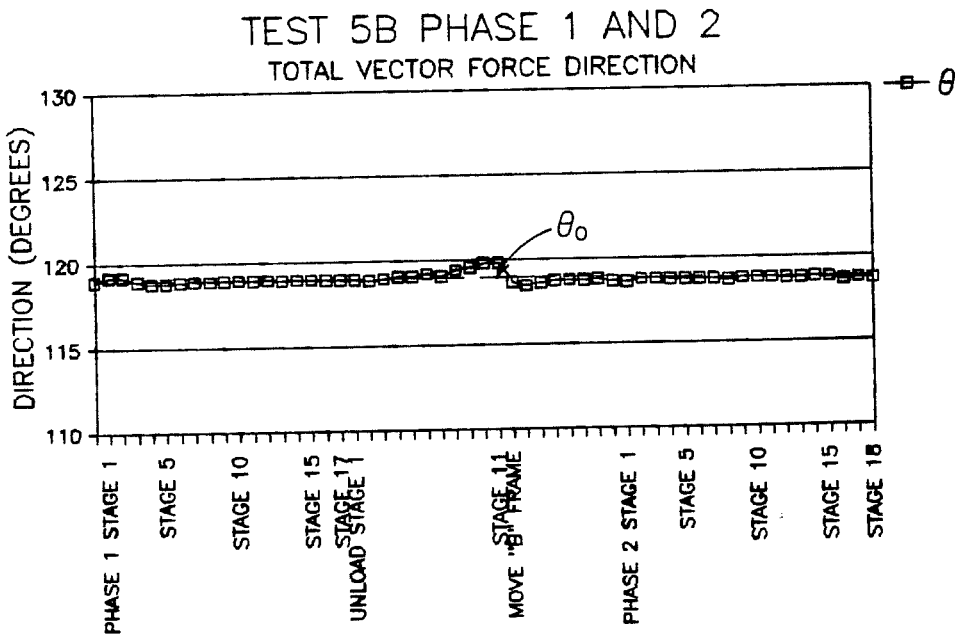
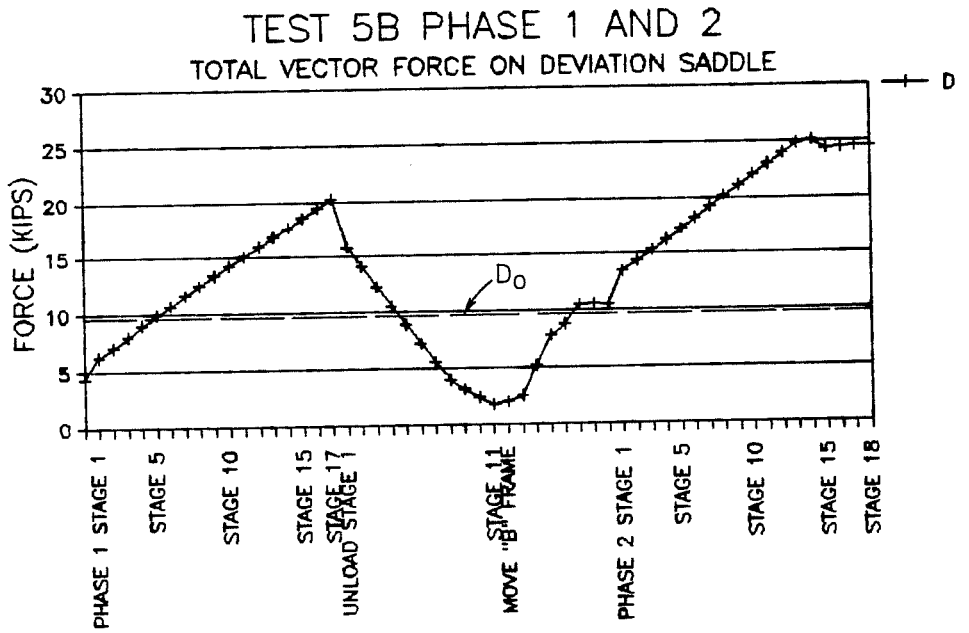


Figure 3.71 Test 5B Loading History

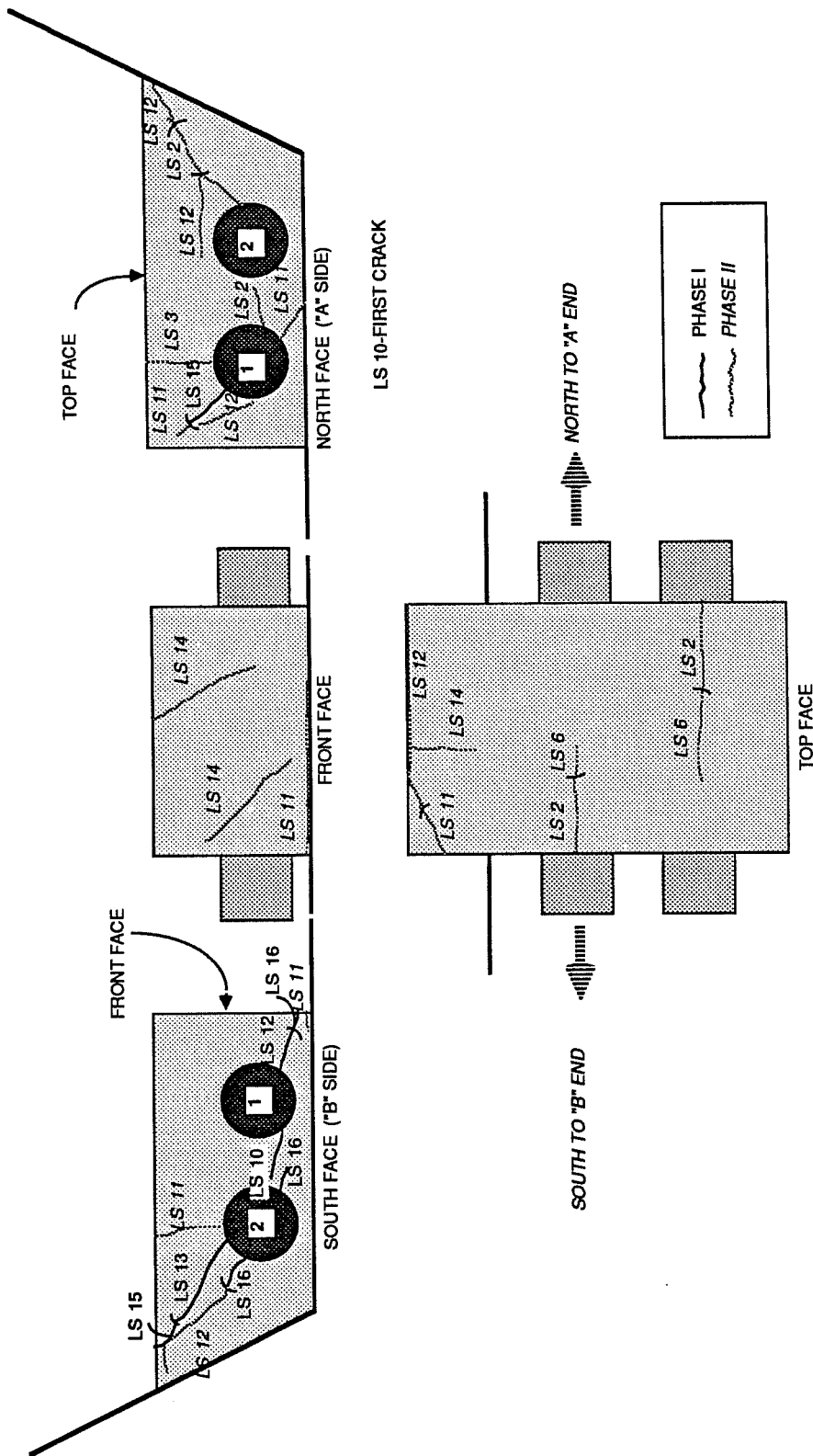


Figure 3.72 Test 5B Crack Patterns

similar. The location of the first crack and the occurrence of the top surface cracks at early load stages of phase 2 were the same for both specimens. Estimated maximum crack width was 1/8 in. at the intersection of the web wall and the top surface. Level of ductility appeared to be higher for this test than that of test 4B which was apparent from the larger cracks that had formed.

The observations for the phase 1 strain data of Fig. 3.73 are as follows:

1) The greatest strain at the end of phase 1 was at the "D" gage which was located on the top of the tendon 2 inner loops. This was also the case in test 4B.

2) The "E" and the "F" gage located on the inner loops between the ducts had the second highest strain with the "F" gage slightly greater than the "E" gage.

3) The "B" and the "H" gage which were located on the reinforcement in the front face did not have the same strain as they did in the previously related tests. A comparison cannot be made with test 4B because the "H" gage had failed before testing.

4) The strain in the "A" gage was lower than it was in test 4B.

5) The other gages were at a lower strain with the strain being the lowest in the "I" gage which was located at the bottom of the tendon 2 inner loop.

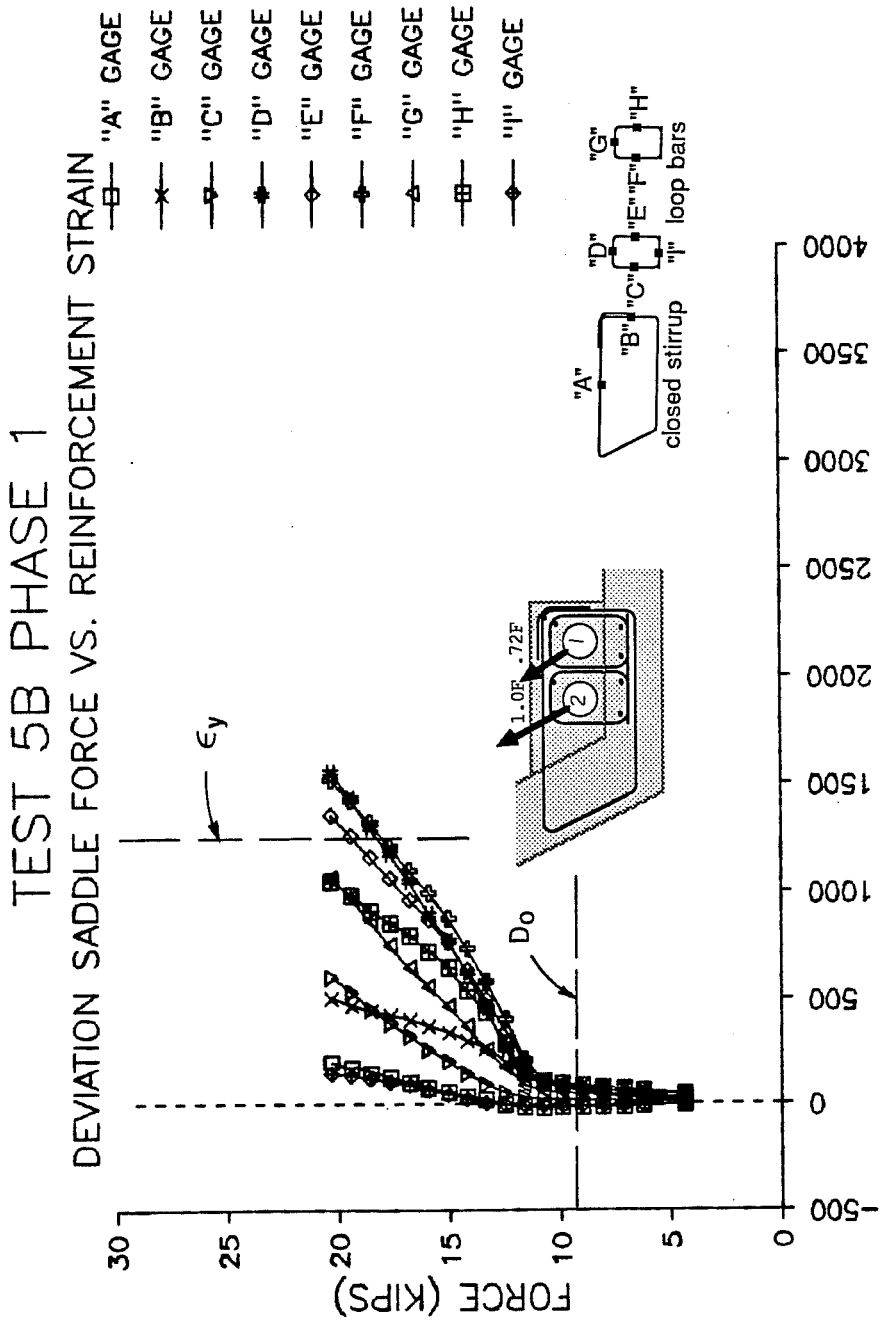


Figure 3.73 Test 5B Reinforcement Strain Data - Phase 1

The observations from the ultimate loading phase 2 strain data (Fig. 3.74) are as follows:

1) All the reinforcement yielded except the "I" gage location. This was not the case in test 4B.

2) Comparing the strain plots for tests 4B and 5B, it appears that the strains reached higher values in test 5B.

As was the case in the other related tests, the inner loops and the vertical leg of the closed stirrup strained due to direct tension and shear friction, and the top of the closed stirrups strained due to the formation of a bending element at the top surface above the ducts.

The reinforcement failure locations are shown in Fig. 3.75. The fracture locations were more irregular than they were in the previous two tests. The before and after failure photographs are shown in Fig. 3.76. The strength comparisons are shown in Fig. 3.77. This bar graph shows that this deviation saddle detail provides a sufficient factor of safety for all the critical load stages.

3.12 Comparison of Epoxy Coated and Uncoated Reinforcement

The comparisons of critical stages of strength of companion specimens are presented in Figs. 3.78 through 3.81 for the corresponding tests of uncoated and epoxy coated reinforcement. Microcracking was not apparent from the strain gage data in tests 1A and 3A, so its strength comparison is not presented in Fig. 3.78.

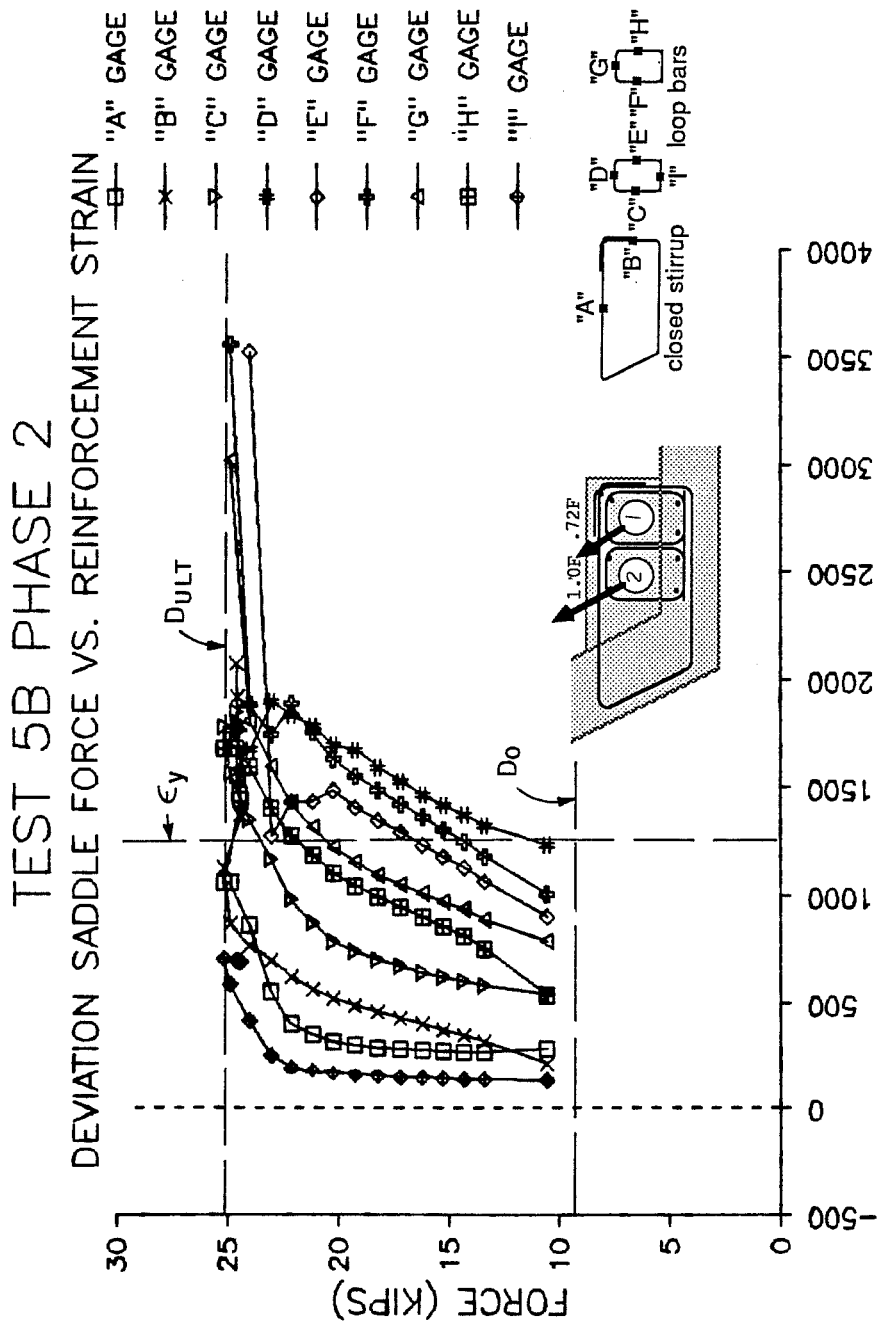


Figure 3.74 Test 5B Reinforcement Strain Data - Phase 2

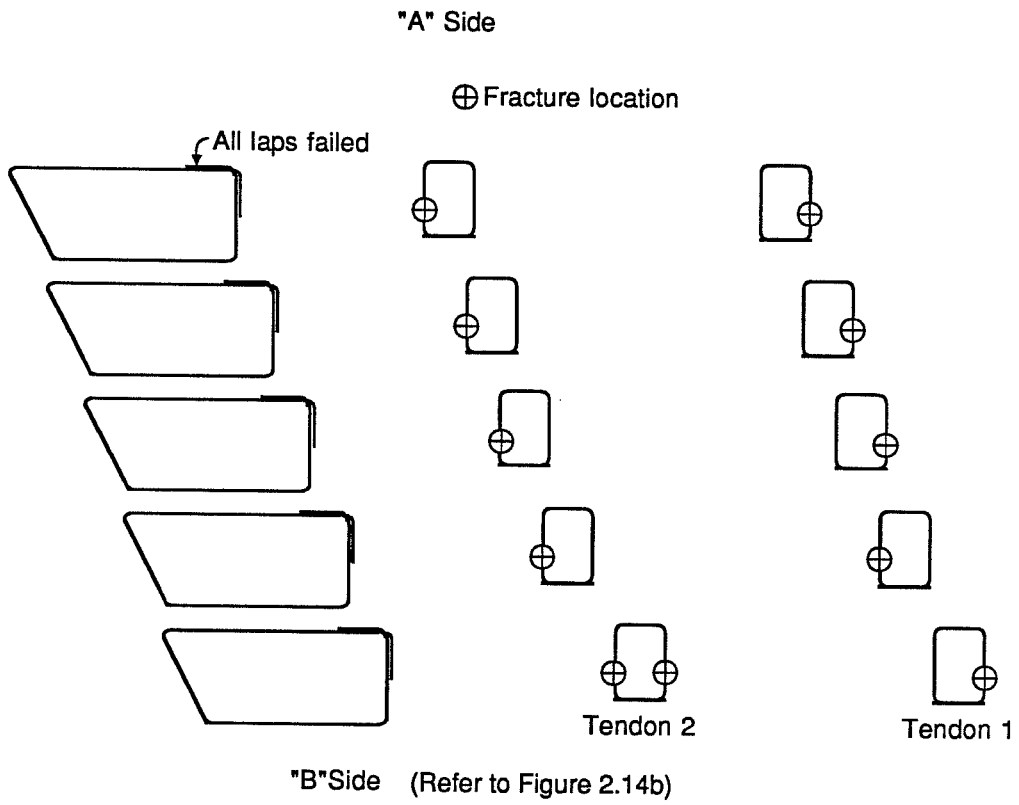


Figure 3.75 Test 5B Reinforcement Failure Locations

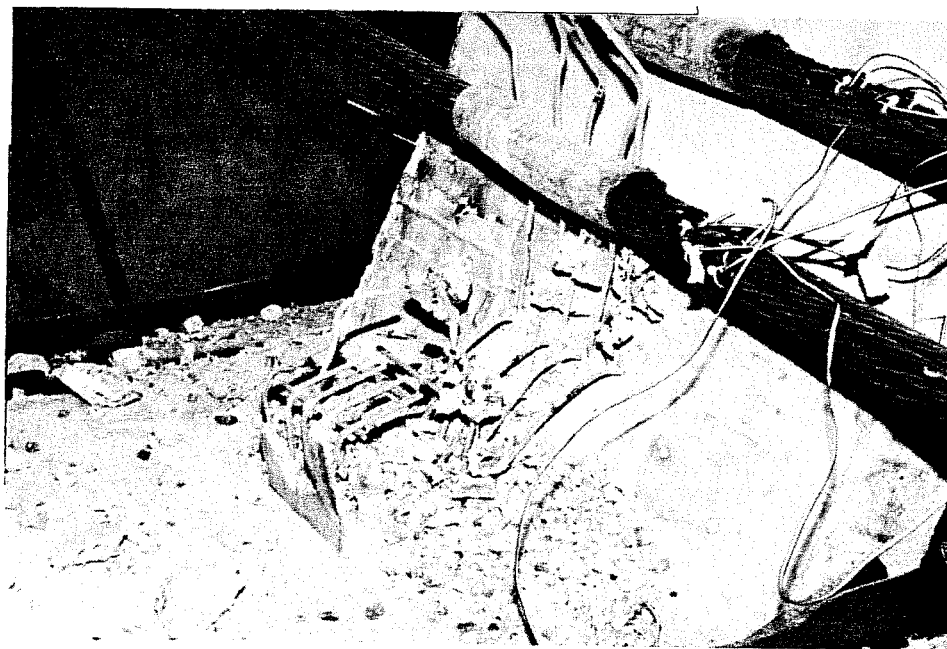
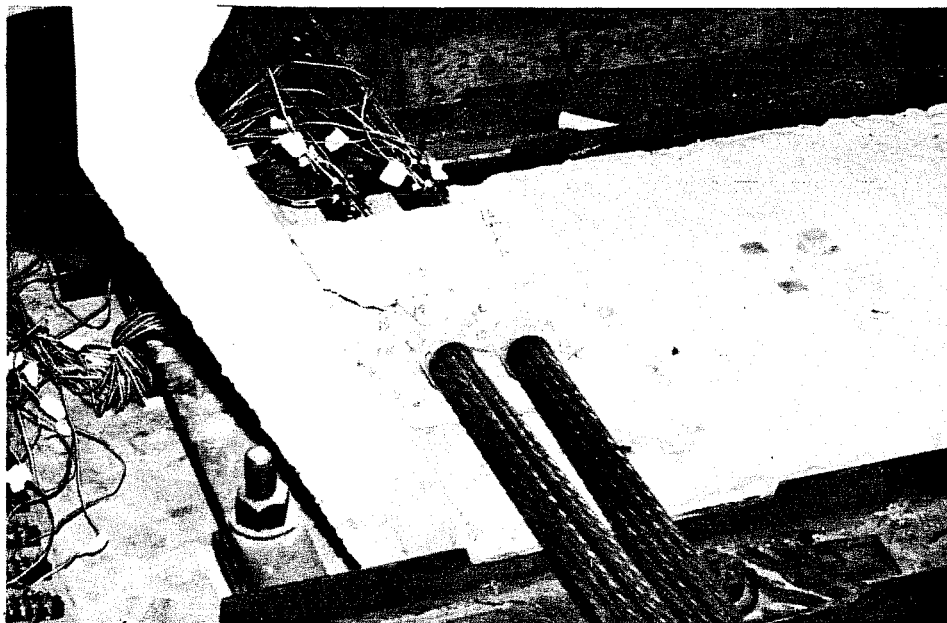


Figure 3.76 Test 5B - Before and After Failure

TEST 5B
RATIO D/D₀ AT CRITICAL STAGES

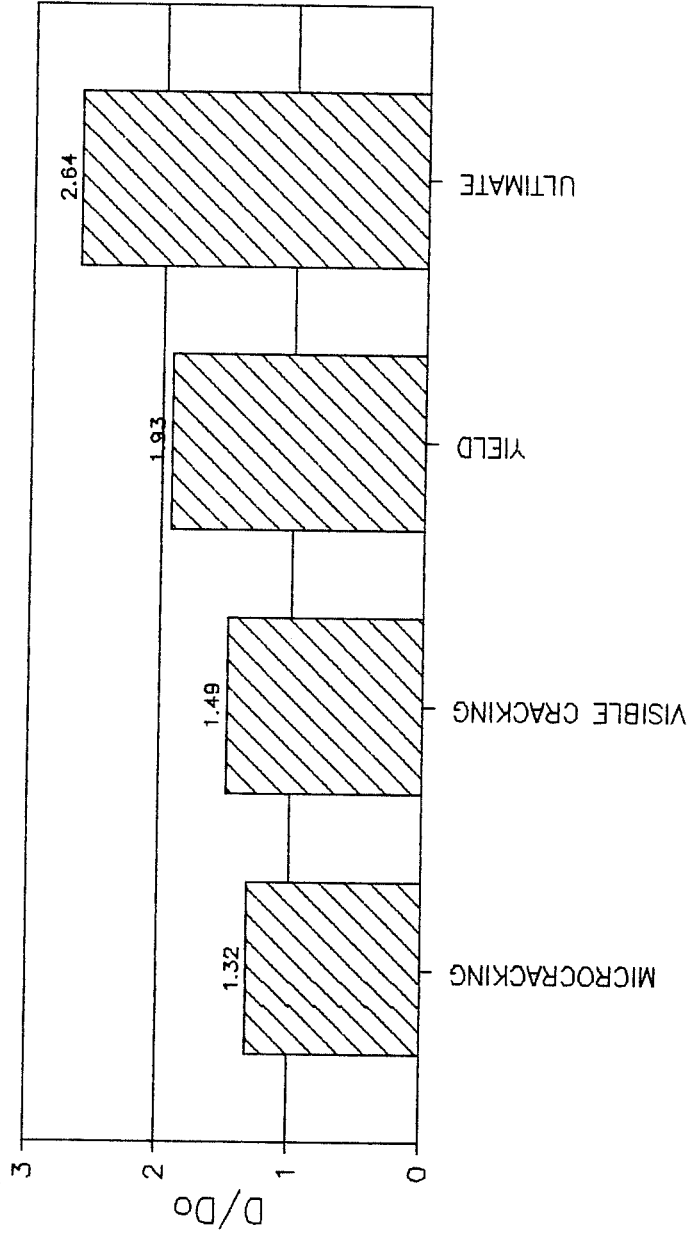
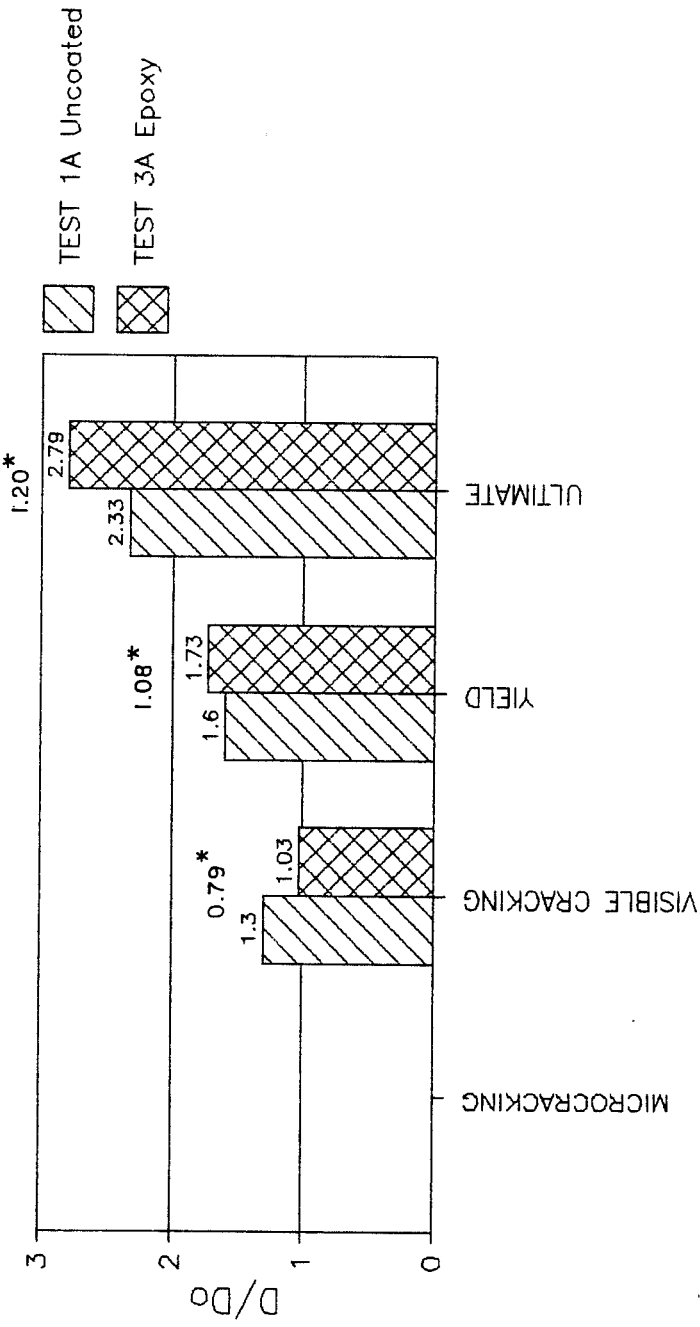


Figure 3.77 Test 5A Strength Comparison

COMPARISON OF TESTS 1A AND 3A

RATIO D/D_0 AT CRITICAL STAGES



*Ratio of epoxy coated reinforcement specimen strength to the uncoated reinforcement specimen strength.

Figure 3.78 Comparison of Tests 1A and 3A

COMPARISON OF TESTS 1B AND 3B

RATIO D/D_0 AT CRITICAL STAGES

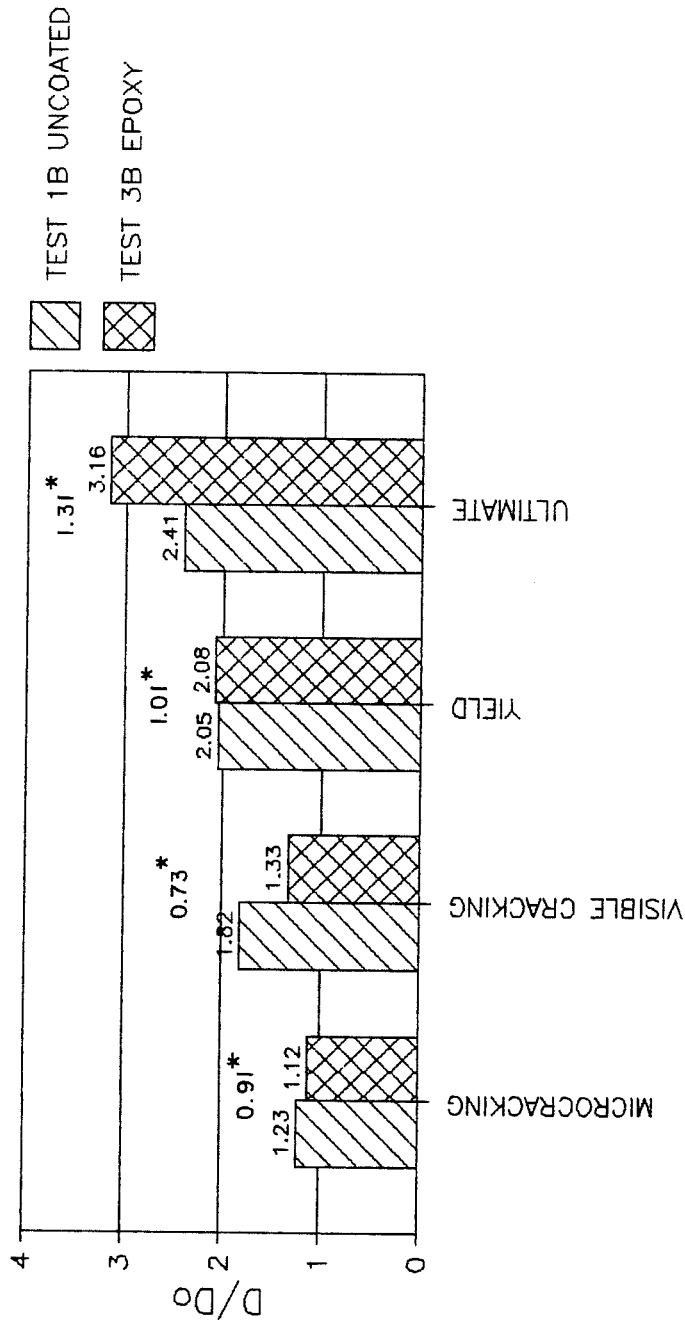
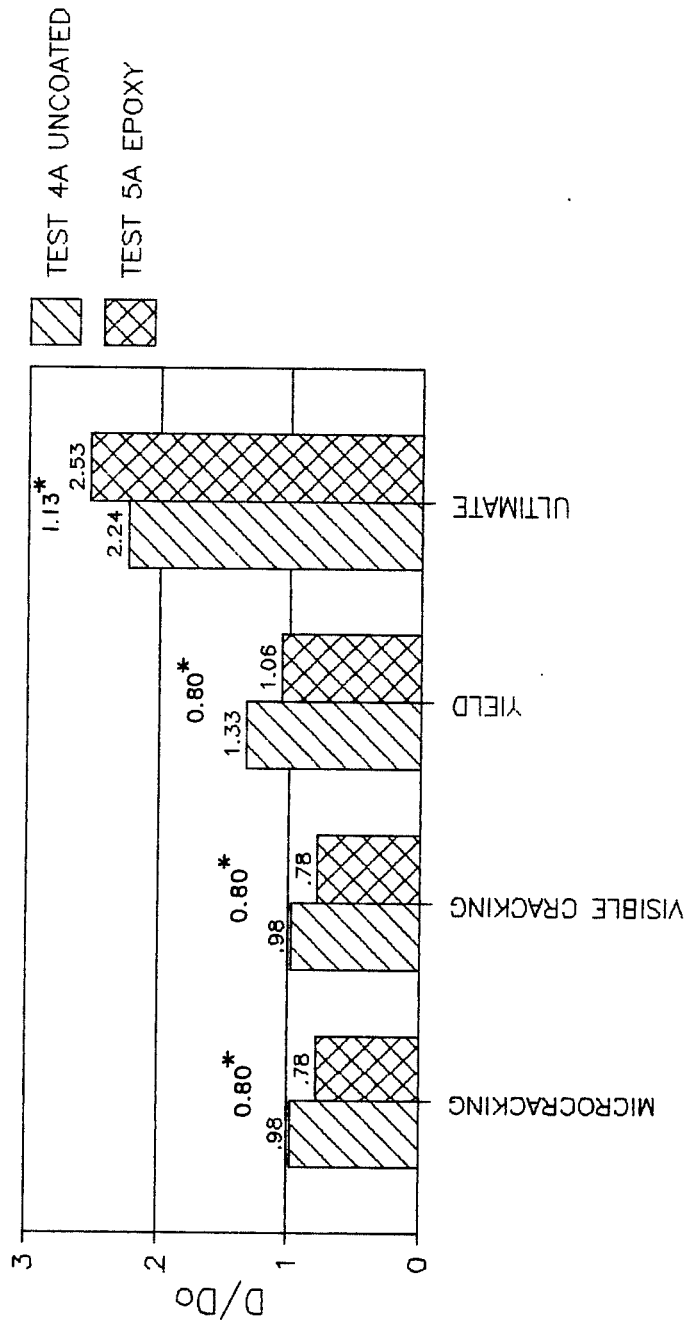


Figure 3.79 Comparison of Tests 1B and 3B

COMPARISON OF TESTS 4A AND 5A

RATIO D/D₀ AT CRITICAL STAGES

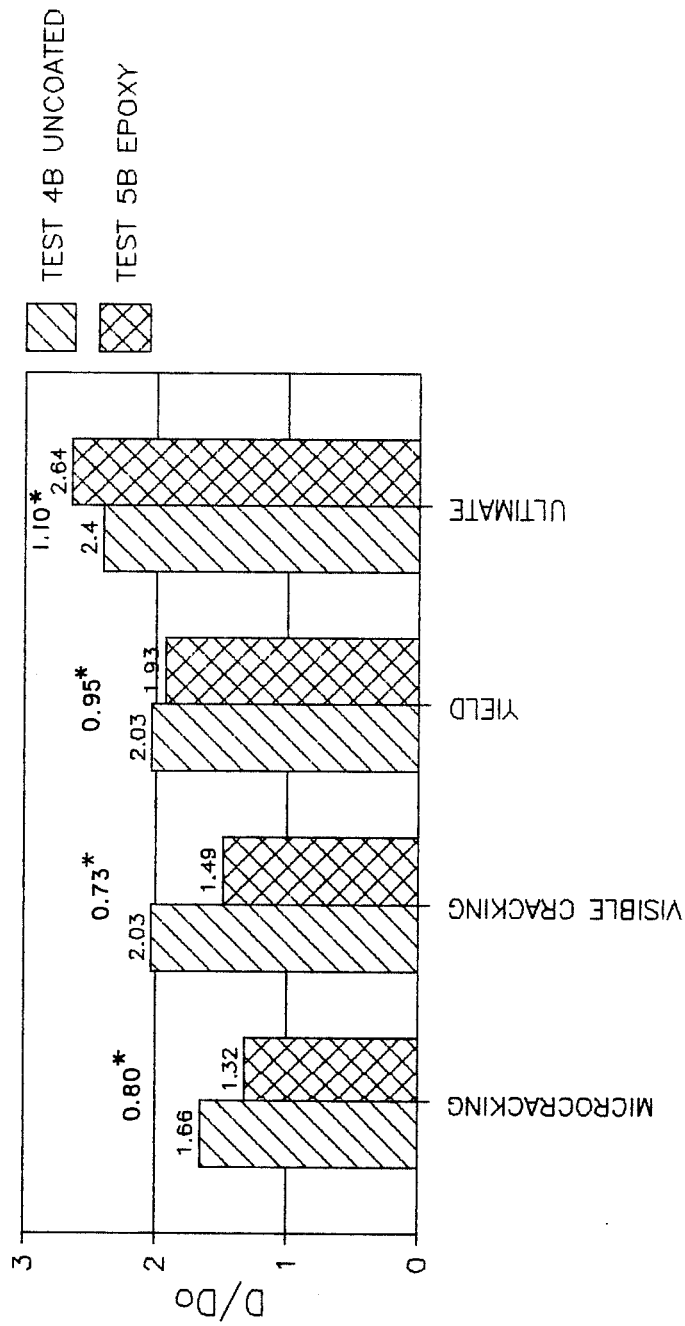


*Ratio of epoxy coated reinforcement specimen strength to the uncoated reinforcement specimen strength.

Figure 3.80 Comparison of Tests 4A and 5A

COMPARISON OF TESTS 4B AND 5B

RATIO D/D_o AT CRITICAL STAGES



*Ratio of epoxy coated reinforcement specimen strength to the uncoated reinforcement specimen strength.

Figure 3.81 Comparison of Tests 4B and 5B

Tests 3A, 3B, 5A, and 5B were fabricated with epoxy reinforcement, while the others were fabricated with uncoated reinforcement.

The results indicate that for microcracking to occur in the epoxy coated reinforcement specimens, the force was between 80% and 91% of that of the uncoated reinforcement specimens averaging 84%. For visible cracking to occur in the epoxy coated reinforcement specimens, the force was between 73% and 80% of that of the uncoated reinforcement specimens averaging 76%. These are reasonable decreases because it is known that epoxy coated reinforcement bonds less with concrete (3).

For yielding of the reinforcement to occur in the epoxy coated specimens, the percentages of force of that of the uncoated specimens varied more widely. The percentages ranged between 80% and 108% averaging 96%. For this critical stage, it is reasonable to expect that both the epoxy coated reinforcement specimens and the uncoated reinforcement specimens would require about the same force to yield the reinforcement. The reason being that in both types of specimens, the entire force is transferred to the reinforcement at this stage and it should not be particularly dependent on the bond characteristics of the reinforcement. With the exception of the comparison of tests 4A and 5A, the other percentages were between 95% and 108% which supports the correlation between the above premise and the results.

It is interesting to note the unexpectedly favorable results for the epoxy coated reinforcement specimens for ultimate strength. A significant percentage increase in strength over that of the uncoated reinforcement specimens developed for the epoxy coated reinforcement specimens. This percentage of strength was between 110% and 131% of that of the uncoated reinforcement specimens averaging 118%. It is unlikely, that the maximum increase in strength for the epoxy coated reinforcement specimens attributable to the coating can be as high as 31% since some of the increase in strength has to be attributed for chair reinforcing inconsistencies which were stated in the preceding sections for the comparison tests 1A and 3A and also 1B and 3B. Specimen 3A and 3B had an increase in strength respectively of 20% and 31%.

However, a reason for this increase in strength in the epoxy coated reinforcement specimens might be attributed to the greater development of the force resisting mechanisms that occurred within the deviation saddle. An explanation for this might be that the local strains are lower for the epoxy coated reinforcement specimens because of the poorer bond of the reinforcement to the concrete; therefore, the reinforcement does not fracture as soon and more force resistance is developed by completely mobilizing other bars. There was a significant increase in strain in the top surface reinforcement for specimens 3A and 3B which possibly did not develop in specimens 1A and 1B because of higher local strains in the link bar which caused it to

fracture at a lower load than that of test 3A and 3B. In specimens 5A and 5B, it is difficult to know how much extra strain was developed in some gages since the gages generally failed at yield of the reinforcement, though, it is somewhat apparent from the plots that strains were higher for these specimens.

In conclusion, the epoxy coating reinforcement had adverse effects on the behavior of the deviation saddle for microcracking and visible cracking. The average reduction in strength for microcracking and visible cracking was 16% and 24% respectively. For the critical strength stage of yielding, coated reinforcement has little effect on the behavior. The reason being that at this stage all the load is transferred to the reinforcement and it should not be particularly dependent on the bond characteristics of the reinforcement. The coated reinforcement favorably effected the behavior of the deviation saddle at ultimate with an average increase in strength of 15% since it allowed for the complete mobilization of all the reinforcement within the deviation saddle.

CHAPTER 4 ANALYSIS OF TEST RESULTS

4.1 Introduction

Deviation saddle behavior can be complex because several different force resisting mechanisms can occur simultaneously. The reinforcement in a deviation saddle must be distributed: (1) to resist direct tension forces caused by the tendon deviations, (2) to resist shear along a cracked plane which may form in the deviation saddle as it tends to separate from the web and flange, and (3) to control and distribute cracks that form on the deviator top surface. In this chapter, the deviation saddle specimens are analyzed by two different methods. The first method utilizes simplified analysis models (Sec. 4.2) and the second method utilizes strut-tie analysis models (Sec. 4.3).

4.2 Evaluation of Results With Respect To Simplified Analysis Models

Observation of the deviation saddles, their cracking pattern, and reinforcement strain indicated that there were three major force resisting mechanisms occurring in the deviation saddles in this test series. Therefore, three simplified analysis behavioral models were developed to analyze these force resisting mechanisms. The analysis models are designated as direct tension model, shear friction model, and beam model. These analysis techniques were introduced by Carter

(1) and modified versions will be utilized for analysis of the entire test series. These behavioral models are shown in Fig. 4.1.

The direct tension model facilitates the analysis of the direct tension reinforcement in the deviation saddle. This is the reinforcement that is the primary tie to the box section. The shear friction model facilitates the analysis of the shear friction reinforcement which transfers the shear across a crack interface which may form below the tendon ducts. The beam model facilitates the analysis of the top surface reinforcement which provides added strength to the deviation saddle to resist pull-out forces. This reinforcement is stressed like tensile reinforcement in a beam. It also distributes surface cracks. The ϕ factor used in comparisons with test results for all simplified analysis models has a value of one since the material strengths and specimen dimensions are known accurately. The actual failures may draw on a combination of mechanisms. This is discussed in Sec. 4.2.4.

4.2.1 Direct Tension Model. The behavior of the direct tension reinforcement in the deviation saddle is straightforward since the reinforcement strength is accurately known for yield and ultimate. This reinforcement closely confines the tendon duct such that the tendon deviation forces are efficiently transferred to this reinforcement. The link bar strength is determined for the two critical strength stages, yield and ultimate. For design purposes, the

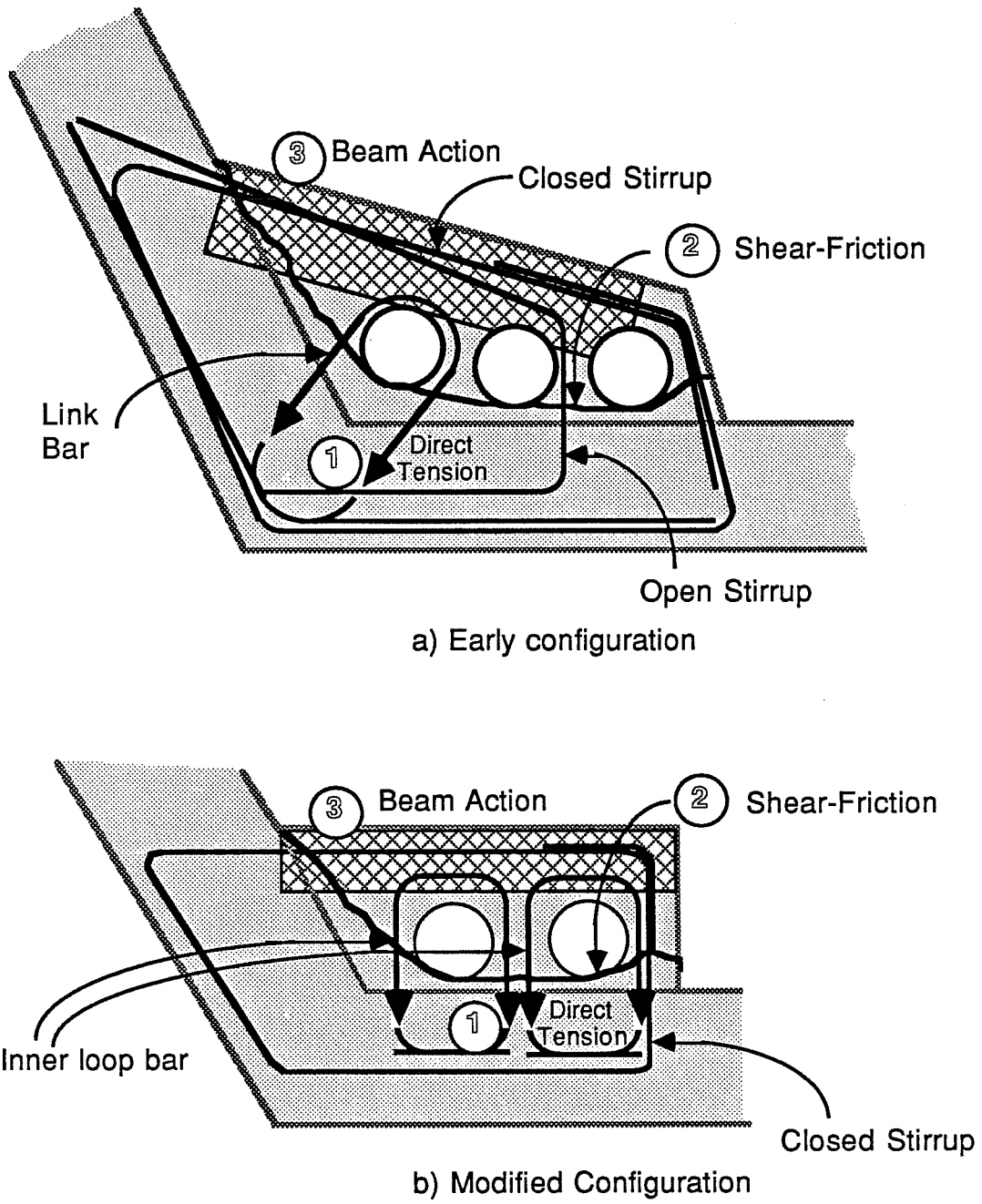
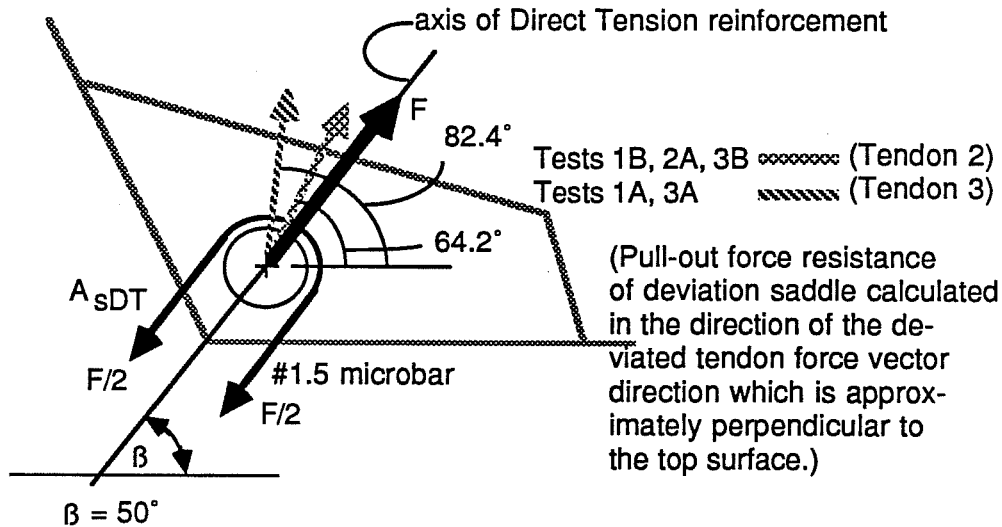


Figure 4.1 Behavioral Models

yield strength of the reinforcement would be utilized rather than the ultimate strength.

In specimens 1A, 1B, 2A, 3A, and 3B, the direct tension reinforcement was the link bar which was at an angle of 50° with the horizontal plane in the direction of the center of the box. Specimen 2B reinforcement scheme did not include the link bar since the objective of the test was to isolate the behavior of the stirrups of tests 1A and 1B. The yield and ultimate strength of the link bar is simply determined by multiplying the yield and ultimate strength of the reinforcement, 45 and 63 ksi respectively, by the total area of the link bar reinforcement. This is the yield and ultimate strength in the direction of the axis of the link bar as shown by the heavy vector in Fig. 4.2. The direction of the deviated component of the tendon force restrained by the link bar for each test is shown as the checkered or the striped arrow in the top sketch. This shows that the axis of the link bar is not directly in line with the deviated tendon force. Therefore, the effective link bar strength in the direction of the force is slightly reduced from the link capacity. The reduction factor is the cosine of the angle between the axis of the link bar and the deviated tendon force.

The direct tension reinforcement of specimens 4A, 4B, 5A, and 5B were rectangular loops that were anchored under the top mat of reinforcement of the box section. The yield and ultimate direct tension strength in the vertical direction is determined by multi-



$$A_{sDT} = 4 \times (2 \times 0.0276 \text{ sq.in.}) = 0.2208 \text{ sq.in.}$$

$$f_y = 45 \text{ ksi} \quad f_u = 63 \text{ ksi}$$

$$\begin{aligned} F_y &= \text{Yield Direct Tension Capacity of Link Bars} \\ &= A_{sDT} \times f_y \\ &= 0.2208 \text{ sq.in.} \times 45 \text{ ksi} \\ &= 9.9 \text{ kips} \end{aligned}$$

Effective Link Bar Strength in the Direction of Deviated Tendon Force

$$\begin{aligned} F_y &= 9.9 \text{ k}(\cos(82.4^\circ - 50^\circ)) = 8.4 \text{ k (1A, 3A)} \\ F_y &= 9.9 \text{ k}(\cos(64.2^\circ - 50^\circ)) = 9.6 \text{ k (1B, 2A, 3B)} \end{aligned}$$

$$\begin{aligned} F_{ult} &= \text{Ultimate Direct Tension Capacity of Link Bars} \\ &= A_{sDT} \times f_u \\ &= 0.2208 \text{ sq.in.} \times 63 \text{ ksi} \\ &= 13.9 \text{ kips} \end{aligned}$$

Effective Link Bar Strength in the Direction of Deviated Tendon Force

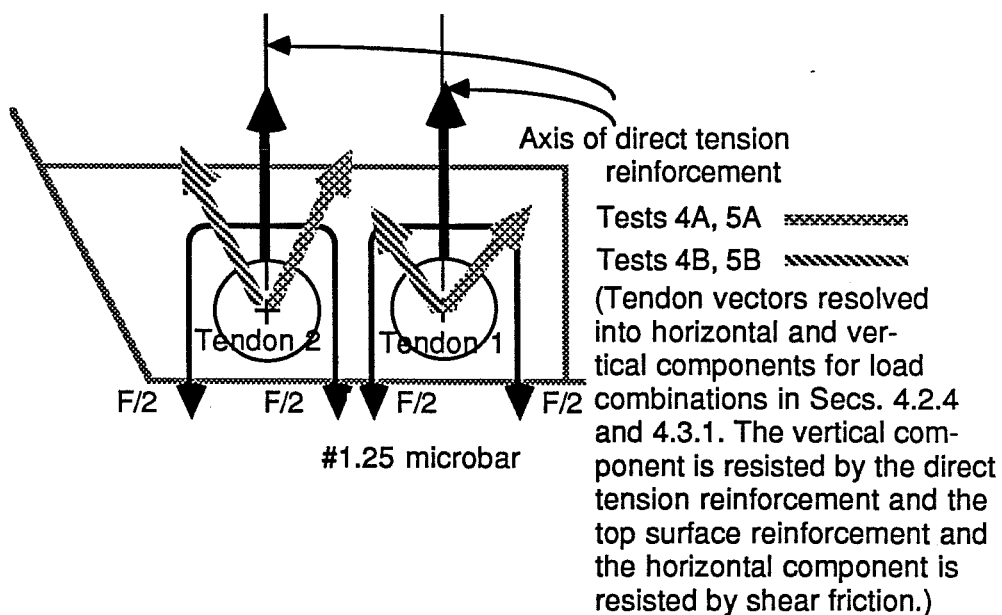
$$\begin{aligned} F_{ult} &= 13.9 \text{ k}(\cos(82.4^\circ - 50^\circ)) = 11.7 \text{ k (1A, 3A)} \\ F_{ult} &= 13.9 \text{ k}(\cos(64.2^\circ - 50^\circ)) = 13.5 \text{ k (1B, 2A, 3B)} \end{aligned}$$

4.2 Direct Tension Model-Tests 1A, 1B, 2A, 3A, 3B

plying the yield and ultimate strength of the reinforcement, 36 and 51 ksi respectively, by the total area of loop bar reinforcement for each tendon. This is shown in Fig. 4.3. In the analysis combinations of Sec. 4.2.4, the tendon deviation forces shown as the checkered or striped arrows in the sketch of Fig. 4.3 are resolved into horizontal and vertical components. The direct tension model is assumed to resist the vertical component, and the shear friction model is assumed to resist the horizontal component.

4.2.2 Shear Friction Model. The behavior of the shear friction reinforcement is somewhat more complex than that of the direct tension reinforcement. Shear friction reinforcement is required to transfer shear across a given plane of a potential crack in the deviation saddle. The physical test results showed that the location of the critical shear plane in this test series was immediately below the tendon ducts.

There has been an extensive amount of research completed on the subject of shear friction by Mattock (4,5,6). The types of test specimens that were utilized in Mattock's investigations were either intentionally cracked across the shear plane before testing, or the shear plane was initially uncracked. The behavior of the tests of the initially uncracked specimens corresponds to the behavior of the deviation saddle since a crack does not form until after loading. Instances where a crack may exist along the shear plane before loading is prevalent in precast concrete connections. Such cracks can occur



$$A_{sDT} = 5 \times (2 \times 0.0192 \text{ sq.in.}) = 0.1920 \text{ sq.in.}$$

$$f_y = 36 \text{ ksi} \quad f_u = 51 \text{ ksi}$$

$$\begin{aligned} F_y &= \text{Yield Direct Tension Capacity of Loop Bars} \\ &= A_{sDT} \times f_y \\ &= 0.1920 \text{ sq.in.} \times 36 \text{ ksi} \\ &= 6.9 \text{ kips (each tendon)} \end{aligned}$$

$$\begin{aligned} F_{ult} &= \text{Ultimate Direct Tension Capacity of Loop Bars} \\ &= A_{sDT} \times f_u \\ &= 0.1920 \text{ sq.in.} \times 51 \text{ ksi} \\ &= 9.8 \text{ kips (each tendon)} \end{aligned}$$

Figure 4.3 Direct Tension Model-Tests 4A, 4B, 5A, 5B

for a variety of reasons unrelated to shear, such as tension forces caused by restrained shrinkage or temperature deformations, or accidental dropping of members, etc. However, these do not apply to the monolithically cast deviation saddle.

Typical test results from Mattock's research are shown in Fig. 4.4, where the average shear stress at failure, v_u , is plotted against ρf_y , where ρ is the ratio of the area of the transverse reinforcement across the shear surface. As shown in the figure, considerably higher strengths were attained for the uncracked sections than for the cracked sections. The conclusions from the shear friction research that relate to this deviation saddle behavior are as follows:

- 1) For 4000 psi normal weight concrete and values of ρf_y between 200 and 1000 psi, the reduction in strength for the specimens with a pre-existing crack is approximately a constant 250 psi.

- 2) Changes in strength, size, and spacing of reinforcement affect the shear strength only insofar as they change the value of the reinforcement parameter ρf_y for f_y less than or equal to 66 ksi.

- 3) Dowel action of reinforcing bars crossing the shear plane is insignificant in the initially uncracked concrete.

- 4) It is appropriate to add the normal stress acting across the assumed crack or shear plane, σ_{Nx} , to the reinforcement parameter ρf_y when calculating shear transfer strength in initially uncracked reinforced concrete. (σ_{Nx} is positive when compression and negative when tension.)

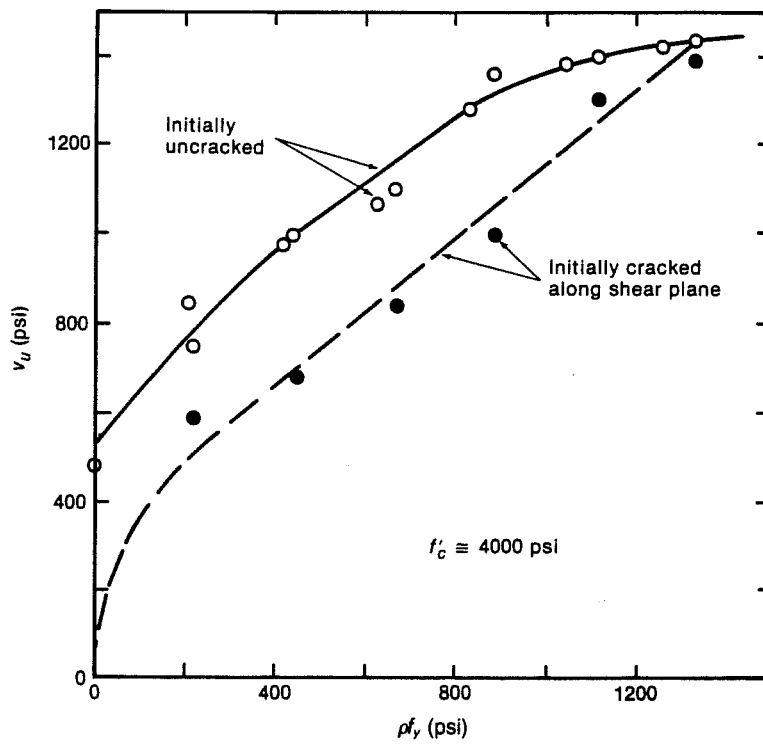


Figure 4.4 Typical Test Results for Shear Friction Study (From Ref. 7)

5) The shear transfer strength of initially uncracked concrete is developed by a truss action after diagonal tension cracking across the shear plane occurs. Failure occurs when the inclined concrete struts fail under a combination of shear and axial force. This is shown in Fig. 4.5. Similar diagonal cracking below the ducts was apparent in some of the tests.

The Mattock and the ACI design equation for shear friction strength were formulated for the more critical case, the initially cracked specimen. This is shown in Fig. 4.6. This makes good sense for design purposes, but for analysis purposes it is desired to have an equation which represents the true initially uncracked behavior. If the lower bound equation is used, it might falsely indicate that shear friction was the direct cause of the failure.

The equation for shear strength of initially cracked specimens formulated by Mattock is $v_u = 400 + 0.8(\rho f_y + \sigma_{Nx})$, which is applicable to the general case of both shear and direct tension or compression acting across a shear plane. This shear stress equation is limited to $v_u \leq 0.3f'_c$. The variable ρ is the ratio of the area of the transverse reinforcement across the shear surface to the area of the shear surface, f_y is the yield point stress of the reinforcement (psi), and σ_{Nx} is the normal stress acting across the shear plane (σ_{Nx} is positive when compression and negative when tension). However, the shear strength across the shear plane in the deviation saddle is somewhat greater since it was initially uncracked. From Fig. 4.4 it

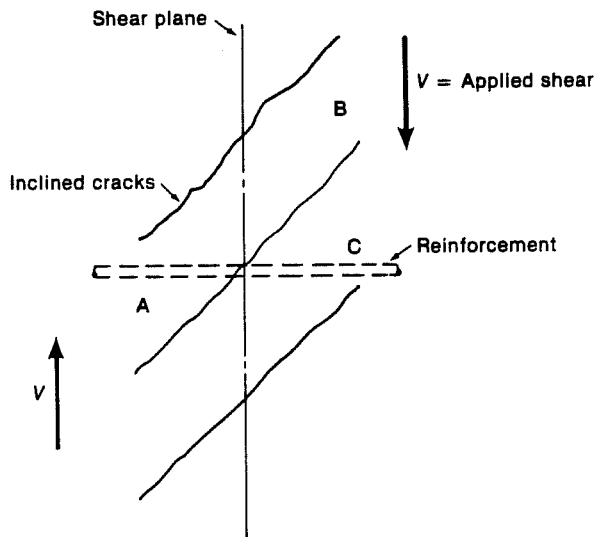


Figure 4.5 Diagonal Tension Cracking Along Previously Uncracked Shear Plane (From Ref. 7)

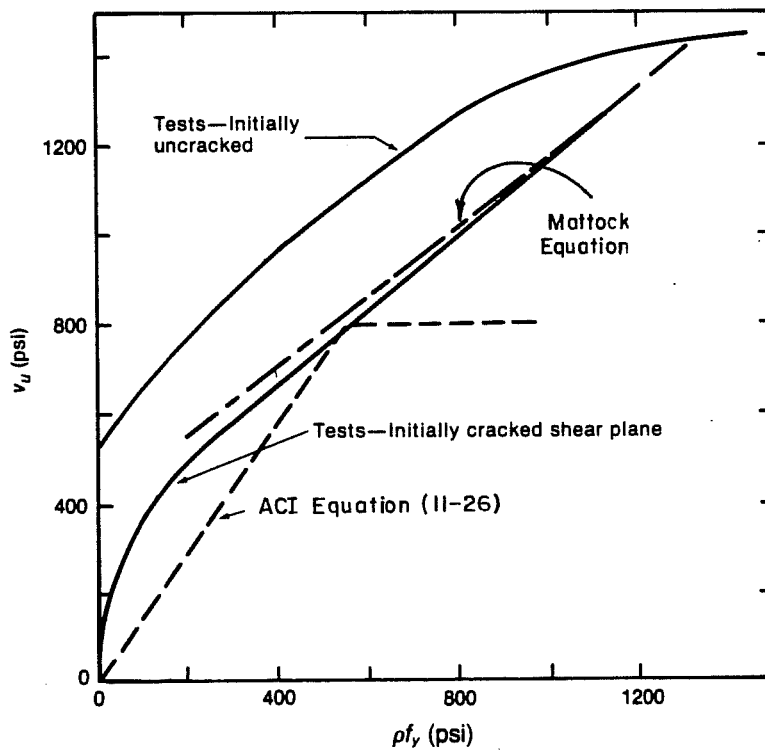
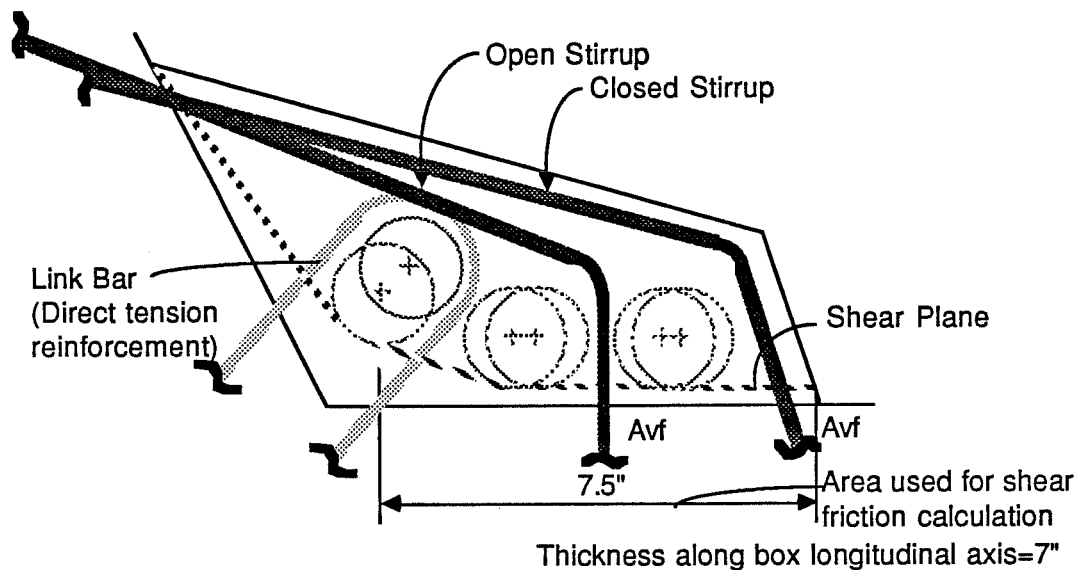


Figure 4.6 Comparison of Mattock Test Results and Design Equations (From Ref. 7)

appears that this extra strength is in the range of 250 psi for ρf_y between 200 and 1000 for 4000 psi concrete. This is an acceptable value for use in analyzing the current series since concrete strength in the deviation saddles was greater than 4000 psi.

Defining exactly what area of concrete and reinforcement contributes to the shear friction strength in the deviation saddle is difficult. It is obvious from the failures that the critical shear plane was located below the tendon ducts. For the loading cases where the total force vector was directed towards the web, it is possible that the shear plane contributing to the shear strength could also extend from the corner duct to the intersection of the top surface of the deviation saddle and the web wall. However, to be conservative in the initial calculation this portion of the shear plane will be disregarded.

The shear friction calculation for tests 1A, 1B, 2B, 3A, and 3B, is shown in Fig. 4.7. This is the ultimate shear friction capacity but is based on yielding of the reinforcement. Shear friction transfer is questionable at strains approaching reinforcement ultimate. Deviator loads at first reinforcement yielding are compared to this ultimate shear friction capacity in Sec. 4.2.4 to provide further comparisons between test results and calculations. The specimen 2A detail did not include the open and closed stirrup. Most of its horizontal force component was resisted by the link bar. In addition, the unreinforced concrete in front of the tendon resisted



(Horizontal shear friction strength compared against total deviated tendon force horizontal component.)

Critical shear plane located below the ducts.

$$v_u = 400 + 0.8(pfy - \sigma_{Nx}) + 250 \quad (\text{psi}) \quad < 0.3f_c$$

$$V_u = 400A_c + 0.8(Asfy - N_x) + 250A_c \quad (\text{lb})$$

Assume direct tension across shear plane is taken by link bar.

$$\text{Therefore, } A_s = A_{vf} \text{ and } \sigma_{Nx} = 0$$

$$A_{vf} = 7(0.0491 \text{ sq. in.}) = 0.34 \text{ sq. in.}$$

$$f_y = 45 \text{ ksi}$$

$$A_c = (7.5")(7.0")(0.5) = 26.3 \text{ sq. in.}$$

Conservative reduction factor for tendon ducts reducing frictional shear stresses on shear plane.

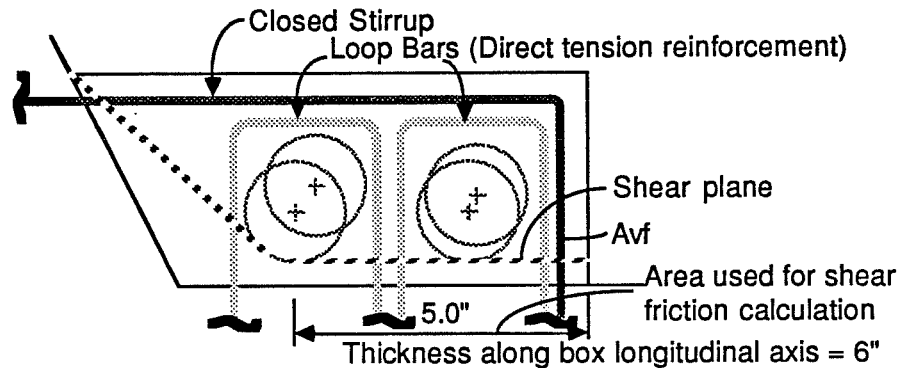
$$V_u = 650 \text{ psi}(26.3 \text{ sq. in.})/1000 + 0.8(0.34 \text{ sq. in.})(45 \text{ ksi}) = 29.3 \text{ k}$$

$$\text{Maximum allowable } V_u = 0.3f_c A_c = 0.3(5500 \text{ psi})(26.3 \text{ sq. in.})/1000 = 43.4 \text{ k O.K.}$$

Figure 4.7 Shear Friction Model-Tests 1A, 1B, 2B, 3A, 3B

the small horizontal force of tendon 1. The shear friction calculation for tests 1A, 1B, 2B, 3A, and 3B is somewhat simplified since the reinforcement for direct tension forces and shear friction was divided into the link bar resisting only tension forces across the shear plane and the stirrups resisting only shear friction. This may not be exactly correct, but is an acceptable starting assumption. The area of shear friction reinforcement is then equal to the area of the seven #2 bars in the front section of the deviation saddle. The yield strength of the reinforcement was 45 ksi. The initial assumption for the concrete area along the shear friction plane is taken as the horizontal distance from the centerline of the corner duct to the front face of the deviation saddle. This area is then reduced by 50% since the total frictional stresses along this plane would be lessened due to the substantial area where the tendon ducts contact the shear plane (chosen as a conservative estimate). When the lower bound shear friction force resistance from this calculation is compared with the total horizontal shear force in Sec. 4.2.4, it is obvious that shear friction was not the direct cause of the failure. However, in tests 1A and 3A where the horizontal shear forces were high from the tendons that were not confined by the link bar, it was obvious from the strain data and failure mechanism that this large horizontal force did influence the behavior with respect to cracking of the deviation saddle and yielding of the open stirrup.

The shear friction calculation for tests 4A, 4B, 5A, and 5B is shown in Figs. 4.8a and 4.8b. As with tests 1A, 1B, 2B, 3A, and 3B, some simplifying assumptions were made for the shear friction calculation. The reinforcement resisting direct tension forces and shear friction is divided into the loop bars resisting only tension forces across the shear plane and the outer closed stirrups resisting only shear friction. The area of shear friction reinforcement is then equal to the five #1.25 bars in the front face of the deviation saddle. This is a very conservative assumption because until the loop bars reach direct tension capacity, there will be some contribution to the shear friction resistance. In this type deviation saddle shown in Fig. 4.1b, the loop bar capacity will be much greater than the tension forces across the shear plane, so some of the loop bar capacity could also contribute to the shear friction resistance. The yield strength of the reinforcement was 36 ksi. The area of concrete utilized in this calculation is that from the centerline of the corner tendon duct to the front face of the deviation saddle. Again as in the shear friction calculation of the other type of deviation saddle detail shown in Fig. 4.1a, the area of concrete is reduced by 50% because of the possible lessening of frictional stresses on the shear plane due to the substantial area where the tendon ducts contact the shear plane. For the above assumptions, the calculations are shown in Fig. 4.8a. When the lower bound shear friction force resistance from this calculation is compared with the total horizontal shear force in



(Tendon vectors resolved into horizontal and vertical components for load combinations in Secs. 4.2.4. The vertical component is resisted by the direct tension reinforcement and the top surface reinforcement and the horizontal component is resisted by shear friction.)

Critical shear plane located below ducts.

$$v_u = 400 + 0.8(pfy - \sigma_{Nx}) + 250 \text{ (psi)} < 0.3f'_c$$

$$V_u = 400A_c + 0.8(Asfy - N_x) + 250A_c \text{ (lb)}$$

Assume tension across the shear plane is resisted by loop bars.

Therefore, $A_s = A_{vf}$ and $\sigma_{Nx} = 0$

$$A_{vf} = 5(0.0192 \text{ sq. in.}) = 0.0960 \text{ sq. in.}$$

$$f_y = 36 \text{ ksi}$$

$$A_c = (2.9" + 2.1")(6.0")(0.5) = 15.0 \text{ sq. in.}$$

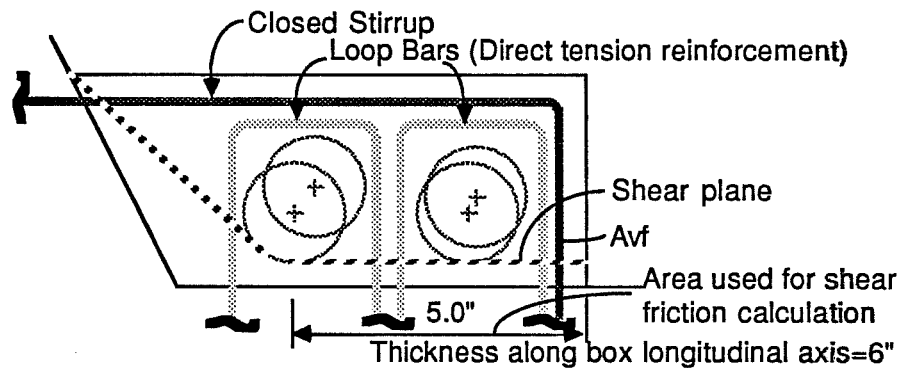
Conservative reduction factor for tendon ducts reducing frictional stresses on shear plane.

$$V_u = 650 \text{ psi}(15.0 \text{ sq. in.})/1000 + 0.8[(0.0960 \text{ sq. in.})(36 \text{ ksi})] = 12.5 \text{ k}$$

$$\text{Maximum } V_u = 0.3f'_c A_c = 0.3(5500 \text{ psi})(15.0 \text{ sq. in.})/1000 = 24.8 \text{ k} > 12.5 \text{ k} \text{ O.K.}$$

This value when compared to the total horizontal shear forces appeared too conservative. Some assumptions were revised. See Fig. 4.8b.

Figure 4.8a Shear Friction Model-Tests 4A, 4B, 5A, 5B-First Trial



(Tendon vectors resolved into horizontal and vertical components for load combinations in Secs. 4.2.4. The vertical component is resisted by the direct tension reinforcement and the top surface reinforcement and the horizontal component is resisted by shear friction.)

Critical shear plane located below ducts.

$$v_u = 400 + 0.8(pfy - \sigma_{N_x}) + 300 \text{ (psi)} < 0.3f_c$$

$$V_u = 400A_c + 0.8(Asfy - N_x) + 300A_c \text{ (lb)}$$

Assume tension across the shear plane is resisted by loop bars.

Therefore, $A_s = A_{vf}$ and $\sigma_{N_x} = 0$

$$A_{vf} = 5(0.0192 \text{ sq. in.}) = 0.0960 \text{ sq. in.}$$

$$f_y = 36 \text{ ksi}$$

$$A_c = (2.9" + 2.1")(6.0")(0.6) = 18.0 \text{ sq. in.}$$

Increased conservative reduction factor for tendon ducts reducing frictional stresses on shear plane.

$$V_u = 700 \text{ psi}(18.0 \text{ sq. in.})/1000 + 0.8(0.0960 \text{ sq. in.})(36 \text{ ksi}) = 15.5 \text{ k}$$

$$\text{Maximum } V_u = 0.3f_c A_c = 0.3(5500 \text{ psi})(18.0 \text{ sq. in.})/1000 = 29.7 \text{ k} > 15.5 \text{ k} \text{ O.K.}$$

Figure 4.8b Shear Friction Model-Tests 4A, 4B, 5A, 5B-Second Trial

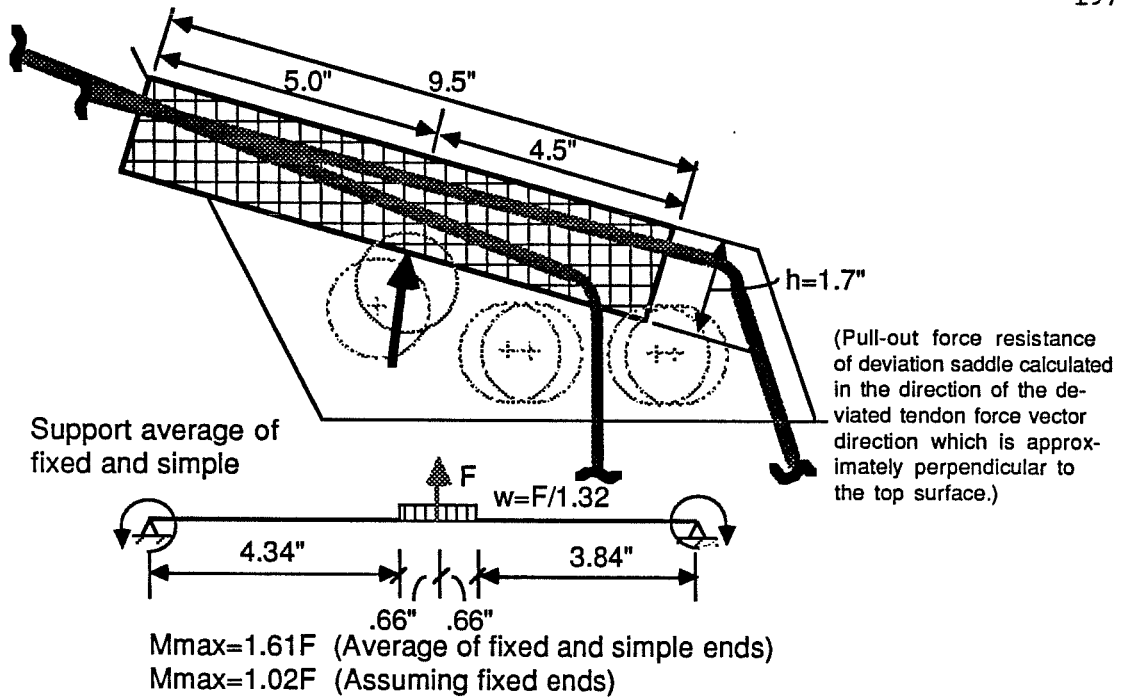
Sec. 4.2.4, it appears that the shear friction strength is only slightly greater than the total horizontal shear force acting on the critical plane. However, it is not believed that the failure was directly due to shear friction capacity being exceeded since the failure appearance was not typical of the failures in Mattock's investigation for initially uncracked specimens subjected to shear and tension across the shear plane. In Mattock's investigation, the shear transfer strength of initially uncracked concrete is developed by a truss action after diagonal tension cracking across the shear plane occurs. The failure was quite brittle and was characterized by the extension of one of the larger diagonal tension cracks roughly parallel to the shear plane, linking up with other diagonal tension cracks, and by compression spalling of the concrete, particularly near the ends of the shear plane. Although similar diagonal cracking below the ducts was apparent in tests 4A, 4B, 5A, and 5B, there was no apparent compression spalling of the concrete near the cracks below the tendon ducts. Therefore, some less conservative assumptions are warranted since it is very likely that the simplifying assumptions were too conservative. The reduction factor for the tendon ducts reducing the frictional stresses on the shear plane which was applied to the area of concrete resisting shear friction might be increased to 0.6 because this 0.5 value was chosen as a very conservative estimate. Also, the factor of 250 psi which was added on to the original shear friction equation because the deviation saddle was

initially uncracked could be increased to at least 300 psi since the 250 psi value was determined for a concrete strength of 4000 psi, whereas the deviation saddle concrete strength was 6000 psi. With the inclusion of these minor adjustments of assumptions, the revised calculations are shown in Fig. 4.8b. When this value is compared to the horizontal shear friction forces in Sec. 4.2.4, it is apparent that the calculated shear strength is 20% to 30% higher than total horizontal shear force in the test. In spite of the increased assumptions, it is still believed that this is a conservative estimate of the shear friction strength.

4.2.3 Beam Model. It is obvious from the tests that reinforcement in the top surface of the deviation saddle was not only effective in distributing surface cracks, but also contributed to the pull-out strength of the deviation saddle. From the strain data and the crack patterns, it is apparent that the reinforcement was stressed much like that of tensile reinforcement in a beam. In specimens 1A, 1B, 2B, 3A, and 3B which were reinforced as shown in Fig. 4.1a, the reinforcement closer (outer closed stirrup) to the top surface had the greatest strain. This is probably due to the fact that the outer closed stirrup was a greater distance from the neutral axis of the assumed beam element. Specimen 2A did not have top surface reinforcement since the objective of the test was to isolate the link bar. It is important to note that this beam element is only an idealization since a beam with only flexural reinforcement would have

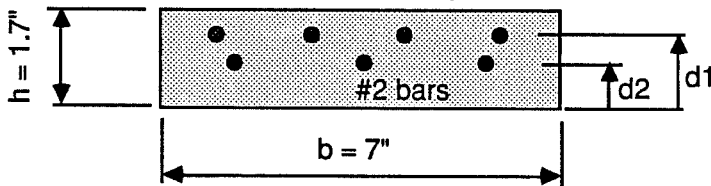
a considerably lower strength than that calculated by this model because it would fail in shear. Beams without web reinforcement fail when inclined cracking occurs or shortly afterwards. However, the inclined cracking of the beam element in the deviation saddle does not cause failure since the loaded surface of the assumed beam element is not free but is attached to the other portion of the deviation saddle.

The calculation for the beam element for tests 1A and 3A is shown in Fig. 4.9, and the calculation for the beam element for tests 1B, 2B, and 3B is shown in Fig. 4.10. The calculation is made only for yield strength of the reinforcement since it does not make sense to consider the absolute ultimate strength of the reinforcement. For these specimens, the top reinforcement was stressed by the deviated force from the tendon with the vertical deviation. The vector direction of this force was almost perpendicular to the top surface of the deviation saddle. This simplifies the overall analysis of the deviation saddle since the force resistance which is not attributed to that of the link bar strength can be attributed to that of the beam element without resolving the tendon vector force into components. The beam element for tests 1A and 3A was significantly different than that for tests 1B, 2B, and 3B. There was a smaller concrete depth above the tendon ducts in specimens 1A and 3A. Therefore, the beam element strength was much less. Also, the location of the force along the beam element was slightly different. The beam element fixity is highly indeterminate. The ends are not free to rotate nor are they totally



(Pull-out force resistance of deviation saddle calculated in the direction of the deviated tendon force vector direction which is approximately perpendicular to the top surface.)

CROSS SECTION:



$$d1 = 1.7" - 0.5" - 0.25"/2 = 1.08"$$

$$d2 = 1.7" - 1.0" = 0.70"$$

$$d = (d1 \times 4 + d2 \times 3) / 7 = 0.91"$$

$$f_y = 45 \text{ ksi}$$

$$f'_c = 5650 \text{ psi (1A)} \quad f'_c = 6000 \text{ psi (3A)}$$

$$A_s = 7 \times 0.0491 \text{ in}^2 = 0.344 \text{ in}^2$$

$$M_n = A_s \times f_y \times (d - a/2)$$

$$a = (A_s \times f_y) / (.85 \times f'_c \times b)$$

$$a = 0.46 \text{ (1A)} \quad a = 0.43 \text{ (3A)}$$

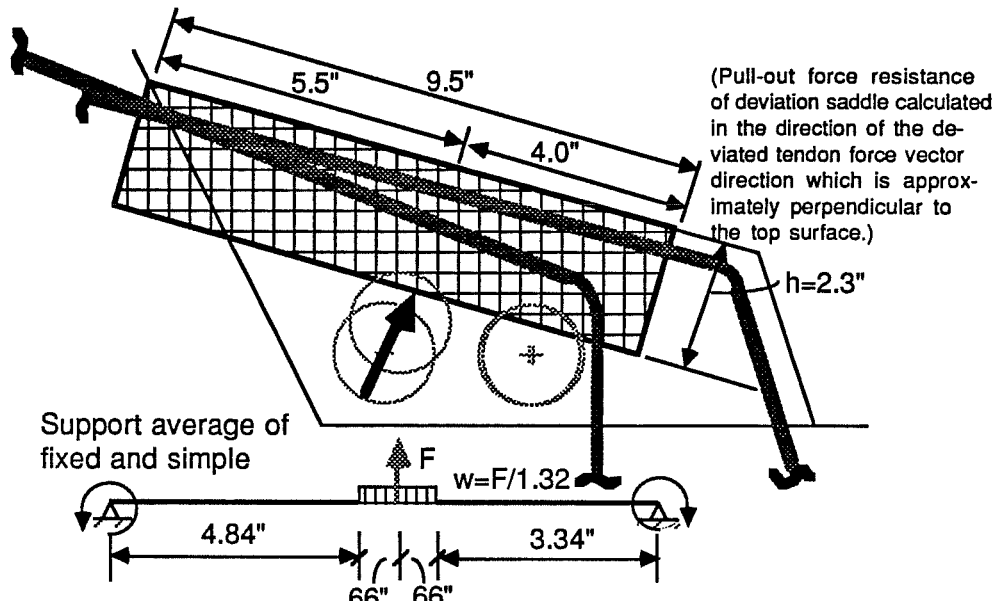
$$M_n = 0.344 \text{ in}^2 \times 45 \text{ ksi} \times (0.91" - 0.46"/2) = 10.5 \text{ k-in. (1A)}$$

$$M_n = 0.344 \text{ in}^2 \times 45 \text{ ksi} \times (0.91" - 0.43"/2) = 10.8 \text{ k-in. (3A)}$$

$M_n = M_{max} \longrightarrow$	$10.5 \text{ k-in.} = 1.61F$ $F = 6.5 \text{ k (1A)}$	Average of fixed and simple ends	$10.5 \text{ k-in.} = 1.02F$ $F = 10.3 \text{ k (1A)}$	Fixed ends
	$10.8 \text{ k-in.} = 1.61F$ $F = 6.7 \text{ k (3A)}$		$10.8 \text{ k-in.} = 1.02F$ $F = 10.6 \text{ k (3A)}$	

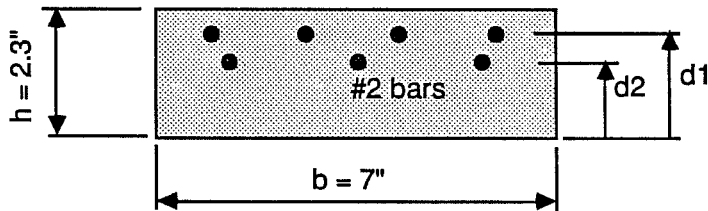
(capacity of top surface reinforcement perpendicular to top surface)

Figure 4.9 Beam Model-Tests 1A and 3A



$M_{max}=1.66F$ (Average of fixed and simple ends)
 $M_{max}=1.17F$ (Assuming fixed ends)

CROSS SECTION:



$d1=2.3"-0.5"-0.25"/2=1.68"$

$d2=2.3"-1.0"=1.30"$

$d = (d1 \times 4 + d2 \times 3) / 7 = 1.52"$

$f_y = 45 \text{ ksi}$

$f'_c = 5650 \text{ psi (1B)}$ $f'_c = 5750 \text{ psi (2B)}$ $f'_c = 6000 \text{ psi (3B)}$

$A_s = 7 \times 0.0491 \text{ in}^2 = 0.344 \text{ in}^2$

$M_n = A_s \times f_y (d - a/2)$

$a = (A_s \times f_y) / (.85 \times f'_c \times b)$

$a = 0.46 \text{ (1B)}$ $a = 0.45 \text{ (2B)}$ $a = 0.43 \text{ (3B)}$

$M_n = 0.344 \text{ in}^2 \times 45 \text{ ksi} (1.52" - 0.46"/2) = 20.0 \text{ k-in. (1B)}$

$M_n = 0.344 \text{ in}^2 \times 45 \text{ ksi} (1.52" - 0.45"/2) = 20.0 \text{ k-in. (2B)}$

$M_n = 0.344 \text{ in}^2 \times 45 \text{ ksi} (1.52" - 0.43"/2) = 20.2 \text{ k-in. (3B)}$

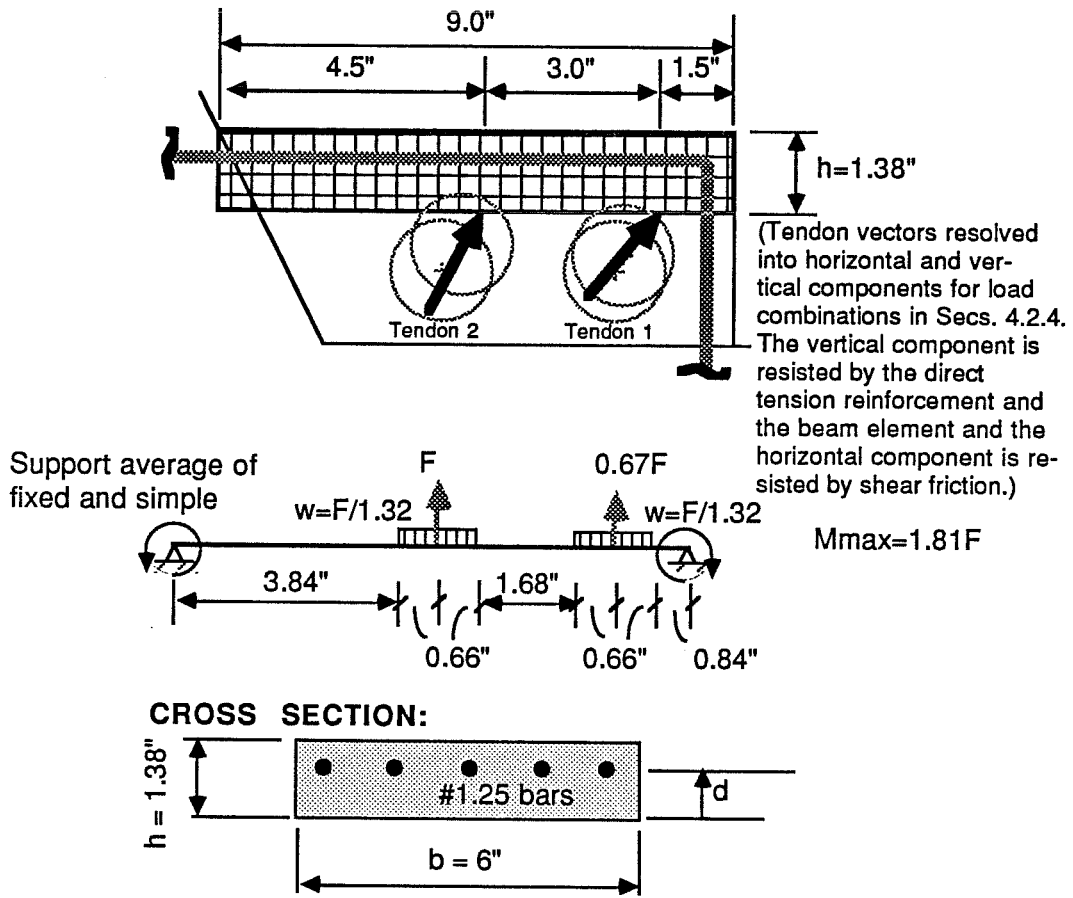
$M_n = M_{max}$	→	20.0 k-in. = 1.66F	Average of fixed and simple ends	20.0 k-in. = 1.17F	Fixed ends
		F = 12.0 k (1B, 2B)		F = 17.1 k (1B, 2B)	
		20.2 k-in. = 1.66F		20.2 k-in. = 1.17F	
		F = 12.2 k (3B)		F = 17.3 k (3B)	

(capacity of top surface reinforcement perpendicular to top surface)

Figure 4.10 Beam Model-Tests 1B, 2B, and 3B

fixed. As a simplifying assumption the beam element supports were assumed to be halfway between fully fixed and simply supported. In addition, the assumed loaded surface is not free but is attached to the lower portion of the deviation saddle, so there is some rotational restraint because of this. In spite of the fact that it would be theoretically incorrect to assume that the ends were fully fixed since the concrete does crack at the web wall and there is no negative moment reinforcement provided per se, calculations were made for fully fixed supports to make further comparisons with the test results. The tendon force was distributed over an area of 75% of the tendon duct diameter because the duct diameter is relatively large in comparison to the length of the beam. The beam length was assumed to be 9.5 in. which went from the intersection of the top surface and the web wall to about halfway between the vertical legs of the open and closed stirrups. This appeared to be a reasonable length of bending because the web wall and the vertical legs of the stirrups provide the downward reactions for the beam element. The difference in concrete strength for related tests proved to make little difference in the calculations. These calculated capacities are utilized in the discussion of force combinations in Sec. 4.2.4. These calculations are utilized for both the yield and the ultimate load stages.

The beam model calculation for tests 4A and 5A is shown in Fig. 4.11, and the beam calculation for tests 4B and 5B is shown in Fig. 4.12. In specimens 4A, 4B, 5A, and 5B, both tendons had to be



$$d = 1.38" - 0.5" - 0.156/2 = 0.80"$$

$$f_y = 36 \text{ ksi}$$

$$f'_c = 5700 \text{ psi (4A)} \quad f'_c = 5400 \text{ psi (5A)}$$

$$A_s = 5 \times 0.0192 \text{ in.}^2 = 0.0960 \text{ in.}^2$$

$$M_n = A_s \times f_y (d - a/2)$$

$$a = (A_s \times f_y) / (.85 \times f'_c \times b)$$

$$a = 0.119 \text{ (4A)} \quad a = 0.125 \text{ (5A)}$$

$$M_n = 0.096 \text{ in.}^2 \times 36 \text{ ksi} (0.80" - 0.119"/2) = 2.56 \text{ k-in. (4A)}$$

$$M_n = 0.096 \text{ in.}^2 \times 36 \text{ ksi} (0.80" - 0.125"/2) = 2.55 \text{ k-in. (5A)}$$

$$M_n = M_{max} \longrightarrow 2.55 \text{ k-in.} = 1.81F$$

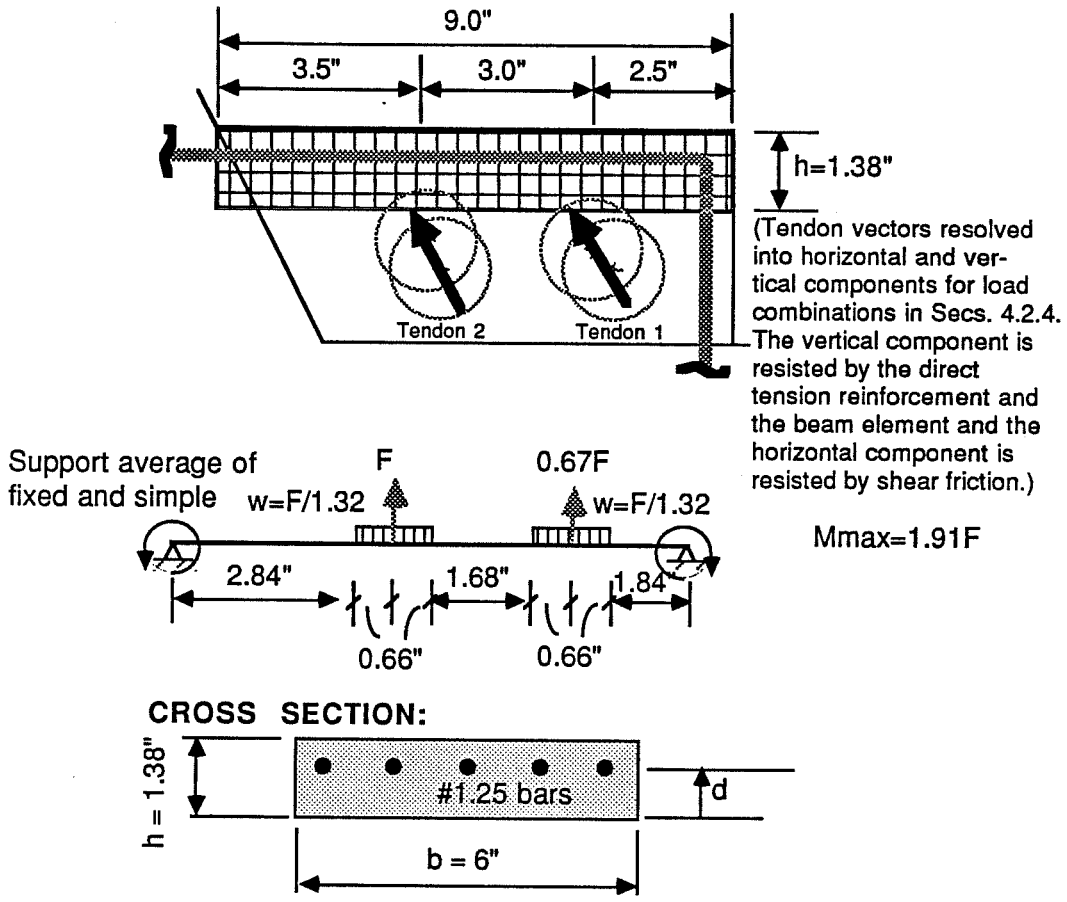
$$F = 1.4 \text{ k (Tendon 2)}$$

$$F = 1.0 \text{ k (Tendon 1)}$$

$$F = 2.4 \text{ k (Total)}$$

(capacity perpendicular to the top surface)

Figure 4.11 Beam Model-Tests 4A and 5A



$$d = 1.38" - 0.5" - 0.156/2 = 0.80"$$

$$f_y = 36 \text{ ksi}$$

$$f'_c = 5700 \text{ psi (4B)} \quad f'_c = 5400 \text{ psi (5B)}$$

$$A_s = 5 \times 0.0192 \text{ in.}^2 = 0.0960 \text{ in.}^2$$

$$M_n = A_s \times f_y (d - a/2)$$

$$a = (A_s \times f_y) / (.85 \times f'_c \times b)$$

$$a = 0.119 \text{ (4B)} \quad a = 0.125 \text{ (5B)}$$

$$M_n = 0.096 \text{ in.}^2 \times 36 \text{ ksi} (0.80" - 0.119"/2) = 2.56 \text{ k-in. (4B)}$$

$$M_n = 0.096 \text{ in.}^2 \times 36 \text{ ksi} (0.80" - 0.125"/2) = 2.55 \text{ k-in. (5B)}$$

$$M_n = M_{max} \longrightarrow 2.55 \text{ k-in.} = 1.91F$$

$$F = 1.3 \text{ k (Tendon 2)}$$

$$F = 0.9 \text{ k (Tendon 1)}$$

$$F = 2.2 \text{ k (Total)}$$

(capacity perpendicular to the top surface)

Figure 4.12 Beam Model-Tests 4B and 5B

resisted by the top surface reinforcement since both tendons had vertical deviations. The vertical force from tendon 1 was approximately 67% of that of tendon 2. The same type of assumptions that were made for the previous specimens were made for these modified specimens. However, the calculations were made only for support fixity halfway between fully fixed and simply supported because this beam element provided a relatively small contribution to the total pull-out capacity of the deviation saddle and thus a change in the end conditions would make very little difference. The beam length was taken as the full length of the top surface of the deviation saddle since the outer closed stirrup extends almost all the way across the top of the deviation saddle. Again as in the previous specimens, the difference in concrete strength appeared to make little difference. The calculated force resisted by the beam element will be utilized in the discussion of force combination in Sec. 4.2.4. As was stated above, these calculations are utilized for both the yield and the ultimate critical load stages.

4.2.4 Analysis Combinations And Comparison of Test Results.

The measured deviator loads at first yield and at ultimate for the entire test series are presented in Table 4.1 and Table 4.2 respectively. These loads will be used for comparison with the analysis method. The first yield load was determined when the strain from any of the strain gages reached the yield strain. The horizontal and vertical components of the deviated forces are given, as well as

TEST	TENDON	YIELD DEVIATOR LOADS			
		HORIZ. FORCE	VERT. FORCE	VECTOR FORCE	ANGLE
		(KIPS)	(KIPS)	(KIPS)	(DEG.)
TEST 1A	1	-1.7	0.0	1.7	180.0
	2	-10.2	0.0	10.2	180.0
	3	1.7	12.3	12.4	82.1
	TOTAL	-10.2	12.3	16.0	129.5
TEST 1B	1	2.0	0.0	2.0	0.0
	2	9.6	19.9	21.3	63.2
	TOTAL	11.6	19.9	23.0	59.8
TEST 2A	1	1.4	0.0	1.4	0.0
	2	4.8	10.0	11.1	64.4
	TOTAL	6.2	10.0	11.8	58.1
TEST 2B	1	1.3	0.0	1.3	0.0
	2	4.7	9.8	10.9	64.4
	TOTAL	6.0	9.8	11.5	58.5
TEST 3A	1	-1.6	0.0	1.6	180.0
	2	-11.5	0.0	11.5	180.0
	3	2.0	13.8	13.9	81.8
	TOTAL	-11.1	13.8	17.3	126.9
TEST 3B	1	2.5	0.0	2.5	0.0
	2	9.6	19.9	22.1	64.2
	TOTAL	12.1	19.9	23.3	58.6
TEST 4A	1	3.5	4.3	5.5	50.9
	2	3.2	6.7	7.4	64.5
	TOTAL	6.7	11.0	12.9	58.8
TEST 4B	1	-4.0	6.1	7.3	123.3
	2	-5.2	10.8	12.0	115.7
	TOTAL	-9.2	16.9	19.3	118.5
TEST 5A	1	2.4	3.0	3.8	51.3
	2	2.9	5.9	6.6	63.8
	TOTAL	5.2	8.9	10.3	59.6
TEST 5B	1	-4.4	6.8	8.1	122.9
	2	-4.5	9.4	10.4	115.6
	TOTAL	-9.0	16.2	18.5	118.9

Table 4.1 Yield Deviator Loads

TEST	TENDON	ULTIMATE DEVIATOR LOADS			
		HORIZ. FORCE	VERT. FORCE	VECTOR FORCE	ANGLE
		(KIPS)	(KIPS)	(KIPS)	(DEG.)
TEST 1A	1	-2.4	0.0	2.4	180.0
	2	-13.8	0.0	13.8	180.0
	3	2.5	18.8	19.0	82.4
	TOTAL	-13.7	18.8	23.3	126.0
TEST 1B	1	2.5	0.0	2.5	0.0
	2	11.2	23.2	25.8	64.2
	TOTAL	13.7	23.2	27.0	59.4
TEST 2A	1	1.9	0.0	1.9	0.0
	2	6.6	13.7	15.2	64.3
	TOTAL	8.6	13.7	16.2	58.1
TEST 2B	1	1.7	0.0	1.7	0.0
	2	5.8	11.9	13.2	64.0
	TOTAL	7.5	11.9	14.1	58.0
TEST 3A	1	-2.5	0.0	2.5	180.0
	2	-18.0	0.0	18.0	180.0
	3	2.9	21.7	21.9	82.4
	TOTAL	-17.6	21.7	27.9	129.0
TEST 3B	1	3.8	0.0	3.8	0.0
	2	14.6	30.2	33.5	64.2
	TOTAL	18.4	30.2	35.4	58.6
TEST 4A	1	5.8	7.2	9.2	51.1
	2	5.5	11.3	12.6	64.0
	TOTAL	11.2	18.6	21.7	58.8
TEST 4B	1	-4.8	7.4	8.8	123.0
	2	-6.1	12.6	14.0	115.8
	TOTAL	-10.9	20.0	22.8	118.5
TEST 5A	1	5.7	7.1	9.1	51.2
	2	6.8	14.0	15.6	64.1
	TOTAL	12.4	21.1	24.5	59.5
TEST 5B	1	-5.3	8.2	9.8	122.9
	2	-6.5	13.4	14.9	115.9
	TOTAL	-11.8	21.6	24.6	118.6

Table 4.2 Ultimate Deviator Loads

the vector forces and directions. The sum of the total deviated forces of all the deviated tendons for each test are given below the individual tendon forces.

The comparison of test results and analysis calculations is made with the use of tables. Tests 1A, 1B, 2A, 2B, 3A, and 3B are tabulated together, while tests 4A, 4B, 5A, and 5B are tabulated together. This was done because tests 1A through 3B were based on the same representative deviation saddle detail shown in Fig. 4.1a, and tests 4A through 5B were based on the same modified deviation saddle detail shown in Fig. 4.1b. Comparisons at yield and ultimate are presented in separate tables. Comparison of pull-out capacities and test results are presented differently for the two separate details. For tests 1A, 1B, 2A, 2B, 3A, and 3B, the pull-out capacity is governed by the single tendon which is vertically deviated. Therefore, all pull-out force resistance is calculated in the direction of this vector force which for all these tests is approximately perpendicular to the top surface. This is a rational basis to compare results since it eliminates the need to resolve the force vector into components and the pull-out resistance is approximately in this direction (link bar axis is slightly different which is taken into account). For tests 4A, 4B, 5A, and 5B, the pull-out capacity is calculated in the vertical direction since reinforcement is placed in the vertical and horizontal directions. Forces for these tests are resolved into vertical and horizontal

directions. For the entire test series, all shear friction capacities and total horizontal forces are oriented in the horizontal direction because the critical shear plane is approximately horizontal.

For tests 1A, 1B, 2A, 2B, 3A, and 3B, comparisons between the analysis results and the test results are presented for yield and ultimate load stages in Table 4.3 and Table 4.4 respectively. The explanations for the values in the table are as follows:

Row 1- Calculation of the capacity of the direct tension reinforcement (link bar) in the direction of the tendon vector which it encloses. This value is determined from reinforcement yield strength for yield and from reinforcement ultimate strength for ultimate.

Row 2- Calculation of the capacity of the beam element for a force perpendicular to the top surface. The top value is for the beam fixity assuming the supports halfway between fixed and simple, while the value in brackets is for the beam fixity assuming the supports fully fixed. This value is based on reinforcement yield strength and so is the same for yield and ultimate as was stated in Sec. 4.2.3.

Row 3- Sum of row 1 and 2 assuming that these force resisting mechanisms are additive because they utilize different reinforcement and resist forces in approximately the same direction. As in row 2, the top value is for the beam fixity assuming the supports halfway between fixed and simple, while the value in brackets is for the beam fixity assuming the supports fully fixed.

	TEST	TEST 1A	TEST 1B	TEST 2A	TEST 2B	TEST 3A	TEST 3B
1.	LINK BAR N_y (1) (CALC) (KIPS)	8.4	9.6	9.6	N/A	8.4	9.6
2.	BEAM ELEMENT N_y (2) (CALC) (KIPS)	6.5 [10.3]	12.0 [17.1]	N/A	12.0 [17.1]	6.7 [10.6]	12.2 [17.3]
3.	N_y TOTAL (CALC) (KIPS)	14.9 [18.7]	21.6 [26.7]	9.6	12.0 [17.1]	15.1 [19.0]	21.8 [26.9]
4.	N_y (TEST) (KIPS)	12.4	21.3	11.1	10.9	13.9	22.1
5.	N_y (TEST)/ N_y (CALC)	0.83 [0.66]	0.99 [0.80]	1.16	0.91 [0.64]	0.92 [0.73]	1.01 [0.82]
6.	V_u (CALC) (KIPS)	29.3	29.3	N/A	29.3	29.3	29.3
7.	V_y (TEST) (KIPS)	10.2	11.6	N/A	6.0	11.1	12.1
8.	V_y (TEST)/ V_u (CALC)	0.35	0.40	N/A	0.20	0.38	0.41

(1) Direct tension strength in direction of tendon vector.

N_u (CALC)=9.9 k(cos 32.4)=8.4 k (TEST 1A, 3A)

N_u (CALC)=9.9 k(cos 14.2)=9.6 k (TEST 1B, 2A, 3B)

(2) Flexural strength perpendicular to top surface which is almost the same direction as tendon vector (assuming supports halfway between fixed and simple). The brackets denote calculation assuming fixed ends.

Table 4.3 Comparison of Test Results to Simplified Analysis Results
Yield Load Stage - Tests 1A, 1B, 2A, 2B, 3A, 3B

	TEST	TEST 1A	TEST 1B	TEST 2A	TEST 2B	TEST 3A	TEST 3B
1.	LINK BAR Nu (1) (CALC) (KIPS)	11.7	13.5	13.5	N/A	11.7	13.5
2.	BEAM ELEMENT Nu (2) (CALC) (KIPS)	6.5 [10.3]	12.0 [17.1]	N/A	12.0 [17.1]	6.7 [10.6]	12.2 [17.3]
3.	Nu TOTAL (CALC) (KIPS)	18.2 [22.0]	25.5 [30.6]	13.5	12.0 [17.1]	18.4 [22.3]	25.7 [30.8]
4.	Nu (TEST) (KIPS)	19.0	25.8	15.2	13.2	21.9	33.5
5.	Nu (TEST)/Nu (CALC)	1.04 [0.86]	1.01 [0.84]	1.13	1.10 [0.77]	1.19 [0.98]	1.30 [1.09]
6.	Vu (CALC) (KIPS)	29.3	29.3	N/A	29.3	29.3	29.3
7.	Vu (TEST) (KIPS)	13.7	13.7	N/A	7.5	17.6	18.4
8.	Vu (TEST)/ Vu (CALC)	0.47	0.47	N/A	0.26	0.60	0.63
9.	FAILURE TYPE	P.O.	P.O.	P.O.	P.O.	P.O.	P.O.

(1) Direct tension strength in direction of tendon vector.
 $Nu(CALC)=13.9 \text{ k}(\cos 32.4)=13.5 \text{ k}$ (TEST 1A, 3A)
 $Nu(CALC)=13.9 \text{ k}(\cos 14.2)=11.7 \text{ k}$ (TEST 1B, 2A, 3B)

(2) Flexural strength perpendicular to top surface which is almost the same direction as tendon vector (assuming supports halfway between fixed and simple). The brackets denote flexural strength assuming fixed ends.

"P. O." Pull-out Forces

Table 4.4 Comparison of Test Results to Simplified Analysis Results
 Ultimate Load Stage - Tests 1A, 1B, 2A, 2B, 3A, 3B

Row 4- Test result for the vector force of the single tendon which is vertically deviated (tendon 3 for tests 1A and 3A, and tendon 2 for tests 1B, 2A, 2B, 3B) and which is approximately perpendicular to the top surface. The angle difference between this vector force acting on the deviation saddle and the perpendicular to the top surface is insignificant since the cosine of the angle difference between them is greater than 0.98. Hence, the beam element capacity which is based on the resistance perpendicular to the top surface does not have to be adjusted for the direction of the deviated tendon force direction.

Row 5- Ratio of test result to calculation for the pull-out capacity of the deviation saddle as determined by adding the link bar and beam element capacities (row 4/row 3). As in rows 2 and 3, the ratio is provided for the alternate calculations assuming different end fixity.

Row 6- Calculation of the horizontal shear friction strength at the critical plane located below the tendon ducts. This calculation is made for the ultimate shear friction capacity, however it is also presented in the yield table to make comparison with the total horizontal shear force at yield.

Row 7- Test result for the total horizontal force acting on a horizontal shear surface through the deviator.

Row 8- Ratio of test result to calculation for the horizontal shear friction capacity of the deviation saddle (row 7/row 6).

Row 9- Critical failure type as determined by comparisons of test to calculated ratio for either the pull-out forces or the horizontal shear friction forces. This is presented only for the ultimate load stage.

For the comparison at yield (Table 4.3), the ratio $N_y(\text{Test})/N_y(\text{Calc})$ in row 5 for the additive link and beam based on the assumed end fixity halfway between fixed and simple for the beam element, shows fairly good correlation between the yield deviator loads and the yield capacity. At the extremes, the calculation is 20% higher than the test result for test 1A and 14% lower than the test result for test 2A. For this ratio in row 5 in brackets based on the assumption of end fixity fully fixed, the agreement is poor (the test result being 18% to 36% below the calculated value). The comparisons indicate that for design based on first yielding, the deviation saddle reinforcement could be very conservatively proportioned for the link bar pull-out capacity since it is the controlling mode of failure. However, for design purposes of deviators reinforced similar to Fig. 4.1a, it would be much more reasonable to add the link bar mechanism capacity to the beam mechanism capacity assuming the end fixity somewhere between fully fixed and simple. However, the agreement between test and calculations assuming fixity halfway between fully fixed and simply supported is still somewhat unconservative for yield loads. It would be more conservative in design to add the link bar mechanism capacity to the beam mechanism capacity assuming the end

fixity simply supported which will produce a lower contribution for the beam element mechanism in the total pull-out capacity. This will produce a safe design. While not shown, the ratios in line 5 would vary from a low of 0.94 to a high of 1.16 for this case. From the ratio of the total horizontal force at first yield to the horizontal ultimate shear friction capacity (row 8), it is shown that the ultimate horizontal shear friction capacity is substantially greater than the total horizontal shear forces at yield and this mode did not govern.

The physical test results showed that in all failures except that of test 2B, the link bars fractured in direct tension. For test 2B, in which no link bar was provided, a tension net of the top surface reinforcement formed and then the concrete crushed. There was no fracturing of the reinforcement. In tests 1A, 1B, 2B, 3A, and 3B, the ratio $V_u(\text{Test})/V_u(\text{Calc})$ in row 8 of Table 4.4 indicated that the total horizontal shear force developed at failure was significantly smaller than the calculated conservative estimate of horizontal shear friction strength. It does not appear that the shear friction failure mode controlled. However as was stated in Sec. 4.2.2, in tests 1A and 3A where the horizontal shear forces were high from the tendons that were not confined by the link bar (tendon 1 and 2), it was obvious from the strain data and failure mechanism that this large horizontal force did influence the behavior with respect to cracking of the deviation saddle and yielding of the open stirrup. Line 5 shows that

the ratio $Nu(\text{Test})/Nu(\text{Calc})$ was much closer to 1.0. For tests 1A and 1B the correlation between the test result and the calculation was excellent. For tests 2A and 2B the test results are 10% to 13% higher than those of the calculations. Since these tests represented an attempt to separate the link bar and the beam element behavior, it was expected that the sum of the ultimate loads for tests 2A and 2B (28.4 k) would be equal to the ultimate load for test 1B (25.8 k) which combined both mechanisms. However, the sum of the link bar mechanism in test 2A and the stirrup beam mechanism in test 2B is about 10% higher than the combined specimen 1B. This appears quite reasonable. For tests 3A and 3B with epoxy coated reinforcement, the test results appear to be significantly higher (19% to 30%) than the calculations. Some of this difference may be attributed to the tensile contribution of the additional reinforcement chair present in these specimens as discussed in the last chapter. However, it appears likely that the extra strength was due to increased beam element relative end fixity which is highly indeterminate in this system. If the beam element end conditions were assumed to be fully fixed, the values shown in brackets show that the test results and the calculations correlate much better for tests 3A and 3B, although such an assumption would be very unconservative for test 1A, 1B, and 2B. As was concluded in chapter 3, it is possible that the local strains at critical sections were lower in the link bars made with epoxy coated reinforcement (specimens 3A and 3B) because of the lower effective bond of the

reinforcement to the concrete. Thus, relatively more force resistance could be developed in the deviation saddle by more completely mobilizing the full plastic moment capacity of the top surface reinforcement before local fracture of the link bars. This may be the explanation for the higher test result values for epoxy reinforced tests 3A and 3B than the directly comparable conventional reinforcement tests 1A and 1B.

It is important to note that with reinforcement patterns as shown in Fig. 4.1a the total deviator force vector acting on the specimen is not the vector force which is directly compared to the pull-out capacity. The reason for this is that the deviator force from other deviated tendons not enclosed within the primary direct tension reinforcement (tendons 1 and 2 for test 1A and 3A, and tendon 1 for test 1B, 2A, 2B, and 3B) had little influence on the direct tension reinforcement. In tests 1B, 2A, 2B, and 3B, the deviated force in the tendon with only horizontal deviation (tendon 1) which was directed away from the web wall was relatively small. In test 2A, this tendon was not enclosed in any reinforcement and still did not influence the failure because the force was too low. This force is easily taken by the shear strength of the concrete. In tests 1A and 3A, the deviated force from the tendons with only horizontal deviation (tendon 1 and 2) which was directed into the web was a rather large force. However, it still did not influence the stresses in the direct tension reinforcement. The reason for this is that the tendon duct for the

tendon with vertical deviation is placed much higher in the deviation saddle than the ducts for tendons with just horizontal deviation (see Fig. 4.9). It is possible that if the duct had been located lower in the deviation saddle, then the compressive forces from the horizontal forces might have reduced the stress in the direct tension reinforcement.

The simplified analysis model results for tests 4A, 4B, 5A, and 5B are given for yield and ultimate load stages in Table 4.5 and Table 4.6 respectively in much the same way as for the early tests. There are several differences in the specimens which cause the results to be presented in a slightly different form. One difference is that with deviators similar to those shown in Fig. 4.1b, both tendons within the deviation saddle have vertical deviation. Therefore, direct tension reinforcement was provided around both tendons. Because of this, the results and calculations for each test are presented for two cases. One case compares the vertical component of the deviated force of tendon 2 to the calculated strength of the direct tension reinforcement placed around tendon 2 plus the added resistance of the beam element for tendon 2. The other case compares the vertical component of the total deviated force acting on the deviation saddle to the calculated strength of all the direct tension reinforcement plus the beam element resistance. Alternate calculations were provided since it is possible to have a failure when the tendon 2 loop bars initially reach ultimate capacity or it is possible that there might

TEST	TEST 4A		TEST 4B		TEST 5A		TEST 5B	
	TENDON 2	TOTAL TENDONS	TENDON 2	TOTAL TENDONS	TENDON 2	TOTAL TENDONS	TENDON 2	TOTAL TENDONS
1. LOOP Ny (1) (CALC) (KIPS)	6.9	13.8	6.9	13.8	6.9	13.8	6.9	13.8
2. BEAM ELEMENT Ny (2) (CALC) (KIPS)	1.4	2.4	1.3	2.2	1.4	2.4	1.3	2.2
3. NyTOTAL (CALC) (KIPS)	8.3	16.2	8.2	16.0	8.3	16.2	8.2	16.0
4. Ny (TEST) (KIPS) (3)	6.7	11.0	10.8	16.9	5.9	8.9	9.4	16.2
5. Ny (TEST)/Ny (CALC)	0.81	0.68	1.32	1.06	0.71	0.55	1.15	1.01
6. Vu (CALC) (KIPS)	N/A	15.5	N/A	15.5	N/A	15.5	N/A	15.5
7. Vy (TEST) (KIPS) (4)	N/A	6.7	N/A	9.2	N/A	5.2	N/A	9.0
8. Vy (TEST)/Vu (CALC)	N/A	0.43	N/A	0.59	N/A	0.34	N/A	0.58

(1) Direct tension strength in the vertical direction.

(2) Flexural strength perpendicular to top surface which is in the vertical direction (assuming supports halfway between fixed and simple).

(3) Vertical component of tendon 2 force vector and vertical component of total tendon vector.

(4) Horizontal component of total tendon vector.

Table 4.5 Comparison of Test Results to Simplified Analysis Results
Yield Load Stage - Tests 4A, 4B, 5A, 5B

TEST	TEST 4A		TEST 4B		TEST 5A		TEST 5B	
	TENDON 2	TOTAL TENDONS	TENDON 2	TOTAL TENDONS	TENDON 2	TOTAL TENDONS	TENDON 2	TOTAL TENDONS
1. LOOP Nu (1) (CALC) (KIPS)	9.8	19.6	9.8	19.6	9.8	19.6	9.8	19.6
2. BEAM ELEMENT Nu (2) (CALC) (KIPS)	1.4	2.4	1.3	2.2	1.4	2.4	1.3	2.2
3. Nu TOTAL (CALC) (KIPS)	11.2	22.0	11.1	21.8	11.2	22.0	11.1	21.8
4. Nu (TEST) (KIPS) (3)	11.3	18.6	12.6	20.0	14.0	21.1	13.4	21.6
5. Nu (TEST)/Nu (CALC)	1.01	0.85	1.14	0.92	1.25	0.96	1.21	0.99
6. Vu (CALC) (KIPS)	N/A	15.5	N/A	15.5	N/A	15.5	N/A	15.5
7. Vu (TEST) (KIPS) (4)	N/A	11.2	N/A	10.9	N/A	12.4	N/A	11.8
8. Vu (TEST)/Vu (CALC)	N/A	0.72	N/A	0.70	N/A	0.80	N/A	0.76
9. FAILURETYPE	P.O.		P.O.			P.O.		P.O.

(1) Direct tension strength in the vertical direction.

(2) Flexural strength perpendicular to top surface which is in the vertical direction (assuming supports halfway between fixed and simple).

(3) Vertical component of tendon 2 force vector and vertical component of total tendon vector.

(4) Horizontal component of total tendon vector.

"P.O." Pull-out Forces

Table 4.6 Comparison of Test Results to Simplified Analysis Results
Ultimate Load Stage - Tests 4A, 4B, 5A, 5B

be redistribution of force which allows the deviation saddle to reach a higher total force equal to the capacity of the entire deviation saddle. For design, the deviation saddle capacity should be based on the lower capacity of individual tendon reinforcement because redistribution of force within the deviation saddle should not be relied on. In line 6 the horizontal shear friction capacity is calculated only for the second case of total horizontal shear force since it does not make sense to compare the shear strength for an individual tendon.

For the comparison at yield (Table 4.5), the ratio of $N_y(\text{Test})/N_y(\text{Calc})$ in row 5 suggests that for tests 4A and 5A the test results are significantly lower (19% and 29%) than the calculated pull-out capacity determined by adding the loop bar mechanism to the beam element mechanism assuming end fixity midway between fully fixed and simply supported. For design, the deviation saddle reinforcement would be proportioned for the pull-out capacity utilizing only the yield strength of the reinforcement. However, the ratios in row 5 indicate that for these two specimens it is not safe to include the beam mechanism capacity in the total pull-out capacity which should be based only on the loop bar mechanism capacity. In fact, in test 4A the vertical component of the deviated tendon 2 force is almost identical to the loop bar yield capacity while in test 5A the test value is only 85% of the loop bar yield capacity. The beam element mechanism contribution is relatively small in comparison to the loop

bar mechanism contribution, so excluding it will not influence the design greatly. However, this outer stirrup will still be required to distribute surface cracks (also, it increases the absolute ultimate strength which is shown later). From the comparison of the total horizontal shear force at yield to the calculated lower bound shear friction capacity (row 8), it appears that the shear friction capacity is significantly greater than the total horizontal force at yield. The ratio is somewhat higher for tests 4B and 5B because these specimens attained higher loads than those of tests 4A and 5A before yield was indicated by the strain gages.

As in the early specimens, the actual failures showed fracture of the direct tension reinforcement. In tests 4A, 4B, 5A, and 5B, the ratio $V_u(\text{Test})/V_u(\text{Calc})$ in row 8 (Table 4.6) indicated that the total horizontal shear force developed at failure was smaller (20% to 30%) than the calculated conservative estimate of horizontal shear friction strength. It does not appear that the shear friction failure mode controlled. Line 5 shows that much closer agreement to 1.0 exists in the ratios of the test results to the calculations for the pull-out capacity determined by adding the loop bar mechanism capacity to the beam element mechanism capacity. At ultimate, it is apparent from this comparison that it is possible to include the beam element mechanism contribution to the total pull-out capacity. This differs from the first yield load stage where the beam element capacity could not be safely included. In comparing the alternate calculations in row 5, it

is likely for test 4A that failure occurred when the tendon 2 ultimate reinforcement capacity was reached. For test 4B, calculation based on only tendon 2 slightly underestimates the test result, while, the calculation for total tendons overestimates the test result. It is probable that there was some redistribution of force when tendon 2 loop bars reached capacity. For tests 5A and 5B with epoxy reinforcement, it appears that the specimen was not as sensitive to fracture when the tendon 2 capacity was reached. The lower bond efficiency of the coated bars apparently allowed further redistribution, and the failure occurred when the total ultimate reinforcement capacity was reached. These results correlate well with the conclusions of chapter 3 which showed that with the epoxy coated reinforcement there is increased redistribution of force within the deviation saddle.

4.3 Evaluation of Results With Respect To Strut-Tie Model

Two different types of zones usually exist in a structure (9). One type of zone is where plane strain assumptions can be made. This type of zone is known as a B-region which stands for either beam or Bernoulli. The other type of zone has strain distribution which is significantly non-linear. This type of zone is known as a D-region which stands for discontinuity, disturbance, or detail. These type of zones are shown in Fig. 4.13. The strut-tie model is applicable for design of D-regions, whereas, the traditional truss model is suitable for design of B-regions. The deviation saddle is a prime example of a

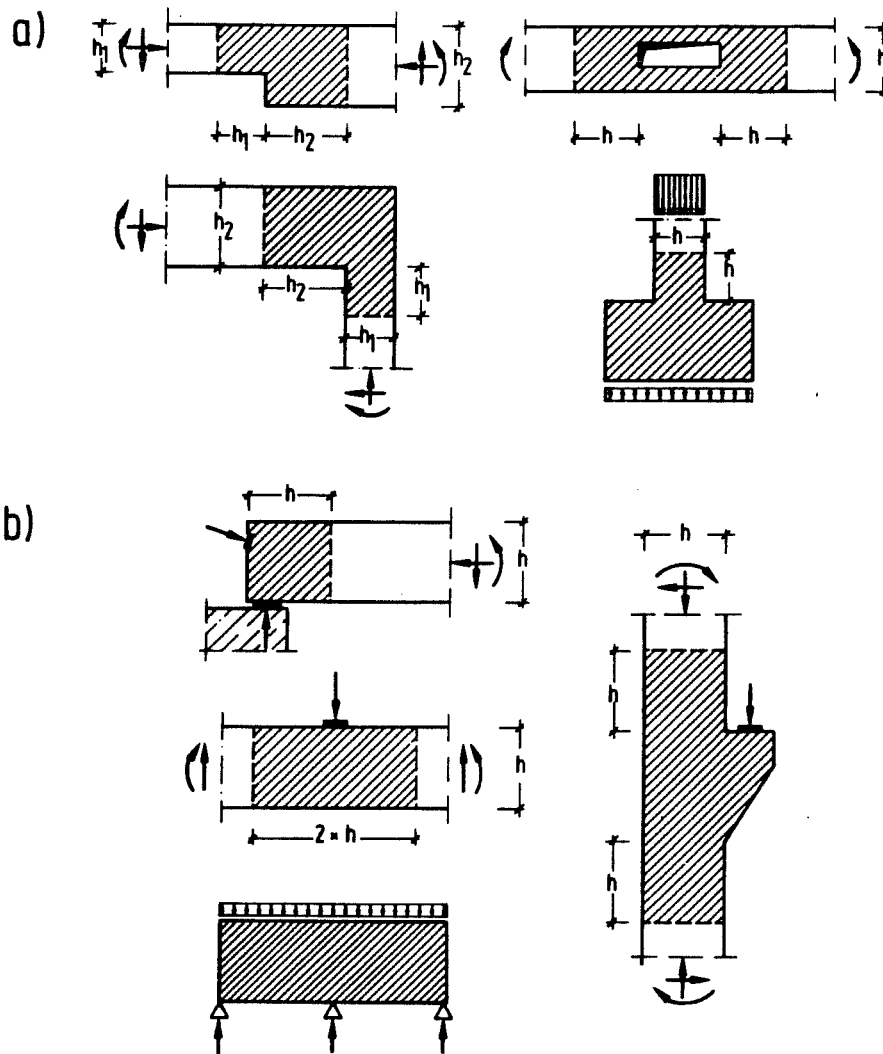


Figure 4.13 "D" Regions (Shaded Areas) with Nonlinear Strain Distribution (From Ref. 9)

D-region; therefore, strut-tie models were used to analyze all ten specimens. A comparison is made with the test results and the simplified analysis models. Refer to Sec. 4.4 for comparison with the simplified analysis models. Two separate strut-tie models will be provided for each specimen, one for the primary direct tension reinforcement and the other for the top surface reinforcement. The force resistance of the two strut-tie models are additive since they are both equilibrium based models which resist pull-out force in approximately the same direction. These two strut-tie models will be combined in Sec. 4.3.1.

The strut-tie model is based on the premise that reinforced concrete structures carry load through a set of compressive stresses which are distributed and interconnected by tensile ties. In this test series, the ties were the micro reinforcing bars. However, prestressing tendons or concrete tensile stress fields may also function as ties for a particular structure. A ϕ factor of one was utilized since material properties and dimensions are accurately known.

The tension ties are one-dimensional elements between two nodes and the concrete struts are two-dimensional stress fields, tending to spread between two adjacent nodes. The struts are the resultants of the stress fields. The nodes of the model are a simplified idealization of reality. A node indicates an abrupt change of the direction of forces. In this analysis, concentrated nodes were

assumed rather than smeared nodes. Concentrated nodes are usually utilized when one of the struts or ties represents a concentrated stress field where the deviation of force tends to be locally concentrated. The strength of the concrete in compression fields depends to a large extent on the multiaxial state of stress and on the disturbances from cracks and reinforcement. Since this analysis is at ultimate state, it is especially important to take into account the disturbances from cracking. From the test observations in this program, most cracks could be classified as skewed to the concrete struts that were selected for the analysis. According to criteria proposed by Schlaich, Schafer, and Jennewein (9), the simplified concrete strengths applicable for this test series are as follows:

$f_{cd}^* = 0.6f_{cd}$: for skew cracking or skew reinforcement

$f_{cd}^* = 0.4f_{cd}$: for skew cracks with extraordinary crack width. Such cracks must be expected if modelling of the struts departs significantly from the theory of elasticity's flow of internal forces (e.g., due to redistribution of internal forces in order to exploit a maximum ultimate capacity).

The symbol f_{cd} is the concrete strength, f'_c , multiplied by safety factors for design. Since this strut-tie method is being utilized for analysis of actual test results, f_{cd} is taken as the concrete strength, f'_c , without any safety factors. The crack widths were large for all specimens except 1B and 3B. For analyses of 1B and 3B, it is

likely that the concrete strength factor should be 0.6. For the other specimens, a value of 0.4 is used. In a structure with reasonable dimensions which is not over-reinforced, the concrete compressive stresses are usually not the main concern. However, as shown later, the concrete strengths were critical for specimens 1A, 2B, and 3A.

The reinforcement utilized in direct tension in the deviation saddles (link bars for specimens 1A, 1B, 2A, 3A, 3B and loop bars for specimens 4A, 4B, 5A, 5B) are simply tension ties linking the deviation force to the box reinforcement. This is shown in Fig. 4.14. In both cases, the direct tension reinforcement closely confined the tendon duct. For this reason, only a small volume of concrete was located between the reinforcement and the tendon duct. This facilitates an efficient transfer of force from the tendon ducts to the reinforcement. This is much like the transfer of force in a properly detailed corbel where the bearing plate is directly attached to the primary tension reinforcement. The tension tie capacity is determined for yield and ultimate and is the same as that presented in the direct tension model of Sec. 4.2.1.

The analysis of the other types of reinforcement is somewhat more complicated. The strut-tie model for the top surface reinforcement resistance is a combination of compression struts branching from the average location of the tendon duct to the tension tie which is the top surface reinforcement. Only the tendons with vertical deviation are used in the analysis since those tendons cause

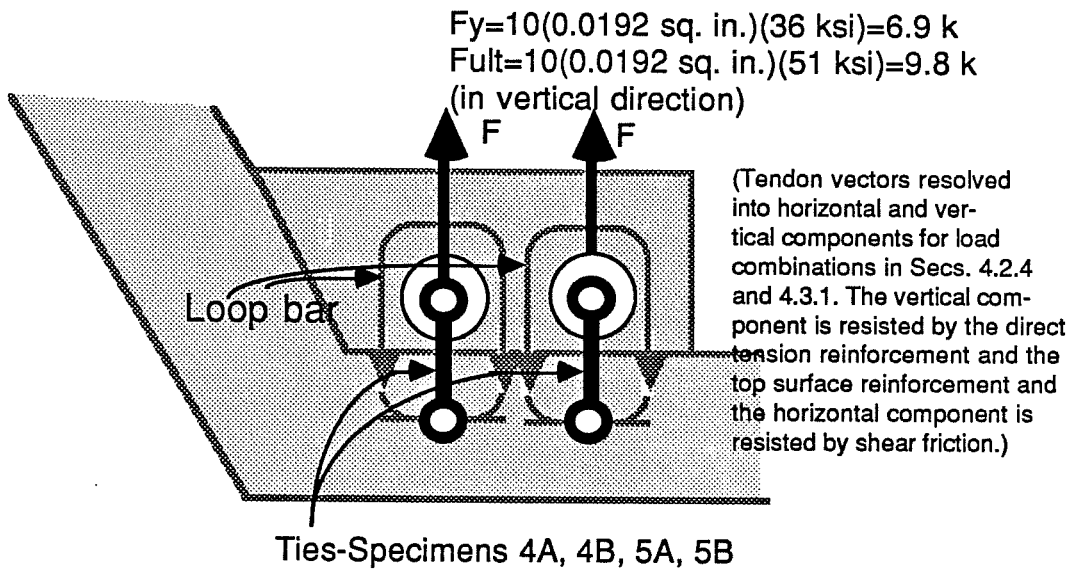
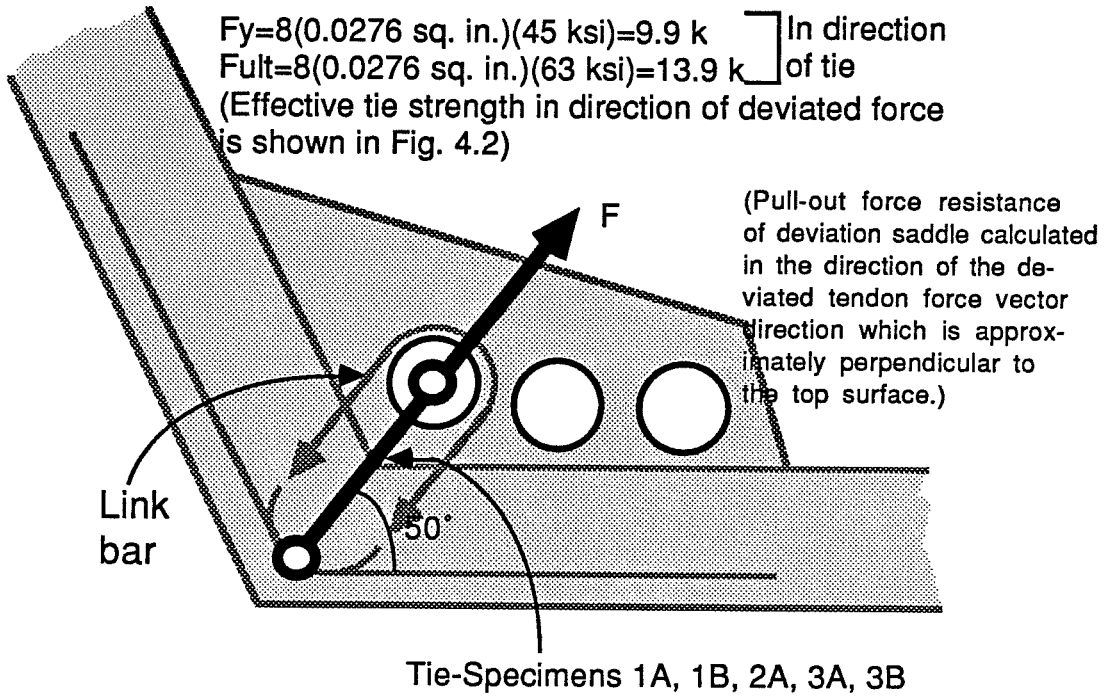


Figure 4.14 Strut-Tie Models-Primary Reinforcement

the stress in the top surface. Specimens 1A, 1B, 2B, 3A, and 3B have only one tendon with vertical deviation (tendon 3 in tests 1A and 3A, and tendon 2 in tests 1B, 2B, 3B), whereas, specimens 4A, 4B, 5A, and 5B have two tendons with vertical deviation (tendons 1 and 2).

The strut-tie models for the top surface reinforcement for specimens 1A, 1B, 2B, 3A, 3B are shown in Figs. 4.15-4.17. The tie was assumed to be at the centroid of the top surface reinforcement with one reaction located halfway between the vertical legs of the stirrups and the other at the web wall. An assumption of the maximum tie force based on yield of the reinforcement is made since it is unlikely the top surface reinforcement reached strain hardening because deformations were limited by the restraint of the direct tension reinforcement (all tests except 2B). Therefore, this strut-tie model for the top surface reinforcement will be used in the load combinations of Sec. 4.3.1 for yield and ultimate load stages. The size of the concrete compression struts was determined by drawing the truss to scale. The thickness of the struts in the deviation saddle was controlled by the size of the tendon duct. A maximum thickness so that the struts did not overlap at the tendon duct was determined from the scaled truss drawing to be 0.75". The angle of the struts which was controlled by the tendon duct and tension tie location was measured from the scaled drawings. The concrete strut widths were 7" which was the width of the deviation saddle. The concrete struts on the outside (AD and CD) carry the force to the assumed reactions. The

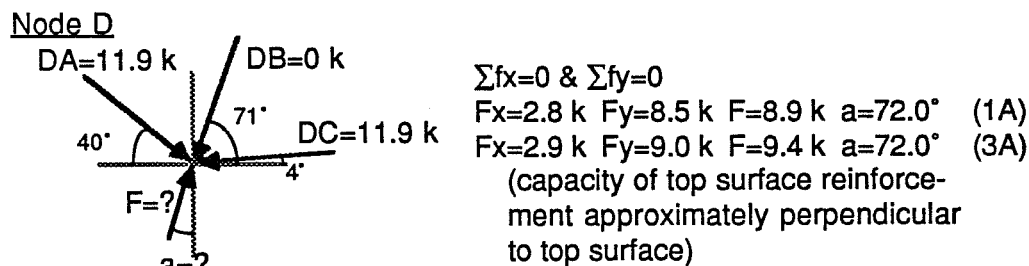
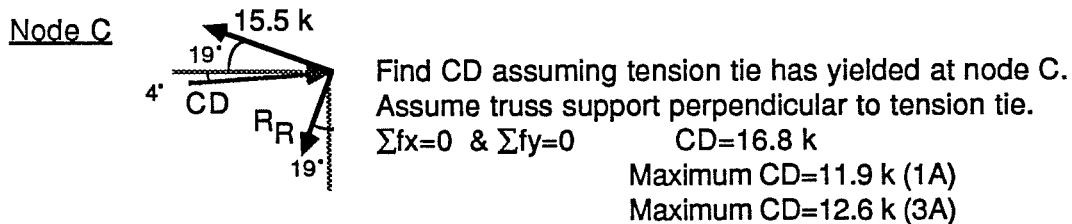
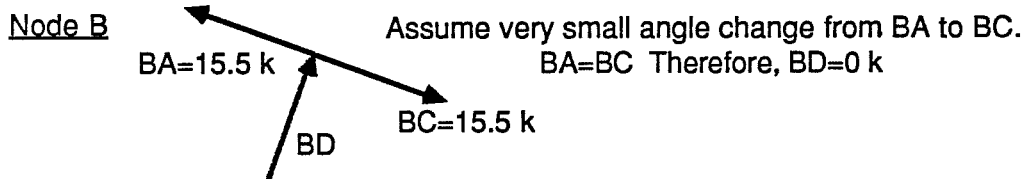
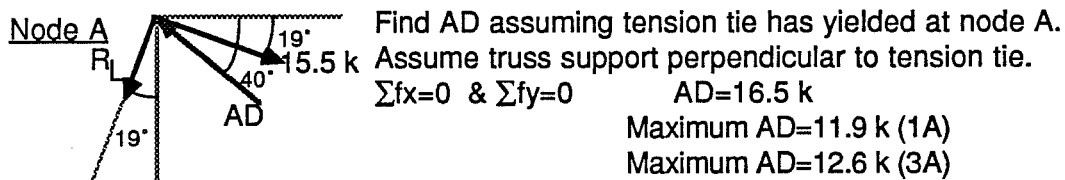
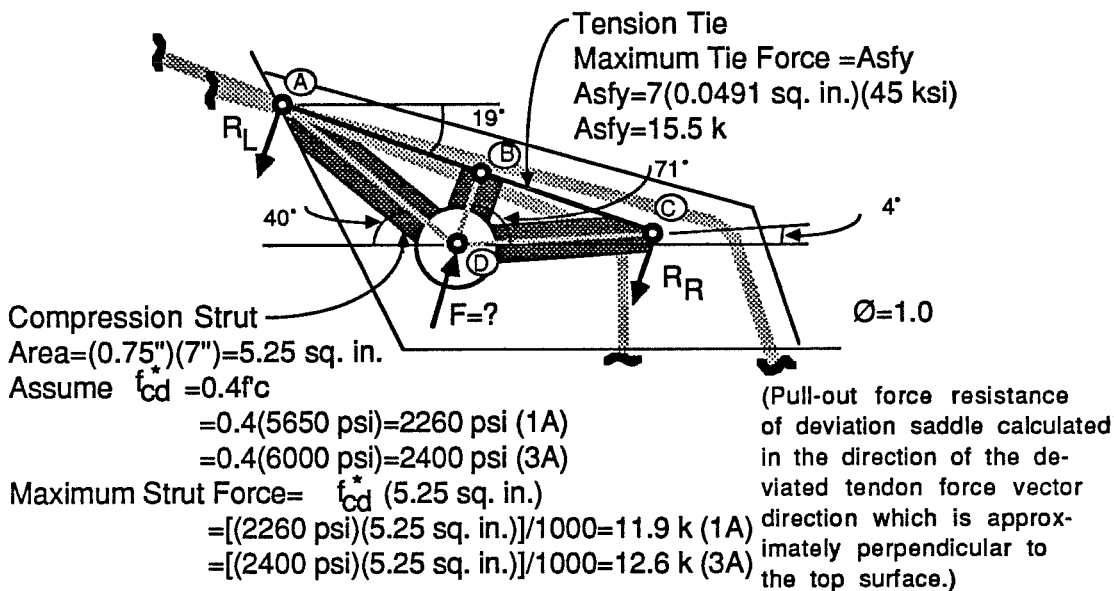


Figure 4.15 Strut-Tie Model -Top Surface Reinforcement-Tests 1A, 3A

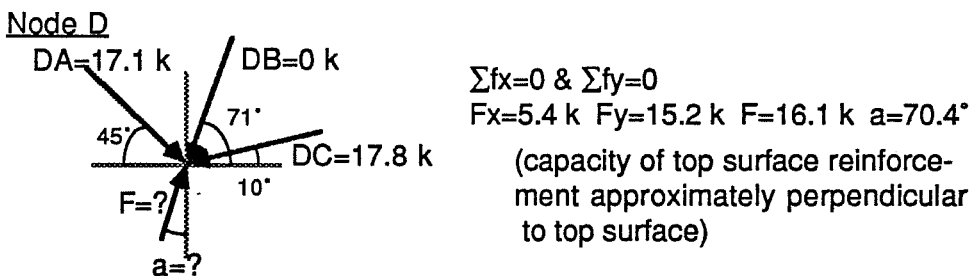
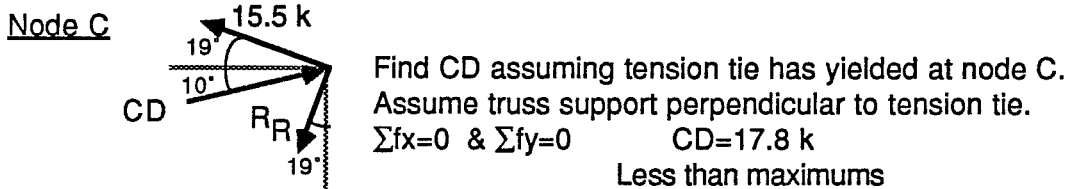
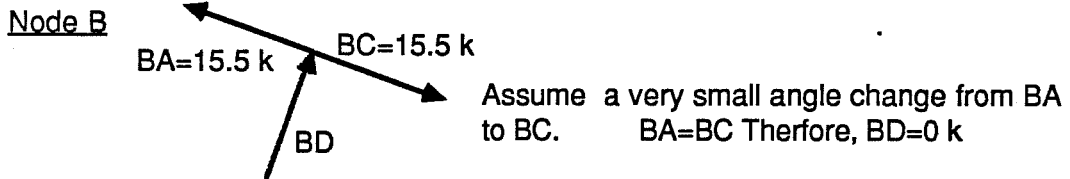
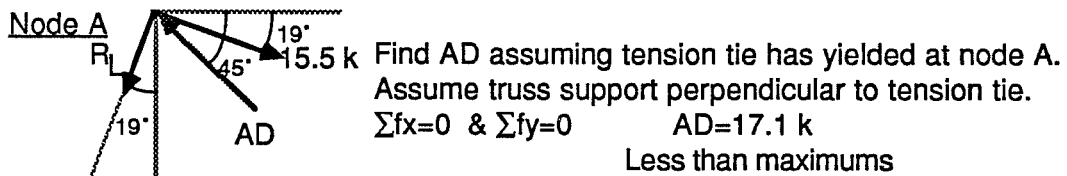
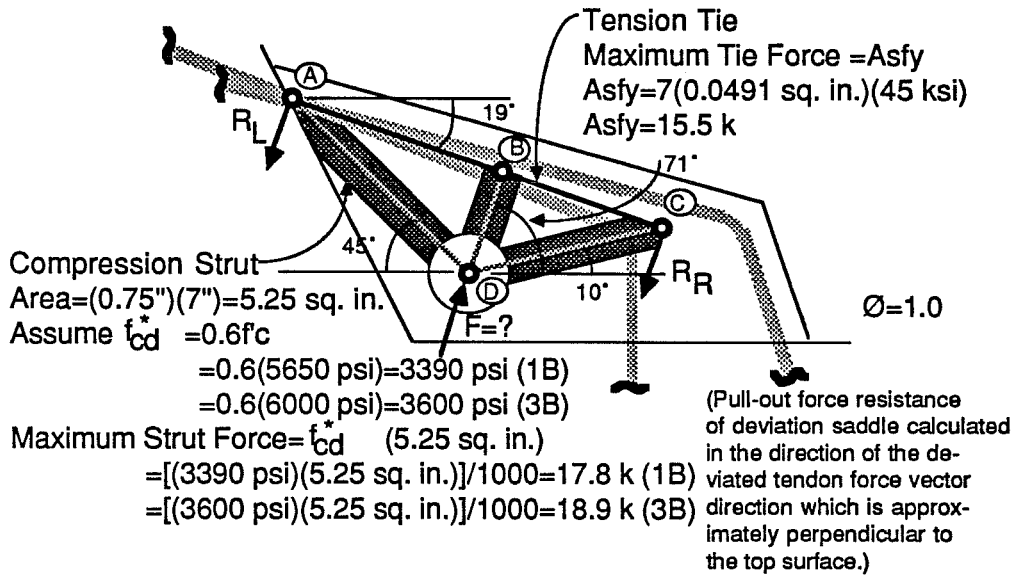
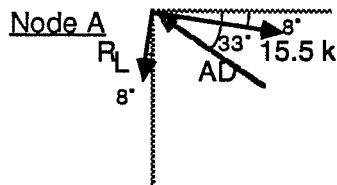
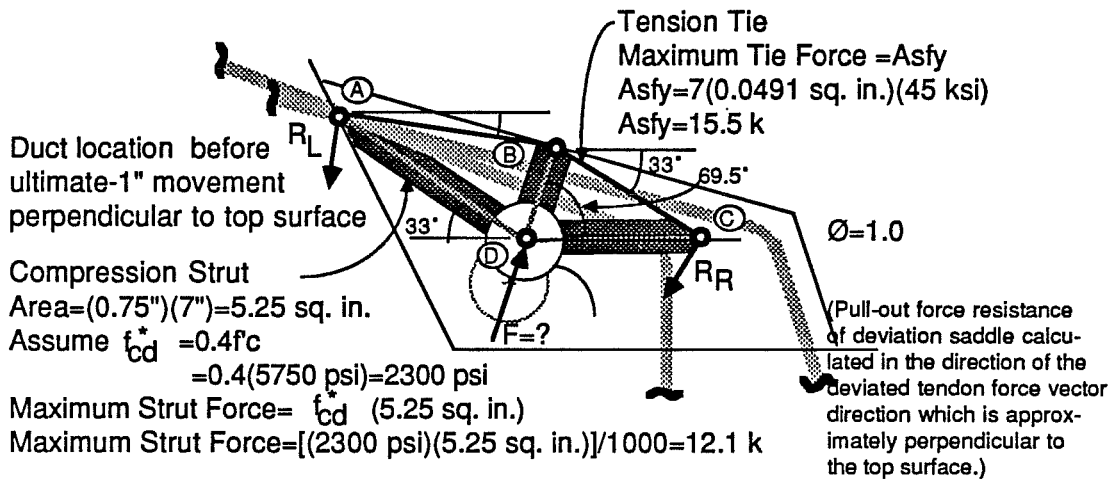
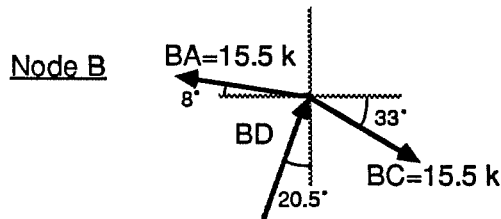


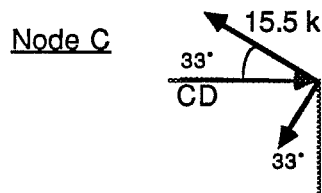
Figure 4.16 Strut-Tie Model -Top Surface Reinforcement-Tests 1B, 3B



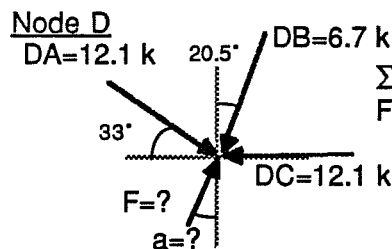
Find AD assuming tension tie has yielded at node A.
 Assume truss support perpendicular to tension tie.
 $\sum f_x=0$ & $\sum f_y=0$ AD=17.1 k
 Maximum AD=12.1 k



$\sum f_x=0$ & $\sum f_y=0$
 BD=6.7 k
 Less than maximum



Find CD assuming tension tie has yielded at node C.
 Assume truss support perpendicular to tension tie.
 $\sum f_x=0$ & $\sum f_y=0$ CD=18.2 k
 Maximum CD=12.1 k

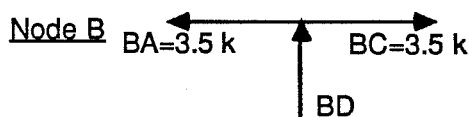
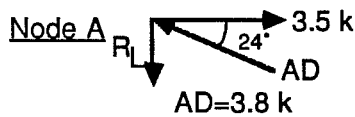
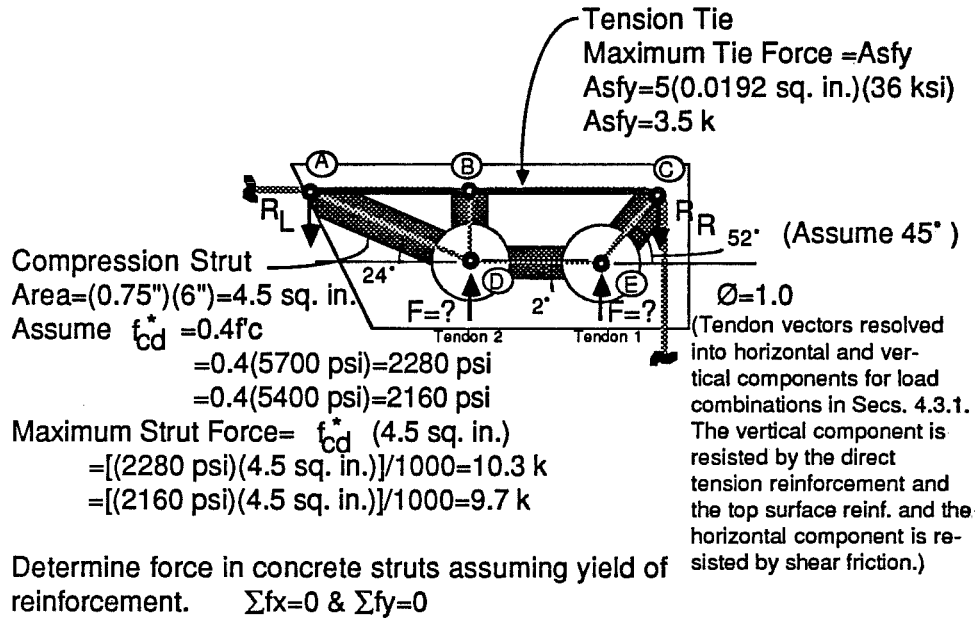


$\sum f_x=0$ & $\sum f_y=0$
 $F_x=4.3$ k $F_y=12.7$ k $F=13.4$ k $a=71.3^\circ$
 (capacity of top surface reinforcement approximately perpendicular to top surface)

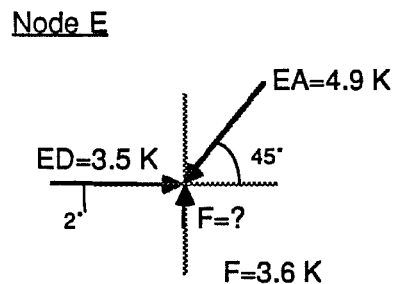
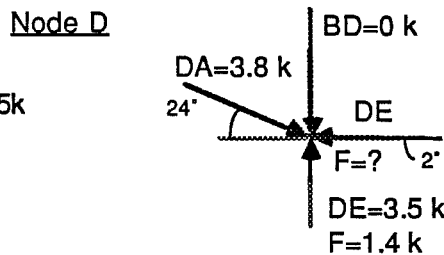
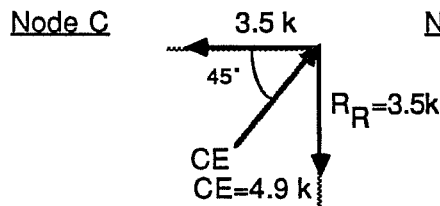
Figure 4.17 Strut-Tie Model -Top Surface Reinforcement-Test 2B

middle strut (BD) was provided because this is a location where a hinge forms. The force in the concrete struts was determined by initially assuming the maximum tie force which was based on yield of the reinforcement. The corresponding compressive strut forces were then calculated as shown. In tests 1A, 3A, and 2B the calculated force for the compression struts (AD and CD) was greater than the maximum compressive strut force allowed for the maximum simplified concrete strength f_{cd}^* discussed above. Therefore, for the calculation of the force resistance in these specimens, the lower strut force based on the f_{cd}^* value was taken. The calculations indicate that the force in the middle strut BD was essentially zero for all tests except test 2B which did not have the link bar to limit deviation saddle deformation. In test 2B, large deformations occurred before failure which was taken into account in the analysis by assuming a 1" deformation perpendicular to the top surface. This test was the only test where deformations were great enough that it might be anticipated that the top surface reinforcement reached a higher stress than that of yield. However as was concluded from the calculation, greater force resistance could not be developed since this specimen was over-reinforced which resulted in the truss being controlled by the maximum strut forces based on f_{cd}^* . The angle of the calculated force resistance was approximately perpendicular to the top surface. This resistance is utilized in the load combinations of Sec. 4.3.1.

The strut-tie models for the top surface reinforcement for specimens 4A, 4B, 5A, and 5B are shown in Figs. 4.18 and 4.19. In these tests both tendons produced significant stress in the top surface reinforcement. The tie is provided by the top surface reinforcement. Strut sizes and angles were selected by the graphical method that was discussed previously for the other detail. The concrete struts AD and CE are provided to take the upward force to the reactions. A vertical concrete strut (BD) is provided above tendon 2 because a hinge forms at this location. However, vertical deformation was limited because of the restraint provided by the loop bars. The force in this vertical compression strut is assumed to be zero since there was only a small angle change in the tie at the hinge. The maximum concrete strut force was assumed to be $f_{cd}^* - 0.4f_{cd} = 0.4f'_c$ which did not enter into the force resistance calculation since this specimen was not over-reinforced and all strut compressive stresses were below f_{cd}^* . The force resistance at node E for tendon 1 force deviation is much greater than that which can be developed because the analysis shows that the force resistance provided by the top surface reinforcement is critical at node D. At this node only 1.4 to 1.6 kips additional force resistance can be provided by the top surface reinforcement to restrain tendon 2. The vertical deviation force of tendon 1 is 67% of that of tendon 2, so the total vertical force resistance is 1.67 times tendon 2 vertical deviation force. Thus this reinforcement only restrains 2.4 to 2.7 kips additional vertical



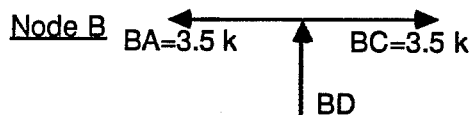
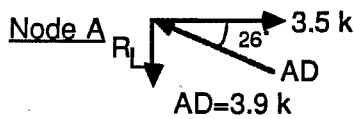
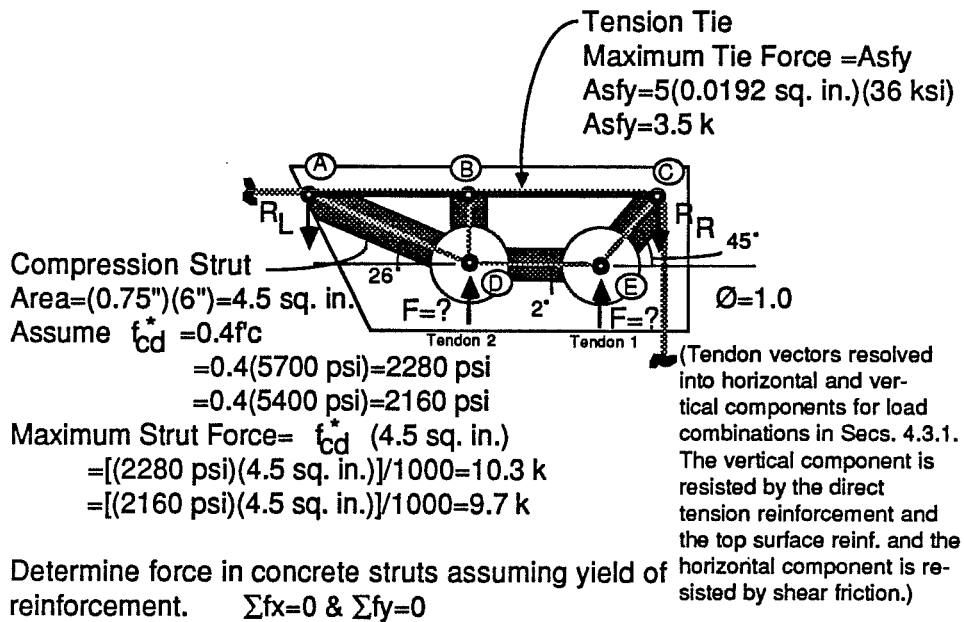
Assume a small angle change between BA and BC. $BD = 0 \text{ k}$



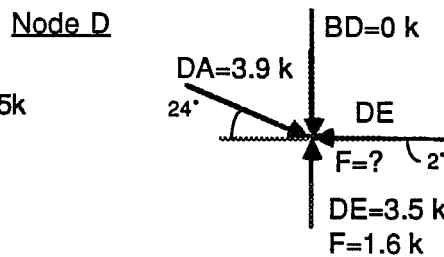
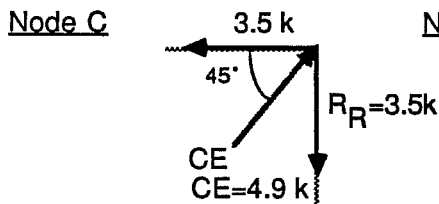
Critical condition occurs when tendon 2 vertical deviation force reaches 1.4 k.

Tendon 2 = 1.4 k
 Tendon 1 = $0.67(\text{Tendon 2}) = 1.0 \text{ k}$
 Total Vertical Force Resistance = 2.4 k
 (capacity perpendicular to the top surface)

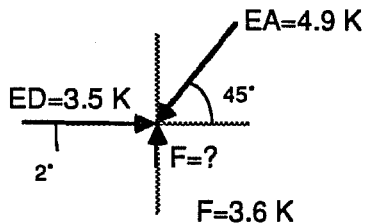
Figure 4.18 Strut-Tie Model -Top Surface Reinforcement-Tests 4A, 5A



Assume a small angle change between BA and BC. $BD = 0 \text{ k}$



Node E



Critical condition occurs when tendon 2 vertical deviation force reaches 1.6 k.

Tendon 2 = 1.6 k
 Tendon 1 = $0.67(\text{Tendon 2}) = 1.1 \text{ k}$
 Total Vertical Force Resistance = 2.7 k
 (capacity perpendicular to top surface)

Figure 4.19 Strut-Tie Model -Top Surface Reinforcement-Tests 4B, 5B

deviation force. The vertical resistance of specimens 4B and 5B is a little greater than specimens 4A and 5A because tendon 2 was located closer to the web.

4.3.1 Analysis Combinations And Comparison To Test Results.

Test results and calculations for the strut-tie model are given in Tables 4.7 through 4.10 in the same general way as for the simplified analysis models except that shear friction is not included since it is not modelled with a strut-tie model.

The test results and calculations for specimens 1A, 1B, 2A, 2B, 3A, and 3B are given in Table 4.7 for the yield load stage and in Table 4.8 for the ultimate load stage. For the yield load stage, the ratio $N_y(\text{Test})/N_y(\text{Calc})$ (row 5) indicates for all tests except 2A that the total strut-tie calculation determined by adding the link bar tie strength to the top surface reinforcement strut-tie model strength overestimates the test results by 16% to 40%. Thus it can be concluded that at the indication of first yield, it is not possible to assume that all the critical strut-tie model reinforcement is completely mobilized to yield. It is likely that the top surface reinforcement does not yield until after considerable straining in the link bar. For design where the deviation saddle capacity is based on first yield of any reinforcement, some contribution of the top surface reinforcement lower than that obtained assuming maximum strut and tie forces would be conservative (perhaps 50% of that obtained from the calculation). For the ultimate load stage, the ratio of test result to calculation

	TEST	TEST 1A	TEST 1B	TEST 2A	TEST 2B	TEST 3A	TEST 3B
1.	LINK BAR N_y (1) (CALC) (KIPS)	8.4	9.6	9.6	N/A	8.4	9.6
2.	TOP SURFACE REINF. N_y (2) (CALC) (KIPS)	8.9	16.1	N/A	13.4	9.4	16.1
3.	N_y TOTAL (CALC) (KIPS)	17.3	25.7	9.6	13.4	17.8	25.7
4.	N_y (TEST) (KIPS)	12.4	21.3	11.1	10.9	13.9	22.1
5.	N_y (TEST)/ N_y (CALC)	0.72	0.83	1.16	0.81	0.78	0.86

(1) Tie strength in direction of tendon vector.

N_y (CALC)=9.9 k(cos 14.2)=9.6 k (TEST 1B, 2A, 3B)

N_y (CALC)=9.9 k(cos 32.4)=8.4 k (TEST 1A, 3A)

(2) Top reinforcement strength perpendicular to top surface
which is almost in the same direction as the tendon vector.

Table 4.7 Comparison of Test Results to Strut-Tie Analysis Results
Yield Load Stage - Tests 1A, 1B, 2A, 2B, 3A, 3B

	TEST	TEST 1A	TEST 1B	TEST 2A	TEST 2B	TEST 3A	TEST 3B
1.	LINK BAR Nu (1) (CALC) (KIPS)	11.7	13.5	13.5	N/A	11.7	13.5
2.	TOP SURFACE REINF. Nu (2) (CALC) (KIPS)	8.9	16.1	N/A	13.4	9.4	16.1
3.	Nu TOTAL (CALC) (KIPS)	20.6	29.6	13.5	13.4	21.1	29.6
4.	Nu (TEST) (KIPS)	19.0	25.8	15.2	13.2	21.9	33.5
5.	Nu (TEST)/Nu (CALC)	0.92	0.87	1.13	0.99	1.04	1.13
6.	FAILURE TYPE	P.O.	P.O.	P.O.	P.O.	P.O.	P.O.

(1) Tie strength in direction of tendon vector.

Nu(CALC)=13.9 k(cos 14.2)=13.5 k (TEST 1B, 2A, 3B)

Nu(CALC)=13.9 k(cos 32.4)=11.7 k (TEST 1A, 3A)

(2) Top reinforcement strength perpendicular to top surface
which is almost in the same direction as the tendon vector.

P.O. Pull-out Forces

Table 4.8 Comparison of Test Results to Strut-Tie Analysis Results
Ultimate Load Stage - Tests 1A, 1B, 2A, 2B, 3A, 3B

TEST	TEST 4A		TEST 4B		TEST 5A		TEST 5B	
	TENDON 2	TOTAL TENDONS	TENDON 2	TOTAL TENDONS	TENDON 2	TOTAL TENDONS	TENDON 2	TOTAL TENDONS
1. LOOP Ny (1) (CALC) (KIPS)	6.9	13.8	6.9	13.8	6.9	13.8	6.9	13.8
2. TOP SURFACE REINF. Ny (2) (CALC) (KIPS)	1.4	2.4	1.6	2.7	1.4	2.4	1.6	2.7
3. Ny TOTAL (CALC) (KIPS)	8.3	16.2	8.5	16.5	8.3	16.2	8.5	16.5
4. Ny (TEST) (KIPS) (3)	6.7	11.0	10.8	16.9	5.9	8.9	9.4	16.2
5. Ny (TEST)/Ny (CALC)	0.81	0.68	1.27	1.02	0.71	0.55	1.11	0.98

(1) Tie strength in the vertical direction.

(2) Top reinforcement strength perpendicular to top surface which is in the vertical direction.

(3) Vertical component of tendon 2 force vector and vertical component of total tendon vector.

**Table 4.9 Comparison of Test Results to Strut-Tie Analysis Results
Yield Load Stage - Tests 4A, 4B, 5A, 5B**

TEST	TEST 4A		TEST 4B		TEST 5A		TEST 5B	
	TENDON 2	TOTAL TENDONS	TENDON 2	TOTAL TENDONS	TENDON 2	TOTAL TENDONS	TENDON 2	TOTAL TENDONS
1. LOOP Nu (1) (CALC) (KIPS)	9.8	19.6	9.8	19.6	9.8	19.6	9.8	19.6
2. TOP SURFACE REINF. Nu (2) (CALC) (KIPS)	1.4	2.4	1.6	2.7	1.4	2.4	1.6	2.7
3. Nu TOTAL (CALC) (KIPS)	11.2	22.0	11.2	22.3	11.4	22.0	11.4	22.3
4. Nu (TEST) (KIPS) (3)	11.3	18.6	12.6	20.0	14.0	21.1	13.4	21.6
5. Nu (TEST)/Nu (CALC)	1.01	0.85	1.11	0.90	1.25	0.96	1.18	0.97
6. FAILURETYPE	P.O.		P.O.			P.O.		P.O.

(1) Tie strength in the vertical direction.

(2) Top reinforcement strength perpendicular to top surface which is in the vertical direction.

(3) Vertical component of tendon 2 force vector and vertical component of total tendon vector.

P.O. Pull-out Forces

**Table 4.10 Comparison of Test Results to Strut-Tie Analysis Results
Ultimate Load Stage - Tests 4A, 4B, 5A, 5B**

(row 5) for tests 1A and 1B shows that the strut and tie analysis overestimates the ultimate strength by 8% and 13% respectively. The comparison is the same as for the other analysis method for test 2A because the link bar is treated the same in both analyses. For test 2B, the strut-tie model is very good for estimating the contribution of the strength of the top surface reinforcement. For tests 3A and 3B, the results are 4% to 13% higher than the calculations. This appears quite reasonable. The underestimation of strength may be due to the added reinforcement chair placed in these specimens. For tests 2B, 3A and 3B the strut and tie models seems to do a better job of predicting the top surface reinforcement contribution than the previous beam element analysis. As found with the other analysis method, it is apparent that the pull-out capacity of the deviation saddles was exceeded in all cases and that this governed failure.

The test results and calculations for specimens 4A, 4B, 5A, and 5B are given in Table 4.9 for the yield load stage and in Table 4.10 for the ultimate load stage. There is very little difference in analysis methods for these specimens since the tension tie (loop bars) capacity which is the same for both analyses governs. The ratios in row 5 of the tables are exactly the same for this analysis method as for the simplified analysis method for tests 4A and 5A, and they are very close for tests 4B and 5B. The same conclusions can be reached for this analysis method as for the simplified analysis method. For the yield load stage, the ratio of $N_y(\text{Test})/N_y(\text{Calc})$ in row 5 suggests

that for tests 4A and 5A the test results are significantly lower (19% and 29%) than the calculated pull-out capacity determined by adding the loop bar mechanism to the top surface reinforcement mechanism. For design, the deviation saddle reinforcement would be proportioned for the pull-out capacity utilizing the yield strength of the reinforcement. However, the ratios in row 5 indicate that at first yield it is not possible to include the top surface reinforcement mechanism capacity in the total pull-out capacity, which should be restricted to the loop bar mechanism capacity. For the ultimate load stage shown in Table 4.10, it is apparent from the comparison in row 5 that it is possible to include the top surface reinforcement mechanism contribution to the total pull-out capacity as limited by the tendon 2 capacity with uncoated reinforcement and the total tendon capacity with epoxy coated reinforcement. This differs from the yield load stage. When comparing the alternate calculations (tendon 2 and total tendons) presented for each test in row 5, the same trend is apparent for these results at ultimate as with the other analysis method. There is a capacity for redistribution of force in the epoxy coated specimens (5A and 5B) that is not obtainable with the directly comparable conventional reinforcement tests 4A and 4B.

4.4 Comparison Of Analysis Methods

For the calculation of the total pull-out capacity of the deviation saddle, the only difference between the simplified analysis method and the strut-tie analysis method is in the treatment of the

top surface reinforcement. The calculation of direct tension reinforcement (the link bars for tests 1A, 1B, 2A, 3A, 3B, and the loop bars for tests 4A, 4B, 5A, and 5B) for both methods is identical. For the simplified analysis method, the top surface reinforcement is assumed to be the tensile reinforcement for an assumed beam element which has a depth equal to the average concrete cover of the tendon ducts. For the strut-tie analysis method, the top surface reinforcement is assumed to be the tie of an assumed truss which incorporates compression struts branching from the average location of the tendon duct. There are subjective assumptions that must be made for both the beam element analysis and the strut-tie analysis for the top surface reinforcement. For the beam analysis, these are the consideration of the degree of fixity of the ends of the beams. For the strut-tie analysis, these are the consideration of the proper strut-tie model to use and also the maximum strut and tie forces. Maximum strut forces are dependent on the strength of the concrete which in turn depends to a large extent on the multiaxial state of stress and on the disturbances from cracks and reinforcement. Maximum tie forces are easily determined if it can be assumed that yield stress of the tie was attained. The subjective assumptions for the strut-tie analysis are critical only when the specimens are over-reinforced as was the case for several of the tests. For under-reinforced specimens, the reinforcement will yield and the maximum allowable concrete strut stresses will be significantly greater than

the calculated values based on yield of the reinforcement. In other words, selection of concrete strut dimensions and maximum stresses will not be critical in under-reinforced specimens.

In tests of the early deviator configuration of Fig. 4.1a with specimens 1A, 1B, 2B, 3A, and 3B, (specimen 2A did not have top surface reinforcement) the top surface reinforcement contribution to the total pull-out capacity of the deviation saddle was significant (40% to 60%), whereas the contribution of the top surface reinforcement in the modified specimen of Fig. 4.1b (tests 4A, 4B, 5A, and 5B) accounted for only a small amount of the total pull-out capacity of the deviation saddle ($\approx 12\%$). For the modified specimens, pull-out capacity calculated using the two different analysis methods was exactly the same for tests 4A and 5A, and had only a negligible difference of 0.3 kips for tests 4B and 5B. However, there was a substantial difference in the calculations by the two analysis methods for specimens 1A, 1B, 2B, 3A, and 3B in which the top surface reinforcement had a significant effect on the total pull-out capacity of the deviation saddle. Comparisons of the top surface reinforcement capacities as determined by the two analysis methods are shown in Fig. 4.20. The values on the vertical axis are the pull-out capacity for the top surface reinforcement expressed in kips for each analysis method for each test. These results are only presented for tests 1A, 1B, 2B, 3A, and 3B because the specimen 2A detail did not include the two stirrups which reinforced the top surface. Tests 4A, 4B, 5A, and

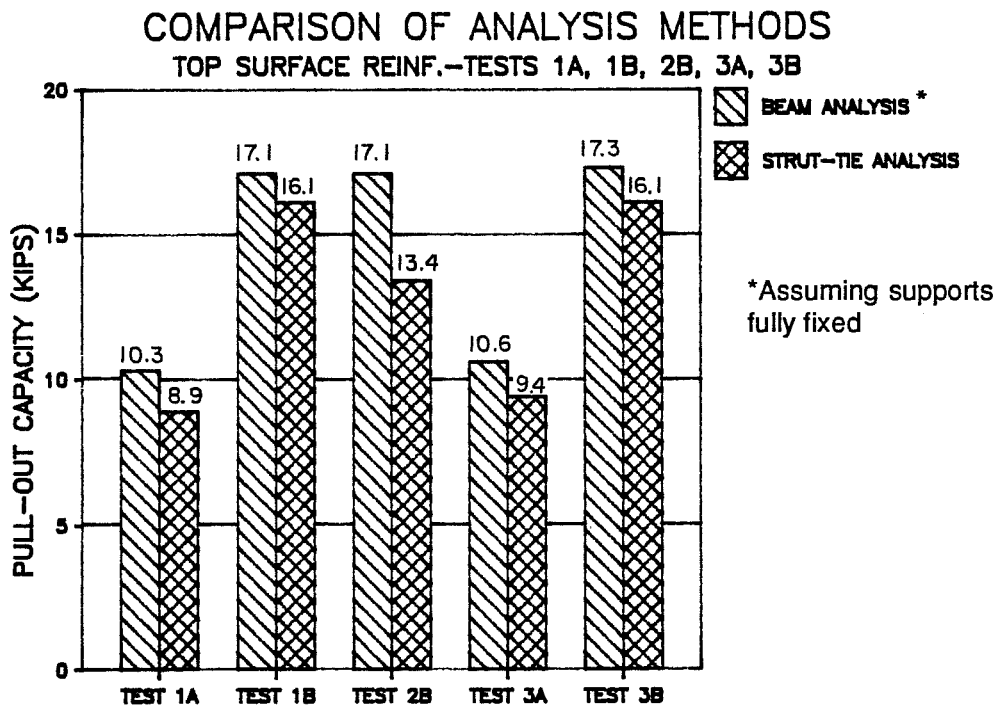
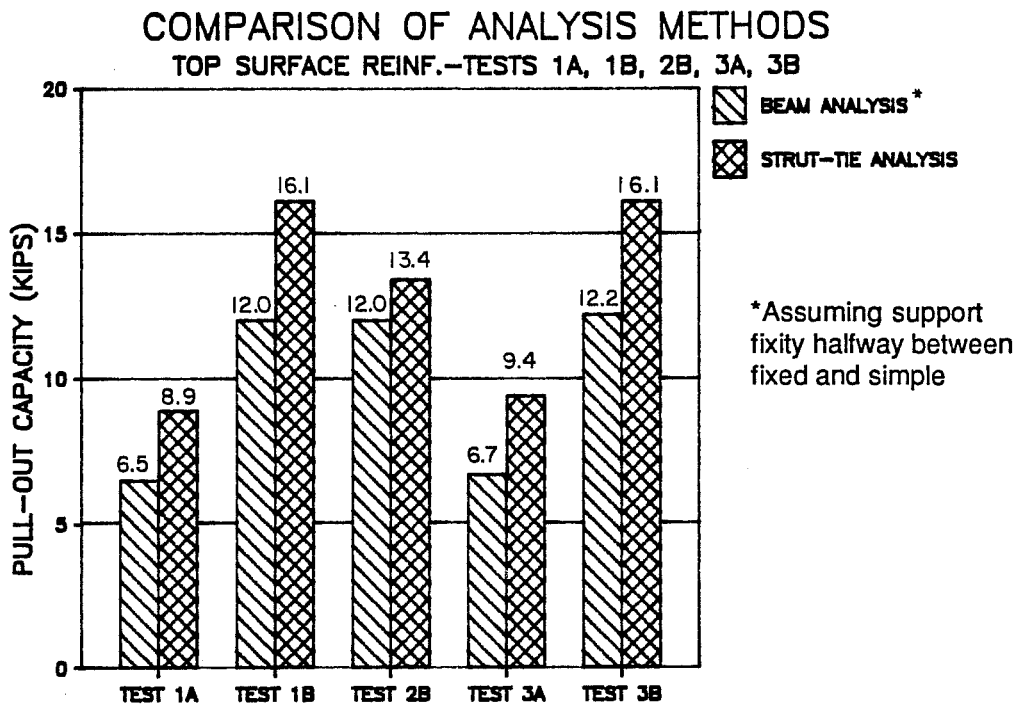


Figure 4.20 Comparison of Analysis Methods for Supplementary Top Surface Reinforcement Only

5B are not shown since the difference in analysis methods for these tests is insignificant. The bar graph at the top of Fig. 4.20 is the comparison between the strut-tie model analysis (top reinforcement only) and the beam analysis (simplified analysis model) assuming support fixity halfway between fixed and simple. From this bar graph it is apparent that the strut-tie model values are 12% to 40% greater than the beam analysis values. The bar graph at the bottom of Fig. 4.20 is the comparison between the strut-tie model and the beam analysis model assuming supports are fully fixed. It can be seen from this bar graph, that beam analysis values are only 6% to 16% greater than the strut-tie analysis values, with the exception of test 2B. The correlation between analysis methods is improved when the supports are assumed fully fixed for the beam analysis. One reason why the comparison is poor for specimen 2B (27% difference) may be due to the dissimilar behavior of this specimen compared to the other specimens. The deformations for specimen 2B were substantially greater because the specimen overall detailing did not include the link bars which limit the deformation. These deformations could be taken into account in the strut-tie analysis method by utilizing the deformed deviation saddle configuration and also a lower allowable concrete stress which takes into account the large crack widths. However for the beam element analysis, it is not possible to take these factors into account.

To summarize, much closer correlations between analysis methods were apparent for tests 1A, 1B, 3A, and 3B, when the beam element for the simplified analysis model was assumed fixed and the strut-tie analysis for the top surface reinforcement was assumed to have maximum tie and strut forces. There was no difference for test 2A because the link bar reinforcement is treated the same in both analyses. For test 2B, the simplified analysis method with the beam element assuming supports halfway between fixed and simple correlates best with the strut-tie model which takes into account the deformed deviation saddle with maximum tie and strut forces. For the modified specimens (4A, 4B, 5A, 5B), the analysis methods compare well for the simplified analysis model with the beam element assuming supports halfway between fixed and simple and the strut-tie model assuming maximum tie and strut forces.

Each analysis method has its own advantages. As was apparent in the preceding sections for the loading combinations in Secs. 4.2.4 and 4.3.1, it is sometimes not possible to count on mobilization of the full capacity of the top surface reinforcement in the total pull-out capacity for the yield load stage. Sometimes at ultimate it is not a conservative assumption to include the full capacity of the top reinforcement. Because of this, the beam analysis offers some versatility because it was found that the end conditions can be altered to produce a lower contribution of the top surface reinforcement so that the design is more conservative. For example it

was determined in Sec. 4.2.4, for tests 1A, 1B, 2B, 3A, and 3B at first yielding load stage that load combinations based on the simplified analysis method assuming simple beam element end conditions would produce a conservative design. Whereas for the strut-tie model, the truss would have to be altered (lower stress than yield in the tie) to reflect the lower contribution of the top surface reinforcement for some tests. This was shown in Sec. 4.3.1. However, the main advantages of strut-tie models are their transparency and adaptability to arbitrary geometry and loading configurations (10). This is an important consideration since there are a wide variety of possible deviation saddle configurations.

Both analysis methods appear to produce reasonable correlations with the test results. However, both methods rely on subjective assumptions for the analysis of the top surface reinforcement. For this reason, it would be more rational for the deviation saddle design to utilize a detail such as the modified specimen of Fig. 4.1b and specimens 4A, 4B, 5A, and 5B, and ignore the contribution of the top surface reinforcement since it would only account for about 12% of the total capacity. This would simplify the design greatly. However, if a deviation design was to include the contribution from the top surface reinforcement, the strut-tie method appears to be a better tool for modelling because of its adaptability to arbitrary deviation saddle geometry and loading configurations.

4.5 Conclusions

The pull-out forces from the vertically deviated tendon(s) were resisted by the combination of the direct tension reinforcement and the top surface reinforcement in the deviation saddle. Horizontal shear across the critical crack plane located below the tendon ducts was resisted by shear friction. Test observations and analysis indicated that in these tests shear friction did not appear to be a critical factor in the failure of the deviation saddle. All failures in this test series (except test 2B which had no direct tension reinforcement) were the result of the fracture of the direct tension reinforcement. This reinforcement can be easily analyzed and is highly efficient. The critical force which acts on the deviation saddle is the maximum tendon deviation force. In this test series, this is the force that was closely confined by the direct tension reinforcement. In the early specimens (Fig. 4.1a) this was the corner tendon which had both vertical deviation and horizontal deviation. The direction of this deviated tendon force was approximately perpendicular to the top surface. The other tendons of the early specimens did not greatly influence the pull-out capacity of the specimens because they were not enclosed within the critical reinforcement (direct tension reinforcement). In the revised specimens (Fig. 4.1b) both tendons were enclosed in separate direct tension reinforcement, but the corner tendon was more critical since it had greater vertical deviation than the other tendon. The basic direct tension reinforcement around the

critical tendon should be proportioned for this maximum tendon deviation force. The other tendons could be provided with the same reinforcement to simplify detailing or, if desired, some lesser amount determined by a similar analysis based on the individual tendon deviated force.

At first yield load stage for specimens 1A, 1B, 3A, and 3B (early configuration - Fig. 4.1a), the capacity of the deviation saddle can be determined by adding the yield strength of the link bars to a contribution of the top surface reinforcement which can be calculated by either analysis method presented in this chapter. Utilizing the beam analysis method, it was stated in Sec. 4.2.4 that this top surface reinforcement contribution could be conservatively estimated assuming a beam element across the top surface with simply supported end conditions. This was concluded because some of the ratios for $N_y(\text{Test})/N_y(\text{Calc})$ based on the assumption of supports halfway between fixed and simple were below 1.0 in Table 4.3. Utilizing the strut-tie analysis models of Sec. 4.3, the total calculated pull-out capacity exceeded the actual yield loads by 16% to 40%. The contribution of the top surface reinforcement as calculated based on the maximum strut and tie forces produced an excessive contribution to the total pull-out capacity of the deviation. It can be concluded from Table 4.7 that the capacity of the top surface reinforcement which should be utilized for estimating the yield loads should be no greater than 50% of that calculated as the maximum. For

specimens 4A, 4B, 5A, and 5B (modified configuration - Fig. 4.1b), it was apparent from both analysis methods that at first yield only the contribution of the direct tension reinforcement should be considered for determining the capacity.

In summary, at the yield load stage of the deviation saddle for the early configuration (Fig. 4.1a), much uncertainty exists as to the contribution of the top surface reinforcement. It is shown that this contribution can be included in the yield load capacity if conservative oversimplified assumptions of simply supported end conditions are utilized for a beam model analysis. For the revised specimens (Fig. 4.1b), it is not safe to include the contribution from the top surface reinforcement in computing yield load capacity.

At the ultimate load stage, there was very good overall agreement between the pull-out capacity calculated from the analysis methods and the test results. For the simplified analysis method, a conservative estimate of the pull-out capacity of the fully detailed deviation saddle (Fig. 4.1a and 4.1b) was made by adding the ultimate capacity of the direct tension reinforcement and the beam element capacity assuming beam element supports halfway between fixed and simple. For the strut-tie analysis, a fairly good estimate of the pull-out capacity of the fully detailed deviation saddle was obtained by adding the ultimate strength of the direct tension reinforcement and of the strut-tie model assuming maximum strut and tie forces. The comparison in row 5 of Table 4.8 shows a slight overestimation of the

pull-out capacity for the conventionally reinforced early deviation saddle detail (Fig. 4.1a) for this method. Both analysis methods based on the above stated assumptions produced conservative pull-out capacities for the epoxy coated reinforcement specimens. However, closer agreement was seen with the strut-tie method. For epoxy coated reinforcement specimens, if the beam analysis of the simplified analysis models is modified to assume that the beam element supports are fully fixed, then a better correlation exists.

At the ultimate load stage, it can be concluded that varying amounts of force were mobilized in the force resisting mechanisms which were added to the primary direct tension reinforcement depending on the bond characteristics of the reinforcement. For the epoxy coated specimens 3A and 3B, the top surface reinforcement was able to develop a greater amount of resistance to the pull-out force than the directly comparable conventional reinforcement specimens 1A and 1B. For the epoxy coated specimens 5A and 5B, once the reinforcement around the highly loaded tendon 2 reached capacity, additional load was carried by the direct tension reinforcement around the other tendon. This trend was not apparent in the directly comparable conventional reinforcement tests 4A and 4B. It can be concluded from these tests that with the somewhat less locally bonded epoxy coated reinforcement there is increased redistribution of force within the deviation saddle before fracture of the direct tension reinforcement. This extra capacity should not be incorporated in the design.

Although the ultimate capacity of the test specimens developed the full ultimate of the reinforcement (which fractured), for design purposes, the highest reinforcement strength utilized should be the yield point stress of the reinforcement. A rational basis for the design of the deviation saddle for the pull-out force must consider the proportional amounts of resistance provided by the direct tension reinforcement and the top surface reinforcement. In tests of the early deviator configuration of Fig. 4.1a (specimens 1A, 1B, 3A, and 3B), the top surface reinforcement contribution to the total pull-out capacity of the deviation saddle was significant (40% to 60%), whereas the contribution of the top surface reinforcement in the modified specimen of Fig. 4.1b (tests 4A, 4B, 5A, and 5B) accounted for only a small amount of the total pull-out capacity of the deviation saddle ($\approx 12\%$). From this test series, it is seen that the pull-out resistance of the top surface reinforcement was somewhat complicated to analyze and some of the assumptions which were used are highly subjective. In addition, there is some uncertainty as to how much of the contribution of the top surface reinforcement can be utilized for the yield capacity of the deviation saddle. Generally, this top surface reinforcement is not as efficiently utilized as the direct tension reinforcement. For these reasons, it would be more practical to proportion the reinforcement in the deviation saddle design detail to be basically direct tension reinforcement such as in the modified specimen of Fig. 4.1b, and ignore the contribution of the

top surface reinforcement since it would only account for about 12% of the total capacity. This would greatly simplify the design. A shear friction check should be made after proportioning the reinforcement for the pull-out forces and additional shear friction reinforcement should be furnished if necessary.

CHAPTER 5
DEVIATOR DESIGN RECOMMENDATIONS

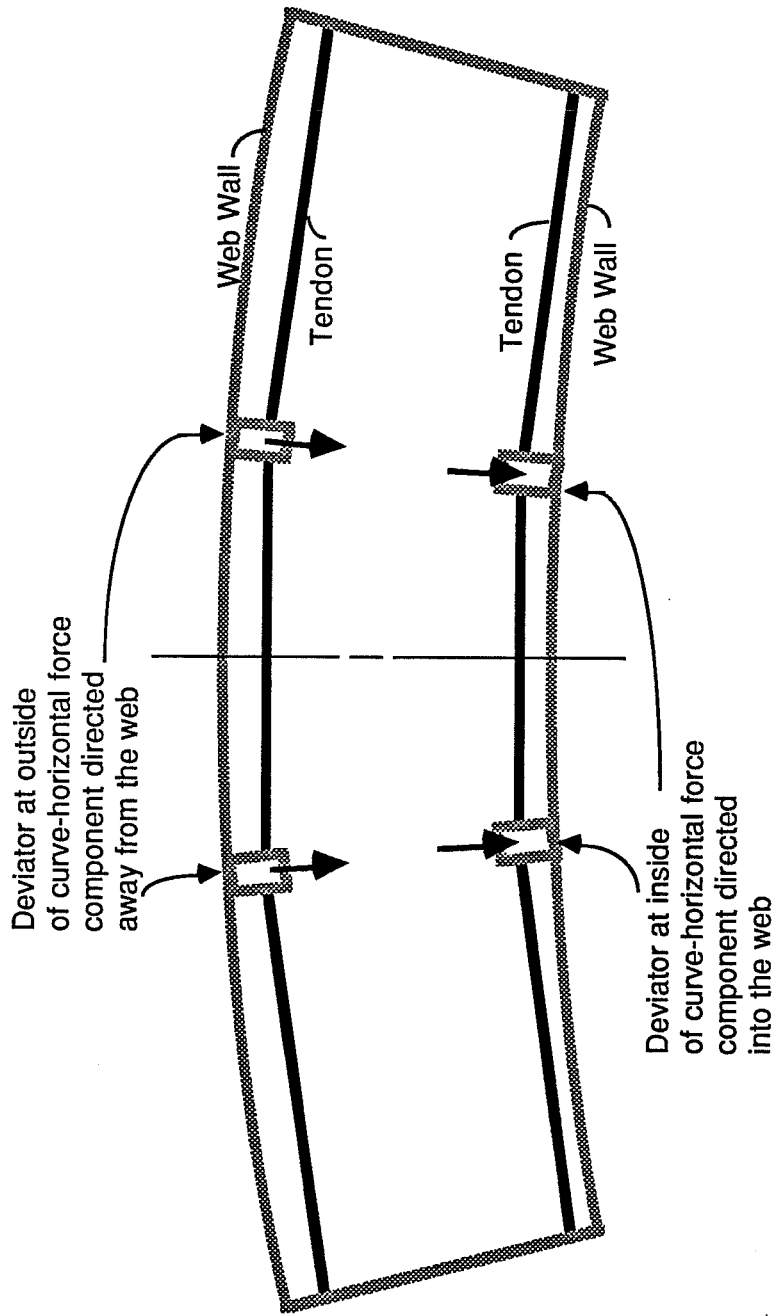
5.1 General Approach

Deviator design recommendations are presented in this chapter. These design recommendations are based on strength, resistance to cracking, constructability, and simplicity of analysis. The majority of the discussion of this chapter is directed towards the deviation saddle since it is the weakest of the three basic types of tendon deviators. However, recommendations for the deviation saddle can be conservatively applied to the diaphragm and the rib or stiffener since these type of deviators generally have added strength contribution from the concrete.

Deviator configurations vary depending on the requirements of the bridge. The most important factor influencing the deviator configuration is the tendon profile because it determines the locations and spacing of the deviators, and the number of tendons deviated within each deviator. The location along the span determines the tendon angular deviations since the closer the tendon deviator is to the pier anchorages, the higher the deviation angles must be. The number of tendons deviated within a deviator is a significant factor affecting the configuration. In the design of any deviator, the most important factor is the number of tendons with vertical deviation at that deviator because they have the greatest impact on the design. The horizontal curvature of the span also has an effect on the deviator

design since an additional horizontal component must be taken into account. The resulting horizontal component of force will be directed away from the web on the outside of the curve, and it will be directed towards the web on the inside of the curve. This is illustrated in Fig. 5.1. Specimens 4A through 5B in the test series represented deviation saddles typical of a curved span. As was learned in this study, deviation saddles on the outside of small radius curves are the most critical because the extra horizontal component is directed away from the web. It can be generally stated that at service loads horizontal force components directed towards the web for either a curved span or straight span should have no damaging effect on the deviator since the force is transferred to the box section by compression of the saddle concrete which generally has excess capacity.

The spacing of the deviation saddles affects the maximum allowable height of the deviation saddle since clearance is required for the adjacent deviated tendons. The problem of interference of deviated tendons from adjacent deviation saddles is minimal in a deep box girder bridge since the tendon deviation angles will be much greater. However, it is not practical to adjust the depth of the box section to suit the requirements of the deviation saddle. Deeper box sections are more common in bridges over water, whereas, highway bridges are usually more shallow. The reason being the vertical clearance constraints are not usually as restrictive over water.



Plan View of Horizontal Curved Span

Figure 5.1 Horizontal Force Components on Deviators of Curved Span

A problem unique to the diaphragm and the rib or stiffener is the geometry complications of the pass-through tendons. This was mentioned in Chapter 1. Pass-through tendons are defined as deviated tendons from adjacent deviators which must pass through the deviators which are located closer to the anchorage zones. Holes are placed in the deviators which require a tendon to pass through. No contact is made between the pass-through tendons and the deviator. Geometry complications are increased on a horizontally curved span because the bridge is curving while the deviated tendons remain on a straight path.

Total service load design forces for the deviator should be the sum of the vertical and horizontal components of the deviated force from each tendon. These can be calculated as the maximum allowable initial jacking force multiplied by the sine of the angle change for the vertical and horizontal planes of the tendon. Under AASHTO Specification (2), the maximum allowable initial jacking force is limited to 80% of the ultimate strength of the tendon ($0.8(f_{pu})(A_{ps})$). At service load levels, reinforcement stresses would be limited to the specified allowable stresses in AASHTO Sec. 8.15.2. For load factor design, neither AASHTO nor ACI (8) specify clearly an appropriate load factor for the prestress tendon force. In order to guarantee a reasonable factor of safety commensurate with other load and resistance factor combinations, it is suggested that the load factor on prestress force should be at least 1.7. Conventional

reinforcement should be assumed at the yield point and the ϕ factor that should be used in the design of the direct tension reinforcement should be 0.90 since the primary acting force is tension. The ϕ factor for the shear friction calculation should be 0.85.

The recommended design detail will be very similar to the last four models (specimens 4A, 4B, 5A, and 5B) that were tested in this investigation because for the most part this deviation saddle detail functioned very well. This detail is shown in Fig. 5.2. It was originally designed for a total factor of safety (LF/ϕ) against pull-out of about 1.6 for yield and about 2.2 for ultimate. These factors of safety were calculated assuming a pull-out capacity determined by adding the direct tension capacity of the loop bars and the beam type capacity of the top surface reinforcement. The tendon deviation horizontal force components were assumed to be resisted by shear friction which appeared to be less critical than the pull-out capacity. Test results of Chapter 3 indicated safety factors for cracking and yield were too low for the tendon configuration that represents a deviation saddle on the outside of a curve (specimens 4A and 5A which had a horizontal force component in the direction of the center of the box). Therefore, recommendations will be made to remedy this deficiency.

The general approach to the design of the deviation saddle is to rely only on the efficiently utilized direct tension reinforcement for the pull-out force resistance of the deviation saddle. Any

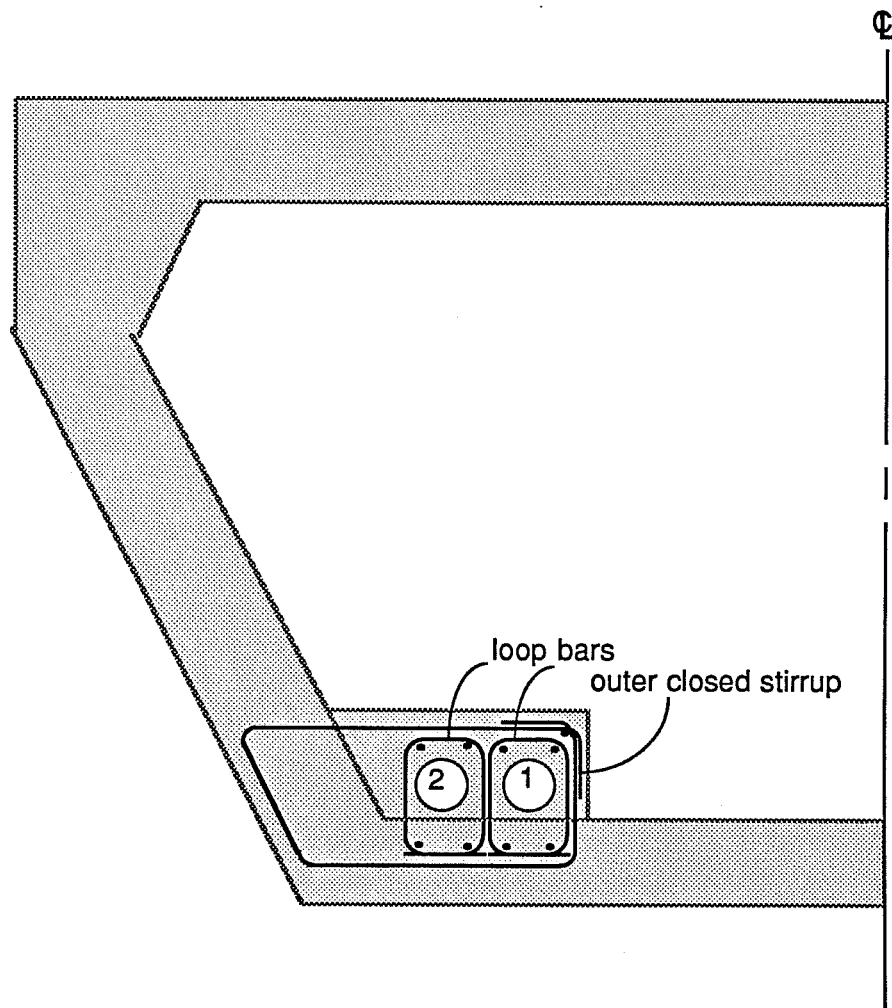


Figure 5.2 Modified Deviation Saddle Detail

contribution to the pull-out resistance from the concrete is ignored as is any additional resistance from any beam type element above the ducts. The concrete contribution cannot be utilized because no compression struts form in the deviation saddle unless the tendon deviation forces are horizontal and directed into the web. The comparison in Chapter 4 for specimens 4A and 5A of the analyses and the test results proved that it was not possible to add the direct tension capacity of the loop bars and the top surface reinforcement capacity at the yield load stage. At this stage, the designer can only depend on the tendon loop bar capacity. Neglecting the contribution of the top surface reinforcement does not influence the design greatly since it was shown in Chapter 4 that the contribution from the top surface reinforcement in the modified specimen was only about 12% of the total pull-out capacity. In addition to designing the deviation saddle for pull-out forces, a shear friction check should be completed.

5.2 Deviation Saddle Geometry And Size

The deviation saddle geometries utilized in this investigation began with the deviation saddle with a sloping top surface and front face shown in Fig. 5.3. This was later modified to a horizontal top surface with vertical sides shown in Fig. 5.2. This was done with the goal of simplifying the shape to make fabrication of the segments easier. In addition, it is imperative in shallow highway bridge structures that the height of the deviation saddle be as low as

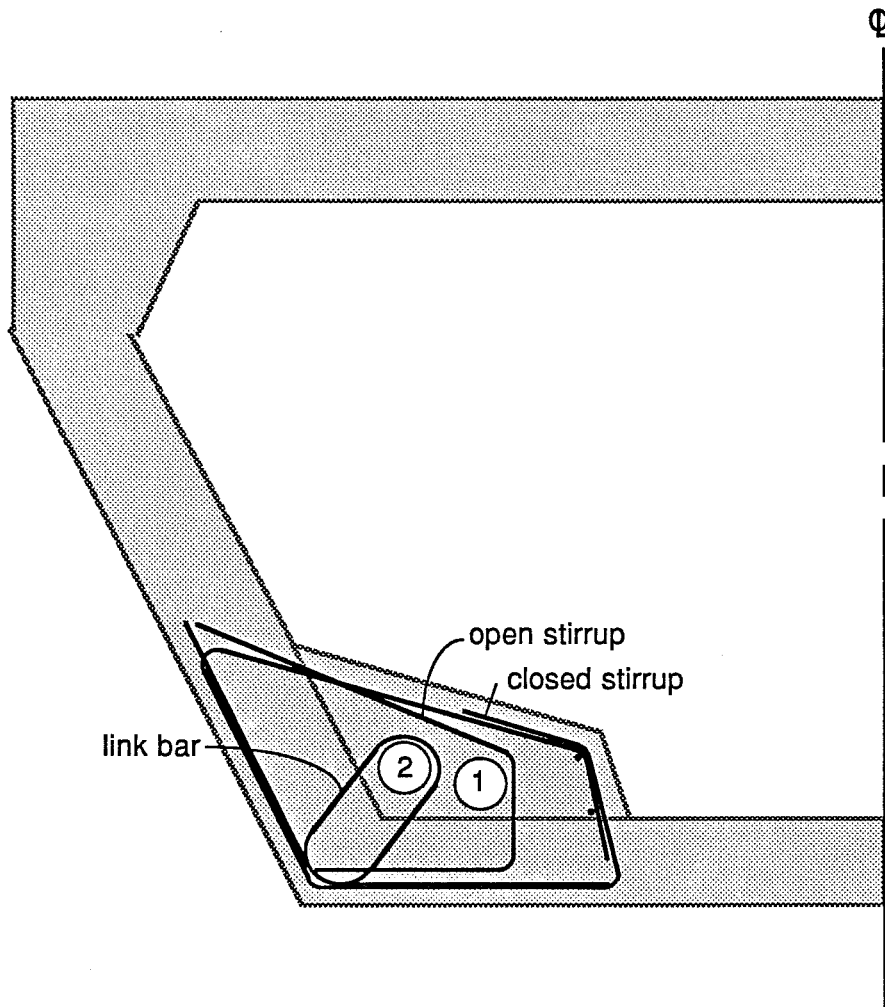


Figure 5.3 Early Deviation Saddle Detail

possible so that there is clearance for the deviated tendons of the adjacent deviation saddle.

For deviation saddles located on the inside and outside of curved spans, it was apparent from the investigation that the factors of safety for ultimate were approximately the same (specimens 4A, 4B, 5A, and 5B). However, the specimens which represent a deviator on the inside of the curve with lateral confinement from the web wall to resist the horizontal force (4B and 5B) had a substantially greater factor of safety against cracking and yielding when compared to the specimens which represent a deviator on the outside of the curve (4A and 5A). This is shown in Table 5.1. These factors of safety were based on the ratio D/D_0 which is the ratio of the total vector force acting on the deviation saddle to the nominal design reference force from Chapter 3. The factor of safety against yielding can be increased by placing additional reinforcement. However, to minimize cracking is difficult because the deviation saddle is primarily a direct tension member which requires the concrete to crack for the reinforcement to be effective.

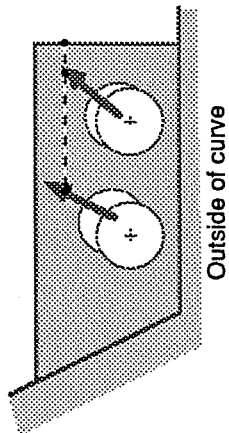
	Side of Curve	Micro cracking	Visible cracking	Yielding	Ultimate
Test 4A	Outside	0.98	0.98	1.33	2.24
Test 4B	Inside	1.66	2.03	2.03	2.40
Test 5A	Outside	0.78	0.78	1.06	2.53
Test 5B	Inside	1.32	1.49	1.93	2.64

Table 5.1

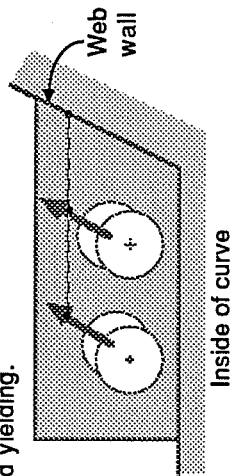
A possible solution to lessen the difference between deviation saddles located on the inside and outside of the curve would be to provide confinement for the front face of deviation saddles located on the outside of the curve. Then the factor of safety for cracking and yielding could be equalized for both tendon configurations (inside and outside of the curve). This could be done by either providing a full bottom flange width deviation saddle (see Fig. 5.4) or providing extra confining reinforcement. The placement of extra ties transversely is not a practical solution because of interference problems with the tendon ducts.

The placement of the full bottom flange width deviation saddle is probably only required for small radius curve spans when all tendons in a deviation saddle have a large horizontal component. For straight spans, when the horizontal tendon angles are small (less than 3°), it should only be necessary to use a deviation saddle which is similar to those tested. These assumptions are based on the observed behavior of the test series. For specimens which represented deviation saddles from a straight span and had smaller horizontal deviation angles (specimens 1A, 1B, 3A, 3B), the factors of safety were acceptable for cracking and yielding. Although the factor of safety for cracking was a little low for specimen 3A which was epoxy coated. It may also be beneficial to provide the full bottom flange width deviation saddle no matter what the tendon deviations are when epoxy

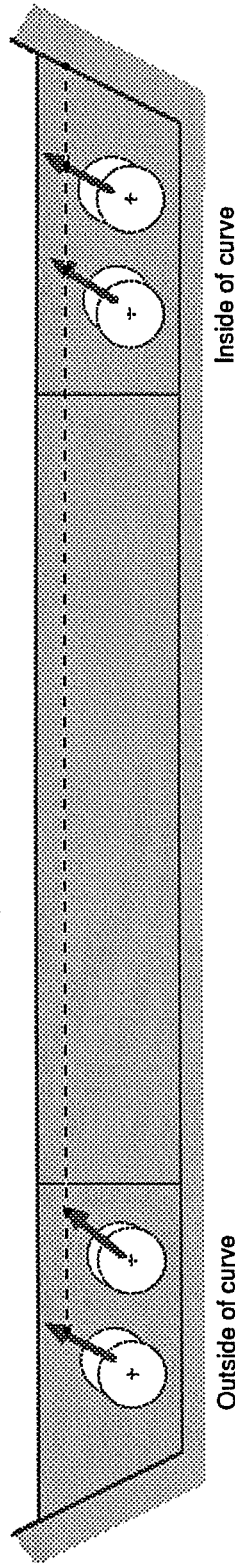
No confinement provided.
Therefore, early crack
formation and yielding.



Confinement provided by web wall.
Therefore, higher resistance to cracking
and yielding.



Both sides confined



Assuming full bottom flange width deviation saddle

Figure 5.4 Recommendation for Full Bottom Flange Width Deviation Saddle - Small Radius Curved Spans

coated reinforcement is being utilized because it was observed in this test series that the specimens with epoxy coating reinforcement cracked at a much lower load than that of the conventionally reinforced specimens (averaged 24% lower). Since the reinforcement is being epoxy coated because of the severe corrosion conditions, it would be advantageous to go one step further and provide the full bottom width deviation saddle which will substantially increase the factor of safety against cracking.

A drawback to the recommendation of the full bottom flange width deviation saddle is the extra dead load. However, it is a great improvement over that of the use of full height diaphragms or ribs (not only because of dead load but also because of geometry complications). A reduction in concrete volume for the full bottom flange width deviation saddle could be made by reducing the longitudinal dimension of the deviation saddle by one-half in the center of the bottom flange at a certain distance from the tendon ducts. Near the webs the deviation saddle would be the same as the models tested but would be joined to the opposite deviation saddle by a concrete strut half the dimension of the deviation saddle. This is illustrated in Fig. 5.5.

Another possible drawback to placing a deviation saddle across the bottom flange of the box section is that it might cause inconvenience for the constructor because equipment often needs to be rolled through the box section during construction. However, it may

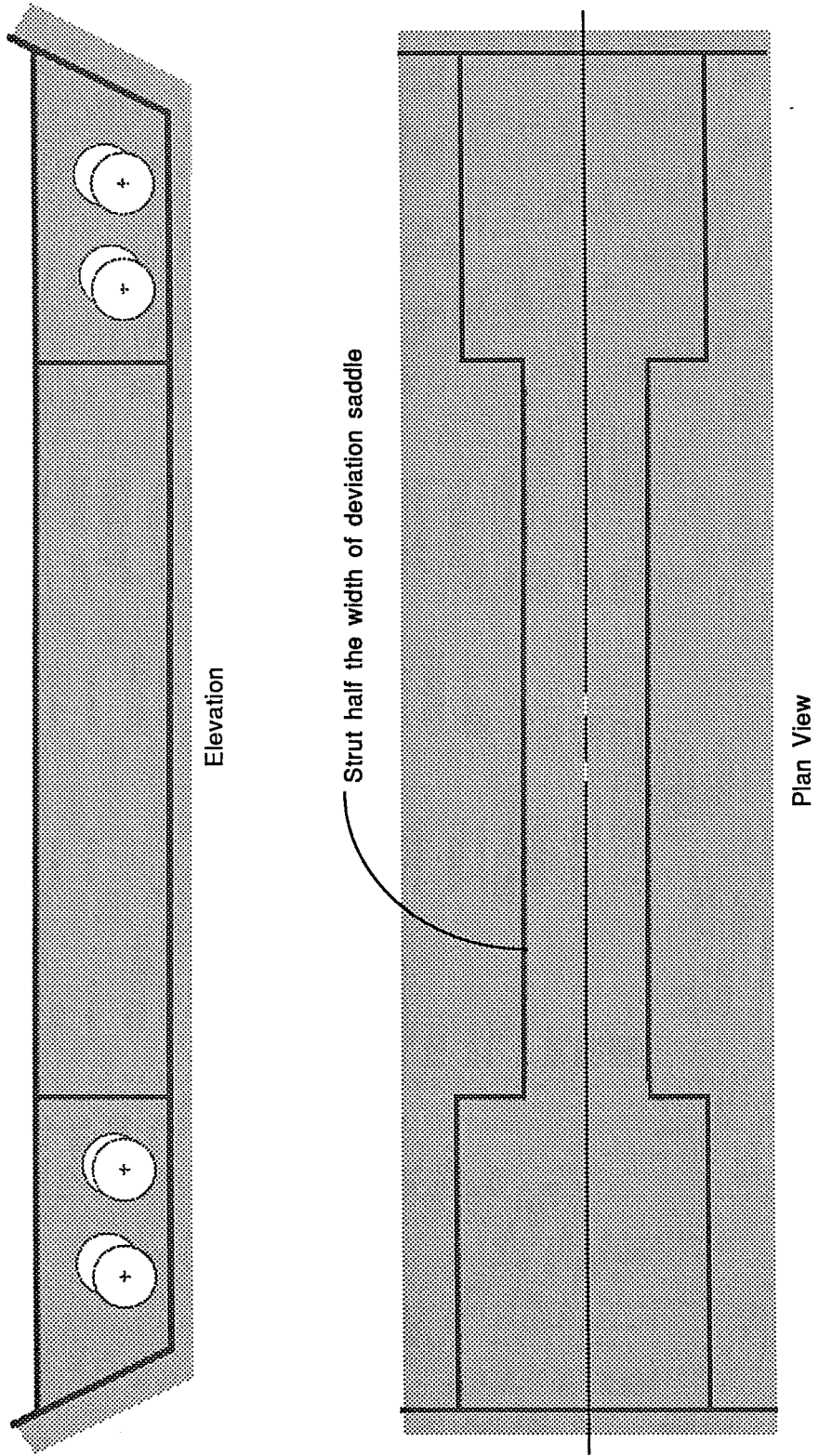


Figure 5.5 Plan And Elevation of Full Bottom Flange Deviation Saddle

reduce temporary post-tensioning hardware which is required, because for small boxes the temporary post-tensioning is usually applied through hardware which bolts to the middle of the bottom flange. This hardware would not be needed since the temporary post-tensioning rods could be placed through the center of the full bottom flange width deviation saddle.

The concrete dimensions of the deviation saddle are controlled by the requirements of the tendon duct curvatures and outer diameter, reinforcement clearances, and cover requirements. The lowest point of the tendon duct above the top of the bottom flange should be based on required clearance (1" to 2") for constructability (protective sheathing placed on extension of tendon duct is generally used for external post-tensioning). The location of the ducts transversely should be as close as possible to the web wall since it is desirable to have as small an eccentricity to the web as possible to minimize bending moments in the bottom flange. The width of the deviation saddle longitudinally is dependent on the spacing and amount of reinforcement (4" to 6" center to center reinforcement spacing is recommended to allow constructability). Also, it is dependent on the minimum radius that the tendon duct can be bent. The curved span deviation saddle models were based on a prototype deviation saddle which had a longitudinal dimension of about 30". It is important not to make the longitudinal dimension too small since

the large concentrated force may have adverse effects on the box girder.

5.3 Reinforcement

From the construction standpoint, it is important to have a deviation saddle reinforcement scheme which minimizes possibilities for fabrication errors and which maximizes versatility so that it can be utilized for the wide array of deviation saddle configurations which may be prescribed by the overall bridge constraints. This was the primary criticism in the first reinforcement scheme that was investigated in this series and which consisted of the link bar with the two confining stirrups. This detail is shown in Fig. 5.3. It was felt by some design professionals that the reinforcement scheme was too restrictive. In the case of a deviation saddle with more than one vertically deviated tendon, an entirely different link bar pattern would have to be fabricated leading to greater complexity in the reinforcement scheme. One of the most important considerations for the reinforcement scheme of the later deviation saddle models for the test series was to find a reinforcement detail which would function like the link bar of the early specimens but that could be utilized for all the tendons within a deviation saddle. This was accomplished by utilizing a small closed rectangular stirrup which looped around each tendon duct and then was anchored under the top mat of reinforcement of the bottom flange. The name coined for this bar pattern is loop bar. Also, an outer closed stirrup which encloses the entire deviation

saddle was also placed to distribute surface cracking as in the first deviation saddle details investigated.

In addition to standardizing the reinforcement patterns, this reinforcement scheme made fabrication of the reinforcement cage easier. These small loop bars and outer closed stirrups could be assembled outside the box reinforcement cage and held in position by longitudinal bars whose length was slightly less than the width of the deviation saddle. These small cages could then be dropped into the completed box reinforcement cage (only the longitudinal reinforcement bars of the box section cage which would run inside the small cages are left out of the completed cage). The small cages of loop bars could then be securely tied to longitudinal bars which are placed in each bottom corner. These longitudinal should be loosely attached to the box section cage so that they can be moved transversely in the formwork to adjust for the tendon duct locations. After the small cages are aligned with the final duct locations in the formwork, the longitudinal bars could be securely fastened to the box section cage. This facilitates placement of the small loop bars because these bars closely confine the tendon ducts and the tendon duct locations may be different from segment to segment. The cage construction scheme is illustrated in Fig. 5.6.

From the analysis standpoint, the modified reinforcement scheme is less complicated to analyze. All the tendon deviation force is assumed to be resisted by the direct tension reinforcement. In

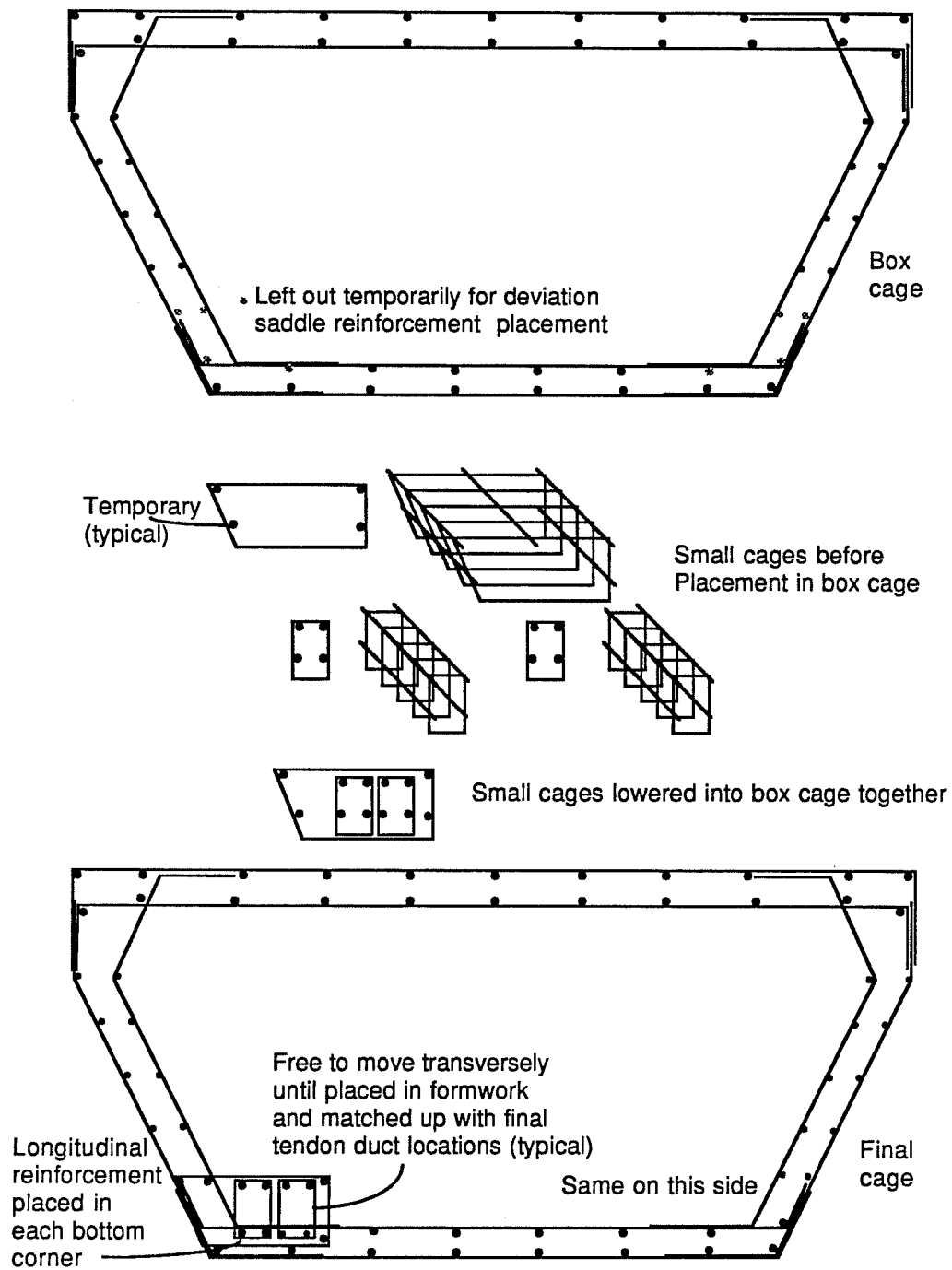


Figure 5.6 Construction Scheme for Box Reinforcement

contrast, in the other reinforcement scheme (Fig. 5.3) considerable pull-out force resistance is provided by the top surface reinforcement. To analyze this top surface reinforcement, some very subjective assumptions must be made and the reinforcement is not nearly as efficiently utilized as the direct tension reinforcement.

As was discussed in the preceding section, the load factor against yielding was only 1.33 and 1.06 for specimens 4A and 5A respectively. The anticipated load factor for the specimens for yield was 1.6 and for ultimate was 2.2. These factors of safety were based on the pull-out capacity determined by adding the loop bar mechanism to the top surface reinforcement mechanism. However it was concluded in Chapter 4 at the yield load stage, that it is not possible to include any contribution from the top surface reinforcement. Also as stated in Sec. 5.1, the load factor for yielding should be at least 1.7. This indicates the requirement for more reinforcement than was present in the model. However, there is ample room to place extra reinforcement, and the additional cost for the extra reinforcement is insignificant. Utilizing a load factor of 1.7 and ϕ factor of 0.9 and the assumption of only including the capacity of the direct tension reinforcement, this will provide an increase in the amount of reinforcement over that present in the models and should produce very satisfactory results.

As was stated above, the deviator reinforcement consists of the loop bars and the outer stirrups. An individual loop bar group

should be designed with the specified load factors and ϕ factors to take the full pull-out force of the tendon with the largest vertical deviation. It will be more economical and error proof to provide the other tendons with the same reinforcement regardless of their tendon deviation forces. Light reinforcement should be provided at the top surface to control and distribute surface cracks (reinforcement neglected in the calculation of the pull-out capacity). This reinforcement should be provided as closed stirrups which enclose the entire deviation saddle. An amount of closed stirrups in the same proportions as the link bar reinforcement will produce very satisfactory results. This reinforcement will then be sufficient to distribute top surface cracking and also provide extra pull-out force capacity to the deviation saddle. In the case that a full bottom flange width deviation saddle is not provided, a shear friction calculation should be completed. In most cases, extra shear friction reinforcement will not have to be provided since there is usually an excess of direct tension reinforcement at the critical shear plane. Also, the outer closed stirrups contribute to the shear friction reinforcement. The shear friction equation that should be used for the check is equation 8-10 of AASHTO (2) which is more conservative and easier to use than Mattock's equation which was used for the analysis in Chapter 4. The net tension across the shear plane is taken into account by subtracting it from the total capacity of the reinforcement crossing the shear plane. The maximum allowable shear strength

or $360A_{CV}$ where A_{CV} is the area of concrete section resisting shear transfer. This area is assumed to be the area below the tendon ducts from centerline of the tendon closest to the web wall to the front face of the deviation saddle. The μ factor is taken as 1.4 since the deviation saddle is monolithically cast. The design recommendations will be illustrated in Sec. 5.4.

The dimensions of the loop bars and the outer closed stirrup are based on the tendon duct curvatures and outer diameters, reinforcement clearances, and development lengths. For the loop bar, the minimum clearance at the highest point of the tendon duct should be approximately 1". The vertical inside dimension of the outer closed stirrup should be at least 2" larger than the loop bars. The maximum bar size utilized for the loop bars should be limited to a deformed #5 size so as to be able to fully develop the 90° hook.

In all models tested, additional bottom flange and web wall reinforcement was provided at the deviation saddle. The amount was approximately double that of the regular bottom flange and web wall reinforcement. This amount of supplementary box reinforcement should be provided for local load distribution at all deviation saddles. If a full bottom flange width deviation saddle is provided, the center strut portion should be provided with nominal surface reinforcement in both directions.

5.4 Design Examples

Two design examples are presented to help clarify the design recommendations discussed above. The first one is shown in Fig. 5.7a-b for a deviation saddle from a straight span. Since the horizontal deviations are less than 3° , a deviation saddle similar to those tested is assumed. The second design example is shown in Fig. 5.8a-b for a deviation saddle from a curved span. A full bottom flange width deviation saddle is assumed because the horizontal angles are quite significant.

5.5 Conclusions

A rational basis for design of deviation saddles was presented. A simplified deviation saddle detail was recommended that differs from the early deviation saddle details which were utilized in bridges in the United States. The reinforcement patterns are standardized to minimize possibilities for fabrication errors and to maximize versatility. Use of this pattern also simplifies and makes assembling of the reinforcement cage significantly easier. The concrete geometry is also simplified to facilitate fabrication and yet provide a low height deviation saddle which is imperative in shallow highway bridges. A recommendation to provide a full bottom flange width deviation saddle is made for deviation saddles in small radius curved spans. Two example designs are made.

Example Design Calculation- Straight Span -Two tendons

Tendon 2-19-0.5"Ø 270 ksi strands $A_{ps}=2.91$ sq. in. (closest to web wall)

Tendon 1-12-0.5"Ø 270 ksi strands $A_{ps}=1.84$ sq. in.

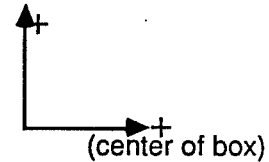
$f'_c=6000$ psi Grade 60 reinforcement

Maximum Allowable Jacking Force= $0.8(f_{ps})(A_{ps})$

Tendon 2 $= (0.8)(270 \text{ ksi})(2.91 \text{ sq. in.})=628.6 \text{ k}$

Tendon 1 $= (0.8)(270 \text{ ksi})(1.84 \text{ sq. in.})=397.4 \text{ k}$

Tendon	Horiz. Dev.	Vert. Dev.	Horiz. Force	Vert. Force
2	+2.93°	+8.22°	+32.1 k	+89.9 k
1	+1.84°	0°	+12.8 k	0 k
Total			+44.9 k	+89.9 k



Load Factor=1.7

$\phi=0.9$ (Tension)

$\phi=0.85$ (Shear)

Design tendon loops based on 89.9 k

$F_u=\phi(A_s)(f_y)$

$A_s=F_u/(\phi f_y)=(89.9 \text{ k})1.7/((0.90)(60.0))=2.83 \text{ sq. in.}$

Assume #4 bars $A_s=0.20 \text{ sq. in.}$

of loops= $2.83 \text{ sq. in.}/(2(0.20 \text{ sq. in.}))=7.1$ use 7-#4 loops each tendon
use 7-#4 closed outer stirrups

Shear friction check

$V_u=(\phi A_s f_y - N_u)\mu$ AASHTO Sec. 8.15.4.3

Area equal to two legs of 7 loops for each tendon and one leg of 7 outer closed stirrups

$A_s=7(5)(0.20 \text{ sq. in.})=7.00 \text{ sq. in.}$

$N_u=(89.9 \text{ k})(1.7)=152.8 \text{ k}$

$\mu=1.4$ (monolithically cast)

$f_y=60 \text{ ksi}$

$\phi=0.85$

$V_u(\text{req'd})=(44.9 \text{ k})(1.7)=76.3 \text{ k}$

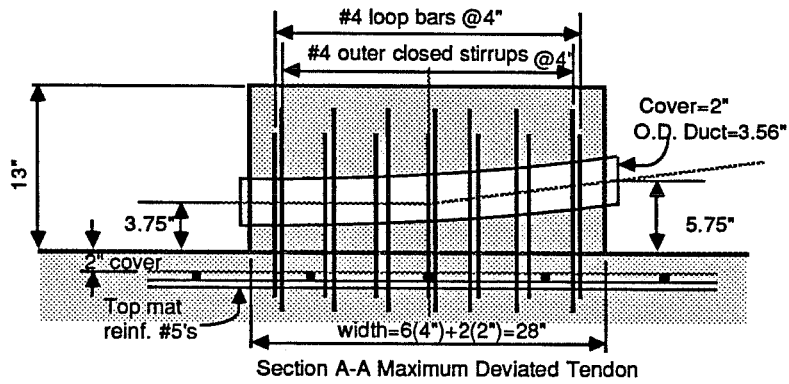
$V_u(\text{provided})=[(0.85)(7.0 \text{ sq. in.})(60 \text{ ksi})-152.8 \text{ k}]1.4=286.9 \text{ k} > 76.3 \text{ k}$ O.K.

$V_u(\text{max provided})=360A_{cv}=360(15.5 \text{ in.})(28 \text{ in.})/1000=156.2 \text{ k} > 76.3 \text{ k}$ O.K.

From Fig. 5.7b

See Fig. 5.7b for dimensioning of reinforcement and concrete

Figure 5.7a Design Example for Straight Span



Link bar vertical dimension = $3.75 + 3.56/2 + (12)(\tan 8.22) + 2 + 2(5/8) + 1 + 2(1/2) = 12.5$
 (out-to-out dimension) use 13"

Link bar horizontal dimension = $3.56 + (12)(\tan 2.93) + 1 + 2(1/2) = 6.2$
 (out-to-out dimension) use 6"

Outer stirrup vertical dimension (out-to-out) = $13 + 3 = 16$ "

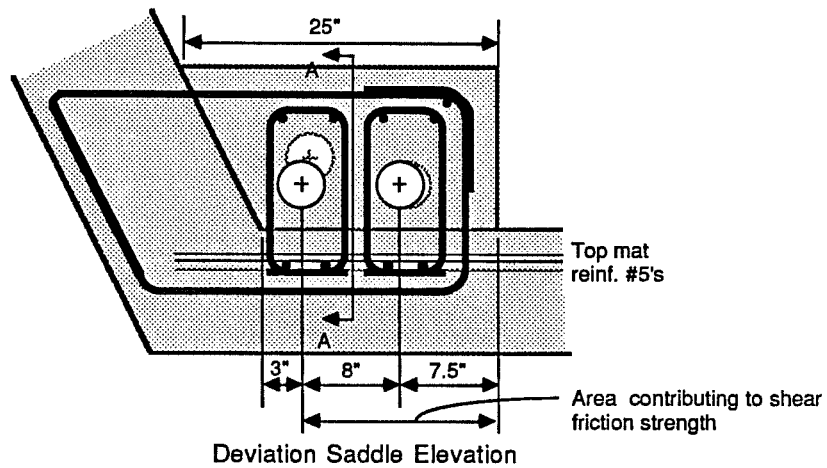
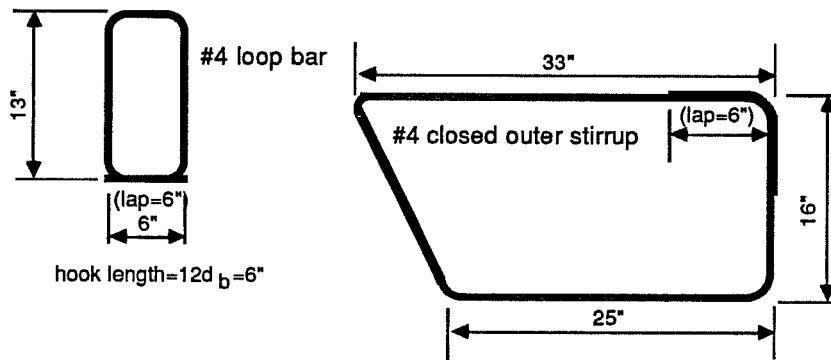


Figure 5.7b Design Example For Straight Span

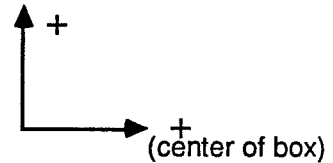
Example Design Calculation- Curved Span -Two tendons

Provide full bottom flange width deviation saddle since small radius curved span

Tendon 2-19-0.6"Ø 270 ksi strands $A_{ps}=4.09$ sq. in. (closest to web wall)
 Tendon 1-19-0.6"Ø 270 ksi strands $A_{ps}=4.09$ sq. in.
 $f_c=6000$ psi Grade 60 reinforcement

Maximum Allowable Jacking Force= $0.8(f_{ps})(A_{ps})$
 Tendon 2 $= (0.8)(270 \text{ ksi})(4.09 \text{ sq. in.})=883.4 \text{ k}$
 Tendon 1 $= (0.8)(270 \text{ ksi})(4.09 \text{ sq. in.})=883.4 \text{ k}$

Tendon	Horiz. Dev.	Vert. Dev.	Horiz. Force	Vert. Force
2	+, -4.0°	+8.0°	+, -61.8 k	+122.9 k
1	+, -4.0°	+6.0°	+, -61.8 k	+92.3 k
Total			+, -123.6 k	+215.2 k



Load Factor=1.7
 $\phi=0.9$ (Tension)
 $\phi=0.85$ (Shear)

Design tendon loops based on 122.9 k

$F_u = \phi(A_s)(f_y)$

$A_s = F_u / (\phi f_y) = (122.9 \text{ k})1.7 / ((0.90)(60.0)) = 3.87 \text{ sq. in.}$

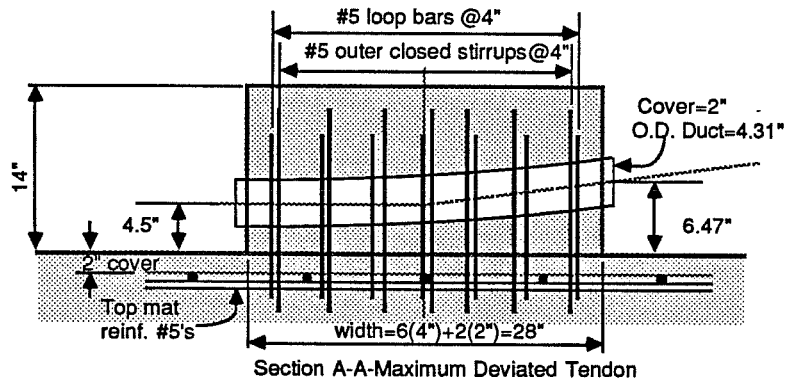
Assume #5 bars $A_s = 0.31 \text{ sq. in.}$

of loops = $3.87 \text{ sq. in.} / (2(0.31 \text{ sq. in.})) = 6.2$ use 7- #5 loops each tendon
 use 7-#5 closed outer stirrups

No shear friction check required since full bottom flange deviation saddle provided

See Fig. 5.8b for dimensioning of reinforcement and concrete

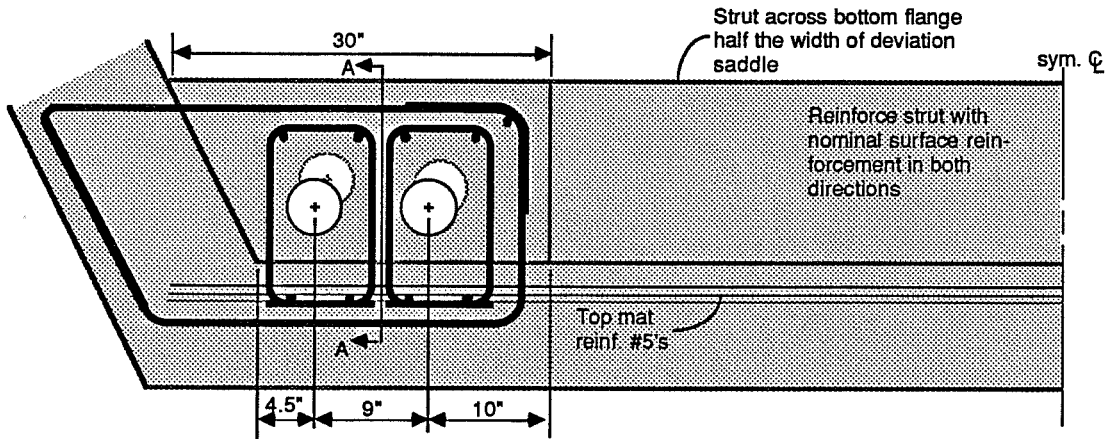
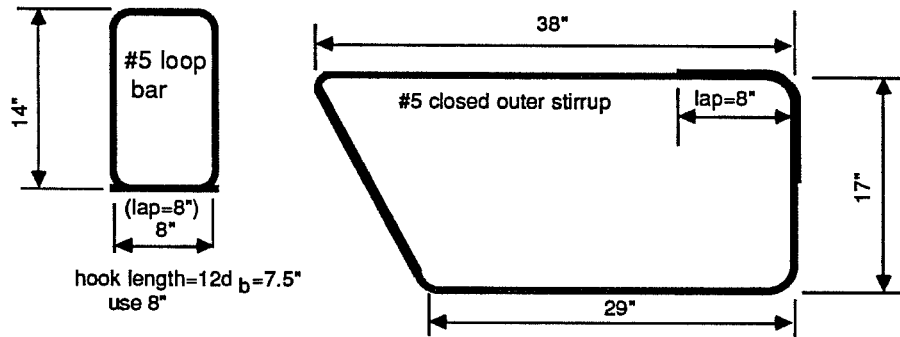
Figure 5.8a Design Example for Curved Span



Link bar vertical dimension = $4.5" + 4.31"/2 + (12")(\tan 8.0^\circ) + 2" + 2(5/8") + 1" + 2(5/8") = 13.8"$
 (out-to-out dimension) use 14"

Link bar horizontal dimension = $4.31" + (12")(\tan 4.0^\circ) + 1" + 2(5/8") = 7.4"$
 (out-to-out dimension) use 8"

Outer stirrup vertical dimension (out-to-out) = $14" + 3" = 17"$



Deviation Saddle Elevation

Figure 5.8b Design Example For Curved Span

CHAPTER 6 CONCLUSIONS AND RECOMMENDATIONS

6.1 Brief Summary

One of the latest and most dramatic developments in segmental technology has been the use of external tendons which are defined as tendons in ducts which are not encased in the concrete of the webs or flanges of the box girder bridge except at the ends of the span. This innovative type of construction has been shown to provide substantial economic savings, as well as savings in construction time. External post-tensioning differs from internal post-tensioning because the tendons are removed from the webs and flanges and placed in the cell-void. The tendon deviators maintain the draped profile of the external tendons and provide the only positive attachment of the tendons to the structure other than at the anchorage zones which makes the deviator a key element of this bridge type.

Uncertainties exist concerning the behavior and proper design criteria for the tendon deviator details. Hence, this study documents an experimental investigation of the tendon deviator details and suggests a design methodology for the deviators.

Three basic kinds of tendon deviators have been utilized in externally post-tensioned segmental box girder bridges; these include the diaphragm, the rib or stiffener, and the saddle or block. These types of deviators are usually monolithically cast in the bridge segments with the correct tendon duct configurations required for the

bridge constraints. The diaphragm and rib or stiffener are usually full web height deviators. The diaphragms usually extend the entire width of the box section and are provided with an access opening for passage along the span. The rib or stiffener extends only a small distance from the web wall. The advantage of using the diaphragm or rib type deviators is that the compressive strength of the concrete may be utilized to resist the tendon deviation forces. A compression strut can develop from immediately above the tendon duct to the top flange which provides these details with higher strength than the saddle or block. However, many disadvantages exist with these details. They create added dead load for the bridge, sometimes offsetting the savings from the efficient web thickness. Other disadvantages are construction related. The formwork for the diaphragm and rib and the geometry for the tendon pass-throughs becomes very complicated, especially for a curved span because the bridge is curving while the tendons remain on a straight path. The block or saddle is usually a relatively small block of concrete located at the intersection of the web and bottom flange. Advantages of utilizing this detail in a bridge are the insignificant additional weight for the structure, the formwork is less complicated than that required for a diaphragm or a rib, and geometry complications are minimized because tendon pass-throughs are not required. However, the disadvantage is that the deviator capacity may be greatly reduced compared to the diaphragm or rib because there is no direct compression strut formed after

cracking. Therefore, the deviator force must be tied back into the box by reinforcement so that it requires greater attention to detailing than that required for a diaphragm or rib.

The laboratory investigation of tendon deviators was directed towards the study of deviation saddles since this detail is the weakest of the three basic types. Also, if the safety of deviation saddles is confirmed by this investigation, then this type offers the most advantages for reducing the structure weight, facilitating the fabrication of segments, and minimizing geometry complications.

The experimental program included fabricating and testing to ultimate of ten reduced scale models of deviation saddles including the two that were completed by Carter (1). Two test specimens were fabricated in each reduced scale single cell box section. They were located on opposite sides of the box section at the intersection of the bottom flange and web wall. The box section was representative of typical single cell box girder bridge sections except that it omitted the cantilever wings. It remained the same for all specimens because it does not influence the behavior of the immediate deviation saddle zone. Supplementary box reinforcement was placed in the bottom flange and web at the deviation saddle for local load distribution.

Specimens 1A and 1B were a typical prototype deviation saddle detail from an existing straight span bridge in the United States. The reinforcement scheme was a link bar with two types of stirrups (designated as open stirrup and closed stirrup). For specimen 1A,

three tendons were deviated which represented a tendon configuration of a deviation saddle located closest to the center of a span. The corner tendon had both a vertical deviation and a slight horizontal deviation directed away from web, and the other tendons had only horizontal deviation directed towards the web. Specimen 1B reinforcement scheme was identical to that of specimen 1A. However, the tendon configuration was different. This deviation saddle only deviated two tendons which represented a deviation saddle located closer to the piers and adjacent to specimen 1A. The corner tendon had both a vertical deviation and a horizontal deviation directed away from the web, and the other tendon only had a slight horizontal deviation directed away from the web. The objective for specimens 2A and 2B was to isolate the behavior of the individual reinforcement patterns of specimens 1A and 1B. These specimens were not intended to be a properly detailed deviation saddles, and they were expected to have an abnormally low factor of safety (D/D_o ratio) for ultimate. Reinforcement details for specimen 2A were based on providing the link bar alone. Specimen 2B reinforcement details were based on providing the two types of stirrups (open and closed stirrups) without the link bars. The tendon pattern for specimens 2A and 2B was identical to specimen 1B. The objective of specimens 3A and 3B was to determine if epoxy coated reinforcement has any effect on the behavior and strength of a deviation saddle. Specimens 3A and 3B were companion specimens to specimens 1A and 1B. The only difference between specimens 3A and

3B and specimens 1A and 1B should have been that the reinforcement was epoxy coated, but some minor differences developed that were not apparent until after fabrication. In spite of this, it was still possible to make comparisons between the epoxy coated specimens (3A and 3B) and the uncoated specimens (1A and 1B). The objective of specimens 4A and 4B was to evaluate a modified reinforcement scheme and deviation saddle geometry. This was an attempt to simplify and standardize reinforcement patterns and deviation saddle geometry for typical deviation saddle details. The reinforcement patterns utilized were a small rectangular closed loop which enclosed each tendon and an outer closed stirrup which enclosed the entire deviation saddle. These bars were anchored under the top mat of reinforcement of the bottom flange. The deviation saddle geometry was changed to a horizontal top surface with vertical sides. The tendon configuration for specimen 4A was representative of a deviation saddle on the outside of a small radius curve. The tendon configuration for specimen 4B was representative of a deviation saddle on the inside of a small radius curved span. Both specimens had two tendons which had both vertical and horizontal deviations. The objective of specimens 5A and 5B was to further evaluate the effect epoxy coated reinforcement has on the behavior and strength of a deviation saddle. Specimens 5A and 5B were companion specimens to specimens 4A and 4B. The only difference between specimens 5A and 5B and specimens 4A and 4B was that the reinforcement was epoxy coated.

A specially designed testing apparatus applied load to the deviator just as it would be loaded in a bridge. This load was applied incrementally to the deviation saddle. The generalized test setup could accommodate a variety of specimen sizes, tendon layouts and loading schemes. Specimens were usually loaded in two cycles. The first load cycle generally continued until yield of the reinforcement, and the second load cycle continued to failure of the specimen. Strain gages were placed internally on the reinforcement of the deviation saddle to determine contributions of individual reinforcement bars.

Physical behavior of each specimen was observed and noted for the full range of loadings. This included general observation of the deviation saddle, their cracking pattern, and strain data.

Two types of initial cracking were apparent in this test series depending on the direction of the total deviated tendon force vector acting on the deviation saddle. If the total force vector was directed towards the center of the box, then the first crack usually formed across the top surface above the tendon with the greatest vertical deviation, and down the sides of the deviation saddle. If the total force vector was directed towards the web, then the first crack usually formed on the sides of the deviation saddle approximately in the direction of the total force vector. All tests except tests 1B and 3B appeared to be ductile and thus gave sufficient warning of the impending explosive failure.

Two separate analysis methods were investigated for each test. The first method utilized simplified analysis models (direct tension model, shear friction model, and beam model) and the second method utilized strut-tie analysis models (tie model for direct tension reinforcement, and strut-tie model for top surface reinforcement). These analyses models were formulated based on the physical behavior of the specimens. The ϕ factor used in comparisons with test results for both analyses had a value of one since the material strengths and specimen dimensions were known accurately.

6.2 Conclusions

The following conclusions can be drawn based on the ten deviation saddle tests of this investigation.

1) All specimens which were intended to be properly detailed deviation saddles (all specimens except 2A and 2B) had an acceptable factor of safety for ultimate load (values ranged from 2.24 to 3.16). The factor of safety was adequate for the yield load stage for the properly detailed deviation saddles 1A, 1B, 3A, 3B, 4B, and 5B (values range from 1.6 to 2.08). However, for tests 4A and 5A, the factor of safety at the yield load stage was unacceptably low, 1.33 and 1.06 respectively. The factor of safety against visible cracking was adequate for specimens 1A, 1B, 3B, 4B, and 5B (1.3 to 2.03). However, it was marginal for specimens 3A, 4A, and 5A (0.78 to 1.03). (Recommendations are made in the following section which would remedy

these deficiencies at the visible cracking stage and at the yield load stage.)

2) The safety of deviation saddles has been verified in this investigation. Properly detailed deviation saddles will perform adequately under service load conditions and have a sufficient factor of safety at ultimate.

3) The epoxy coated reinforcement had adverse effects on the behavior of the deviation saddle at microcracking and visible cracking stages. The average reduction in strength for microcracking and visible cracking was 16% and 24% respectively. However, at the critical strength stage of yielding, coated reinforcement has little effect on the behavior. At this stage, all the load is basically transferred to the reinforcement which if well anchored is not particularly dependent on the local bond characteristics of the reinforcement. The well anchored coated reinforcement favorably affected the behavior of the deviation saddle at the ultimate load stage with an average increase in strength of 15% since it allowed for the complete mobilization of all the reinforcement within the deviation saddle. It can be concluded from these comparisons that the use of epoxy coated reinforcement resulted in an increased redistribution of force within the deviation saddle before fracture of the direct tension reinforcement.

4) All specimens except specimens 1B and 3B exhibited adequate ductility and thus gave sufficient warning of the impending

explosive failure. The specimens which resisted the pull-out force mainly by direct tension reinforcement (specimens 4A, 4B, 5A, and 5B) always displayed adequate ductility because the reinforcement had to strain substantially to fail.

5) From the cracking patterns and the strain data, three behavioral mechanisms were evident in the deviation saddle. They were the pull-out resistance of the direct tension reinforcement, the pull-out resistance of the top surface reinforcement, and the shear friction strength of the specimens across the critical cracked plane which was observed to be directly below the tendon ducts. The pull-out resistance of the direct tension reinforcement and the effective resistance of the top surface reinforcement are additive. Some uncertainty exists concerning the effectiveness of this top surface reinforcement at the yield load stage of the deviation saddle. The top surface reinforcement is beneficial in controlling and distributing cracks on the top surface of the deviation saddle.

6) All final failures (except with special specimen 2B) were the result of the fracture of the direct tension reinforcement. Test observations and analysis indicated that in these tests shear friction did not appear to be critical to the failure of the deviation saddle.

7) The capacity of the specimens could be determined by either the simplified analysis models or the strut-tie analysis models. Both analysis methods appear to produce reasonable correlations with the

test results, although both methods rely on subjective assumptions for the analysis of the top surface reinforcement.

8) In comparing the two types of reinforcement which are utilized to resist pull-out force in this study (direct tension reinforcement and top surface reinforcement), it is obvious that the direct tension reinforcement (the link bar in specimens 1A, 1B, 2A, 3A, 3B and the loop bar in specimens 4A, 4B, 5A, 5B) is significantly more efficient than the top surface reinforcement in resisting the deviated force.

9) The critical force which acts on the deviation saddle is the maximum tendon deviation force. In this test series, this is the force that was closely confined by the direct tension reinforcement. In the early configuration (specimens 1A, 1B, 3A, and 3B) this was the deviated force of the corner tendon which had both vertical deviation and horizontal deviation. The other tendons of the early specimens did not greatly influence the pull-out capacity of the specimens because they were not enclosed within the critical reinforcement (direct tension reinforcement). In the revised configuration (specimens 4A, 4B, 5A, and 5B) both tendons were enclosed in separate direct tension reinforcement, but the corner tendon was more critical since it had greater vertical deviation than the other tendon. The basic direct tension reinforcement around the critical tendon should be proportioned for this maximum tendon deviation force. The other tendons could be provided with the same reinforcement to simplify

detailing or some lesser amount determined by a similar analysis based on the individual tendon deviated force.

6.3 Recommendations

The following recommendations are made based on the ten deviation saddle tests of this investigation. Recommendations are focused on the deviation saddle since it is the weakest of the three basic types of tendon deviators. However, these recommendations can be conservatively applied to the diaphragm and rib or stiffener since these type of deviators generally have added strength contribution from the concrete.

1) Total service load design forces for the deviator should be the sum of the vertical and horizontal components of the deviated force from each tendon. These can be calculated as the maximum allowable initial jacking force multiplied by the sine of the angle change for the vertical and horizontal planes of the tendon. Under the AASHTO Specification (2), the maximum allowable initial jacking force is limited to 80% of the ultimate strength of the tendon ($0.8(f_{pu})(A_{ps})$).

2) At service load levels, reinforcement stresses would be limited to the specified allowable stresses in AASHTO Sec. 8.15.2.

3) For load factor design, neither AASHTO nor ACI (6) clearly specify an appropriate load factor for the prestress tendon force. In order to guarantee a reasonable factor of safety commensurate with other load and resistance factor combinations, it is suggested that

for this specific application the load factor on prestress force should be at least 1.7. Conventional reinforcement should be assumed at the yield point. The ϕ factor that should be used in the design of the direct tension reinforcement should be 0.90 since the primary acting force is tension. The ϕ factor for the shear friction calculation should be 0.85.

4) The recommended design detail is very similar to the modified deviation saddle detail (specimens 4A, 4B, 5A, and 5B) of the test series. The general approach to the design of the deviation saddle should be to rely only on the very efficiently utilized direct tension reinforcement for the pull-out force resistance of the deviation saddle. Any contribution to the pull-out resistance from the concrete is ignored as is any additional resistance from any beam type element above the tendon ducts.

For the direct tension reinforcement, utilize small closed rectangular stirrups (labeled as loop bar) which loop around each individual tendon duct of the deviation saddle and are well anchored under the top mat of reinforcement of the bottom flange. Additionally, provide light reinforcement in the deviator top surface for controlling and distributing surface cracks (this reinforcement should be neglected in the calculation of the pull-out capacity). This reinforcement should be provided as closed stirrups which enclose the entire deviation saddle. An amount of closed stirrups of the same

diameter and spacing as the link bar reinforcement should produce very satisfactory results.

Each individual loop bar group should be designed with the specified load factors and ϕ factors to resist the full pull-out force of the tendon with the largest vertical deviation. It will be more economical and will minimize fabrication errors to provide the other tendons with the same reinforcement regardless of their tendon deviation forces. The dimensions of the loop bars and the outer closed stirrup must be based on the tendon duct curvatures and outer diameters, reinforcement clearances, and development lengths. For the loop bars, the minimum clearance at the highest point of the tendon duct should be approximately 1". The vertical inside dimension of the outer closed stirrup should be at least 2" larger than the loop bars. The maximum bar size utilized for the loop bars should be limited to a deformed #5 size so as to be able to fully develop the 90° hook.

5) Deviation saddle geometry utilized should be a horizontal top surface with vertical sides. This makes fabrication of the segments easier and provides the lowest height deviation saddle possible which is critical in shallow highway bridge structures for clearance of deviated tendons from adjacent deviation saddles.

The concrete dimensions of the deviation saddle are controlled by the requirements of the tendon duct curvatures and outer diameter, reinforcement clearances, and cover requirements. The lowest point of the tendon duct above the top of the bottom flange

should be based on required clearance (1" to 2") for constructability (protective sheathing placed on extension of tendon duct is generally used for external post-tensioning). The location of the ducts transversely should be as close as possible to the web wall since it is desirable to have as small an eccentricity to the web as possible to minimize bending moments in the bottom flange. The width of the deviation saddle in the longitudinal direction of the bridge is dependent on the spacing and amount of reinforcement (4" to 6" center to center reinforcement spacing is recommended to allow constructability). Also, it is dependent on the minimum radius that the tendon duct can be bent.

6) Provide a full bottom flange width deviation saddle for curved spans with small radii when all the tendons in a deviation saddle have large horizontal deviations. For straight spans, when the horizontal tendon angles are small (less than 3°) and the horizontal components are directed either into the web or away from the web, it should only be necessary to use a deviation saddle which is similar to those tested. It may also be a good idea to provide the full bottom flange width deviation saddle no matter what the tendon deviations are when epoxy coated reinforcement is being utilized because it was observed in this test series that the specimens with epoxy coated reinforcement cracked at a much lower load than that of the conventionally reinforced specimens (averaged 24% lower). Since the reinforcement is being epoxy coated because of severe corrosion

conditions, it would be advantageous to go one step further and provide the full bottom flange width deviation saddle which will substantially increase the factor of safety against visible cracking.

A reduction in concrete volume for the full bottom flange width deviation saddle could be made by reducing the longitudinal dimension of the deviation saddle by one-half in the center of the bottom flange at a certain distance from the tendon ducts. Near the webs the deviation saddle would be the same as the models tested but would be joined to the opposite deviation saddle by a concrete strut half the dimension of the deviation saddle.

7) In cases where a full bottom flange width deviation saddle is not provided, a shear friction calculation should be made. In most cases, extra shear friction reinforcement will not have to be provided since there is usually an excess of direct tension reinforcement at the critical shear plane. Also, the outer closed stirrups contribute to the shear friction reinforcement. The shear friction equation that should be used for this check is Equation 8-10 of AASHTO Sec. 8.15.4.3. Any net tension across the shear plane is taken into account by subtracting it from the total capacity of the reinforcement crossing the shear plane. The maximum allowable shear strength provided by this equation is the lesser of the two values, $0.09f'_cA_{cv}$ or $360A_{cv}$ where A_{cv} is the area of concrete section resisting shear transfer. This area is assumed to be the area below the tendon ducts from the centerline of tendon closest to the web wall

to the front face of the deviation saddle. The μ factor is taken as 1.4 since the deviation saddle is monolithically cast.

APPENDIX

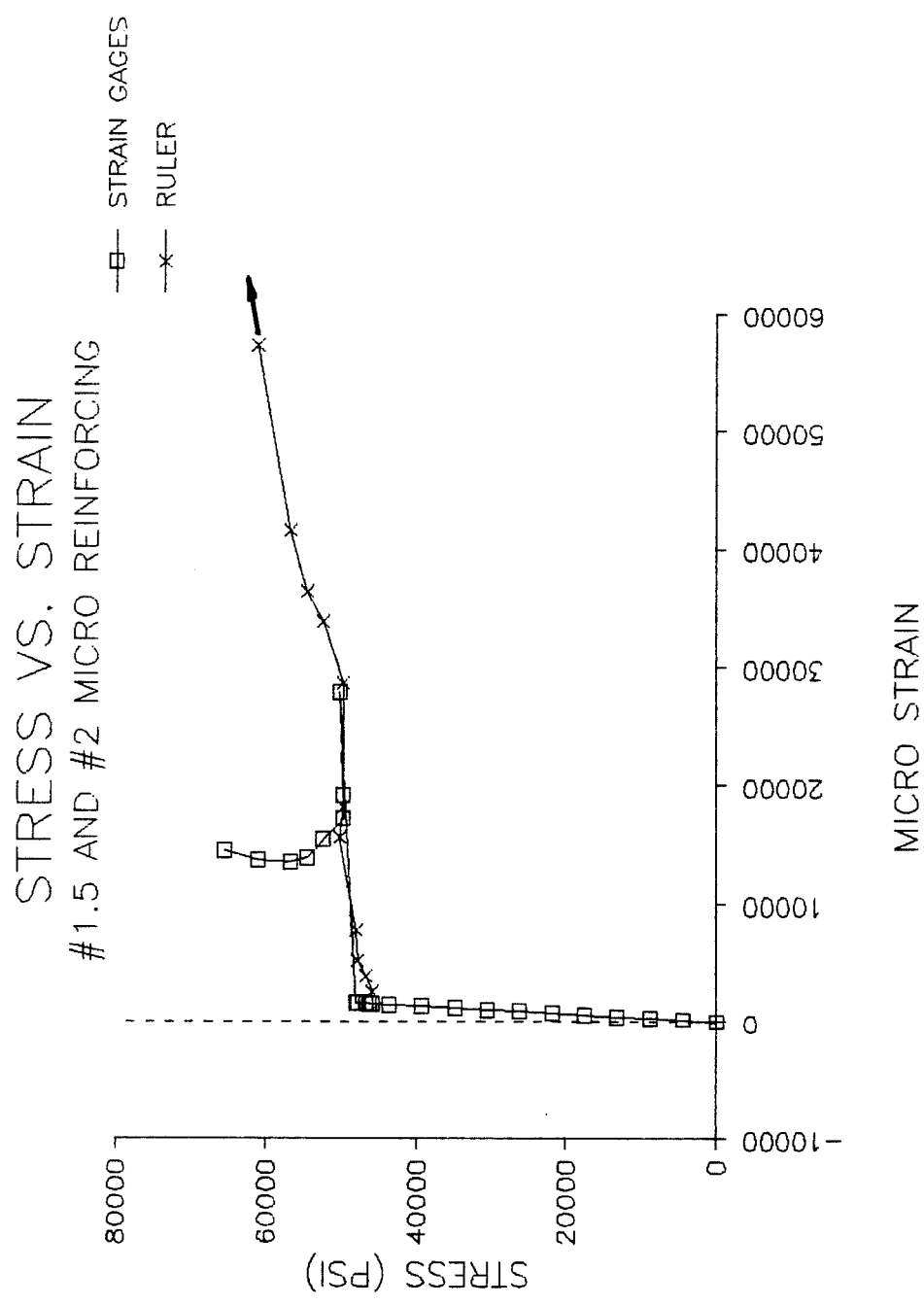


Figure A.1 Typical Stress-Strain Curve for #1.5 and #2 Micro Reinforcing Bars

STRESS VS. STRAIN #1.25 MICRO REINFORCING

—□— STRAIN GAGES
—×— RULER

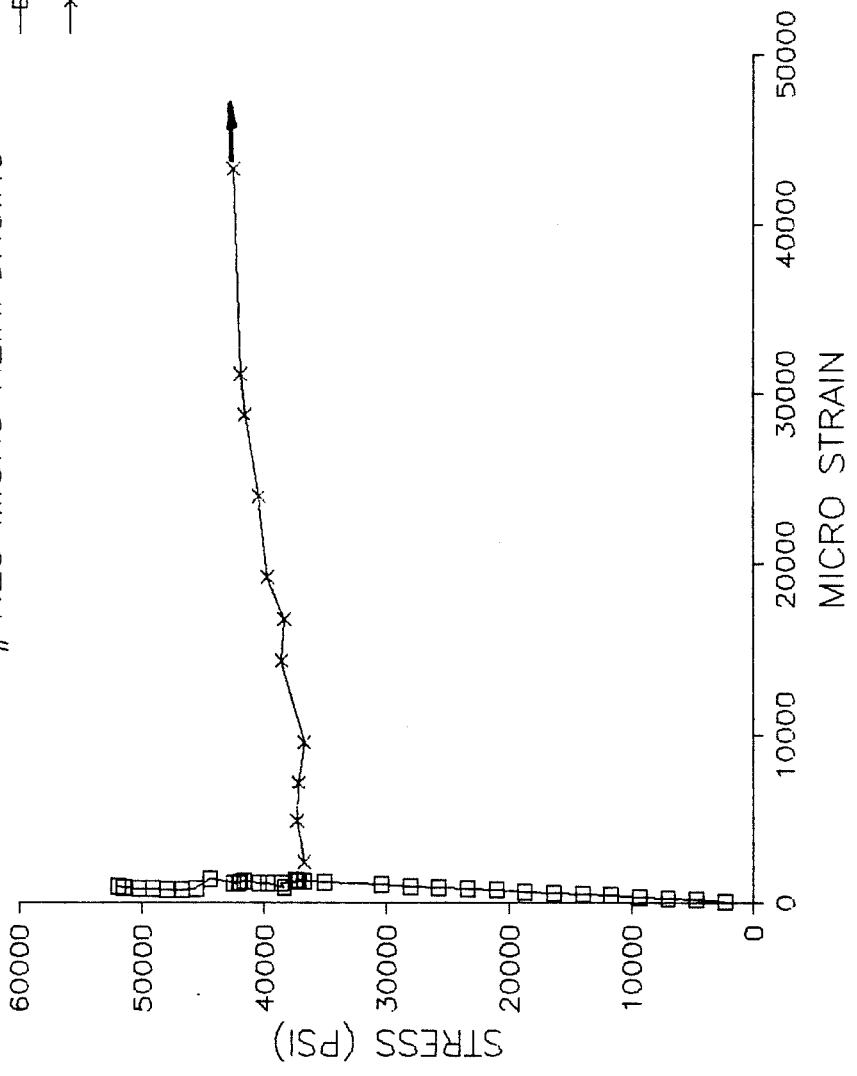


Figure A.2 Typical Stress-Strain Curve for #1.25 Micro Reinforcing Bars

REFERENCES

1. Carter, L.L., "Deviator Behavior in Externally Post-Tensioned Bridges," unpublished Master's thesis, The University of Texas at Austin, August 1987.
2. American Association of State Highway and Transportation Officials, Standard Specification for Highway Bridges, Thirteenth Edition, Washington D. C., 1983.
3. Treece, R., "Bond Strength of Epoxy-Coated Reinforcing Bars," unpublished Master's thesis, The University of Texas at Austin, May 1987.
4. Hofbeck, J.A., Ibrahim, I.O., Mattock, A.H., "Shear Transfer in Reinforced Concrete," ACI Journal, Vol. 66, No. 2, February 1969, pp. 119-128.
5. Mattock, A.H., Hawkins, N.M., "Shear Transfer in Reinforced Concrete - Recent Research," PCI Journal, Vol. 17, No. 2, March-April 1972, pp. 55-75.
6. Mattock, A.H., Johal, L., Chow, H.C., "Shear Transfer in Reinforced Concrete with Moment or Tension Acting Across the Shear Plane," PCI Journal, Vol. 20, No. 4, July-August 1975, pp. 79-93.
7. MacGregor, J.G., Reinforced Concrete-Mechanics and Design, Prentice Hall, New Jersey, 1988.
8. American Concrete Institute, Building Code Requirements for Reinforced Concrete (ACI 318-83), Detroit, 1983.
9. Schlaich, J., Schaefer, K., Jennewein, M., "Towards a Consistent Design of Reinforced Concrete Structures," PCI Journal, Vol. 32, No. 3, May-June 1987.
10. Marti, P., "Truss Models in Detailing," Concrete Institute, Vol. 7, No. 12, December 1985, pp. 66-73.

VITA

Richard James Beaupre was born in Grosse Pointe, Michigan, on August 11, 1961, the son of Charlotte Marchand Beaupre and John Edward Beaupre. After graduating from Leto High School, Tampa, Florida, in 1979, he entered Hillsborough Community College in Tampa, Florida. In January, 1982, he transferred to the University of Florida in Gainesville, Florida. He received the degree of Bachelor of Science in Civil Engineering from the University of Florida in April, 1984. During the following years he was employed as a bridge engineer at Greiner Engineering Sciences, Inc. of Tampa. In September, 1986, he entered The Graduate School of The University of Texas at Austin.

Permanent address: 8220 Vassar Circle
Tampa, Florida

This thesis was typed by the author.

